The
GEOLOGICAL BULLETIN
of the
PUNJAB UNIVERSITY

Number 36 *December 2001*

CONTENTS

Geol. Bull. Punjab Univ. 36, 2001.

PETROGRAPHY OF THE DUNGAN FORMATION EASTERN SULAIMAN RANGE, PAKISTAN.

BY

NAZIR AHMAD AND SHAFEEQ AHMAD
Institute of Geology, Punjab University, Lahore.

Abstract:-*The Dungan Formation is Palaeocene to Early Eocene in age and comprises a 98m thick predominantly carbonate sequence. It extends about 200km from north to south along the Sulaiman Range. The formation consists of nodular to massive limestone with subordinate shale, marl, sandstone and limestone conglomerates. The limestone is dark grey to brown and creamy white, and weathers brown, grey and buff yellow. In the southern Sulaiman Range, the shale becomes more as compared to that of northern part. The shales are dark blue grey, brown and olive in colour, which weathers grey to green. The conglomerates are usually composed of pebbles and cobbles of grey and brown limestone and marl, embeded in a matrix of soft, ash grey calcareous shale.*

The Formation is rich in fossils including foraminifers, gastropods, bivalves and calcareous algae. The foraminifers belong to miliolids, coskinolina, lockhartia, miscellanea, ranikothalia, nummulites, assilina, operculina, alveolina, discocyclina, athecocyclina, actinosiphon, globorotalia and globigerina. The calcareous algae are mainly red algae which includes archaeolithothamnium, lithothamnium, mesophyllum, lithophyllum, and jania, where as the green algae are clypeina, trinocladus; and acicularia. The other fossils are bryozoa, echinoderms, molluscs and corals. The cement types in the formation includes peloidal, neomorphic, isopachous bladed, drusy, and syntaxial overgrowth. On the basis of this study the formation comprises of calcareous mudstone, wackestone, packstone and grainstone.

INTRODUCTION

This paper deals with the petrography of the Dungan Formation which is based on the stained thin sections of the rock samples which are collected from three localities named Raghasar, Zinda Pir and Rakhi Nala (Fig. 1). These stained thin sections are studied under binocular microscope and reflected light microscopy; polished thin sections under cathodoluminescence microscopy and scanning electron microscopy on back scattered mode. A compromise system has been used (based on both Folk, 1959, 1962, and Dunham, 1962) to describe the composition, texture and the framework of the Dungan Formation.

LIMESTONE CLASSIFICATION

Two classification systems are commonly used each with different emphasis. These systems are given by Folk (1959, 1962) and Dunham (1962).

Folk Classification:- Folk's classification (1959, 1962) is based manily on depositional texture and especially on matrix type. He distinguished three components, the allochems (particles or grains); the matrix, chiefly micrite (equivalent to clay in sandstone); and cement, chiefly drusy sparite. An abbreviation for the allochems (bio-skeletal grains; oo-ooids; pel-peloids; and intra-intraclasts) is used as a prefix to micrite or sparite whichever is dominant.

Dunham Classification:- Dunham's classification is based on the depositional texture of the limestone. The fundamental criterion of subdivision is the nature of the framework of the sediments. He classified limestones into: grainstone, grains without matrix (grain supported); packstone, grains in contact with matrix (grain supported); wackestone, coarse grains floating in a matrix, grains are more than 10%, (mud supported); and mudstone, micrite with few grains, grains are less than 10%, (mud supported).

In the present study both type of classifications are used to describe the composition, texture and the types of grains present in the thin sections of the Dungan Formation.

CARBONATE GRAINS

Carbonate grains, broadly the main component of the limestone, are called the allochems. There are two main types of allochems, the skeletal and non-skeletal. The

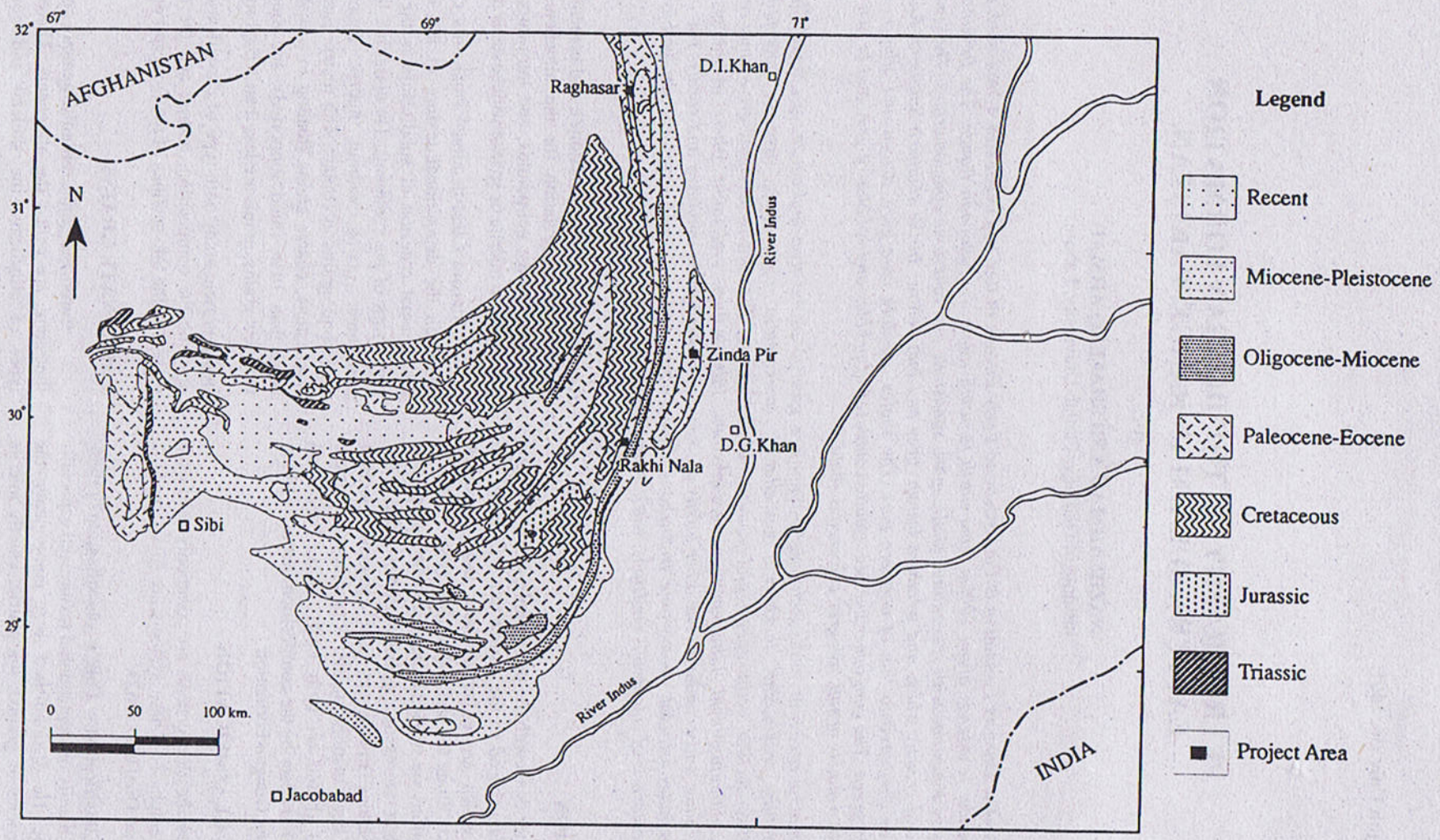

Fig. 1. Generalized geological map of the Sulaiman Basin (modified after Bakr and Jackson, 1964)

Dungan Formation contains both types of carbonate allochems.

SKELETAL ALLOCHEMS

The skeletal allochems of a limestone are formed by carbonate-secreting organisms. In the Dungan Formation these organisms (in order of abundance) are the benthonic foraminifera, algae, bryozoa, echinoderms, molluscs, corals and planktonic foraminifera. The present studies show that the skeletal allochems are the main component of the carbonates of the Dungan Formation.

Benthonic Foraminifera

The benthonic foraminifera present in the Dungan Formation are *Coskinolina, Miliolids, Rotalia, Lockhartia, Miscellanea, Ranikothalia, Nummulites, Assilina, Operculina, Discocyclina, Alveolina, Athenocyclina* and *Actinosiphon* (Davies, 1941; Hunting Survey Corporation, 1961; Latif, 1964; Iqbal, 1969).

i) Miliolids

They are abundantly present in the studied thin sections of Rakhi Nala and Raghasar areas. Their walls are of porcellaneous texture which gives shiny and smooth appearence. The test is made up of randomly oriented micrite grains. In thin section they appear dark in plane polarised light. The walls are composed of high-Mg calcite and the chambers are filled by sparry calcite cement (Plate 1A). Under cathodoluminescence microscopy the micritic wall are non-luminescent whereas the chamber fill cement shows orange luminescence (Plate 1B) in some cases.

ii) Coskinolina

Very few *Coskinolina* foraminifera are present in the few studied thin sections of Rakhi Nala and Raghasar areas. Their walls are of simple agglutinated forms, consisting of a single layer composed of particles. In thin sections the walls appear dark in plane polarized light. Both uniserial and biserial *Coskinolina* are present in the formation. The chambers are filled by non-ferroan sparry calcite cement (Plate 1C).

iii) Lockhartia

This genus of foraminifera is very common in most of the studied thin sections of Raghasar and Zinda Pir areas. Their wall structure is of hyaline texture which is characterised by fine and course perforation, and is originally composed of high-Mg calcite. The high-Mg calcite walls of foraminifera may become ferroan after diagenesis where as low Mg calcitic walls are not (Richter and Fuchtbauer, 1978). In thin section the walls appear light coloured in plane polarised light, and the chambers are filled mainly by sparry calcite cement, and few by micrite (Plate 2A). Under cathodoluminescence microscopy in some cases the walls show orange luminescence and the chamber fill cement are non-luminescent whereas in some cases the walls are non-luminescent and the chamber fill cement shows orange luminescence (Plate 2B).

iv) Miscellanea

This genus is commonly present in few thin sections of the studied areas of Raghasar and Zinda Pir. It is lenticular to subspherical, the walls are of hyaline texture which show the coarse perforation and is composed of high-Mg calcite. In thin sections the walls appear light coloured in the plane polarized light, and the chambers are filled mostly by non-ferroan srary calcite cement. In some cases they are filled partially by ferroan and partially by non-ferraon sparry calcite cement. In few thin sections the walls of the foraminifera are also ferroan (Plate 2C).

v) Ranikothalia

Very few foraminifera of this genus are present in a few of the studied thin sections of the Zinda Pir area. They are mostly present as fragments, very few are in a complete form. The wall structure of this genus is of hyaline texture, which is characterized by perforation and is composed of high-Mg calcite. In thin sections chamber walls appear light coloured in plane polarized light. The chambers are filled with mostly by the non-ferroan sparry calcite cement, and few are partially by non-ferroan sparry calcite cement and partially by micrite. *Ranikothalia* are planispiral and the whorls are 4/5 in A form (Plate 3A).

vi) Nummulites

This genus of benthonic foraminifera is very commonly present in most of the studied thin sections of the Zinda Pir section. They are present mostly in a complete form along with broken fragments. The wall structure of these genera is of hyaline texture, which is characterized by minute perforations and is composed of both low-Mg calcite and high-Mg calcite. In the thin sections the walls appear light coloured in plane polarized light, and show extinction under cross polarized. In a few cases the wall are ferroan (Plate 3B). The chambers are filled mostly by non-ferroan sparry calcite cement. In a few cases the chambers are filled by ferroan sparry calcite cement, and in some cases they are partially filled by ferroan and partially by non-ferroan sparry calcite cement (Plate 3C). *Nummulites* are planispiral and have many whorls. Under cathodoluminescence microscopy the walls of few *Nummulites* show orange luminescence and the cement filled in chambers is non-luminescent (Plate 4A). Similarly in few cases the cement filled in chambers show orange luminescence and the walls are non-luminescent.

vii) Assilina

This genus is commonly present in most of the thin sections of the Zinda Pir section. It is planispiral and has a

tight coil with many whorls. The wall structure of this genera is of hyaline texture, characterized by perforations and is composed of high-Mg calcite. In thin sections the walls are light coloured in the plane polarized light. The chambers are filled mainly by non-ferroan sparry calcite cement, and occasionally by ferroan and non-ferroan sparry calcite cement (Plate 3C). Under cathodoluminescence microscopy the walls of few *Assilina* show orange luminescence and the cement, filled in chambers, does not show luminescence. Similarly in a few cases the cement filled chambers show orange luminescence and the walls are non-luminescent.

viii) Operculina

This type of genus is commonly present in most of the thin sections of the Zinda Pir section. Specimens are planispiral and have a moderately tight coil with three quarters of their whorls in A form. The wall structure of *Operculina* is hyaline with minute perforations. The walls are composed of both high-Mg calcite and low-Mg calcite. The chambers are filled mainly by non-ferroan sparry calcite cement (Plate 3C) and in few cases they are filled partially by sparite and partially by micrite. Under cathodoluminescence microscopy the walls of some *Operculina* show orange luminescence (Plate 4A) and the cement filled chambers are non-luminescent. Similarly in some cases the cement filled in chambers show orange luminescence and the walls are non-luminescent.

ix) Alveolina

Very few foraminifera of this genus were observed in thin sections of the Zinda Pir area. The wall structure of Alveolina is porcelaneous, which gives a shining and smooth appearance under plane polarized light. It is micritic and in thin section it appears dark in plane polarized light. The walls are composed of high-Mg calcite. The chambers are filled by non-ferroan sparry calcite cement (Plate 3A).

x) Discocyclina

This type of genus is commonly present in many of the thin sections of the Zinda Pir area and in some thin sections of the Raghasar area. The genus is present both in complete form and in the form of broken fragments. It is circular in plain and discoidal (Plate 3C). The radial chamberlet walls of equatorial chambers are in adjacent with the annuli usually alternate in position. The wall structure is of hyaline texture characterized by perforations. The walls are composed of both low-Mg calcite and high-Mg calcite. After diagenesis, the high-Mg calcitic wall texture becomes ferroan (Plate 4B) whereas the low-Mg calcitic wall texture does not become ferroan (Richter and Fuchtbauer, 1978). In thin sections the walls appear light coloured in the plane polarized light. The chambers are filled by non-ferroan sparry calcite cement. Under cathodoluminescence microscopy the cement filled in chambers of some specimens show orange luminescence. Similarly the walls of the *Discocyclina* show orange luminescence in some specimens (Plate 4C).

xi) Athecocyclina

This genus of foraminifera is commonly present in some thin sections of the Zinda Pir area. Specimens are present mostly in the form of broken fragments, some are present in a complete form. Tests are circular in plane. The radial chamber walls are more or less absent. The wall structure of *Athecocyclina* is of hyaline characterized by minute perforations. These walls are composed of low-Mg calcite. In thin sections the walls appear light coloured in plane polarized light (Plate 3C). The chambers are filled by non-ferroan sparry calcite cement.

xii) Actinosiphon

Few foraminifera of this genus are present in thin sections of the Zinda Pir area. Mostly they are present in a complete form and very few are in broken fragments. The embryonic chambers are bilocular, and are completely surrounded by a ring of about eleven periembryonic chambers. The equatorial chambers are irregular radial row, each with a large median intercameral foramen. The wall structure of the *Actinosiphon* is hyaline, characterized by minute perforations which are composed of low-Mg calcite. In thin sections the walls appear light coloured in plane polarized light.

Calcareous Algae

The calcareous algae present in the carbonates of Dungan Formation are mainly the red calcareous algae along with few green calcareous algae. The genera of red calcareous algae are the *Archaeolithothamnium, Lithothamnium, Mesophyllum, Lithophyllum*, and *Jania* and the genera of green algae are *Trinocladus, Clypeina* and *Acicularia* (Davies, 1941; Khan and Haque, 1956; Hunting Survey Corporation 1961).

A) Calcareous Red Algae

i) Archaeolithothamnium

This genus of red calcareous algae is very commonly present in most of the thin sections of Raghasar area, moderately in Zinda Pir area. In the Raghasar area most of the algae are in a complete form along with few fragments, whereas in Zinda Pir section they are mainly in the form of fragments. In the Raghasar area this genus of algae mainly adopts a rhodolithic structure. The structure is formed of individual layers of cells, each of which can be differentiated into hypothallus and perithallus. The hypothallium is multilayered, developing parallel to the substrata. The perithallial tissue is generally thick and

composed of regular rows of cells. The sporangia are not in conceptacles but occur loose in rows (Plate 5A), this is a distinctive characteristic of this genus. In thin section the tissues appear dark and micritic under plane polarized light. The conceptacles appear light and sparry calcitic under plane polarized light. In some cases the rhodoliths are encrusted by bryozoa. Under cathodoluminescene microscopy in several cases the tissues of the algae show orange luminescence (Plate 5B).

ii) Lithothamnium

This genus is abundantly present in most of the studied thin sections of Raghasar and few in Zinda Pir and Rakhi Nala sections. In the Raghasar area they are present mainly as complete rhodoliths. In the Zinda Pir section they are mostly in the form of broken fragments, and particularly in the Rakhi Nala section they are present in the form of very small fragments. The tissues are composed of numerous layers of cells which can be differentiated into hypothallus and perithallus. The hypothallium is multi-layered, but non coaxial developing parallel to the substrata. The perithallium is usually thick and composed of regular layers of cells (Plate 5C). The sporangia occur in multi-pored conceptacles. The hypothallium and the perithallium appear dark and micritic under plane polarized light in thin section whereas the conceptacles are light coloured and sparitic under plane polarized light. In the Raghasar area few *Lithothamnium* are encrusted by bryozoa. Under cathodoluminescene microscopy, in a very few cases, the hypothallium and perithallium of the algae show orange luminescence.

iii) Mesophyllum

Mesophyllum is commonly present in most of the thin sections of Raghasar area, and in a few thin sections of the Zinda Pir area. In the Raghasar area specimens are preserved well in both complete and fragmental forms. In the Zinda Pir area they are mostly preserved as fragments. In this type of algae the tissues can normally be differentiated into hypothallus and perithallus. The multilayered hypothallium is parallel to the substrata and characteristically coaxial. The perithallium is thick and distinctly layered. The conceptacles are multipored and relatively larger. In thin sections the tissues appear micritic and dark under plane polarized light. The conceptacles are light coloured and sparitic under plane polarized light.

iv) Lithophyllum

This genus of red algae is moderately common in most of the thin section of the Raghasar area. They are mainly in a complete sheet-like form although fragments also occur. The tissues are normally differentiated into a hypothallium and perithallium. The hypothallium is coaxial and the perithallial tissue is thick and composed of regular layers of cells. In a few cases the coaxial hypothallium is surrounded by a thinner marginal perithallium (Plate 6A). The conceptacles have a single aperture. In thin sections the hypothallus and perithallus appear as micrite and are dark under plane polarized light. The conceptacles are light coloured and sparitic under plane polarized light. Under cathodoluminescene microscopy occasionally the tissues of the algae show orange luminescence.

v) Jania

Very few calcareous algae of this genus are present in few thin sections of Raghasar area. They are mostly present in the form of fragments, very few are in a complete form (Plate 6B). The *Jania* develops dichotomously branched thallus made up of cylindrical segments. Medullary filaments are surrounded by a thin zone of cortical filaments. The cells of the medullary filaments are typically wedge-shaped and successive rows of cells join along irregular lines. The conceptacles occur in axial positions. In thin sections the tissues appear dark and micritic under plane polarized light. The conceptacles are sparitic and light coloured under plane polarized light.

B. Calcareous Green Algae

i) Clypeina

This genus of calcareous algae belongs to family dasycladaceae. This type of algae are rarely present in few of the thin sections of Raghasar area. They are present both in complete and fragmental forms. Specimens look like a bowl-shaped disc which corresponds to the whorls of primary branches (Plate 6C). The central stem is moderately large and sporangia occur in the lower ends of the branches. The stem and branches appear dark and micritic in thin section under plane polarized light. The sporangia are light coloured and sparitic under plane polarized light and show extinction under cross polarized.

ii) Trinocladus

This genus also belongs to dasycladaceae family. Very few *Trinocladus* algae are present in thin sections of Raghasar area. They are mostly present in the form of fragments. Specimens have a cylindrical thallus with moderately large central stem. Primary branches, occuring in regular whorls, give rise to secondary branches and these in turn to clusters of tertiary branches. The primary branches are thick, widen outward and probably contain the sporangia (Plate 6C). In thin sections the stem and branches appear dark and micritic under plane polarized light.

iii) Acicularia

This genera of calcareous algae belongs to family dasycladaceae. Specimen are rarely present in very thin sections of Raghasar area. They are mostly present in the form of fragments. The plant appears like a disc which is

made up of radially arranged rays that contain spherical sporangial cavities. These rays or fragments may result from the disaggregation of the apical disc (Plate 6C). In thin section the disc and the rays appear dark and micritic under plane polarized light. The sporangial cavities are light coloured and sparitic under plane polarized light, and show extinction under cross polarized.

Bryozoa

Bryozoan colonies are very commonly present in most of the thin sections of Raghasar and Zinda Pir areas, and in few sections of Rakhi Nala area. The colonies (zoaria) are generally small about one centimeter in diameter and they appear as lacy networks, as thin encrustation on algae, as rows of small beads, and as spiderlike webs. The colonies have a cellular arrangement of zooecia and the thin calcareous walls are of a granular texture. The zooids are generally less than 0.5 mm in diameter and colonies may comprise several hundred individuals. The bryozoans are characterized by their cellular colonial structure with tubes and pores of various widths and parallel arrangements. The diameter of their chambers is intermediate between those of coral and red calcareous algae. The zooecium is calcareous and cylindrical or polygonal in shape. The bryozoa are composed of high-Mg calcite. A few bryozoa colonies encrust the red calcareous algae. In thin section the walls appear dark in plane polarized light. The chambers are generally filled by non-ferroan sparry calcite cement, but in a few cases they are partially filled by micrite and partially by sparry calcite cement. Usually the wall and the chambers do not show luminescence, but sometimes, the sparry calcite cement, filled in chambers show orange luminescence (Plate 7A). Similarly in a very few cases the walls of the bryozoa colonies show orange luminescence.

Echinoderms

The echinoderms are commonly present in most of the thin sections of the Rakhi Nala, Raghasar and Zinda Pir areas. They are mainly echinoids along with a few asteroids. The echinoderms are composed of high-Mg calcite in the form of plates or spines. Each plate or spine behaves as a single crystal of calcite when viewed under plane polarized light and is giving unit extinction under cross polarized. The echinoderms are in the form of plates (Plate 7B), and they generally have a syntaxial overgrowth cement (Plate 7B). Under cathodoluminescence microscopy most of the echinoderm fragments which have the syntaxial overgrowth cement show zoned (orange thin lines and dead thick part) luminescence (Plate 5B), whereas in a few cases the whole fragment show bright orange luminescence.

Molluscs

Molluscs fragments are abundantly present in most of the thin sections of Rakhi Nala, Raghasar, and Zinda Pir areas. They are mainly bivalves including oysters, and gastropods. The bivalve shells are originally composed of aragonite which after diagenesis recrystallized to a mosaic of sparry calcite. In thin sections they are randomly oriented. Original shell shapes are discernible by means of a fine coating or micrite "dust rim". The oyster shells have a calcitic foliated structure with a mixed mineralogy, the outer layers are calcitic and the inner layers are aragonitic which dissolved during diagenesis and later on filled by sparry calcite cement (Plate 7B). The dense structure of oysters makes them relatively resistant to fragmentation. They are well preserved in the rocks. The shells of aragonitic bivalves do not preserve their original structures. The entire shells have been dissolved leaving voids which are later filled by calcite spar. Under cathodoluminescence microscopy very few of the sparry calcite cement void infillings show orange luminescence, and the micritic wall does not show any luminescence. The gastropod shells are present only in a few thin sections. These shells are composed of aragonite and have a cross-lamellar structure. The skeletal structure of gastropod is not preserved due to their original aragonitic composition which, after diagenesis, is replaced by non-ferroan sparry calcite cement. Under cathodoluminescence microscopy they do not show any luminescence.

Corals

Very few corals are present in thin sections of Raghasar and Zinda Pir areas. The corals are mainly the *Scleractinia* and were originally composed of fine, fibrous aragonite which later is replaced by sparry calcite cement after diagenesis. The chambers are filled by sparry calcite cement. Coral colonial skeletons may be distinguished from bryozoa skeleton by their tendency to form large colonies, the larger size of the body cavities, the presence of nodes, spines and septa projecting into the body cavity and their relatively thick, uniform walls. In thin section the septa appear as micrite and dark under plane polarized light and the chambers (trabecular canals) light coloured because of sparry calcitic infilling (Plate 7C). Under cathodoluminescence microscopy they do not show any luminescence.

Planktonic Foraminifera

The planktonic foraminifera are abundantly present in few of the thin sections of Zinda Pir area. They are mainly the *Globorotalia* and *Globigerina* (Davies 1941; Hunting Survey Corporation 1961; Latif 1964; Iqbal 1969) and have thinner test wall than the benthonic foraminifera, composed of low-Mg calcite. The walls appear dark, micritic under plane polarized light. The chambers are relatively large. They are filled by non-ferroan sparry calcite cement (Plate 8A). They appear as light coloured and sparry under plane polarized light, and show extinction

under cross polarized. Under cathodoluminescence microscopy they do not show any luminescence.

NON-SKELETAL ALLOCHEMS

In the Dungan Formation the non-skeletal allochems are very few, consisting of ooids and intraclasts.

Ooids

In the studied area the ooids are found in 7-8 thin sections of the Rakhi Nala section only. The ooids are spherical to subspherical grains consisting of multi-laminate concentric lamellae. The nucleus generally is a foram or any other skeletal fragment or a quartz grain. The ooids are normally 0.3 to 0.5 mm. in diameter and do not show any fracture. They are well preserved and appear dark under plane polarized light. They are encircled by calcitic envelope, which shows orange luminescence (Plate 8B).

Intraclasts

Very few intraclasts are found in thin sections of Zinda Pir and Raghasar areas. The intraclasts are of biomicrite of the same formation. In thin sections they are recognised on the basis of sharp boundaries between the intraclasts and the primary part of the formation.

NON CARBONATE GRAINS

In the Dungan Formation non-carbonate grains are moderately common in most of the thin sections of Rakhi Nala area, but very few are present in the Raghasar and Zinda Pir areas. The non-carbonate grains are mainly quartz grains, along with a few pyrite crystals. The quartz grains are uni-crystalline and medium to coarse grained, sub-angular to sub-rounded. They are characterized by low birefringence, lack of cleavage and twinning, and low positive relief, and show extinction under cross-polarized light. The pyrite crystals are opaque in plane-polarized light and in cross-polarized light, whereas it gives yellow shining appearance in the reflected microscopy.

CEMENT TYPES

This study established several different types of cement in Dungan Formation. These cement types are peloidal, neomorphic, isopachous bladed, drusy, and syntaxial overgrowth cements.

PELOIDAL CEMENT

This type of cement is found in some thin sections of Raghasar and Zinda Pir areas. In thin sections peloids appear dark with a little light coloured sparry calcite in between them under plane polarized light. The micritic peloids are subspherical bodies of 20 to 50 μm in diameter. They are composed of micrite of less than 3 μm. The microspar cement crystals are 5 to 8 μm in diameter and appear light coloured and cloudy. The peloids do not show fibrous structure. In other words it is a microcrystalline sparry calcite cement with the micrite (in the form of peloids). The boundaries between the micrite and the microspar calcite are irregular. In modern carbonate sediments such type of cements are composed of high-Mg calcite (Scoffin, 1987). Under cathodoluminescence microscopy the peloids are non-luminescent.

NEOMORPHIC SPAR

This type of cement is present in several of the thin sections of Raghasar area. The neomorphism is the regrowth of fine grained spar (microspar, crystal size between 4 to 8 μm) in place of sparry calcite cement (crystal size between 10 to 50 μm) (aggrading neomorphism). Crystals are characterized by irregular intercrystalline boundaries, the irregular crystal size distribution, the gradational boundaries to areas of neomorphic spar and the presence of skeletal grains floating in coarse spar (Plate 8C).

In general the development of the neomorphic spar takes place commonly on the margins of the large shell fragments of molluscs, which are originally composed of aragonite. They are now represented by relatively coarse mosaic of pseudospar (Plate 7B). The crystals are characterized by irregular boundaries and great variations of size. The fabric of these crystals is very similar to that of sparry calcite cement, but it lacks the characteristic pore filling spar, and containing small patches of micrite. Under cathodoluminescence microscopy they do not show any luminescence.

ISOPACHOUS BLADED CEMENT

The isopachous bladed cement occurs in thin sections of Rakhi Nala, Raghasar, and Zinda Pir areas. It is in the form of crust or a thin uniform fringe around the foraminifera and ooliths with a uniform thickness (Plate 9A). These fringes have grown outward into the pore space at right angle to the surface of the grains (foraminifera and oolite). Under plane polarized light they appear light coloured, and under cathodoluminescence microscope they show bright orange luminescence (Plate 8B).

DRUSY CEMENT

This type of cement is commonly present in most of the studied thin sections of the Rakhi Nala, Raghasar and Zinda Pir areas. This cement fills mainly the intergranular pore spaces and the intragranular spaces (i.e. the chambers of foraminifera, bryozoa, and corals). The drusy mosaic cement is composed of anhederal crystals of small longitudinal or prismatic calcite. The size of the crystal increases towards the centre of the pore (Plate 9B). The cement is mainly non-ferroan, but in few cases it is ferroan as well. The boundaries between the crystals are usually sharp and irregular. The drusy cement is composed of low-

Mg calcite. Under plane-polarized light it appears light coloured, and shows extinction under cross-polarized light. Under cathodoluminescence microscopy most of the drusy cement show a dull luminescence, but in a few cases this cement shows orange luminescence.

SYNTAXIAL OVERGROWTH CEMENT

The syntaxial overgrowth cement occurs in most of the thin sections which contain echinoderm fragments. Large single crystals are developed on echinoderm fragments, in optical continuity with the calcite of the echinoderm. They can be distinguished from the allochems in the thin sections under plane polarized light, but under cross-polarized light they extinguish as a single crystal. The rim or overgrowth cement usually consists of non-ferroan clear crystals (Plate 10A).

Evamy and Shearman (1965) were able to resolve the successive stages of the development of syntaxial sparry calcite overgrowth around echinoderm fragments by staining techniques. They traced the distribution of ferrous iron in the calcite crystal and identified iron free and variably iron bearing zones. They found that the calcite of the echinoderm debris and of the inner parts of the overgrowths remained unstained. Under cathodoluminescence microscope these zones are clearly established. The iron free zones are non-luminescent whereas the iron bearing zones are showing orange to dull luminescence on the basis of iron enrichment (Plate 10B).

MATRIX

The matrix is a material in which the grains (allochems) are embedded. This is fine grained, and composed of high-Mg micro crystalline calcite. It is present in most of the studied thin sections of Rakhi Nala, Raghasar, and Zinda Pir areas. It ranges from 0% of the total rock to 89.2%. It appears dark under plane-polarized light and does not show any luminescence under cathodoluminescence microscopy.

POROSITY

In the studied thin sections of Rakhi Nala, Raghasar, and Zinda Pir areas the porosity is mainly secondary which includes mouldic, vug, and fracture. The mould (Plate 9C) and vug porosities are formed by solution of grains, after thorough leaching by meteoric ground water, and fractures are formed through tectonic movements and pressures. All these porosity types are filled by non-ferroan sparry calcite cement, with some ferroan calcite cement. Under cathodoluminescence microscopy the calcite cement of the pores does not show any luminescence.

COMPACTION AND PRESSURE SOLUTION

Compaction refers to any process that decreases the bulk volume of rocks. This includes mechanical processes that decrease the bulk volume of single grains (grain deformation) or that cause closer packing of grains (re-orientation) and pressure solution which decreases the volumes of grains and of cement minerals.

The effects of compaction are seen in thin sections from the Zinda Pir area in the form of mechanical process and pressure solution. The skeletal grains in these sections show slight deformation in their shapes and have a concavo-convex contacts between them. This shows the weak compactional effect on them (Plate 10C). The other sections of Rakhi Nala and Raghasar areas do not show any significant compactional effect on the grains.

Similarly the effect of pressure solution is seen in most of thin sections of the Zinda Pir area in the form of dissolution seams and stylolite structures. In other sections of Rakhi Nala and Raghasar areas they are not significantly present. The dissolution seams are seen in a few thin sections of argillaceous carbonate rocks. They are smooth, undulose seams of insoluble residue which lack the distinctive suture of stylolite (Plate 10C).

The stylolites are thin zones of discontinuity within rocks, and are developed locally due to the pressure solutions. In thin sections they appear like zig-zag sutures. The stylolites are of low peak amplitude, (about 1 mm.), and are parallel to bedding. The seams of stylolites are filled by dark insoluble material (may be clays).

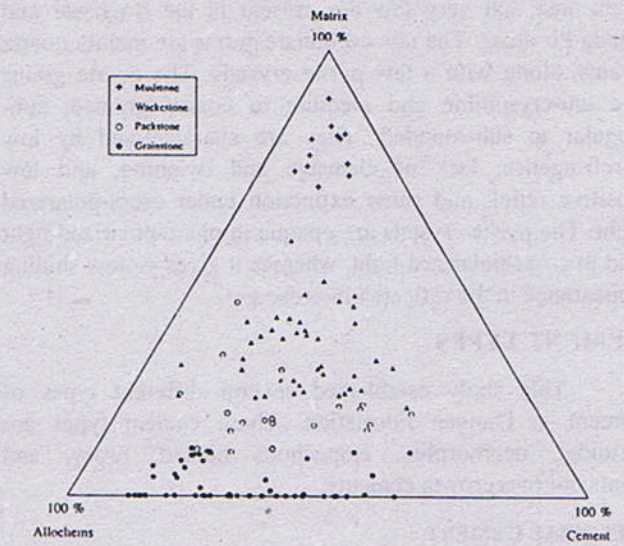

Fig. 2 Plot of the various rock types identified within Dungan Formation, superimposed on Dunham's (1962) classification of limestones.

MICROFRACTURES

The microfractures are seen in most of the thin sections of all the three areas. They are generally small in width and length. The width is 0.2 to 0.5 mm. and few

Plate -1

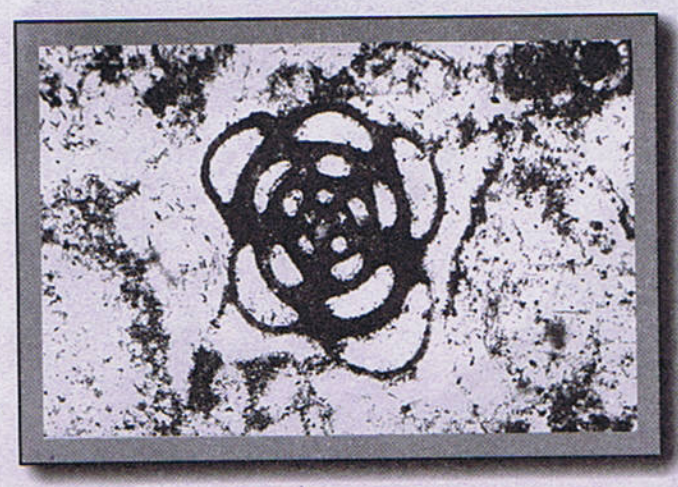

A

200 µm

B

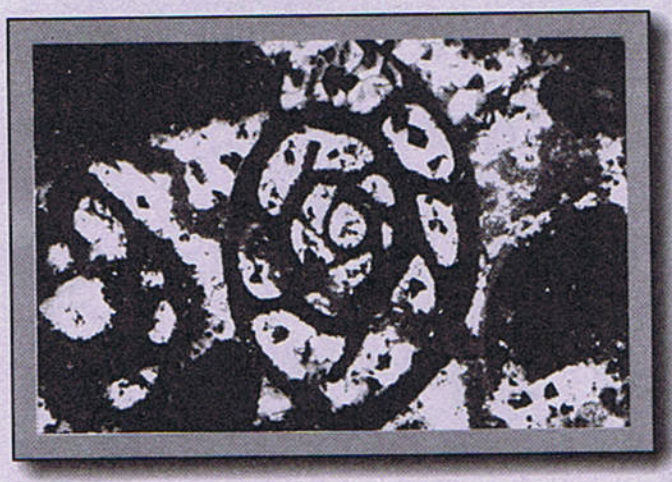

200 µm

C

200 µm

Plate -2

A

200 µm

B

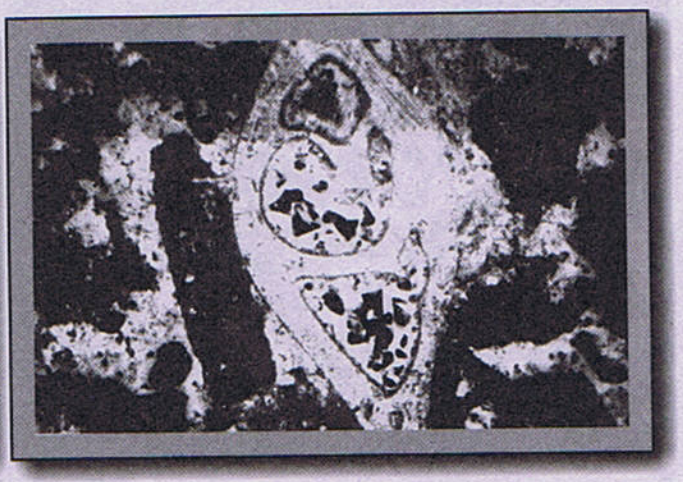

200 µm

C

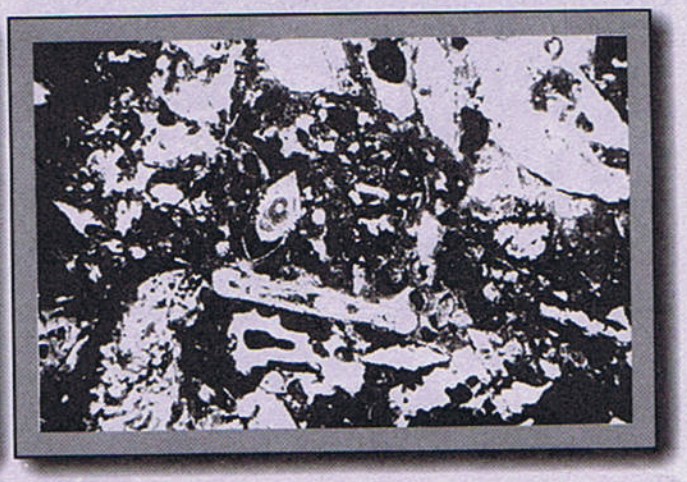

1000 µm

Plate -3

A

1000 µm

B

1000 µm

C

1000 µm

Plate -4

A

400 µm

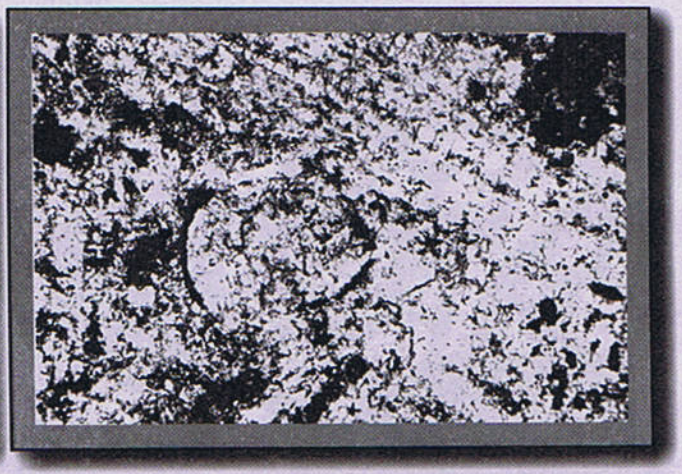

B

200 µm

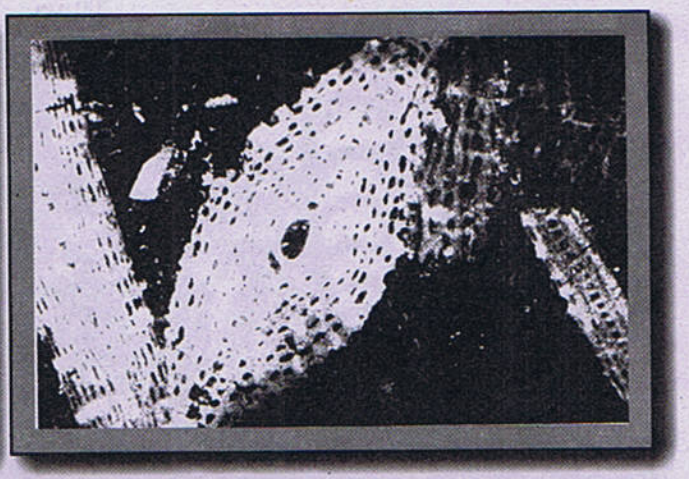

C

400 µm

Plate -5

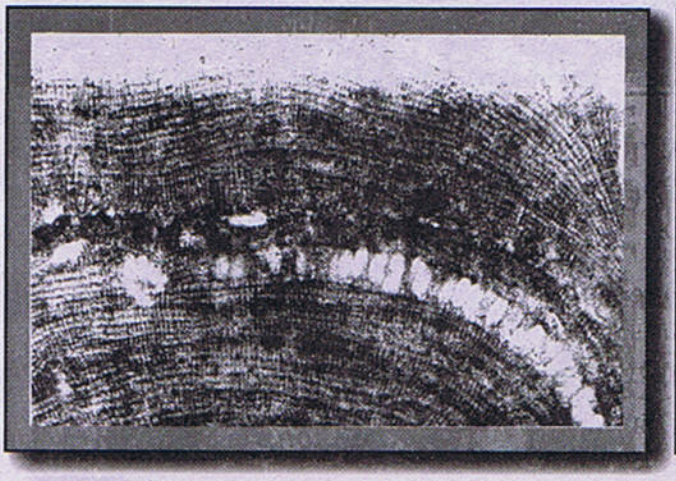

A

200 µm

B

400 µm

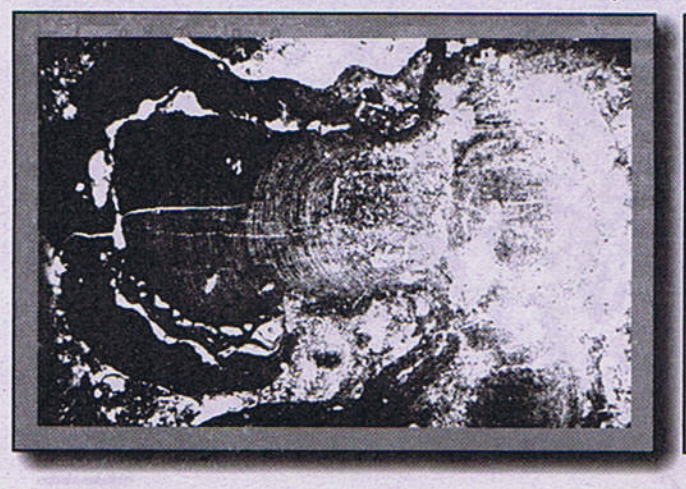

C

1000 µm

Plate -6

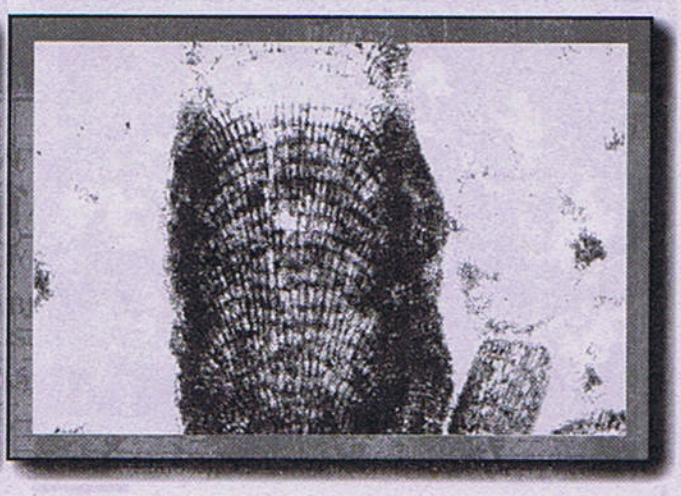

A

200 µm

B

1000 µm

C

1000 µm

Plate -7

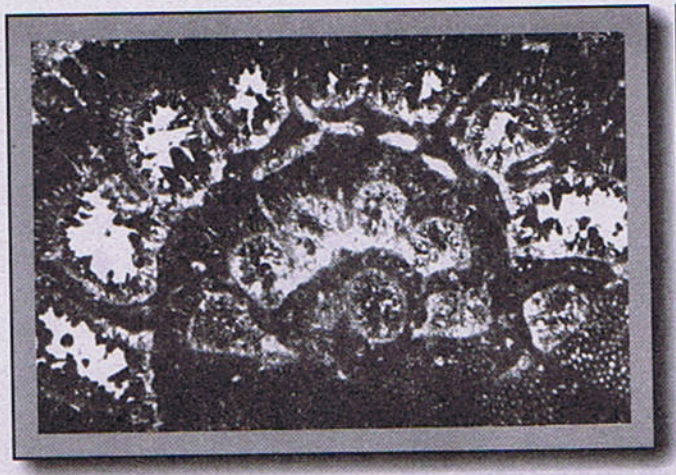

A

200 µm

B

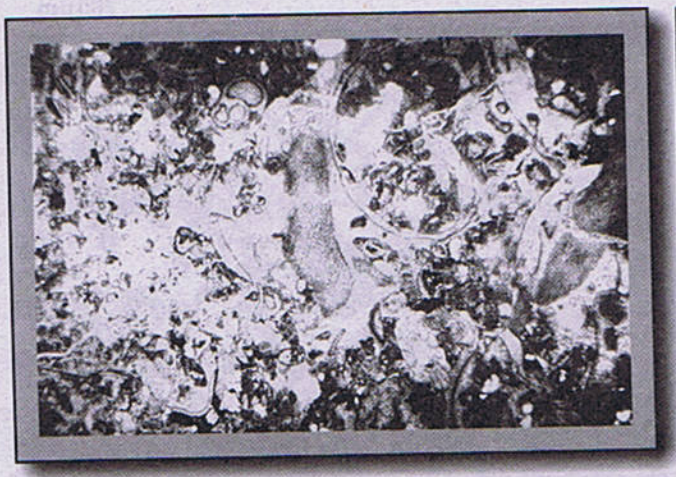

1000 µm

C

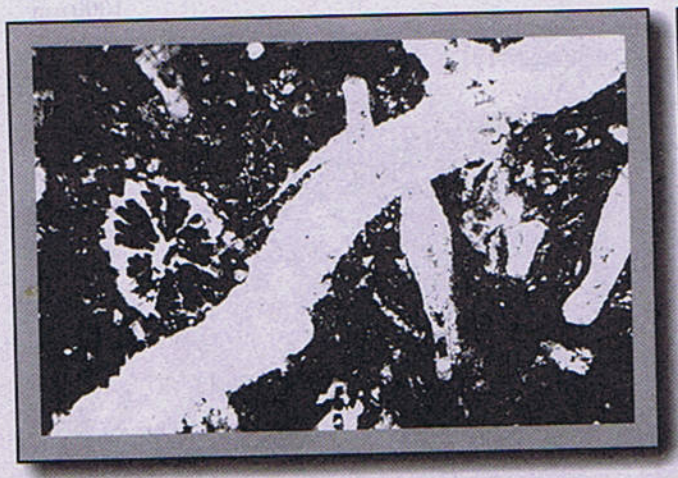

1000 µm

Plate -8

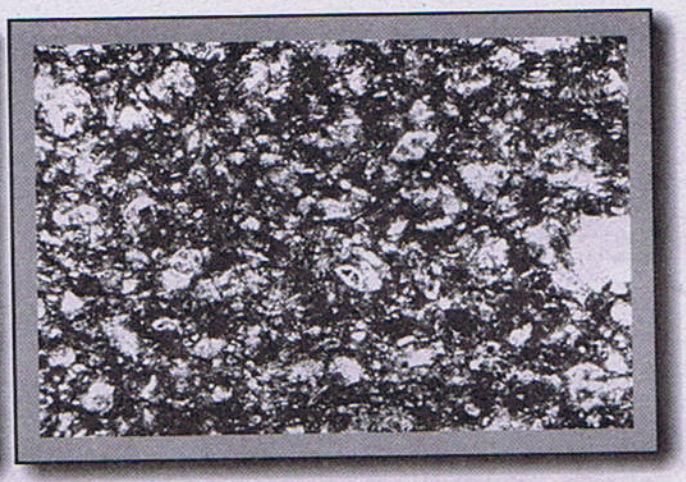

A

200 µm

B

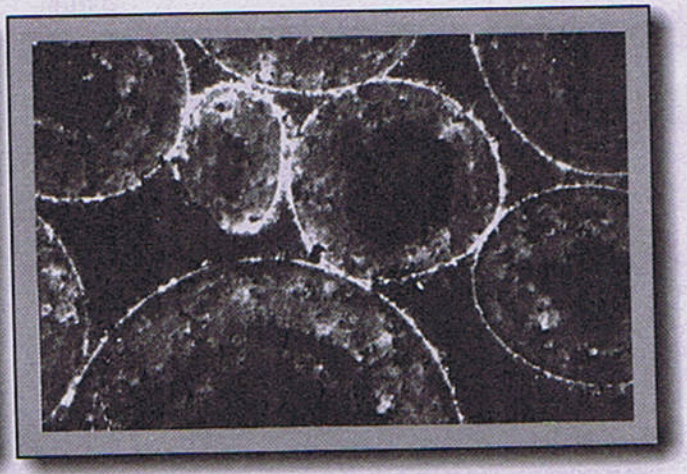

200 µm

C

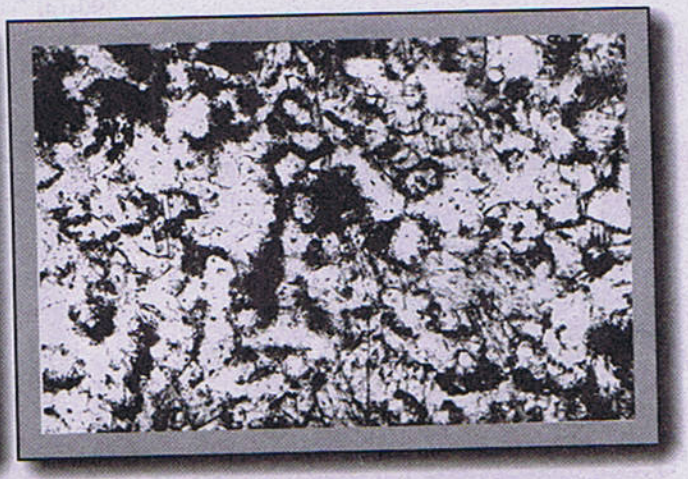

200 µm

Plate -9

A

200 µm

B

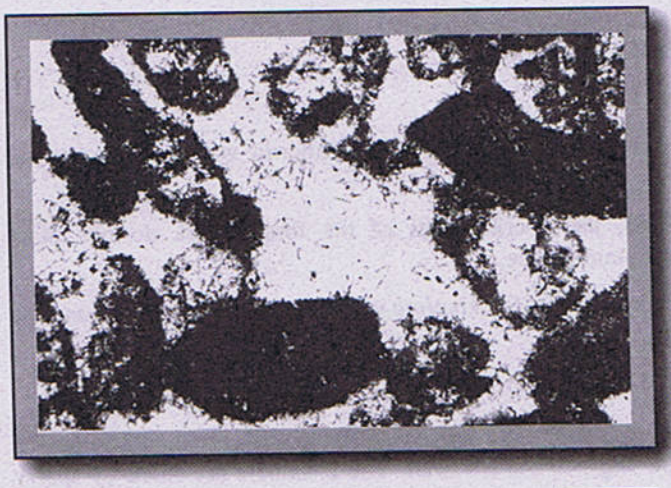

200 µm

C

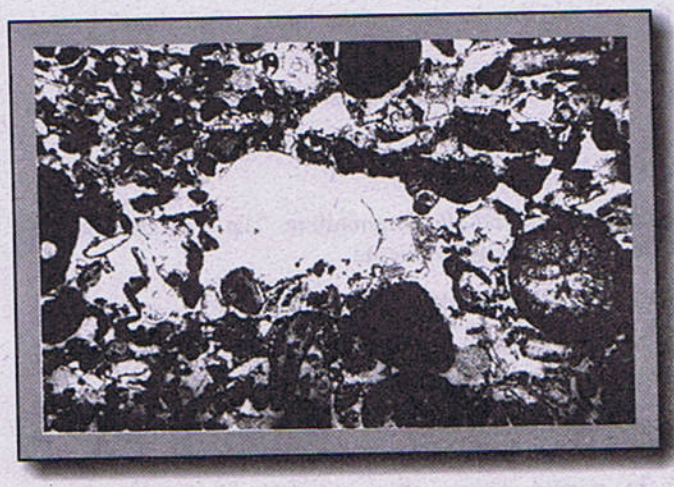

1000 µm

Plate -10

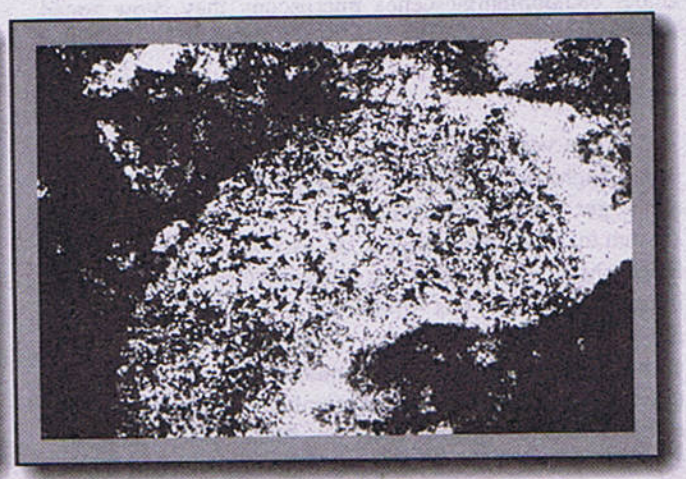

A

200 µm

B

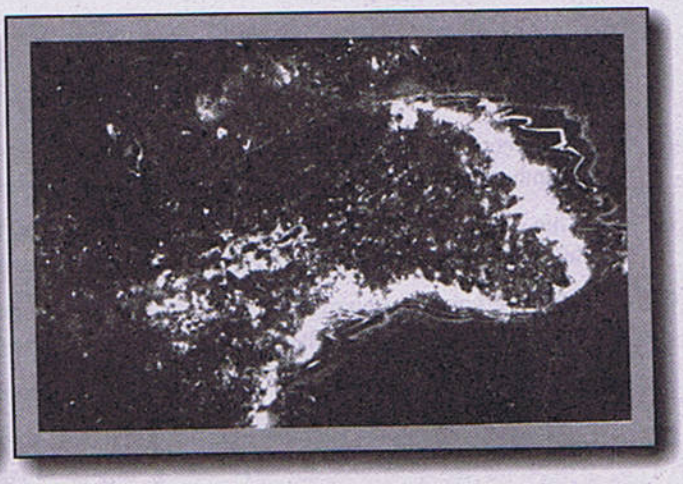

200 µm

C

1000 µm

centimetres long. They are randomly present and most of them are parallel to each other but some are intersecting. The are mainly filled by non ferroan sparry calcite cement. Under cathodoluminescence microscopy they show zoned luminescence.

VEINS

The veins are found in some thin sections of Rakhi Nala, Raghasar, and Zinda Pir areas. The veins are wider and larger than the microfractures. They are generally 0.2 to 10 mm.in width and ranging up to several centimetres in length. Most of the veins are perpendicular to the bedding, intersect the host rock allochems (Plate 7C), and have a sharp boundaries with them. These veins run parallel to each other, some of them are perpendicular and intersect the others. Most of them are filled mainly by non-ferroan sparry calcite cements, whereas some are filled by ferroan sparry calcite cement, which intersect the non-ferroan sparry calcitic veins (Plate 7C). The vein filling calcite crystals are anhedral to subhedral in shape.

CONCLUSIONS

On the basis of present petrographic studies, the Dungan Formation has mainly the skeletal allochems that are (in order of abundance) the benthonic foraminifera, algae, bryozoa, echinoderms, molluscs, corals and planktonic foraminifera. The non-skeletal allochems are ooids and intraclasts. The cement types, in the Dungan Formation, are peloidal, neomorphic, isopachous bladed, drusy, and syntaxial overgrowths.

The Dungan Formation is classified into four types of limestones (Fig. 2). The Calcareous Mudstones in which the grains are 10% on average, the rock is mud supported, the matrix is 78%, and the cement (spar) is 11% of the total rock. Wackestones in which the grains are 38% on average, the rock is mud supported, the matrix is 33%, and the cement (spar) is 29% of the total rock. Packstones in which the grains are 42% on average, the rock is grain supported, the matrix is 18%, and the cement (spar) is 40% of the total rock. Grainstones in which the grains are 67% on average, the rock is grain supported, the matrix is 3%, and the cement (spar) is 30% of the total rock.

EXPLANATION OF PLATES

Plate 1

A. Thin section photomicrograph from sample RG13, showing miliolid foraminifera with micritic wall structure and the chambers are filled by non-ferroan sparry calcite cement.

B. Thin section cl photomicrograph from sample RG 46, the micritic wall of the foraminifera do not show luminescence, whereas the chambers are showing orange luminiscence.

C. Thin section photomicrograph from sample RG4 illustrating biserial *Coskinolina* with micritic wall structure and the chambers are filled by non-ferroan sparry calcite cement.

Plate 2

A. Thin section photomicrograph from sample RG21, showing foraminifera (*Lockhartia*), the walls are thick and have a radial fibrous structure, the fibres being aligned at right angle to the test wall. The chambers are filled by sparry calcite cement.

B. Thin section cl photomicrograph from sample RG 46, the wall and the chambers of the foraminifera showing orange luminescence.

C. Thin section photomicrograph from sample ZP15, showing foraminifera. The wall are thin and the chambers are filled partially by sparite and partially by micrite.

Plate 3

A. a) Thin section photomicrograph from sample Zp15, showing *Ranikothalia* foraminifera. The wall are thick and fibrous, and the chambers are filled partially by sparry calcite and partially by micrite.

b) *Alveolina* foraminifera with micritic wall and the chambers are filled by sparry calcite cement.

B. Thin section photomicrograph from sample ZP 40, illustrating most of the foraminifera chambers are filled by ferroan sparry calcite cement, whereas the walls of most of the foraminifera are unaltered.

C. Thin section photomicrograph from sample ZP40, showing *Nummulites, Assilina, Operculina, Discocyclina* and *Athecocyclina.* The *Nummulites, Assilina* and *Operculina* have a thick fibrous wall structure, and the chambers are filled partially by sparry calcite cement and partially by micrite. *Discocyclina* and *Athecocyclina* have radial chambers, filled by sparry calcite cement.

Plate 4

A. Thin section cl photomicrograph from sample ZP 40, illustrating the dull luminescence of the walls of nummulites, the chamber are non-luminescent.

B. Thin section photomicrograph from sample ZP 39, illustrating the shallow burial environment in which the drusy cement and the walls of the faraminifera became ferroan.

C. Thin section cl photomicrograph from sample ZP 40, the shell structure of *Discocyclina* shows orange luminescence and the sparry cement with in the chamber is non-luminescent.

Plate 5

A. Thin section photomicrograph from sample RG 7, showing algae *Archaeolithothamnium*, the perithallial tissue containing rows of individual Sori.

B. Thin section cl photomicrograph from sample RG 45, the network structure of the calcareous algae showing dull luminescence and the cement filling the structure is non-luminescent.

C. Thin section photomicrograph from sample RG 24, illustrating *Lithothamnium* algae, in the form of rhodolith structure.

Plate 6

A. Thin section photomicrograph from sample RG 10, showing *Lithophyllum* algae, the thick perithallial and hypothallium is coaxial.

B. Thin section photomicrograph from sample Rg 11, illustrating the algea *Jania,* having dichotomously branched thallus.

C. Thin section photomicrograph from sample ZP 55 showing different genera of green algae, such as *Clypecina, Trinocladus* and *Acicularia.*

Plate 7

A. Thin section cl photomicrograph from sample RG 46, the walls of the bryozoa do not show luminescence, whereas the cement filling chambers show dull to orange lumonescence.

B. Thin section photomicrograph from sample RG 5 showing a) echinoderm fragment having syntaxial overgrowth cement, b) molluscs fragments having micritic envelops around them and they are filled by sparry calcite cement.

C. Thin section photomicrograph from sample ZP 14, a) the calcite vein which cuts the structure of foraminifera. The vein is mainly non-ferroan, b) Scleractiniam coral showing septa (central dark line with surrounding trabecular structure) and the partially filling chambers by calcite cement.

Plate 8

A. Thin section photomicrograph (from sample ZP 7A) showing the planktonic and the moulds of planktonic foraminifera, represents the planktonic foraminiferal facies.

B. Thin section cl photomicrograph from sample RK 13 showing the orange luminescence of isopachous bladed cement around the oolites.

C. Thin section photomicrograph from sample RG 29 illustrating the neomorphic spar having irregular boundaries and patches with in the crystals.

Plate 9

A. Thin section photomicrograph from sample ZP 23 illustrating the isopachous bladed cement around the foraminifera. The isopachous bladed cement is non-ferroan whereas the drusy cement is ferroan. The chambers are filled partially by ferroan and partially by non-ferroan calcite cement.

B. Thin section photomicrograph (from sample RG 21) of drusy cement showing irregular boundaries and the crystal size increases towards the centre of the pore space.

C. Thin section photomicrograph from sample RG 8 illustrating the process of dissolution, the ghost structure, the skeletal allochem is totally dissolved, the original structure of the allochem is totally destroyed, creating a mold porosity, which later on filled by sparry calcite cement.

Plate 10

A. Thin section photomicrograph (from sample RG 39) of echinoderm fragment showing the syntaxial overgrowth cement.

B. Thin section cl photomicrograph of the above echinoderm fragment (RG 39). The syntaxial overgrowth cement showing the bright zoned luminescence, indicating different zones of Fe and Mn concentrations.

C. Thin section photomicrograph from sample ZP 20, showing the stylolite solution zone, dark lines are solution interfaces with concentration of insoluble minerals (especially clay minerals). These lines passes around the skeletal grains.

REFERENCES

Ahmad, N. 1996. Palaeoenvironments, diagenesis and geochemical studies of the Dungan Formation (Palaeocene), Eastern Sulaiman Range, Pakistan. Unpublished Ph.D. Thesis, Leicester University, U.K.

Davies, L. M. 1941. The "Dungan" limestone and the Ranikot beds in Baluchistan. *India Geological Survey*, **78**, 316-317.

Dunham, R. J. 1962. Classification of carbonate rocks according to depositional texture. In, W. E. Ham (ed) Classification of Carbonate Rocks. *Mem. Amer. Assoc. Petrol. Geol.*, **1**, 108-121.

Evamy, B. D. and Shearman, D. J. 1965. The development of overgrowths from echinoderm fragments. *Sedimentology*, **5**, 211-233.

Folk, R. L. 1959. Practical petrographic classification of limestones. *Bull. Amer. Assoc. Petrol. Geol.*, **43**, 1-38.

Folk, R. L. 1962, Spectral subdivision of limestone types. In, W. E. Ham (ed) Classification of Carbonate Rocks. *Mem. Amer. Assoc. Petrol. Geol.*, **1**, 68-84.

Hunting Survey Corporation (H. S. C.) 1961. Reconnaissance geology of part of West Pakistan. (Colombo Plan Cooperative Project) Canada Government, Toronto, 1-550.

Iqbal, M. W. A. 1969. The Tertiary pelecypod and gastropod fauna from Drug, Zinda Pir, Vidor (Distt. D. G. Khan), Jhalar and Chharat (Distt. Campbellpur), West Pakistan. *Ibid., Mem. Palaeontologica Pakistanica,* **6**, 1-77.

Johnson, J. H. 1957. Calcareous algae. U.S. Geological Survey, Prof. Pap. 280-E, 209-246.

Johnson, J. H. 1961. Limestone-building algae and algal limestones. Johnson Publishing Company, Boulder, Colo., 1-297.

Johnson, J. H. and Adey, W. H. 1965. Study of Lithophyllum and related algal genera. Quarterly of the Colorado School of Mines, **60**, 1-65.

Khan, and Haque, 1965. Lexique stratigraphique international, 3, Asie, fasc. 8, (a) India, Pakistan, Nepal, and Bhutan. Centre Natl. recherche Start., Paris, 1-404.

Latif, M. A. 1964. Variation in abundance and morphology of Pelagic foraminifera in the Paleocene-Eocene of the Rakhi Nala, West Pakistan. *Punjab University Geological Bulletin,* **4**, 29-109.

Richter, D. K. and Fuchtbauer, H. 1978. Ferroan calcite replacement indicates former magnesian calcite skeletons. *Sedimentology*, **25**, 843-860.

Scoffin, T. P. 1987. An introduction to carbonate sediments and rocks. Chapman and Hall, New York, 1-274.

Tucker, M. E. 1981. Sedimentary Petrology. Blackwell Scientific Publications, London, 1-252.

Wray, J. L. 1977. Calcareous Algae. Elsevier Scientific Publishing Company, Amsterdam, 1-185.

Geol. Bull. Punjab Univ. 36, 2001.

RHYOLITE FROM THE ISLAND ARC SEQUENCE OF THE BELA OPHIOLITE-MELANGE COMPLEX, PAKISTAN.

BY

ZULFIQAR AHMED

Department of Earth Sciences, King Fahd University of Petroleum & Minerals, Dhahran-31261, Saudi Arabia.

AND

AKHTAR ALI SALEEMI

Institute of Geology, University of the Punjab, Lahore - 54590, Pakistan.

Abstract:-*Feldspar-phyric rhyolite occurs as a conspicuous feature of the outcrops near Goth Shafi (GPS= 27° 32.5′ N; 66° 23′ E), north of Wadh town in Balochistan. The rocks occur within a suprasubduction zone island arc complex, that makes an essential component of the Bela ophiolite-melange complex. The major- trace- and rare earth-element contents of the rhyolite, alongwith those of other acidic rocks from the same complex, have been determined. The rhyolite represents the most evolved amongst the igneous rocks of the island arc sequence, and formed by the fractional crystallization of basaltic magma without crustal assimilation. The chondrite-normalized REE patterns of this island arc sequence exhibit progressive enrichment in REE with magmatic evolution, culminating with crystallization of rhyolite.*

INTRODUCTION

The Bela ophiolite-melange complex (abbreviated here as "BOMC") contains ophiolitic rocks generated under three different types of tectonic regimes as depicted by their field features and geochemistry of mafic rocks, and are found as an island-arc related northern terrane and a basinal southern terrane (Ahmed & Ernst, 1999). Acidic igneous rocks form a relatively large volume of the rocks of the BOMC (1999). The granitoids, described earlier by Ahmed (1992, 1993) were identified as plagiogranite. The acidic and intermediate rocks of the BOMC in the island arc related northern sequence display such a large variety and volume which is unsurpassed by any other of the Pakistani ophiolites and is matched by rather few ophiolites of the world (Coleman, 1977). The acidic rocks of the BOMC are restricted to its northern part, which is now regarded as representing an island arc (Ahmed, 1996). These acidic rocks have evolved along two paths: one that led to the formation of trondhjemitic plagiogranite; and the other to the potash-rich granites. The present study finds that the evolution of igneous rocks continued further and probably culminated in the crystallization of a rhyolite and related acidic volcanic rocks. In this context, the present study describes the acidic volcanic rocks from the Goth Shafi area located within the northern part of BOMC, and serves to characterize their chemical composition. These rocks were emplaced probably in the late Cretaceous. This paper provides an insight into the genetic problems of the studied rocks and takes into account their geodynamic significance in the framework of the India- Eurasia collision that occurred in the early Tertiary, about 50 Ma ago, with the closure of the Tethys ocean in this region.

GEOLOGICAL SETTING OF THE RHYOLITE

The BOMC is located along the suture zone that marks the western margin of the Indian lithospheric plate, abutting against the Eurasian plate (Fig. 1). Its outcrops extend for over a 465 km length of the suture zone in a N-S elongation, extending from Goth Allana in the south (GPS: 24° 56′ N, 66 ° 42′ E) at the mouth of Hab river ,west of Karachi, to Sange Siah – Katai section in the north (GPS: 28° 36′ N, 66° 20′ E). The ophiolitic-melange complex is indicated to have formed in a suprasubduction zone environment of a small ocean-basin branch of the Neotethys during late Cretaceous times (Ahmed, 1996).

The geochemistry and field relations of rocks have led Ahmed and Ernst (1999) to recognize two contiguous segments of the BOMC: the northern segment representing an island arc-related tectonic setting and the southern segment being derived from a back-arc basinal setting. Both these segments also contain, the rarer rocks derived from the oceanic island type of tectonic setting. The northern

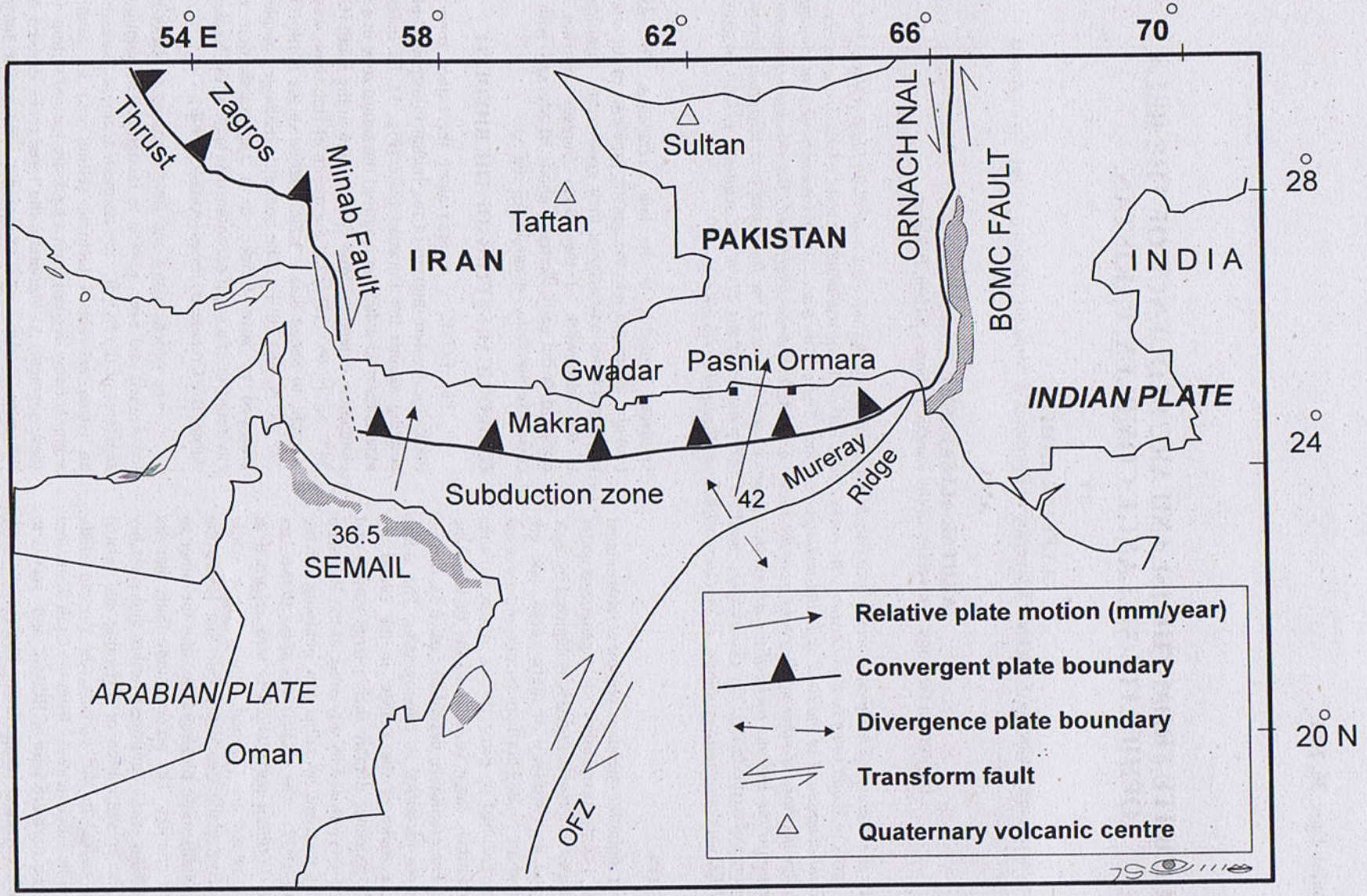

Fig. 1. Location and regional tectonic setting of BOMC and other ophiolites in the region, shown by grayish pattern. OFZ = Owen Fracture Zone.

segment houses a complete sequence of an ophiolite that represents a section through an island arc. The basalts and the other rocks of the arc terrane are characterized by their low-Ti content (Ahmed, 1996).

The lithological varieties developed at the northern, island-arc related ophiolitic sequence of the BOMC include lherzolite, harzburgite, dunite wehrlite, podiform chromitite, clinopyroxenite, layered gabbro, isotropic gabbro, plagiogranite (diorite, quartz diorite, trondhjemite, granite), sheeted dike complex, basaltic to andesitic pillow lavas and flows, red chert, shale, limestone, keratophyre, and grey felsite porphyries and rhyolite described in this paper. The ultramafic rocks are also cut by satellite dikes of dolerite and pyroxenite. An ophiolitic mélange constitutes a large part. The plagiogranite forms major outcrops of upto a few km across; as well as minor, dikes and lensoid bodies. It includes soda-rich trondhjemites as well as potash-bearing and potash-rich granites (Ahmed 1992, 1993). The acidic rocks may be surrounded by rocks of mafic to dioritic composition.

Amongst the ophiolitic complexes of Pakistan, BOMC displays relatively the most voluminous outcrops of plagiogranite, which are entirely restricted to its northern part with that represents the arc-related sequence. Goth Shafi area belongs tectonically to the northern section of BOMC, and contains a variety of lithogies including gabbros, sheeted dike complex, shallow-water basaltic eruptions, variety of acidic rocks, feldspar porphyries, rhyolites and overlying sediments and cherts that host Mn mineralizations. The rocks are dominated by those representing the apical part of an island arc. The area shows typical mélange outcrops, in addition to outcrops with intact ophiolitic sequence. The cherts are well bedded, and associated with blocks of basalt and limestone. Joints and open spaces in chert contain oxides of Mn. Hematite is concentrated in certain brecciated rocks, including the rhyolite described herein.

ANALYTICAL METHODS

The rock samples, as indicated in Table 1, were analyzed for bulk chemistry by X-ray fluorescence (XRF) for their major elements, and by the inductively-coupled plasma (ICP-MS) method for their trace elements and rare earth elements (Table 2). The errors for XRF determinations are lower than 5%.

PETROGRAPHY

The rhyolite samples from near the village of Goth Shafi are mostly feldspar-phyric and some exhibit glomeroporphyritic texture. In many samples, the phenocrysts are euhedral and replaced by calcite, epidote, and albite. Accessory hematite is ubiquitously observed in the rock at this locality, and shows partial alteration to a reddish brown phase, transluscent under the microscope. The mineral assemblage doesn't indicate contamination by crustal sources.

WHOLE-ROCK GEOCHEMISTRY

The sample Z1856 contains acidic SiO_2 content (68.3% by weight; or 69.8 anhydrous wt. %) which is lesser than that of the granites (sample # Z1450, 1440) or trondhjemite (sample # Z1673) of the island arc sequence, as listed in Table 1. But its Mg# is much lower and Zr very high as compared to the granitic rocks. Both parameters show more evolved nature of the rhyolite. The rock belongs to the rhyolite field of the silica versus alkalies diagram of Le Maitre et al. (1989), which establishes the petrographic nomenclature of the rock samples. The composition falls in the rhyolite field close to its boundary line with trachyte. In terms of alkaline versus subalkaline (tholeiitic) divisions, the rock plots in the alkaline field after Kuno (1966) but in the subalkaline or tholeiitic field after Irvine and Baragar (1971). In the classification of Rickwood (1989) using the K_2O versus SiO_2 plot, the rock belongs to the high-K calc-alkaline series. Zr is considered a rather immobile element and is commonly used as an indicator of the degree of fractionation even when the rocks are secondarily altered. The Mg# and Zr content of the rhyolite samples from Goth Shafi (Nos. Z1856 and Z1775), show that it is more evolved rock than the rocks of the island arc sequence as reported herein as well as those reported in an earlier study (Ahmed, 1996).

The rhyolite sample is metaluminous, although it is fairly close to being peralkaline, which would qualify it for the name pantellerite. Its molar $K_2O + Na_2O$ (= 0.114) is close to its molar CaO (= 0.119). The rhyolite is pantellerite, according to the IUGS –recommended nomenclature based on the Al_2O_3 versus total FeO composition (after Macdonald, 1974). Amongst associated acidic rocks, some pink granite (Z1886) and trondhjemite (Z1673) are metaluminous; but other associated granites (Z1865, Z1440, Z1450) are peraluminous. The ratio K_2O/Na_2O is 1.0355 for the rhyolite, but it varies for the granites from 0.4422 to 1.2750. For the trondhjemite, it is 0.0271. The rhyolite is close to being a peralkaline, i.e., its molar ratio $(Na_2O + K_2O)/Al_2O_3$ exceeds 1. The associated granites are also peralkaline; unlike the associated trondhjemite.

Many studies have suggested that the rare earth elements (REE) are amongst the least soluble trace elements and are relatively (though not totally) immobile during weathering, hydrothermal alteration and low-grade metamorphism (e.g., Michard, 1989; Rollinson, 1993). In slightly altered rocks, REE are used to represent the composition and pattern of variation in the original rock.

Table 1

Bulk-rock major- and trace- element analyses of acidic rocks from the arc-related part of the BOMC.

Anal. No. Sp. No. *	1 Z1856	2 Z1886	3 Z1865	4 Z1450	5 Z1440	6 Z1673
SiO_2	68.30	70.40	75.00	77.23	74.62	74.04
TiO_2	0.24	0.50	0.18	0.18	0.32	0.22
Al_2O_3	12.20	14.10	12.90	12.74	12.62	12.91
Fe_2O_3	6.39	2.97	1.76	1.01	3.09	4.64
MnO	0.24	0.02	0.01	0.12	0.14	0.13
MgO	0.06	0.41	0.36	0.28	1.04	0.20
CaO	1.83	0.85	1.89	1.19	0.76	2.16
Na_2O	4.22	4.22	3.71	4.37	4.93	5.90
K_2O	4.37	5.38	2.70	2.41	2.18	0.16
P_2O_5	0.01	0.10	0.03	0.02	0.06	0.03
LOI	2.05	1.10	0.45	0.71	1.06	0.65
Total	99.91	100.05	98.99	100.26	100.80	101.04
mg #	1.826	21.491	28.884	35.502	40.108	7.981
Trace elements in ppm:						
Rb	125	126	62	49	31	1
Sr	47	66	147	125	69	114
Ba	188	425	567	460	1084	19
Zr	1540	893	189	125	140	159
Ta	ND	ND	ND	2.60	0.50	1.09
Hf	ND	ND	ND	3.67	3.74	4.07
Zn	ND	ND	ND	6.0	43.2	6.3
Th	32.70	12.20	12.10	4.83	7.16	ND
U	7.70	1.20	0.20	1.14	2.33	0.05
Y	139	55	14	30	34	42
Nb	277.0	30.0	14.0	13.8	8.6	7.1
Ga	ND	ND	ND	11.8	10.3	15.2
Pb	ND	ND	ND	3.0	2.4	0.9
Cu	ND	ND	ND	10.6	29.1	4.5
Cr	ND	ND	ND	5.8	43.9	54.2
Ni	ND	ND	ND	2.0	8.0	13.9
V	ND	ND	ND	24.0	29.0	26.2

ND = Not determined.
* = Samples are described in Table 2.

Table 2

Whole-rock REE analyses of acidic rocks and island arc rock suite of Goth Shafi area.

Anal. No. / Sp. No.	1 Z1856	2 Z1775	2 Z1886	3 Z1865	4 Z1450	5 Z1440	6 Z1673	7 Z1776	8 Z1777
La	199.0	123.9	77.3	22.7	21.4	19.6	4.3	5	6.7
Ce	386.0	251.5	177.0	39.0	41.7	38.0	12.1	13.4	15.7
Pr	37.20	28.79	19.40	3.70	4.66	4.51	2.00	1.93	2.20
Nd	142.00	98.60	85.40	12.90	19.02	16.00	11.06	9.5	10.2
Sm	29.70	19.57	17.40	3.50	3.97	3.98	3.44	2.92	3.08
Eu	1.62	3.96	1.19	0.64	0.73	1.03	1.32	0.99	1.05
Gd	22.80	17.43	12.80	2.80	3.85	4.37	4.78	3.95	4.12
Tb	3.70	ND	1.80	0.40	ND	ND	ND	ND	ND
Dy	24.00	18.76	11.90	2.70	4.27	5.07	6.31	4.83	5.05
Ho	5.24	3.55	2.21	0.61	0.82	0.98	1.22	0.94	0.98
Er	15.90	10.54	6.80	1.80	2.57	3.09	3.93	2.88	3.03
Tm	2.20	ND	1.10	0.30	ND	ND	ND	ND	ND
Yb	15.60	10.43	6.50	2.30	2.83	3.09	3.89	2.79	2.92
Lu	2.24	1.52	1.04	0.37	0.43	0.47	0.58	0.42	0.43

ND = Not determined.

Z1856 = Acidic volcanic rock from Goth Shafi area, Topographic Sheet 35 I/6.

Z1775 = Grey, feldspar-phyric rhyolite from Goth Shafi area, Topographic Sheet 35 I/6.

Z1886= Pink granite from Rehmat Killi, east of Porali river, Topographic Sheet # 35 I/8.

Z1865 = Plagiogranite, containing diorite xenoliths and surrounded by diorite, from north Belar area, Topographic Sheet # 35 I/8.

Z1450 = Granite from the Purwait Bhut area: GPS: 27 degrees 12.53 minutes N; 66 degrees 20.33 minutes E.

Z1440 = Granite from Laya Garr area; GPS: 27 degrees 16.23 minutes N; 66 degrees 20.55 minutes E.

Z1673 = Trondhjemite from Mamir area, GPS: 27 03.68 N; 66 17.72 E (Topographic Sheet 35 I/8).

Z1776 = Gabbro from Goth Shafi area, Topographic Sheet 35 I/6.

Z1777= Basalt, with pillow structure, from Goth Shafi area, Topographic Sheet 35 I/6.

The REE data (Table 2) normalized to chondritic values after Nakamura (1974) are plotted in Fig.2.

Comparison of the chondrite-normalized REE between the rhyolite and the basalts, andesites and other rocks of the same island arc suite show that the rhyolite is highly enriched in LREE as well as HREE and displays a negative Eu anomaly similar to that shown by the associated K-bearing granites. As Eu is preferentially incorporated as Eu^{2+} in feldspars, the Eu / Eu* values (Ahmed, 1993) of the whole rocks depend upon whether the rocks are feldspar cumulates (Eu / Eu* >1), frozen melts modified by feldspar accumulation processes (Eu / Eu* ≈1) or residual liquids after accumulation of feldspar (Eu / Eu* <1). Thus the Eu / Eu* values of 1 or below 1suggest these rocks might be former liquids, parental or residual ones. These can be used to constrain liquid evolution trends. Rocks with Eu / Eu* >1 are either plagioclase cumulates or possess certain percentage of accumulated feldspar, and these record in principle, how much plagioclase was accumulated during fractionation of a liquid. This indicates that the samples of acidic rocks in Fig. 2, with large Eu anomalies, represent former liquid compositions.

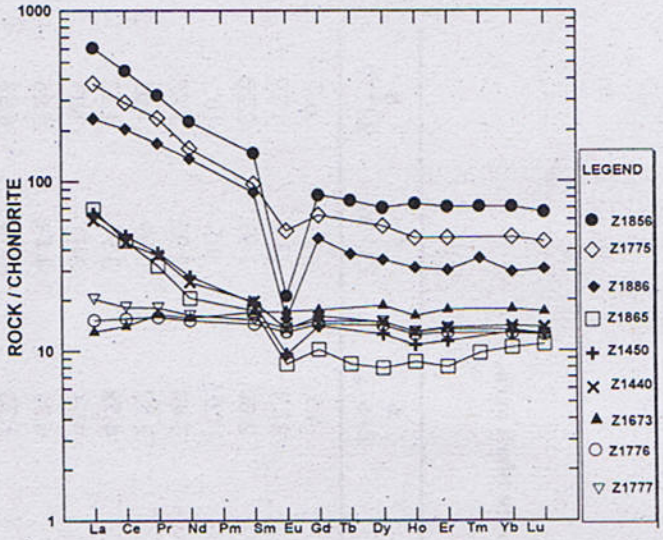

Fig. 2. Chondrite-normalized rare earth element plots for the acidic rocks of the island arc sequence and the lithologies exposed at the Goth Shafi outcrop. Sample numbers are explained in Table 2.

Table 3

^{87}Sr / ^{86}Sr data for the island-arc sequence of BOMC (after Ahmed, 1996).

Sp. No.	Rock type	87Sr / 86Sr	SiO_2 (wt. %).	Mg #	Zr (ppm)
Z1450	Granite	0.7044720	77.23	35.502	125
Z1673	Trondhjemite	0.7045850	74.04	7.981	159
Z1580	Andesite	0.7053100	58.19	33.284	47
Z1572	Gabbro	0.7051365	43.73	76.564	16
Z1445	Gabbronorite	0.7046908	44.01	73.460	11

DISCUSSION

Large-scale rhyolite magmatism is a common feature on the back-arc sides of convergent margins (Takagi et al., 1999), such as the rhyolites of the Taupo Volcanic Zone of New Zealand (Wilson et al., 1995) and west-central Mexico (Mahood, 1981). Such rhyolites may form by the fractional crystallization of basaltic magma (Cameron et al., 1980), partial melting of crustal materials (Graham et al., 1992; Barbieri et al., 2001).) and fractional crystallization of basaltic magmas with crustal fusion (McCulloch et al., 1994). The Goth Shafi rhyolite possess many of the properties of such a back-arc rhyolite.

The ophiolitic plagiogranite originally named by Coleman and Peterman (1975) include a variety of soda-rich and potash-poor acidic and intermediate rocks such as trondhjemite, albite granite, tonalite, quartz diorite, keratophyre, albitite and diorite. These form by fractionation from subalkaline basaltic magma. Plagiogranite has also been demonstrated to form by partial melting of basic rocks under hydrous conditions (Gerlach et al., 1981; Flagler and Spray, 1991).

The chemical variations in the Na-rich trondhjemites are consistent with crystal fractionation model for the plagiogranite adopted by many previous workers (e.g., Coleman and Peterman, 1975;Coleman, 1977). The arc lavas of BOMC have been indicated previously by Ahmed (1996) to have produced andesites. Such arc-andesites can form by fractional crystallization from melts generated

from the hydrous peridotites of the mantle wedge as a result of the dehydration of the underlying slab (e.g., Fyfe and McBirney, 1975).

From the studies like those of the arc lavas of Shirahama Group, Japan, it is indicated that rhyolitic liquids can develop from the calc-alkaline arc magmas (Tamura, 1995). Arc rhyolites can be produced by differentiation from mantle-derived magmas without crustal contamination (Tamura and Nakamura, 1996).

In terms of the Sr-Nd isotopic ratios, Ahmed (1996) reported isotopic heterogeneity between low-Ti andesite of arc-related rocks of BOMC and the high-Ti basalts.

The evolution of arc lavas to rhyolite could have preeded with or without crustal assimilation. Crustal assimilation increases both SiO_2 and $^{87}Sr / ^{86}Sr$ values. The acidic magma generated by crustal melting would enhance the $^{87}Sr / ^{86}Sr$ ratio of the magma because basement crustal rocks generally possess higher $^{87}Sr / ^{86}Sr$ than the mantle derived magmas. For the island-arc sequence, for the five samples $^{87}Sr / ^{86}Sr$ is as given in Table 3. It shows that a linear relationship between Mg# or Zr contents and the $^{87}Sr / ^{86}Sr$ of this rock suite; but there is no such relation between SiO_2 and $^{87}Sr / ^{86}Sr$. Thus the enhanced $^{87}Sr / ^{86}Sr$ do not go parallel with crustal assimilation; but do increase sympathetically with magma evolution.

CONCLUSIONS

The island arc sequence developed at BOMC displays a large petrographic variety and its most evolved igneous rock is a metaluminous rhyolite that makes a large outcrop near Goth Shafi. This rhyolite is the final product of the liquid line of descent of the arc-forming magmas of the BOMC. The rhyolite could have been derived by fractional crystallization of the mantle-derived magmas that also crystallized the andesites. This process of magmatic evolution probably didn't involve crustal assimilation. The REE of the island-arc related igneous rocks show progressively increasing contents with fractionation. It shows extreme enrichment in REE compared to the rest of the rocks from the same arc-related sequence. Its REE pattern shows strong LREE enrichment and a strong negative Eu anomaly.

ACKNOWLEDGEMENTS

Zulfiqar Ahmed thanks the King Abdul Aziz City for Science and Technology (KACST), Riyadh, and the King Fahd University of Petroleum and Minerals, Dhahran, for providing research facilities and support.

REFERENCES

Ahmed, Z., 1992. Bulk-rock and mineral chemistry of anatectic and fractionated acidic rocks coexisting in the Bela ophiolite. *Kashmir Journal of Geology* **10**, 53- 74.

Ahmed, Z.,1993. Leucocratic rocks from the Bela ophiolite, Khuzdar District, Pakistan. In: *"HIMALAYAN TECTONICS"* Treloar, P.J. & Searle, M.P. (Eds.); *Geological Society of London Special Publication* No.74, 89-100.

Ahmed, Z., 1996. Chromite from the Bela arc-basin ophiolite, Pakistan. *International Geology Review*, **38** (7), 607-624.

Ahmed, Z., 1996. Nd- and Sr-isotopic constraints and geochemistry of the Bela ophiolite-melange complex, Pakistan. *International Geology Review*, **38 (4),** 304-319.

Ahmed, Z. & Ernst, W.G.,1999. Island-arc related, back-arc basinal, and oceanic-island components of the Bela ophiolite-melange complex, Pakistan. *International Geology Review*, **41 (8),** 739-763.

Ahmed, Z. & Ernst, W.G. (2000) Island-arc related, back-arc basinal, and oceanic-island components of the Bela ophiolite-melange complex, Pakistan. *In:* TECTONIC STUDIES OF ASIA AND THE PACIFIC RIM, Ernst, W.G. & Coleman, R.G. (Eds.) International Book Series, Geological Society of America, **3**, 178-214.

Barbieri, M., Castorina, F., Masi, U., Garbarino, C., Nicoletti, M., Kassoli-Fournaraki, A., Filippidis,and Mignardi, S., 2001. Geochemical and isotopic evidence for the origin of rhyolites from Petrota (Northern Thrace, Greece) and geodynamic significance. Chemie der Erde **61,** pp. 13-29.

Cameron. M., Bagby, W.C., Cameron, K.L., 1980. Petrogenesis of voluminous mid-Tertiary ignimbrites of the Sierra Madre Occidental, Chihuahua, Mexico. Contrib. Mineral. Petrol. **74**, 271-284.

Coleman, R.G., 1977. OPHIOLITES --- ANCIENT OCEANIC LITHOSPHERE ? Springer - Verlag, Berlin. pp. 130 -134.

Coleman, R.G. & Peterman, Z.E. 1975. Oceanic plagiogranite. *Journal of Geophysical Research* **80** (8), 1099-1108.

Flagler, P.A. & Spray, J.G. 1991.Generation of plagiogranite by amphibolite anatexis in oceanic shear zones. *Geology* **19,** 70 - 3.

Fyfe, W.S. and McBirney, A.R., 1975. Subduction and the structure of andesitic volçanic belts. Amer. Journal of Science **275-A**, 285-297.

Gerlach, D. C., Leeman, W. P. & Ave Lallemant, H. G. 1981. Petrology and geochemistry of plagiogranite in the Canyon Mountain ophiolite, Oregon. *Contributions to Mineralogy and Petrology* **77,** 82-92.

Graham, I.J., Gulson, B.L., Hedenquist, J.W., Mizon, K., 1992. Petrogenesis of late Cenozoic volcanic rocks from the Taupo Volcanic Zone, New Zealand, in the light of new lead isotope data. Geochim. Cosmochim. Acta **56,** 2797-2819.

Irvine, T.N., and Baragar, W.R.A., 1971. A guide to the chemical classification of the common volcanic rocks. Canadian Journal of Earth Sciences, **8,** 523-548.

Kuno, H., 1966. Lateral variation of basalt magma types across continental margins and island arcs. Bull. Volcanol., **29**, 195-222.

Le Maitre, R.W., Bateman, P., Dudek, A., Keller, J., Lameyre Le Bas, M.J., Sabine, P.A., Schmid, R., Sorensen, H., Streckeisen, A., Woolley, A.R. and Zanettin, B., 1989. A Classification of Igneous Rocks and Glossary of Terms. Blackwell Publishers, Oxford.

Macdonald, R. 1974. Bulletin Volcanologique **38,** 498-516.

Mahood, G.A., 1981. A summary of the geology and petrology of the Sierra La Primavera, Jalisco,Mexico. J. Geophys. Res. 86 (B11), 10137-10152.

McCulloch, M.T., Kyser, T.K., Woodhead, J.D., Kindkey, L., 1994. Pb-Sr-Nd-O isotopic constraints on the origin of rhyolites from the Taupo Volcanic Zone of New Zealand: evidence for assimilation followed by fractionation from basalt. Contributions to Mineralogy and Petrology, **115**, 303-312.

Michard, A. 1989. Rare earth element systematics in hydrothermal fluids. Geochim. Cosmochim. Acta, **53**, 275-282.

Nakamura, N. 1974. Determination of REE, Ba, Fe, Mg, Na and K in carbonaceous and ordinary chondrites. *Geochimica et Cosmochimica Acta* **38,** 757-775.

Rickwood, P.C., 1989. Boundary lines within petrologic diagrams which use oxides of major and minor elements. Lithos **22,** 247-263.

Rollinson, H. 1993. Using Geochemical Data: Evaluation, Presentation, Interpretation. Longman Scientific and Technical, Harlow, UK, 352 p.

Takagi, T. Orihashi, Y., Naito, K. and Watanabe, Y., 1999. Petrology of a mantle-derived rhyolite, Hokkaido, Japan. Chemical Geology **160**, 425-445.

Tamura, Y., 1995. Liquid lines of descent of island arc magmas and genesis of rhyolites: evidence from the Shirahama Group, Japan. Journal of Petrology **36 (2),** 417-434.

Tamura, Y., and Nakamura, E., 1996. The arc lavas of the Shirahama Group, Japan: Sr and Nd isotopic data indicate mantle-derived bimodal magmatism. Journal of Petrology **37 (6),** 1307-1319.

Wilson, C.J.N., Houghton, B.F., McWilliams, M.O., Lanphere, M.A., Weaver, S.D., Briggs, R.M., 1995. Volcanic and structural evolution of Taupe Volcanic Zone, New Zealand: a review. Journal of Volcanology and Geothermal Research **68**, 1-28.

Geol. Bull. Punjab Univ. 36, 2001

FLUID INCLUSION STUDY OF THE STRATABOUND TUNGSTEN AND STRATIFORM LEAD-ZINC MINERALISATIONS CHITRAL, NORTHERN PAKISTAN

BY

MOHAMMAD ZAHID
Department of Geology, University of Peshawar, Peshawar 25120, Pakistan

DAVID H. M. ALDERTON
Department of Geology, Royal Holloway, University of London, Egham, Surrey TW20 0EX, UK

AND

CHARLIE J. MOON
Department of Geology, University of Leicester, Leicester LE1 7RH, UK

Abstract:- *Stratabound tungsten and stratiform lead-zinc mineralisations lie within the Hindu Kush terrane, Chitral, northern Pakistan. Scheelite has been found mainly in the calc-silicate quartzite and subordinate tourmalinite associated with metapelite at Miniki Gol. Whereas the stratiform and stratabound lead-zinc mineralisation is mainly confined to the marble horizon at Besti Gol. The conformability of the sulphide mineralisation with the host marble indicates that the lead-zinc mineralisation has been precipitated in synsedimentary environment. In contrast, tungsten at Miniki Gol appears to be genetically related to leucogranite that is exposed 400m away from the scheelite mineralisation.*

Miniki Gol metasediments have undergone at least two deformational events accompanying Barrovian-type of metamorphism followed by the emplacement of leucogranite.

The fluid inclusion study of the Miniki Gol tungsten deposits and Besti Gol lead-zinc deposits indicates the presence of two contrasting hydrothermal fluids. The former is dominantly aqueous whilst the later contains substantial amount of volatiles including CO_2, CH_4 and ± N_2. The consistency of the fluid inclusions both within leucogranite and calc-silicate rocks signify a genetic link between the scheelite mineralisation and the possible post-magmatic hydrothermal fluids. Both the salinity and temperature of the hydrothermal fluids decrease from leucogranite and pegmatite to scheelite-bearing calc-silicate quartzite indicating an influx of possible meteoric water.

The presence of CO_2 in the Miniki Gol pegmatite and the occurrence of calcite in the calc-silicate rocks probably suggest two phases of the same fluid, the earlier CO_2-rich and later aqueous fluids. The volatiles such as CO_2 and B in the ore-forming solutions may have played a role in the transportation of tungsten. Subsequent removal of CO_2 and high pH value in the tungsteniferous fluids have probably facilitated the precipitation of scheelite. On the basis of thermometric data, a temperature of 450 ± 50°C is proposed for the growth of scheelite in the study area.

INTRODUCTION

Stratabound tungsten and stratiform lead-zinc mineralisations of Chitral, Northern Pakistan, lie within the Hindu Kush range, approximately 50 km to the northwest of the Main Karakoram Thrust (Figs. 1, 2). Arkari Formation hosts the tungsten and lead-zinc mineralisations at Miniki Gol and Besti Gol, respectively (Figs. 2, 3). This Formation is dominantly composed of garnet mica schist, phyllite, calc-silicate quartzite and marble. These rocks have undergone at least two phases of deformation and metamorphism that are related to continent-arc collisions during the Cretaceous and Eocene respectively (Fletcher, 1985; Leake et al., 1989). The leucogranite has been emplaced after the peak of Barrovian type of metamorphism.

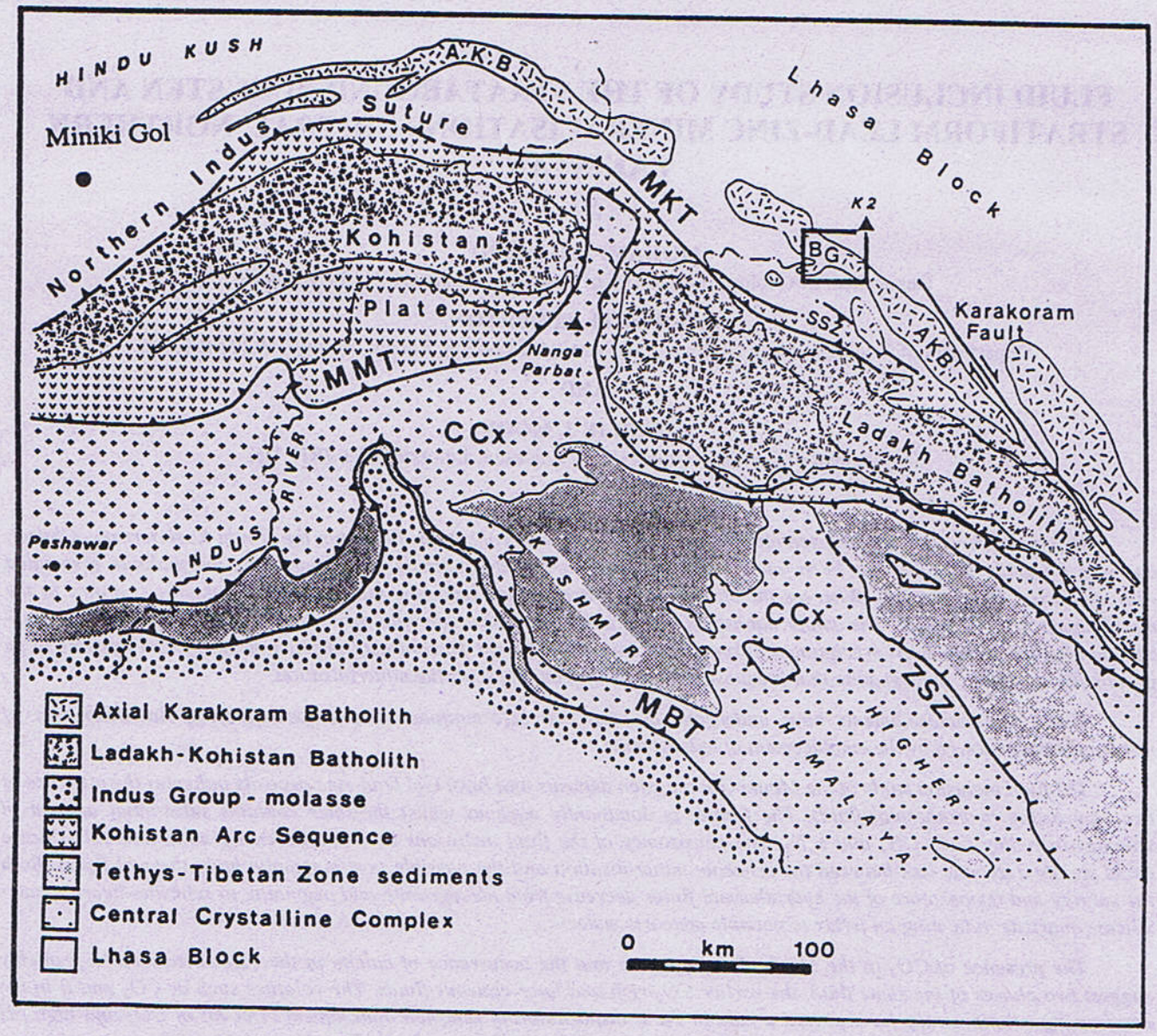

Fig. 1. Geological sketch map of the north-west Himalaya and Karakoram showing Karakoram batholith, Kohistan-Ladakh island arc and tectonic zones of Himalaya (after Parrish and Tirrul 1989). MKT = Main Karakoram thrust; MMT = Main Mantle thrust; MBT = Main Boundary thrust; SSZ = Shyok suture zone; ZSZ = Zanskar shear zone; BG = Baltoro granite

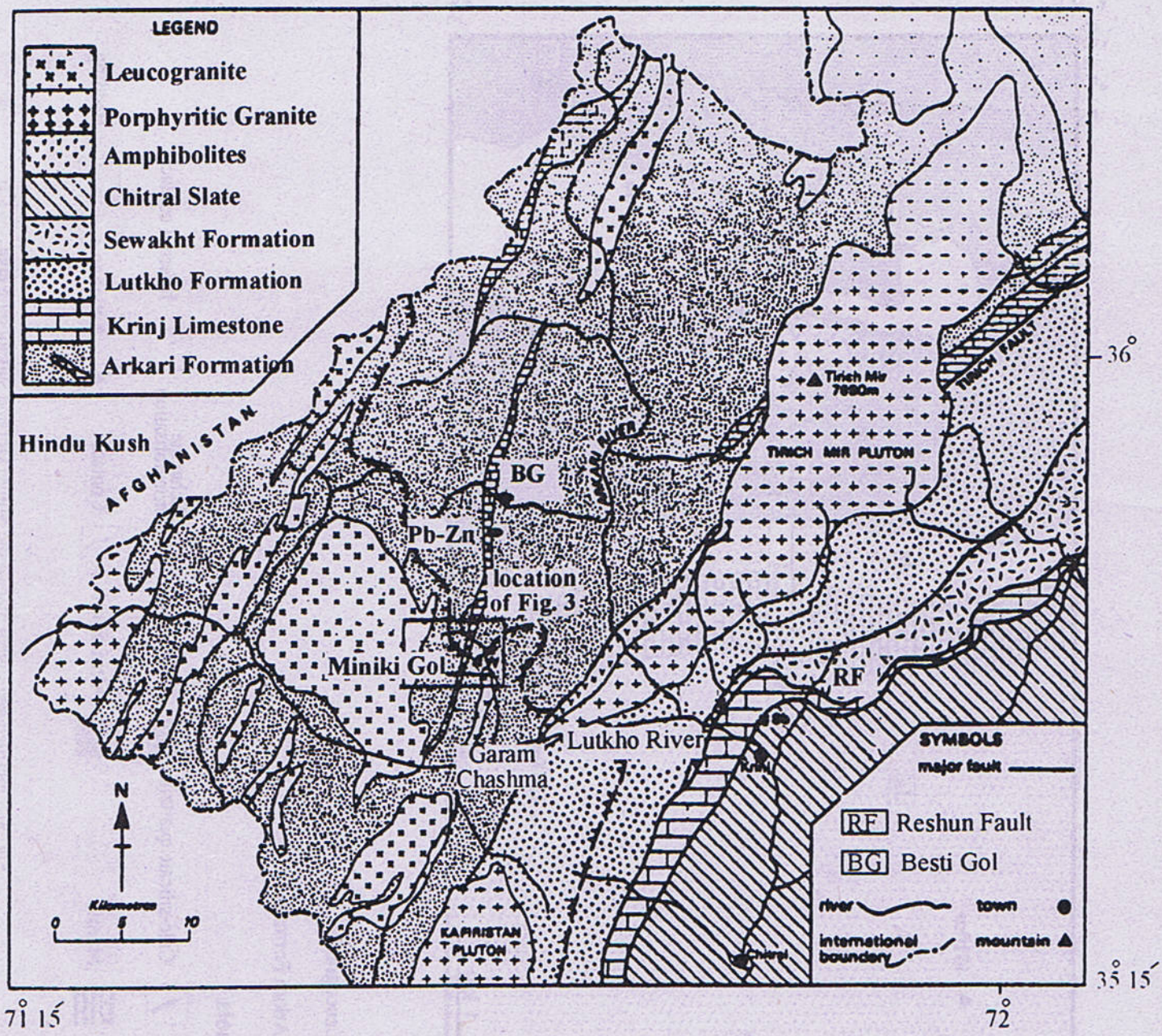

Fig. 2. Geological map of the Garam Chashma area showing Arkari Formation that hosts W and Pb-Zn mineralisations (after Leake et al. 1989).

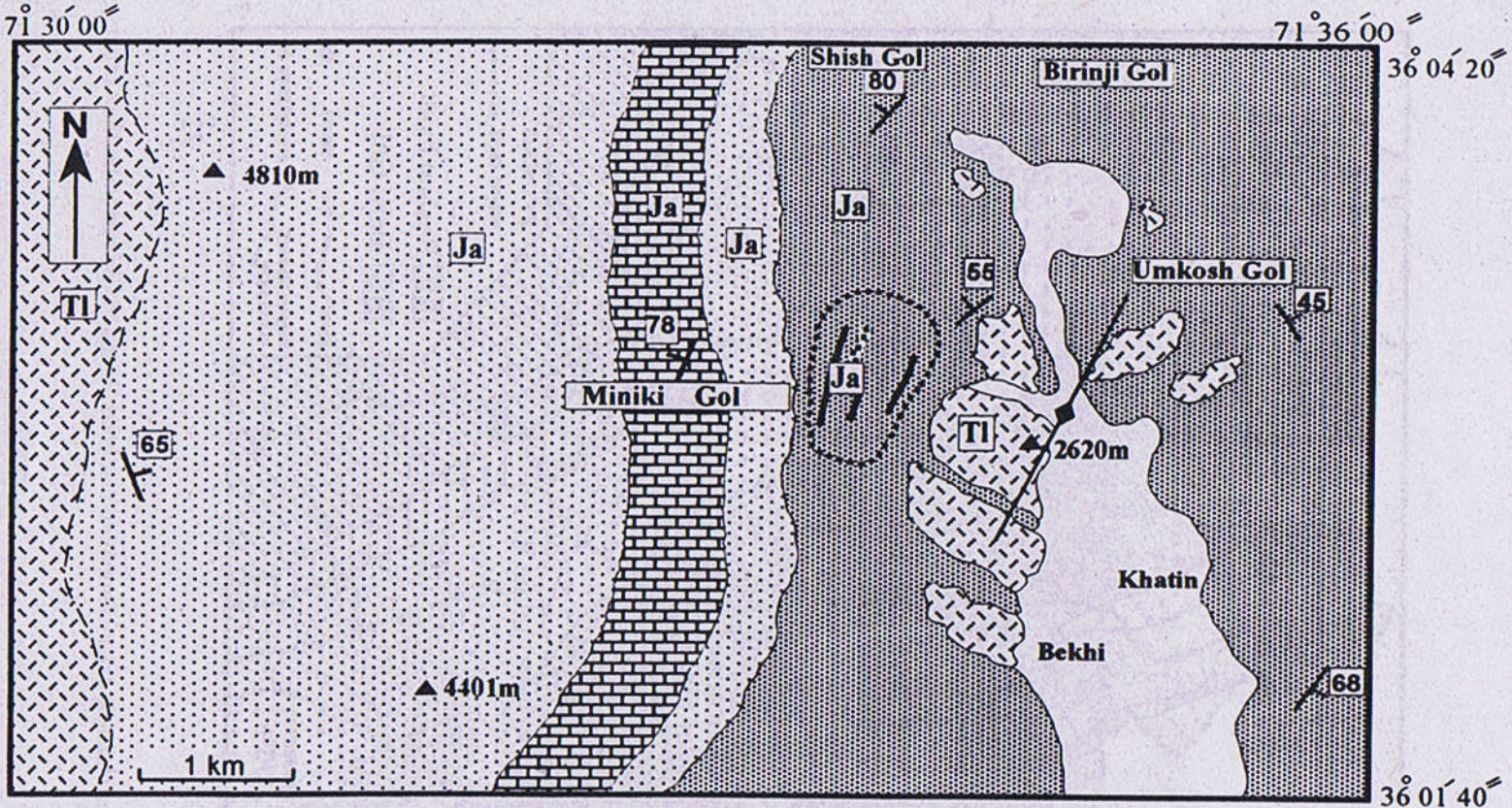

LEGEND

Tl Tertiary Leucogranite

Ja Jurassic Arkari Formation

Key to symbols

Alluvium; Calc-silicate quartzite; Tourmalinite; Scheelite mineralisation; Inferred contact

Phyllite; Marble; Mica schist; Contact; Anticline; Bedding

Fig. 3. Simplified geological map of the Miniki Gol and surrounding area.

Scheelite in the study area is concentrated mainly in calc-silicate quartzite and subordinate tourmalinite. The calc-silicate rock is composed of clinozoisite, quartz, calcic-amphibole, plagioclase, chlorite, biotite, calcite, sphene, garnet and scheelite. This represents a skarn-type mineral assemblage. The percentage of the clinozoisite varies but reaches up to 60 % by volume and is intergrown with scheelite grains. The growth of scheelite seems to be post-granitic in the study area.

In contrast, Pb-Zn mineralisation has been found within marble at Besti Gol area that lies about 8 km further away to the north of Miniki Gol (Fig. 2). Pb-Zn mineralisation includes a substantial amount of sphalerite and hydrozincite together with subordinate galena and pyrite. This mineralisation seems to be synsedimentary and reconcentrated during regional metamorphism.

Fluid inclusion study has been carried out to establish the genesis of these two contrasting style of mineralisations. Miniki Gol scheelite mineralisation has previously been considered as metamorphic in origin (Leake et al., 1989). However, the present investigation characterises the genetic linkage between tungsten mineralisation and the emplacement of Miniki Gol leucogranite. This conclusion is based on the similar style and consistency of the fluid inclusions found both within leucogranite and calc-silicate rocks. Miniki Gol leucogranite is essentially composed of two-feldspar, quartz, muscovite and subordinate biotite, garnet, tourmaline and apatite. Muscovite is more abundant than biotite in these leucogranites. Such a mineralogy is considered as the characteristic feature of the felsic variety of S-type granite or two-mica leucogranite (Barbarin, 1990).

GEOLOGICAL SETTING

Hindu Kush terrane, Karakoram and Himalayas were formed as result of collision between Indo-Pakistan plate and Asian plate. The first contact of the Kohistan arc with the Karakoram terrane along Main Karakoram Thrust occurred between 100 and 80 Ma ago (Coward et al., 1986; Pudsey, 1986), which corresponds to the initiation of the northward subduction and consumption of Tethys ocean. Subduction of Indo-Pakistan plate continued in the direction of north and northeast and the final collision of the Indo-Pakistan plate with the Asian plate along the Main Mantle Thrust took place between 50 and 40 Ma ago (Molnar and Tapponnier, 1975; Petterson and Windley, 1985).

The subduction and subsequent crustal shortening and thickening have produced the Barrovian type of metamorphism followed by the intrusion of granodiorite and leucogranite within these two plates.

The Kohistan terrane which has been proposed as island arc is bounded by major suture in the south, The Main Mantle Thrust and in the north by Main Karakoram Thrust (Shyok suture zone) see (Fig. 1). This complex is composed of Jijal Complex, Kamila amphibolite, Chilas ultramafic, Kohistan batholith (granodiorite-quartz-diorite), Island arc volcanic and metasediments (Tahirkheli, 1982; Coward et al., 1982; Jan, 1979,1980).

Pudsey et al. (1985) divided the geology of western Karakoram and Hindu Kush between the Pak-Afghan border and northern suture into two tectonic units: (1) the northwestern unit between Pak-Afghan border and Reshun Fault and (2) the Central unit between Reshun Fault and relatively CO_2-rich compared with the inclusions found in the muscovite pegmatite.

Pegmatite

Only aqueous fluid inclusions were recognised in the quartz grains OF THE MUSCOVITE pegmatite (ZC 21, Table 1, Fig. 4B). These muscovite pegmatite patches area and has been found mainly in calc-silicate quartzite. Although minor occurrences and showings are extended up to Garam Chashma area, the best grade tungsten mineralisation zone has been found within a 2-3 km belt in the vicinity of Miniki Gol (Leake et al., 1989). Two-mica leucogranite is emplaced at the mouth of Miniki Gol, approximately 400 meters to the south-east of mineralised zone (Figs. 2, 3) but is generally unmineralised. No evidence of association between leucogranite and tungsten mineralisation has been noticed at least on the surface, however, their possible genetic relationship can not be ruled out.

Scheelite occurs as discontinuous patches, stringers and conformable small veins within the calc-silicate quartzite and can be considered as stratabound type.

Stratiform lead-zinc mineralisation is confined to a prominent belt of marble extending from Hot springs (Garam Chashma) to Besti area within the Arkari Formation (Fig. 2). Sphalerite, hydrozincite and galena are the main phases identified and occur as more or less continuous layers along the strike of the enclosing marble. The extension of Pb-Zn mineralisation along its strike length at Besti Gol is unknown. No leucogranite plutons have been found in the near vicinity, however, quartz veins that are generally unmineralised, are associated with the mineralised zone.

SAMPLE PREPARATION AND ANALYTICAL TECHNIQUES

Representative samples from leucogranite, pegmatite, scheelite-bearing calc-silicate quartzite and quartz veins closely associated with Pb-Zn-bearing marble, were selected from both Miniki Gol and Besti Gol areas. In

all a total of 36 doubly polished wafers of about 200 μm in thickness from these rocks were prepared. Out of these only 9 were selected for the fluid inclusion study as the fluid inclusions found in other samples were very small.

The fluid inclusion study was carried out at Royal Holloway and Bedford New College, University of London. For the thermometric studies (i.e. heating and freezing), doubly polished wafers were analysed using a Linkam TH 600 programmable heating-freezing stage attached to a Zeiss transmitted-light microscope. The stage has a wide range of temperature between -180°C and 600°C with the following accuracy;

-180°C to -20°C = ± 0.1°C

-20°C to + 50°C = ± 0.2°C

50°C to 500°C = ± 0.5°C

The stage was calibrated using synthetic fluid inclusions in quartz crystals.

FLUID INCLUSIONS CHARACTERISTICS

Both primary and secondary inclusions were recognised in the study area. These inclusions were found mostly in the granular quartz grains. Microthermometric measurements were carried out mainly on the primary inclusions, although the total homogenisation temperatures were also noted in some of the secondary fluid inclusions. The main characteristics of both types of inclusions are as follow:

Primary inclusions

The studied primary fluid inclusions were subdivided into non-aqueous gas inclusions and aqueous H2O inclusions. The following is the subdivision of these fluid inclusions in different rock types.

Quartz veins

Three phase inclusions (liquid H_2O, liquid CO_2 and vapour $CO_2 \pm CH_4$), have been identified in the quartz veins spatially associated with marble-hosted lead-zinc mineralisation at Besti Gol (ZM 109, Table 1, Fig. 4A). Aqueous fluid inclusions were also found in these quartz veins. The size of these fluid inclusions ranges from 15 to 40 μm in diameter. These fluid inclusions are relatively CO2-rich compared with the inclusions found in the muscovite pegmatite.

Pegmatite

Only aqueous fluid inclusions occur in the quartz grains of the tourmaline pegmatite (ZC 23, Table 1) however, both CO_2-bearing and aqueous fluid inclusions were recognised in the quartz grains of the muscovite pegmatite (ZC 21, Table 1, Fig. 4B). These muscovite pegmatite patches are located within the Miniki Gol leucogranite. Fluid inclusions vary in size, ranging from 5 to 35 μm in diameter.

Leucogranite

Primary aqueous fluid inclusions with liquid H_2O and vapour H_2O are relatively abundant in the Miniki Gol leucogranite (Fig. 5A). No CO_2-bearing fluid inclusions were observed within the Miniki Gol leucogranite. These aqueous fluid inclusions range from 20 to 25 μm in diameter.

Scheelite-bearing calc-silicate quartzite

As in leucogranite, only aqueous fluid inclusions were found in the Miniki Gol scheelite-bearing calc-silicate quartzite (Fig. 5B) and no CO_2-bearing fluid inclusions were observed within the scheelite-bearing calc-silicate quartzite. The fluid inclusions in these rocks range from 15 to 20 μm in diameter and have been found in the granular quartz grains that are intergrown with clinozoisite and scheelite grains.

Secondary inclusions

These fluid inclusions comprise of two-phase and mono-phase fluid inclusions. Two phase aqueous fluid inclusions were noted in the Miniki Gol leucogranite, whereas mono-phase inclusions occur in leucogranite, pegmatite and scheelite-bearing calc-silicate quartzite.

MICROTHERMOMETRY

Fluid inclusion data from the study area are summarised in the Table 1. The data such as (salinity, freezing temperature and the gas contents) of quartz veins from Besti Gol are significantly different from those of Miniki Gol rocks (Table 1).

The final melting of clathrate (TMclath) of the primary CO_2-bearing fluid inclusions in the quartz vein at Besti Gol, is recorded between 1.5 and 9.5°C, corresponding to salinities between 2 to 14 wt % NaCl equivalent (Table 1). These CO_2-bearing fluid inclusions were frozen down to -165°C because at this temperature every phase was solidified. During the reheating, the first melt of solid CO_2 appeared at - 79°C and the final melting ($TMCO_2$) was completed at temperatures, ranging from -56.6°C to -71°C. This temperature is well below the melting temperature of pure solid CO_2 (-56.6°C), indicating the presence of volatile compounds such as CH_4, N_2 or even H2S, in addition to CO_2 (Almeida and Noronha, 1988). The presence of CH_4 was also confirmed as the final clathrate dissociation (TMclath) of the CO_2-bearing fluid inclusions occurred at 16°C (Table 1). However, nothing can be said about the amount of N_2 and H_2S as they have not been

(A) 75 μm

(A) 75 μm

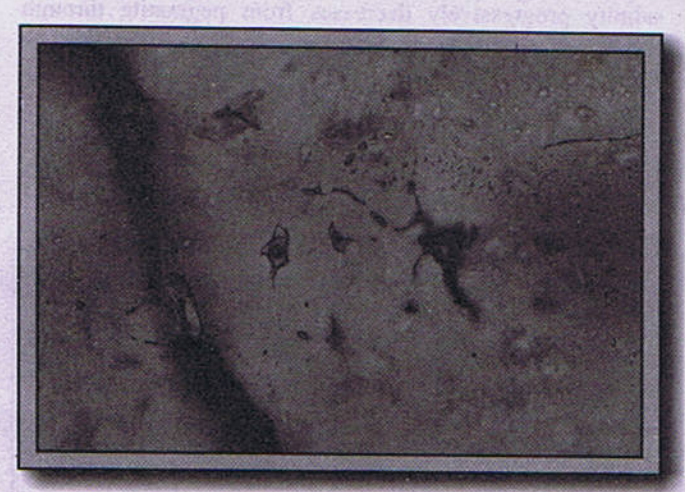

(B) 75 μm

(B) 75 μm

Fig. 4 (A). Primary CO_2-bearing fluid inclusions in the Besti Gol quartz vein with degree of fill (F) = 0.5 (sample ZM 109). **(B)** Primary aqueous fluid inclusions in the quartz of muscovite pegmatite at Miniki Gol (sample ZC 21).

Fig. 5 (A). Primary aqueous fluid inclusions in the quartz of Miniki Gol leucogranite (sample ZC 20). **(B)** Primary fluid inclusions along with mono-phase inclusions in the quartz grains of the scheelite-bearing calc-silicate quartzite at Miniki Gol (sample ZC 67).

analysed and also their behaviour is not fully known. The CO_2 content of these fluid inclusions reaches up to 28.6 wt %. Total densities of the fluid inclusions and CO_2 were calculated as 0.52 and 0.4 g cm-3 respectively. The partial homogenisation temperature ($ThCO_2$) of the CO_2-bearing fluid inclusions in the quartz veins, were recorded between 30.9°C and 31.1°C. The total homogenisation (TH) in the Besti Gol quartz vein, occurred at temperature between 240°C and 415°C (Fig. 6B), with a maximum decrepitation temperature (TD) of 410oC. It should be noted, that the study on the quartz veins at Besti Gol is preliminary as it was carried out only on three CO2-bearing fluid inclusions in one sample.

The salinity of CO_2-bearing fluid inclusions in the muscovite pegmatite at Miniki Gol ranges from 8 to 10 wt % NaCl equivalent (Table 1). However, aqueous fluid inclusions both in the muscovite and tourmaline pegmatite show low salinity, ranging from 0.5 to 10 wt % NaCl equivalent, with the exception of one analysis of 13 wt % NaCl equivalent (Table 1, Fig. 7B). The final melting of solid CO_2 ($TMCO_2$) was recorded at temperature -56.6°C, along with (TMclath below + 10°C), indicating a pure CO_2 gas (ZC 21, Table 1). These fluid inclusions are characterised by a low fluid density (0.3 g cm-3) and relatively high CO_2 density (0.6 g cm-3) with 20.4 wt % CO_2. The partial homogenisation temperature ($ThCO_2$) occurred between 29.3°C and 31.1°C. The non-aqueous fluid inclusions in the pegmatite homogenised at maximum temperature of 495°C with TD of 390°C, whereas in the aqueous fluid inclusions it occurred between 100 and 400°C (Fig. 6A).

The Miniki Gol leucogranite contains both primary and secondary aqueous fluid inclusions. The primary fluid inclusions are characterised by relatively low salinity (between 0 and 8 wt % NaCl equivalent), and with TH, ranging from 100°C up to 440°C (Table 1, Figs. 6C, 7B). The salinity of the secondary fluid inclusions in the studied leucogranite was recorded up to 5 wt % NaCl equivalent and homogenised at temperature between 150-200°C with leakage up to 330°C. Some melt inclusions were also found in the analysed leucogranite.

The aqueous fluid inclusions in the scheelite-bearing calc-silicate quartzite, is represented by very low salinity and the maximum value is noted as 2 wt % NaCl equivalent (Table 1). The homogenisation of two phases in these inclusions, occurred at temperature between 160 and 500°C (Table 1, Fig. 7A). It is also worth mentioning that the salinity progressively decreases from pegmatite through leucogranite to scheelite-bearing calc-silicate quartzite at Miniki Gol (Table 1).

Table 1.
Microthermometric analyses of the primary fluid inclusions (except ZC 20, secondary inclusions) from Miniki and Besti Gol areas

Samples	No	Composition	T_MCO_2 (°C)	T_M (°C)	$T_M$clath (°C)	Salinity Wt. % NaCl equ.	T_H (°C)
ZM 109	7	$CO_2 \pm CH_4$-H_2O-NaCl	– 56.6 to – 71	-------	1.5, 9.5, 16	2 to 14	240 to 415
ZC 21	8	CO_2-H_2O-NaCl	– 56.6	-------	– 2 to 6.1	8 to 10	450 to 495
ZC 21	7	H_2O-NaCl	-------	– 0.5 to – 9	-------	1 to 13	140 to 400
ZC 23	9	H_2O-NaCl	-------	– 0.3 to – 6.5	-------	0.5 to 10	100 to 220
ZS 19	2	H_2O-NaCl	-------	– 3.5 to – 4.5	-------	6.5 to 8	100 to 170
ZS 19	4	H_2O±NaCl	-------	0.0 to – 2.5	-------	0.0 to 5	150 to 330
ZC 20	4	H_2O ± NaCl, H_2O only	-------	0.0 to – 1	-------	0.0 to 2	390 to 440
ZC 65	4	H_2O only	-------	0.0	-------	0.0	210 to 280
ZC 67	3	H_2O only	-------	0.0	-------	0.0	396 to 500
ZC 67A	2	H_2O ± NaCl , H_2O only	-------	0.0 to – 1	-------	0.0 to 2	160 to 400
ZC 70	5	H_2O only	-------	0.0	-------	0.0	205 to 450

ZM 109 (Quartz vein), ZC 21 (Muscovite pegmatite), ZC 23 (Tourmaline pegmatite), ZS 19 and ZC 20 (Leucogranite), ZC 65, ZC 67, ZC 67A and ZC 70 (Calc-silicate quartzite).

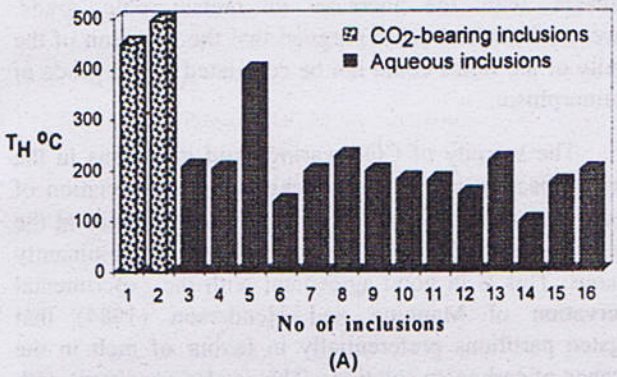

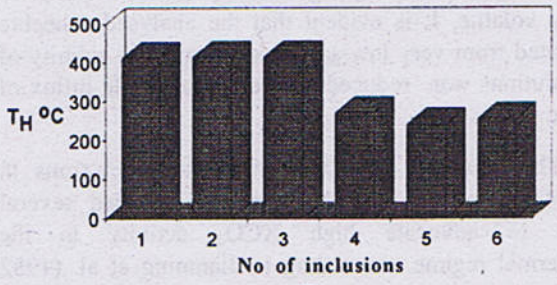

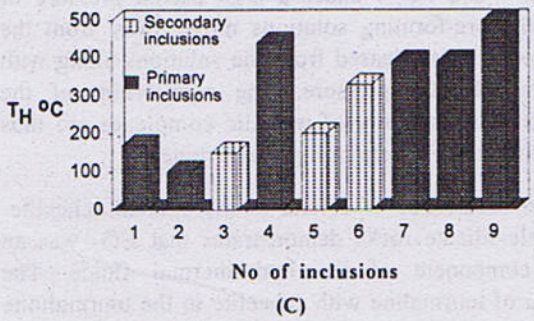

Fig. 6. Charts showing total homogenisation temperature (T_H): **(A)** Primary CO_2-bearing and aqueous fluid inclusions in pegmatite at Miniki Gol. **(B)** Primary CO_2-bearing fluid inclusions in the Besti Gol quartz vein **(C)** Primary and secondary fluid inclusions in the Miniki Gol leucogranite.

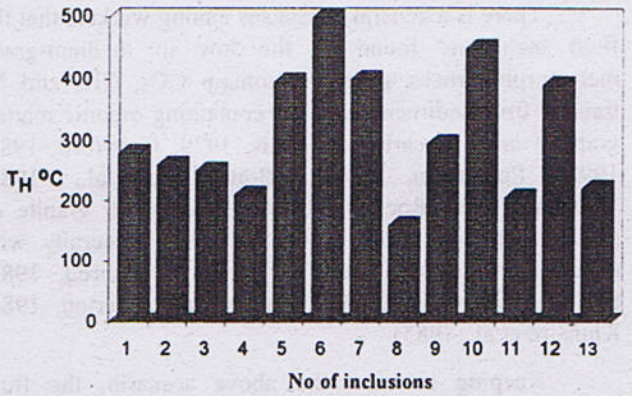

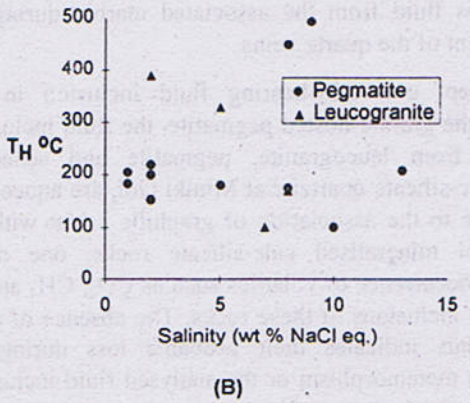

Fig. 7 **(A).** Total homogenisation temperature (T_H) of Miniki Gol Scheelite-bearing calc-silicate quartzite. **(B)** Relationship of salinity with (T_H) of Miniki Gol leucogranite and pegmatite.

DISCUSSION

The study area has experienced at least two phases of deformation accompanying metamorphism up to upper amphibolite facies. The emplacement of the leucogranite appears to be contemporaneous with the peak of metamorphism that was followed by retrogression. Many ingredients may have been added to the trapped fluids or lost during these tectonic events.

There is a general consensus among workers that the fluid inclusions found in the low to medium-grade metamorphic rocks generally contain CO_2, CH_4 and N_2 trapped from sedimentary rocks containing organic matter, graphite or hydrocarbons (Mullis, 1979; Crawford, 1981, 1992; Poutiainen, 1990; Bottrell et al., 1988; Wilkinson,1990; Roedder, 1984). In contrast, granite or shallow intrusive rocks are characterised generally with aqueous or CO_2-rich fluid inclusions (Weisbrod, 1981; Bottrell and Yardley, 1988; Rankin and Alderton, 1985; Kinnaird et al., 1985).

Keeping in view the above scenario, the fluid inclusions in quartz vein associated with marble and graphitic schist at Besti Gol area, contain CH4 and possibly N_2, in addition to CO_2. Theses volatiles are significantly different from those found in the rocks at Miniki Gol. Their occurrence probably indicates the local remobilization of the aqueous fluid from the associated marble during the emplacement of the quartz veins.

Except one CO_2-bearing fluid inclusion in one sample of the granite-hosted pegmatite, the fluid inclusions in quartz from leucogranite, pegmatite and scheelite-bearing calc-silicate quartzite at Miniki Gol, are aqueous in nature. Due to the association of graphitic schist with the Miniki Gol mineralised calc-silicate rocks, one might expect the occurrence of volatiles such as CO_2, CH_4 and N_2 in the fluid inclusions of these rocks. The absence of these volatiles thus indicates their probable loss during the progressive metamorphism or the analysed fluid inclusions represent the later phases of hydrothermal alteration.

The striking feature of the aqueous fluid inclusions from the scheelite-bearing calc-silicate quartzite is their lower salinity compared with that of leucogranite. Moreover, the salinity of the CO_2-bearing fluid inclusions in the Miniki Gol pegmatite is relatively higher than the aqueous fluid inclusions. The general falling temperature trend from CO_2-bearing fluid inclusions to aqueous fluid inclusions within the Miniki Gol pegmatite, is correlated with a decline in salinity (Table 1), indicating the mixing of these fluids with meteoric water. This phenomenon is the characteristic feature of many hydrothermally (including greisen) related tungsten deposits such as Xihuashan tungsten deposits, China (Giuliani et al., 1988) and Cligga Head, SW England (Spooner, 1981). The low salinity could also be related to the lack of albite in the scheelite-bearing calc-silicate rocks. Some authors have related the variation of salinity to the metamorphic grade and according to Poutiainen, (1990) the salinity of aqueous solutions decreases with the increase in metamorphic grade. However, Crawford (1981) argued that the variation of the salinity of the fluids could not be correlated with a grade of metamorphism.

The scarcity of CO_2-bearing fluid inclusions in the scheelite-bearing calc-silicate rocks and the association of clinozoisite with the scheelite suggest that the fluids at the time of growth of these minerals, were predominantly aqueous. This is in good agreement with the experimental observation of Manning and Henderson (1984) that tungsten partitions preferentially in favour of melt in the presence of carbonate solutions. This is also consistent with the laboratory experiments of Keppler and Wyllie (1991) that solubility of W is very high in the presence of water as the only volatile. It is evident that the analysed scheelite precipitated from very low-saline solutions. The salinity of these solutions was reduced due to the probable influx of meteoric water.

The presence of CO_2-bearing fluid inclusions in many of the world's tungsten deposits, has led several workers to advocate high XCO_2 activity in the hydrothermal regime. According to Jianming et al. (1982 and references therein), the complex anion of tungsten (WO4) 2-is only stable together with corresponding cations (Ca^{2}+, Mn^{2}+ and Fe^{2}+) under a high partial pressure of CO_2. As the ore-forming solutions move away from the source area, CO_2 is released from the solutions along with the decline of CO_2 pressure. The equilibrium of the solutions and the stability of metallic complexes are thus lost, resulting in the precipitation of ore minerals.

The occurrence of calcite in the studied scheelite-bearing calc-silicate rocks demonstrates that CO_2 was an essential component of the hydrothermal fluids. The association of tourmaline with scheelite in the tourmalinite also indicates that B was also predominant volatile in the hydrothermal fluids. Volatiles such as CO_2, H_2O and B in the Miniki Gol tungsteniferous fluids with low pH may have driven away tungsten and brought to the site of deposition (calc-silicate rocks) during the last phase of hydrothermal activity. As pointed out by Absar (1991), clinozoisite usually forms from a high pH and CO_2-deficient fluids whilst calcite precipitates from a CO_2-rich fluids. It is obvious that calcite in the studied calc-silicate quartzite fractionated first from the CO_2-rich fluids. The continuous separation and consumption of CO_2 by calcite from the hydrothermal fluids may have increased the pH of the fluids. This has facilitated the deposition of clinozoisite

together with scheelite from the CO_2-deficient fluids It would, however, be a mere speculation to propose two separate fluids, responsible for the deposition of calcite and clinozoisite. It is also very difficult to assess the time gap of these events and also the paragenetic sequence between the precipitation of scheelite in the subordinate tourmalinite and calc-silicate rocks.

Most of fluid inclusions from the world's metamorphosed scheelite deposits, such as Felbertal scheelite deposit (Schenk et al., 1990) and metamorphic scheelite deposit in N. Norway (Larsen, 1991), contain CH_4 and N_2 in addition to CO_2. Keeping in view the above discussion, it can be said that the fluid inclusion data from the Miniki Gol rocks are not compatible with those formed by regional metamorphic fluids. In addition, the consistency of the fluid inclusions both within leucogranite and calc-silicate rocks suggest that scheelite has been precipitated from the post-magmatic tungsteniferous fluids.

The occurrence of secondary fluid inclusions, low-temperature aqueous fluid inclusions (up to 200oC, Table 1) and mono phase inclusions within the leucogranite also indicate low-temperature hydrothermal activity within the leucogranite and pegmatite. The presence of kaolin in the analysed pegmatite is also consistent with low-temperature activity. Such a low-temperature and low-salinity fluids have also been reported in the kaolinized St. Austell granite, SW England. According to Alderton and Rankin (1983) this represents the influx of meteoric water through cooled granite during or after the last phase of hydrothermal activity.

The fluid inclusion study of the scheelite-bearing rocks shows two sets of homogenisation temperatures (400-500°C and 160-390°C). The falling temperature trend of fluid inclusions within the scheelite-bearing rocks could be related to the mixing of meteoric water. It can be inferred from these studies that scheelite partitioned around 450 ± 50°C and continued till the lower-green schist facies.

CONCLUSION

The fluid inclusion study of the Miniki Gol tungsten deposits and Besti Gol lead-zinc deposits shows the presence of two contrasting hydrothermal fluids. The former was dominantly aqueous whilst the later contains substantial amount of CO_2 together with CH_4 and possibly N2. The aqueous fluid inclusions in the leucogranite and scheelite-bearing calc-silicate quartzite are similar in nature, indicating a possible genetic linkage between these two fluids. The present fluid inclusions data suggest that scheelite has been precipitated from the post-magmatic tungsteniferous fluids and Miniki Gol leucogranite can be considered as a source of these fluids. The salinity of the hydrothermal fluids decreases from leucogranite and pegmatite to scheelite-bearing calc-silicate quartzite. The falling temperature and salinity could be related to the mixing of ground water with the hydrothermal fluids.

The presence of CO_2 in the Miniki Gol pegmatite and the occurrence of calcite in the calc-silicate rocks probably demonstrate two phases of the same fluid, the earlier CO_2-rich and later aqueous fluids. The removal of CO_2 and high pH value in the tungsteniferous fluids may have favoured the precipitation of scheelite. On the basis of thermometric data, a temperature of 450 ± 50°C is proposed for the growth of scheelite in the study area.

ACKNOWLEDGEMENTS

The Association of Commonwealth Universities in UK financed this study. Mr. Colin Cunnighan prepared the polished thin sections (double wafers) in the Department of geology, University of Leicester.

REFERENCES

Absar, A., 1991. Hydrothermal epidote- an indicator of temperature and fluid composition. *J. Geol. Soc., India* **38,** 625-628.

Alderton, D. H. M. and Rankin, A. H., 1983. The character and evolution of hydrothermal fluids associated with the kaolinized St. Austell granite, SW England. *J. Geol. Soc. London,* **140,** 297-309.

Almeida, A. and Noronha, F., 1988. Fluids associated with W and Ag-Au deposits of the Mirandale area, NE Portugal: an example of peri-granitic zoning. *Bull. de Min.,* **111,** 331-341.

Barbarin, B., 1990. Granitoids: main petrogenetic classifications in relation to origin and tectonic setting. *Geol. J.,* **25,** 227-238.

Bottrell, S. H. and Yardley, B. W. D., 1988. The composition of a primary granite-derived ore fluid from S.W. England, determined by fluid inclusion analysis. *Geoch. Cosm. Acta,* **52,** 585-588.

Bottrell, S. H. Carr, L. P. and Dubessy, J., 1988. A nitrogen-rich metamorphic fluid and coexisting minerals in slates from North Wales. *Min. Mag.,* **52,** 451-457.

Coward, M. P. Jan, M. Q. Rex, D. Tarney, J. Thirlwall, M. and Windley, B. F., 1982 Geotectonic framework of the Himalaya N. Pakistan. *J. Geol. Soc. London,* **139,** 299-308.

Coward, M. P. Windley, B. F. Broughton, R. D. Luff, I. W. Petterson, M. G. Pudsey, C. J. Rex, D. C. and Asif Khan, M., 1986. In: Collision tectonics in the NW Himalayas (Ed. M. P. Coward and A. C. Ries), Collision tectonics. *Geol. Soc. Spec. Publication,* **19,** 203-219.

Crawford, M. L., 1981. Fluid inclusions in metamorphic rocks- low and medium grade. In: Short course in fluid inclusion (Ed. L. S. Hollister and M. L. Crawford), *Applications to petrology Miner. Ass. Canada,* **6,** 157-181.

Crawford, M. L., 1992. Fluid inclusions-what can we learn? *Earth Sci. Rev.,* **32,** 137-139.

Desio, A., Zanettin, B. (1970) Geology of the Baltoro basin. Italian expeditions to the Karakoram (K2) and Hindu Kush (leader A. Desio), Scien. Rep. Sec. 11 Brill Leiden 2: 308.

Einaudi, M. T., Meinert, L. D., Newberry, R. J. (1981) Skarn deposits. *Econ. Geol. 75th Anniv.* Vol. 317-391.

Fletcher, C. J. N., 1985. Gold, antimony and tungsten mineralisation in the Chitral District, Northwest Frontier Province, Pakistan. Report for Sarhad Development Authority, Peshawar.

Giuliani, G. Li, Y. D. and Sheng, T. F., 1988. Fluid inclusion study of Xihuashan tungsten deposit in the southern Jiangxi province, *China. Mineral. Deposita,* **23,** 24-33.

Jan, M. Q., 1979. Petrography of pyroxene granulites from northern Swat and Kohistan. *Geol. Bull. Univ. Peshawar Spec. Issue,* **11,** 65-87.

Jan, M. Q., 1980. Petrology of the obducted mafic-ultramafic metamorphites from the southern part of the Kohistan island arc sequence. *Geol. Bull. Univ. Peshawar Spec. Issue,* **13,** 95-108.

Jianming, C. Ruolan, L. and Guangsheng, Z., 1982. Study on fluid inclusion and its relation to mineralisation of Pangushan tungsten deposit, Jiangxi Province, China. In: Tungsten Geology Jiangxi, China (Ed. J. V. Hepworth and Y. H. Zhang), (ESCAP RMRDC) Bandung, Indonesia, 233-243.

Keppler, H. and Wyllie, P. J., 1991. Partitioning of Cu, Sn, Mo, W, U and Th between melt and aqueous fluid in the systems haplogranite-H2O-HCl and haplogranite-H2O-HF. *Cont. Min. Pet.,* **109,** 139-150.

Kinnaird, J. A. Batchelor, R. A. Whitley, J. E. and Mackenzie, A. B., 1985. Geochemistry, mineralisation and hydrothermal alteration of the Nigerian high heat producing granites. In: High heat production (HHP) granites, hydrothermal circulation and ore genesis. Inst. Mini. Met., 169-195.

Larsen, R. B., 1991. Tungsten skarn mineralizations in a regional metamorphic terrain in northern Norway: a possible metamorphic ore deposit. *Mineral. Deposita,* **26,** 281-289.

Leake, R. C. Fletcher, C. J. N. Haslam, H. W. Khan, B. and Shakirullah, 1989. Origin and tectonic setting of stratabound tungsten mineralisation within the Hindu Kush of Pakistan. *J. Geol. Soc. London,* **146,** 1003-1016.

Manning, D. A. C. and Henderson, P., 1984. The behaviour of tungsten in granitic melt vapour system. *Cont. Min. Pet.,* **86,** 286-293.

Molnar, P. and Tapponnier, P., 1975. Cenozoic tectonics of Asia: effects of a continental collision. Science, **189,** 419-426.

Mullis, J., 1979. The system methane-water as a geologic thermometer and barometer from the external part of the Central *Alps. Bull. Miner.,* **102,** 526-536.

Newton, R. C. (1989) Metamorphic fluids in the deep crust. Ann. Rev. Earth Planet. Sci. 17: 385-412.

Parrish, R. R. and Tirrul, R., 1989. U-Pb age of the Baltoro granite, northwest Himalaya, and implications for zircon inheritance and monazite U-Pb systematics. Geology, **17,** 1076-1079.

Petterson, M. G. and Windley, B. F., 1985. Rb-Sr dating of the Kohistan arc-batholith in the Trans-Himalaya of N. Pakistan, and tectonic implications. *Earth. Planet. Sci. Lett.,* **74,** 45-57.

Powell, C. M. (1979) A speculative tectonic history of Pakistan and surroundings: some constraints from Indian ocean. In: Farah, A. and Dejong, K. A. (eds), Geodynamics of Pakistan, *Geol. Surv. Pakistan, Quetta* 5-24.

Pudsey, C. J., 1986. The Northern Suture, Pakistan: margin of a Cretaceous island arc. *Geol. Mag.*, **123,** 405-423.

Pudsey, C. J. Coward, M. P. Luff, I. W. Shackleton, R. M. Windley, B. F. and Jan, M. Q., 1985. Collision zone between the Kohistan arc and the Asian plate in NW Pakistan. Trans. Roy. Soc. Edinburgh, **76,** 463-479.

Poutiainen, M., 1990. Evolution of a metamorphic fluid during progressive metamorphism in the Joroinen-Sulkava area, southeastern Finland, as indicated by fluid inclusions. *Min. Mag.*, **54,** 207-218.

Rankin, A. H. and Alderton, D. H. M., 1985. Fluids in granites from southwest England. In: High heat production (HHP) granites, hydrothermal circulation and ore genesis. Inst. Mini. Met., 287-299.

Rex, A. J., Searle, M. P., Tirrul, A., Crawford, M. B., Prior, D. J., Rex, D. C., Barnicoat, A. (1988) The geochemical and tectonic evolution of the central Karakoram, N. Pakistan. Phil. Trans. Roy. Soc. London Ser. A 326: 229-255.

Roedder, E., 1984. Fluid inclusions. Rev. Min. 12. Miner. Soc. America.

Schenk, P. Höll, R. München, Ivanova, G. F. Naumov, V. B. and Kopneva, L. A., 1990. Fluid inclusion studies of the Felbertal scheelite deposit. *Geol. Rundschau,* **79,** 451-466.

Searle, M. P., Cooper, D. J. W., Rex, A. J. (1988) Collision tectonics of the Ladakh-Zanskar Himalaya. Phil. Trans. Roy. Soc. London Ser. A 326: 117-150.

Spooner, E. T. C., 1981. Fluid inclusion studies of hydrothermal ore deposits. In: Short course in fluid inclusion (Ed. L. S. Hollister and M. L. Crawford), Applications to petrology, Miner. Ass. Canada, **6,** 209-240.

Tahirkheli, R. A. K., 1982. Geology of the Himalaya, Karakoram and Hindu Kush in Pakistan. *Geol. Bull. Univ. Peshawar,* **15,** 1-51.

Thompson, A. B., Connolly, J. A. D. (1992) Migration of metamorphic fluids: some aspects of mass and heat transfer. Earth Sci. Rev. 32: 107-121.

Weisbrod, A., 1981. Fluid inclusions in shallow intrusives. In: Short course in fluid inclusion (Ed. L. S. Hollister and M. L. Crawford), Applications to petrology, Miner. Ass. Canada, **6,** 241-271.

Wilkinson, J. J., 1990. The role of metamorphic fluids in the development of the Cornubian ore field: fluid inclusion evidence from south Cornwall. *Min. Mag.*, **54,** 219-230.

Zahid, M. (1996) Genesis of stratabound scheelite and stratiform Pb-Zn mineralisation Chitral, Northern Pakistan, and its comparison with S-W England tin-tungsten deposits. Unpubl. Ph.D. thesis Univ. Leicester.

Geol. Bull. Punjab Univ. 36, 2001.

THE STUDY OF THE EVOLUTION OF HAZARA KASHMIR SYNTAXIS IN NORTHERN PAKISTAN AND ITS EFFECTS ON THE CIVIL ENGINEERING STRUCTURES BASED ON GRAVITY AND MAGNETIC DATA

BY

MUHAMMAD RUSTAM KHAN

Institute of Geology, Azad Jammu & Kashmir University, Muzaffarabad, Pakistan

AND

UMAR FAROOQ

Institute of Geology, University of the Punjab, Lahore - 54590, Pakistan

Abstract:-*Gravity and magnetic study in the Hazara and its adjoining areas of Northern Pakistan indicated sedimentary and metasedimentary wedge in the form of Hazara-Kashmir Syntaxis (HKS) which exists on the Precambrian crystalline crust of Indian shield. This study also indicates the presence of decollement under the western limb and absence under the eastern limb of HKS. The gravity modelling shows the crystalline crust of 38 Km which extends all the way in the Lesser and Sub-Himalaya of Northern Pakistan and occurs as faulted blocks between Hazara Lower Seismic Zone (HLSZ) and Bagh Basement Fault (BBF). There is no indication of the pre-existing horst or projection on the leading edge of the Indian plate. The presence of decollement under the western side of Jhelum fault and absence under the eastern side and the collision of Indian and Eurasian plates are responsible for the formation of HKS. The southward migration of sedimentary and metasedimentary wedge of the western limb of HKS developed the Jhelum fault. At present the western limb moves southward between Jhelum and Kalabagh faults. The seismicity in the area along this fault is low due to the presence of decollement but the area is tectonically very active. The western limb of HKS moves southward at a rate of 2cm per year and 41Km net slip was calculated along the Jhelum Fault. The folding, faulting and landsliding along the Jhelum fault, Kalabagh fault and the Salt Range Thrust Front (SRTF) have been observed. As a result of southward movement of western limb of HKS the cracks develop in the RCC structures constructed across the river Jhelum which is running along the Jhelum fault. The roads constructed along the river Jhelum are also damaged due to the active nature of the Jhelum fault.*

INTRODUCTION

The area under study is highly folded and faulted and the complexity of structures is developed in response to stresses caused by the collision of Indian and Eurasian platelets (Powel, 1975) about 45-52Ma ago and by subsequent continuous movement of India towards north. The prominent geological feature of the area is Hazara-Kashmir Syntaxis (HKS). Since the western limb of HKS is structurally more complicated than its eastern counterpart, geological models of Wadia (1931) and Calkins et al. (1975) have explained the tectonic evolution of HKS. All these efforts are based mainly on geological data and need to be constrained by geophysical data. Thus the project was formulated to have a gravity and magnetic study in the area bounded by latitude 33° to 35°N and longitude 72° to 74°E (Fig.1). As the thrust system of the area has brought in contact the terrain of different densities and susceptibilities, it was considered that an advocate coverage of the area by gravity and magnetic study would explain the nature of the evolution of the HKS and its effects on the civil engineering structures.

DENSITY/SUSCEPTIBILITY ZONING OF THE AREA

The thrust system of the study area structurally juxtaposes lateral lithological changes and correspondingly generates five zones of density and susceptibility contrasts (Fig.2). From each zone, representative rock units were sampled, and density and susceptibility measurements were made. In the southern part of the area the post collisional Murree and Siwaliks molasse of Tertiary age are separated from the pre-collisional marine sediments of Eocene to Cretaceous age by the Main Boundary Thrust (MBT). Post

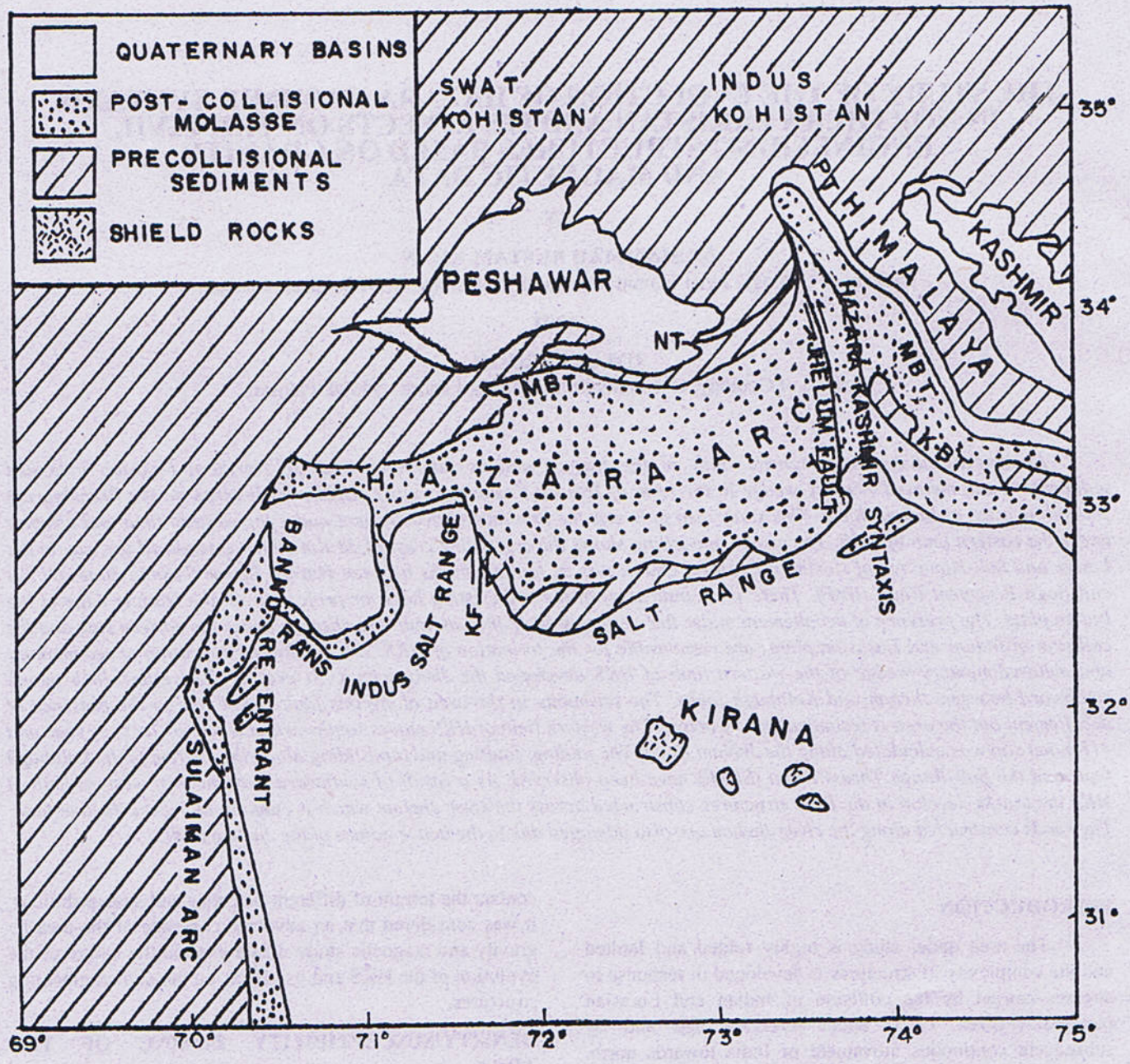

Fig. 1 Tectonic Map of Northern Pakistan. PT – Panjal Thrust, MBT Main Boundary Thrust, KF = Kalabagh Fault after Seeber et al. (1981), Chaudhary & Ghazanfar (1992) and Khan & Ali (1994).

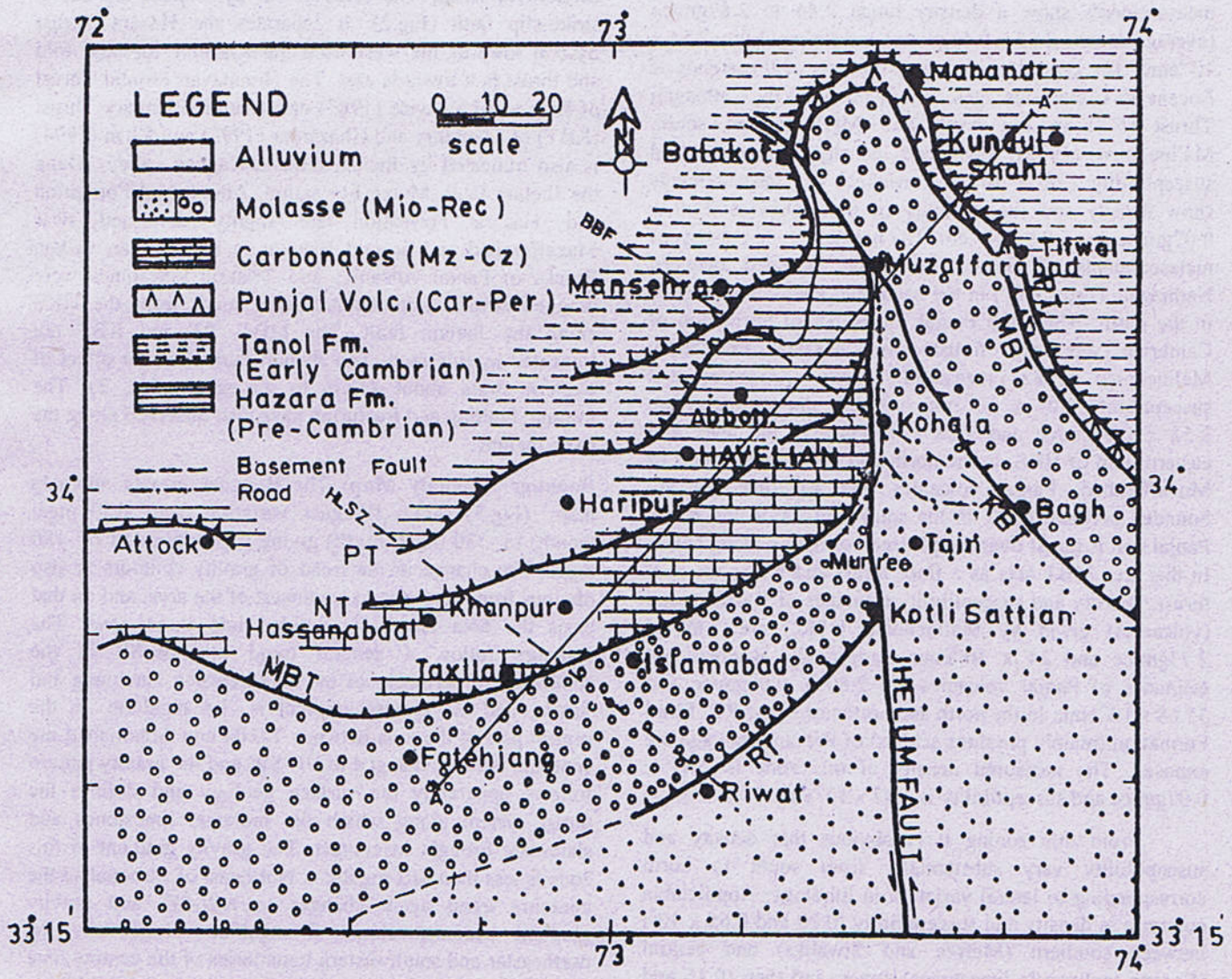

Fig. 2 Generalized tectonic map of Hazara-Kashmir Syntaxis in northern Pakistan. MT – Manshern Thrust, PT = Panjal Thrust, MBT = Main Boundary Thrust, KBT = Kashmir Boundary Thrust, RT = Riwat Thrust, KT = Kahuta Thrust, HLSZ = Hazara Lower Scismic Zone and BBF = Bagh Bascment Fault; (Wadia, 1928; Latif, 1970, 1973; Calkins, et al. 1975; Kazmi and Rana, 1982. Baig and Lawrence, 1987; Greco, 1989; Chaudhry and Ghazanfar, 1993 and Khan and Ali, 1994. Section A-A′,C-C′ and D-D′ are selected for gravity modelling (Khan, 1994).

collisional sediments mainly are the sandstone and shale. The density and susceptibility of these sediments already measured by Malinconico (1982) is 2.64gm/cc and 2.09 x 10^{-5}emu, respectively. Duroy (1986) estimated density 2.3 to 2.5gm/cc on the basis of seismic velocity. Our measurements show a density range 2.44 to 2.67gm/cc (average density 2.55 ± 0.11gm/cc) and susceptibility 2.54 x 10^{-5}emu. The central zone mainly consists of limestones of Eocene to Cretaceous ages, and is bounded by Nathiagali Thrust (NT) in the north and MBT in the south. Malinconico (1982) mentioned density 2.69gm/cc and susceptibility 1.66 x 10^{-5}emu, whereas our measurements show density and susceptibility of limestones as 2.66 ± 0.07gm/cc and 1.89 x 10^{-5}em. The northern zone consists of metasediments of Hazara Formation bounded between Nathiagali Thrust (NT) in the south and Panjal Thrust (PT) in the north. Along the Panjal Thrust Tanol Formation of Cambrian age are thrust over Hazara Formation. Malinconico (1982) measured density 2.53gm/cc and susceptibility 3.07 x 10^{-5}emu, whereas our estimates are 2.52 ± 0.04gm/cc and 3.28 x 10^{5}emu. In the apex and eastern limb of HKS, in the north and north eastern part of Muzaffarabad, Panjal volcanics and Agglomerates are bounded between MBT in the south and PT in the north. Panjal unit is thrust over the Murree Formation along MBT. In this area MBT acts as a floor thrust and PT as the roof thrust. Density and susceptibility estimates of Kalam group (volcanics) given by Malinconico (1982) are 2.69 to 2.73gm/cc and 24 x 10^{-5}emu respectively, whereas our estimates of Panjal volcanics are 2.80 ± 0.05gm/cc and 35.68 x 10^{-5}emu. In the north and northeast of the PT, Tanol Formation (mainly phyllites schists) of Precambrian age are exposed. The measured density of this zone is 2.54 ± 0.07gm/cc and susceptibility is 4.47 x 10^{-5}emu.

From this zoning it is obvious that density and susceptibility vary substantially from south to north corresponding to lateral variation in lithology. Appreciable contrasts in density and susceptibility (0.09 and 0.65 x 10^{5}) between southern (Murree and Siwaliks) and central (Eocene to Jurassic limestones) zones, and then (0.15 and 1.39 x 10^{-5}) central to northern (Precambrian slates) zones, suggest the probability of generation of diagnostic gravity and magnetic signals over different lithologies brought in contact by the thrust system of the area. Near the apex and eastern limb of HKS, Panjal zone shows the highest density and susceptibility as compared to other zones due to the presence of dominant Panjal volcanics. The Tanol zone or Salkhala zone which spreads in the NNE and NW of the Panjal zone, is dominated by slates equivalent to the Hazara slates. The density and susceptibility of this zone is slightly greater than the density and susceptibility of northern zone (Hazara slates) due to the intrusion of granites. For gravity modelling the estimated density of the above rock units, decollement (2.25gm/cc), crystalline crust (2.96gm/cc) and Moho (3.29gm/cc) have been used by Khan (1994).

INTERPRETATION OF MAPS

Structural Map: The HKS is cut by Jhelum left-lateral strike-slip fault (Fig.2). It separates the Hazara Thrust System towards the west from the Kashmir foreland fold and thrust belt towards east. The Himalayan Frontal Thrust of Baig and Lawrence (1987) or Kashmir Boundary Thrust (KBT) of Chaudhry and Ghazanfar (1992) and Khan (1994) is also truncated by Jhelum fault in Kaghan valley. Along the Jhelum fault, Muree Formation, Abbottabad Formation and Hazara Formation are highly deformed near Muzaffarabad and around Balakot in the Kaghan valley. Blocks of Panjal volcanics and Triassic limestones were dragged several kilometres further south from the HKS along the Jhelum fault. The MBT, PT and KBT are truncated by this fault. The Jhelum fault show an offset of western strata about 41Km to the south (Fig. 2). The folding, faulting and fracturing have also observed along the river Jhelum.

Bouguer Anomaly Map: The Bouguer gravity anomaly map (Fig.3) shows Bouguer variation from -150 mgal (south) to -330 mgal (north) giving a gravity relief of -180 mgal. The change in the trend of gravity contours is aiso obvious from northeast to southwest of the area, and on that basis the area clearly is divided into three zone. The contours follow a general trend of NW-SE in the southwestern periphery of the area between Fatehjang and Taxila, and the gravity gradient is -1.6 mgal/km. In the central part of the area between Taxila and Abbottabad the contours trend is changed to NE-SW and the gravity pattern follows apparently the surface geology and defines the thrust system along which the molasse, limestones and slates are brought in contact. The gravity gradient in this zone is less than -0.2 mgal/km. Northeast of Abbottabad the contours trend again changes to NW-SE, and gravity gradient becomes about -2 mgal/km. Noticeably, the northeaster and southwestern boundaries of the central zone with closely spaced contours (high gradient) observed from Mansehra to Bagh and over Taxila are the indicators of basement effects such as the Hazara Lower Seismic Zone of Seeber and Armbruster (1979). The contours trend in the central zone follows appreciably the trend of the Hazara thrust system. In this Bouguer anomaly map (Fig.3) the gravity model selected across the profile A-A′. The Bouguer gravity anomaly map does not show the horst or projection on the Indian crystalline basement un-der the sedimentary wedge of HKS.

Magnetic Anomaly Map: The total magnetic intensity map shown in (Fig.4), describes magnetic variations with respect to the Turnol magnetic base value 49250 gammas at Turnol.

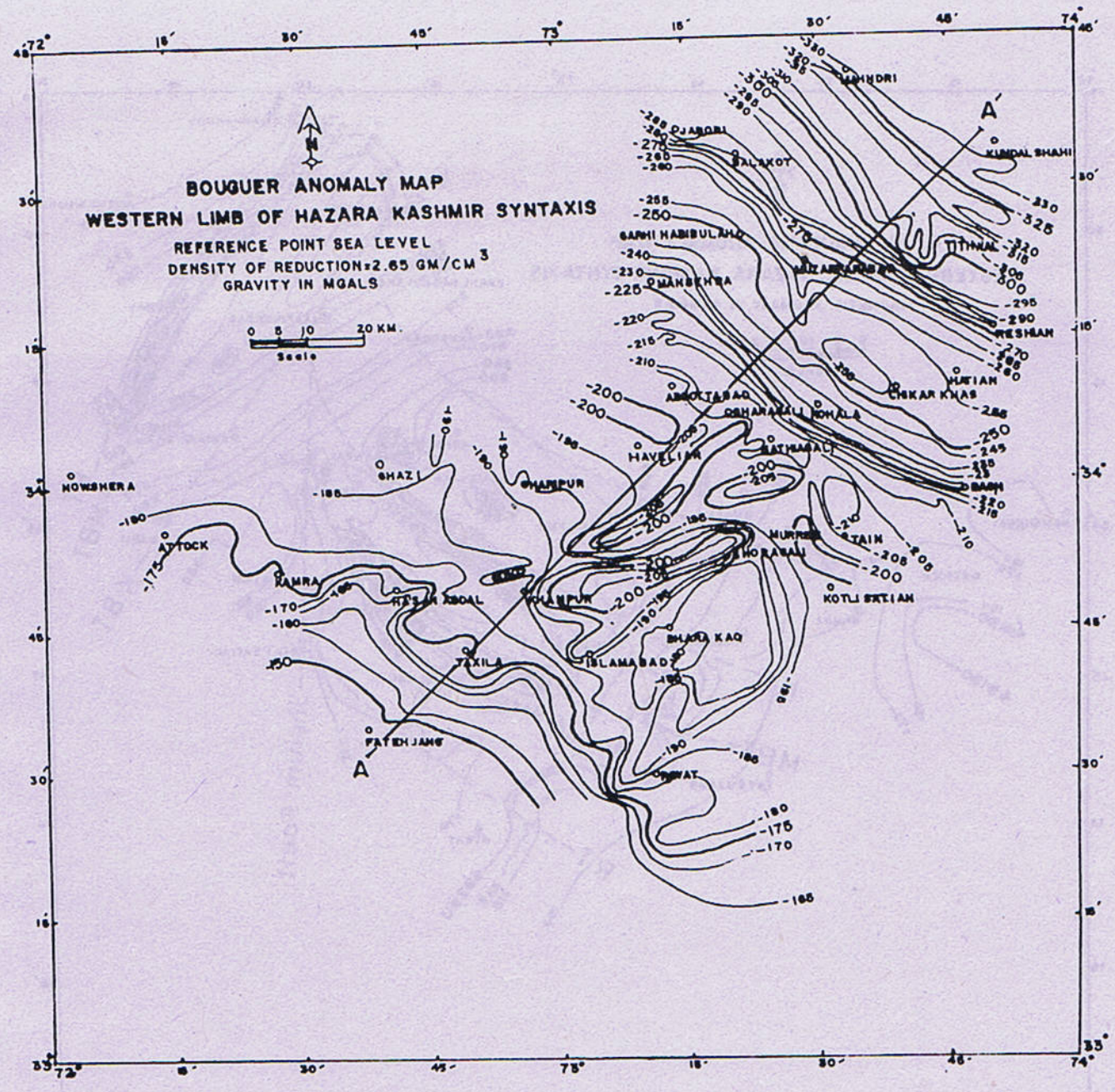

Fig. 3 Boguer gravity anomaly map.

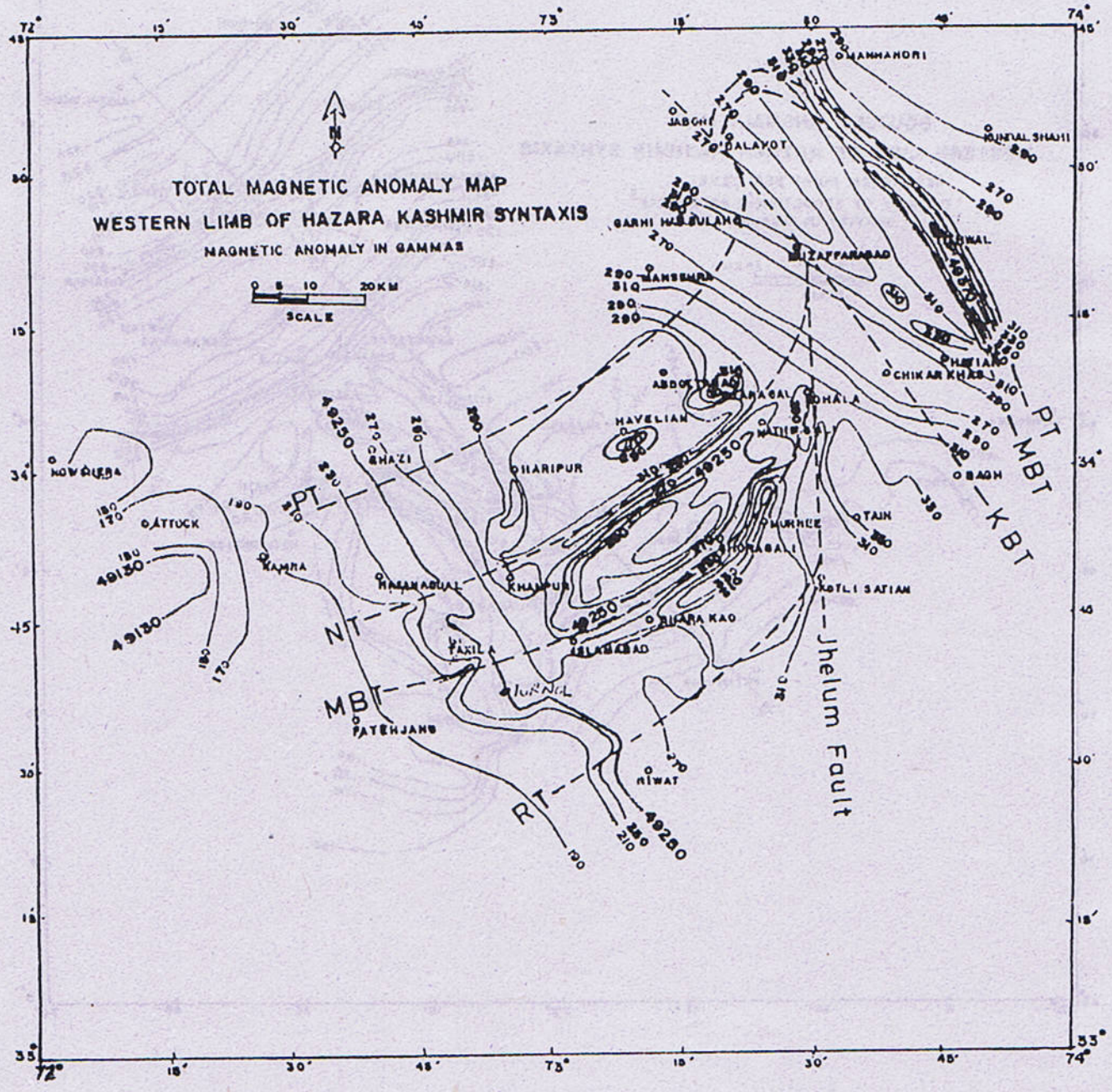

Fig. 4 Magnetic anomaly map.

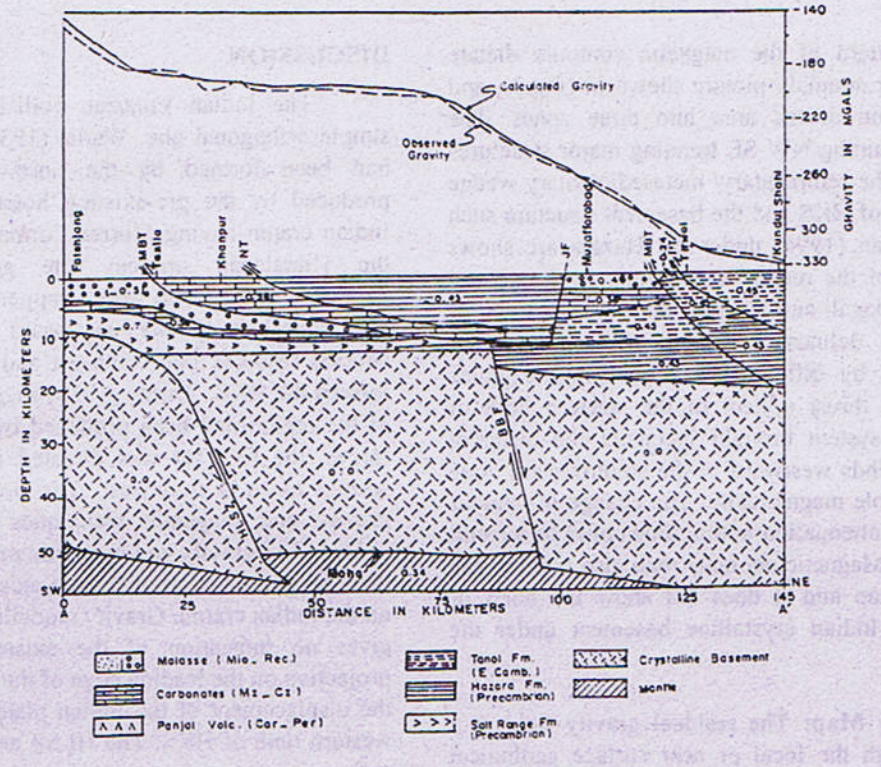

Fig. 5 Gravity model shows the combined sediments and Moho effects along the profile A-A′ (Khan, 1994)

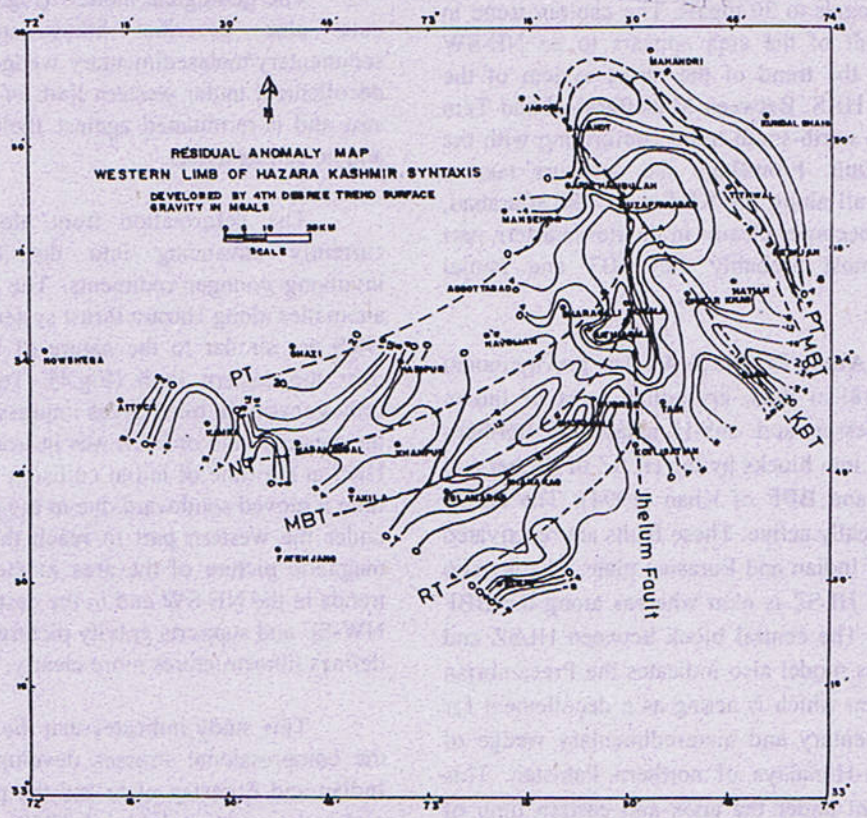

Fig. 6 Residual gravity anomaly map, PT = Panjal Thrust, NT = Nathiagali Thrust, MBT = Main Boundary Thrust, KBT = Kashmir Boundary Thrust, RT = Riwat Thrust.

The trend and pattern of the magnetic contours dictate almost the Bouguer anomaly picture shown in (Fig.3), and confirm the division of the area into three zones. The northern zone containing NW-SE trending major structures (MBT and PT) in the sedimentary/ metasedimentary wedge of the eastern limb of HKS and the basement structure such as the BBF of Khan (1994) under the Hazara arc shows conforming trend of the magnetic contours. In the central zone between Nathiagali and Khanpur the NE-SW trend of magnetic contours delineate possibly the susceptibility contrasts produced by different formations and explains clearly the Hazara thrust system of the western limb of HKS. This thrust system brought incontact the different rock units and extends westward in the southwestern zone where it is not visible magnetically. The change in contour trend and magnetic attenuation in this zone could be a result of thick salt layer. Magnetic anomaly map also confirm the gravity anomaly map and it does not show the horst or projection on the Indian crystalline basement under the HKS.

Residual Anomaly Map: The residual gravity field at a point is related with the local or near surface geological structures having different densities. The residual gravity map of the area is presented in Fig. 5 and shows gravity variation from –0 mgals to 20 mgals. The contour trend in the southwestern half of the area appears to be NE-SW following generally the trend of the thrust system of the western timb of the HKS. Between Muzaffarabad and Tain the contours show a north-south trend conforming with the trend of Jhelum fault. FromBagh the contours take a northwesterly trend all along the KBT upto Muzaffarabad, and the same trend becomes clearer in the northeastern part corresponding to most probably the MBT and Panjal Thrust.

Gravity Modelling Along Profile A-A′: The gravity model (Fig.6) shows the 38Km thick crystalline crust of Indian shield under the lesser and sub-Himalaya of northern Pakistan and faulted into blocks by the HLSZ of Seeber and Armbruster (1979) and BBF of Khan (1994). The HLSZ and BBF are tectonically active. These faults are reactivated after the collision of Indian and Eurasian plate. The net slip calculated along the HLSZ is 6km whereas along the BBF the net slip is 4km. The central block between HLSZ and BBF is uplifted. This model also indicates the Precambrian Salt Range Formation which is acting as a decollement for the overlying sedimentary and metasedimentary wedge of the Lesser and Sub-Himalaya of northern Pakistan. This decollement is absent under the apex and eastern limb of HKS. Similarly in the profile C-C′ and D-D′ indicate the decollement under the western limb of HKS.

DISCUSSION

The Indian Eurasian collision geometry is not a simple orthogonal one. Wadia (1931) suggested that HKS had been formed by the northwest ward indentation produced by the pre-existing horst or projection on the Indian craton having Murree Formation on its top. During the Himalayan orogeny the geosynclinal sediments deposited in the north were wrapped around this projection and consequently the southward directed compressive stresses resolved into southeast and southwest components formed the HKS. Duroy (1986) suggested that the structure of the region had been produced by two successive set of forces, the first set was directed towards south and the second towards southwest. The present studies based on gravity and magnetic techniques disagree with Wadia (1931). The gravity and magnetic maps (Fig.3-4) show that there is no indication of the pre-existing horst or projection on the Indian craton. Gravity modelling of Khan (1994) also gives no indication of the existence of any horst or projection on the leading edge of the Indian plate, but shows the displacement of the Indian plate into blocks under the western limb of HKS. The HLSZ and BBF are tectonically active.

The geological models (Fig.6) derived from gravity data also describe lithostructural nature of the sedimentary/metasedimentary wedge and decollement. The decollement under western limb of HKS thins out towards east and is terminated against Jhelum fault, involving salt and no salt tectonics.

The deformation front along the Hazara arc is currently advancing into the foredeep progressively involving younger sediments. The nature of the magnetic anomalies along Hazara thrust system in the western limb of HKS are similar to the nature of the magnetic anomalies over the eastern limb (Fig.4). This similarity alongwith orthogonality in trend gives impression as if the material of the western limb of HKS was in front of the eastern limb of HKS at the time of initial collision and with the passage of time it moved southward due to the presence of decollement under the western part to reach the current position. The magnetic picture of the area in the western limb of HKS trends in the NE-SW and in the eastern limb it trends in the NW-SE and supports gravity picture (Fig. 5) in general, and defines lithostructures more clearly.

This study indicates that the HKS originated due to the compressional stresses developed by the collision of Indian and Eurasian plate and the presence of decollement under the western limb of HKS. At the later stage the Jhelum fault cut the western limb of HKS and marked the salt and no salt area. The Jhelum fault is the youngest

sinistral fault of the area trending north-south along the River Jhelum. The folding, faulting, fracturing and landslidings are observed along this fault between Muzaffarabad and Tain, which show that Jhelum fault is still tectonically active. The slickensides have been observed in the rock units along this fault and have also indicated the southward movement of the western limb of HKS. The 31Km offset of the western limb of HKS was calculated by Chaudhry and Ghazanfar (1993) along the Jhelum fault. The 41Km net slip of the western limb of HKS was calculated along the Jhelum strike-slip fault, which indicate that the rate of movement is 2cm/year and fault developed nearly 2 million year ago. This tectonically active Jhelum strike-slip fault is very destructive for the RCC structures which are being constructed along and across the River Jehlum. In the long term cracks will develop in the RCC bridges which are constructed across the River Jhelum near Kohala and Muzaffarabad City. The roads are being constructed along the River Jhelum like Kohala to Muzaffarabad, Kohala to Bagh and Kohala to Murree are badly damaged by the landsliding. These landslides near the fault plan are developed by the active Jhelum strike-slip fault whereas the areas 2 to 4Km away from the fault plan are comparatively stable and favourable for the RCC structures. Similarly the folding and faulting observed near SRTF and Kalabagh faults indicated that these faults were active. The RCC structures constructed across these faults are also not fisible, so the detail geophysical investigations are required in the Salt Range and Kalabagh areas as well.

CONCLUSION

There is no any indication of the pre-existing horst or projection on the leading edge of the Indian plate. The rocks of the western limb of HKS were infront of the eastern limb of HKS at the time of initial collision and with the passage of time it moves southward.

The HKS originated due to the compressional stresses developed by the collision of Indian and Eurasian plate and the presence of decollement under the western limb of HKS and absent under the eastern limb.

The folding, faulting, fracturing, landsliding and slickensides along the Jhelum fault plane indicate that the Jhelum fault is tectonically active. The Jhelum fault is the youngest strike-slip fault of the area which developed nearly 2 Ma ago. The western limb of HKS moves southward at a rate of 2cm/year.

The RCC structures constructed across and along the River Jhelum are not feasible. Due to the southward movement of the western limb of HKS cracks are expected in the future in the RCC structures. The roads constructed along River Jhelum are badly damaged by the landsliding due to active nature of the Jhelum fault.

The RCC structure are also not fissile across the SRTF in the south of the study area and Kalabagh strike slip fault in the southwest of the study area. The detail geophysical investigations are required in the Salt Range and Kalabagh area for the constructions of the RCC structures.

ACKNOWLEDGMET

We are thankful to Prof. Dr. M. Ashraf and Prof. Dr. Mirza Shahid Baig for critically reviewing this paper.

REFERENCES

Baig, M.S., and Lawrence, R.D., 1987. Precambrian to early palaeozoic orogensis in the Himalaya, *Kashmir J. Geol.*, **5**, 1-22.

Calkins, J.A., Offield, T.W., Abdullah, S.K.M., and Ali, S.T., 1975. Geology of the southern Himalaya in Hazara, Pakistan and adjacent area. *U.S. Geol. Sun.* No. 716-c, 1-29.

Chaudhry, M.N. and Ghazanfar, M., 1993. Some Tectono stratigraphic observations on NW Himalaya, Pakistan. *Pakistan Jour. Geol.* No. 1, 2, 1-14.

Duroy, 1986. Subsurface densities and lethospheric flexure of the Himalaya foreland in Pakistan interpreted from gravity data. M.S., thesis, Oregon State University, Corvallies, OR., 745.

Greco, A., 1986. Geological investigation in the western Himalayan Syntaxis area (Azad Kashmir NE, Pakistan). Dissertation ETH. Zurich, Nr. 8779 Zurich, 1935.

Kazmi, A.H., and Rana, R.A., 1982. Tectonic map of northern Pakistan. *Geol. Surv. Pakistan,* Quetta.

Khan M.R., and Ali, M., 1994. Preliminary modeling of the western Himalaya. *Kashmir, J. Geol,* 11-12, 59-66.

Khan, M.R., 1994. Tectonic modeling of Hazara and its adjoining areas, unpublished Ph.D. Thesis Quaid-i-Azad University Islamabad, Pakistan. 1-81

Latif, M.A., 1970. Explanatory notes on the geology of south-eastern Hazara to accompany the revised geological map, J. Geol. B.A. Sonderbon, 15, 5-20.

Latif, M.A., 1973. Partial extension of the evaporite facies of the Salt Range to Hazara Pakistan. Nature, 244, 124-125.

Malinconico, L.L. Jr., 1982. Structure of the Himalayan structure zone of Pakistan interpreted gravity and magnetic data unpublished Ph.D. Thesis Dartmouth College, 1-128.

Seeber, L. and Armburster, J., 1979. Seismicity of the Hazara are in northern Pakistan VS basement faulting. In Geodynamics of Pakistan. Farah, A., and Dc Tong, K.A.. eds., *Geol., Surv. Pakistan,* 131-142.

Wadia, D.N., 1928. Geology of Poonch State (Kashmir) and adjacent portion of the Punjab. *Geol. Sur. India, Mem.* **51,** 185-370.

Wadia, D.N., 1931. The syntaxis of the northwest Himalaya its roads, tectonics and Oregon, Rec. *Geol., Surv, India,* **65,** 189-220.

Powell, Mc. A. and Conaghan, P.J. 1975. Tectonic models of the Tibetan Plateau. *Geol.,* **7,** 727-734.

Geol. Bull. Punjab Univ. 36, 2001.

JURASSIC CARBONATE SHELF DEPOSITION, ABBOTTABAD DISTRICT, NORTHERN PAKISTAN

BY

RIAZ AHMED SHEIKH
Institute of Geology, University of the Punjab, Lahore, Pakistan

M. KALEEM AKHTER QURESHI
Geological Survey of Pakistan, 83/D, Model Town, Lahore, Pakistan

SHAHID GHAZI
Institute of Geology, University of the Punjab, Lahore, Pakistan

AND

KHAN RASS MASOOD
Botany Department, University of the Punjab, Lahore, Pakistan

Abstract:-*The depositional style and the diagenetic events in the Jurassic carbonate shelf deposits of the Samana Suk Formation, exposed at Sikhar Ridge (Sangargali) and the Thai Barrier Sections, near Abbottabad (along the Abbottabad-Nathiagali Road) has been studied. As far as twenty-nine microfacies have been identified in both the sections, but few selective have been illustrated. The sediments in the Samana Suk Formation have been subjected to various diagenetic events, of which dolomitization is the most significant. At least two phases of dolomitization have been determined. The zonation in the dolomite crystals represents the nature of the pore water chemistry. Dedolomitization has led to the development of porous horizons.*

INTRODUCTION

The Samana Suk Formation is a widespread carbonate shelf deposit that covered large areas of the Upper Indus Basin including Hazara, Kala Chitta, Kohat, western Salt Range and the Trans Indus Range.

Masood (1989) established seven microfacies in the Samana Suk Formation on the basis of random sampling from different localities of Hazara, without mentioning the number of samples and localities. Qureshi et al (1997) also identified eleven microfacies on the basis of reconnaissance work in Hazara.

The facies model described in this paper emphasizes the relationship between depositional environments, diagenetic events and the rock properties and is based on detailed work relating to microfacies and diagenesis of this formation from Sangargali and Thai Barrier areas, District Abbottabad (Fig.1). Detailed depositional synthesis logs are also being presented, which have been drawn after systematic measurement and sampling (Figs. 2, 3). Critical relationship between marl-mudstone/ wackestone, grainstone and synsedimentary lithification is also discussed.

The Jurassic sequence (the Datta Formation, the Samana Suk Formation and lower part of the Chichali Formation) in the Sangargali overlies the Cambrian Abbottabad Formation while at the Thai Barrier it overlies the Precambrian Hazara Formation. The generalized stratigraphic sequence at these localities is given in Table .1.

SEDIMENTOLOGICAL STUDIES

The depositional model presented in this paper is based on the microfacies variations encountered at different levels in the Samana Suk Formation. Detailed sedimentological studies have been carried out and the following microfacies have been identified. These microfacies are the lithologic suites that represent sediments and precipitates deposited in similar environments.

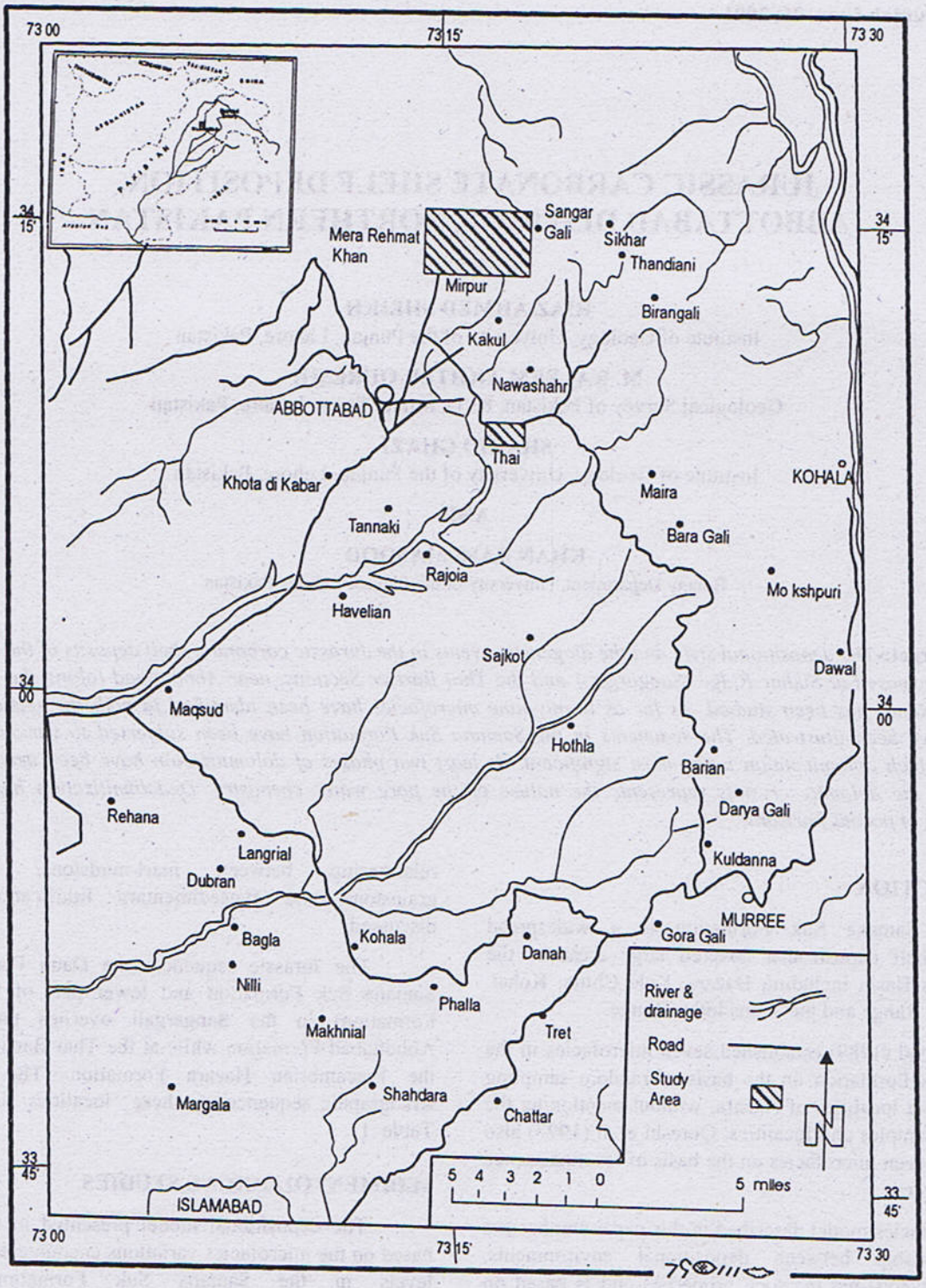

Fig. 1. Location Map of study areas.

Facies fall into the following five (5) broad categories. 1. Shelf facies - open circulation. 2. Shoal facies - agitated water. 3. Restricted marine shoal facies. 4. Restricted marine, shelf/lagoon facies - protected environment. 5. Tidal flat facies.

Significant amount of porosity is found in each facies. The intergranular porosity is the dominant porosity type in the limestone beds of the Samana Suk Formation. Vuggy porosity is also very commonly present.

Table-1
The generalized stratigraphic sequence of the study area.

AGE	SANGARGALI SECTION	LITHOLOGY	THAI BARRIER SECTION
CRETACEOUS	Kawagarh Formation	-Fine grained limestone and marl.	Kawagarh Formation
	Lumshiwal Formation	-Medium to coarse grained glauconitic sandstone	Lumshiwal Formation
	Chichali Formation	Shales and interbedded glauconitic sandstone.	Chichali Formation
----------	------ Disconformity------	----- Disconformity----	------ Disconformity---
JURASSIC	Samana Suk Formation	-Thin to thick-bedded limestones. dolomite and dolomitic limestone	Samana Suk Formation
	Datta Formation	-Sand stone and quartz arenite.	Datta Formation
----------	-------- Unconformity--------	----- Unconformity ------	----------
CAMBRIAN	Abbottabad Formation (Lower Part)	Maroon flaggy and thin bedded sandstone -Faceted boulders in sandy matrix.	Unconformity
----------	-------- Unconformity--------		----------
EO-CAMBRIAN	Hazara Formation	-Slates, sandstones and quartzite. Base not exposed	Hazara Formation

MICROFACIES

1:- Bioclastic lime mudstone and wackestone: (Plate no.1a). The faunal diversity suggests an open marine environment. Fossils are well preserved in sediments of low energy environments. At places, fossils are homogenized through bioturbation.

2:- Cortoid bearing bioclastic packstone and grainstone. On the basis of algal contents this microfacies is divided into two sub-types.

I. Dasycladacean (green algae) Facies, having oysters, echinoderms, pelecypods, gastropods and brachiopods.

II. Red algae bearing Facies, having oysters and brachiopods.

Red algae are very sensitive to salinity variations (Flugel, 1972). Therefore the two facies were deposited under different salinity conditions. The microfacies II, is interpreted to be of normal marine shelf environments while the facies I, shows salinity variations, indicating slight restrictions in circulation of sea water.

3:- Oncoidal, ooidal grainstone. On the basis of algal contents this microfacies has been divided into the following three sub types.

I. Dasycladacean and phylloid green algae, Facies, having pelecypods, brachiopods, gastropods, echinoderm and oysters.

II. Red algae Facies, having echinoderm, brachiopods benthnoic foraminifers and gastropods.

III. Dasycladacean green algae Facies, having pelecypods and echinoderms.

Oncoids and superficial radial ooids with fossil fragments embedded in spar are indicators of shoal environment in agitated water. They show moderately high-energy conditions and shallow water environment. More restricted back shoal conditions are shown by facies no. III than that of facies no. II.

4:- Bioclastic-ooidal-peloidal grainstone. On the basis of faunal content this facies has been subdivided as follows:

I. It consisted of oyster shell fragments, pelecypods, gastropods, brachiopods, echinoderms and green algae.

II. It consisted of oysters, brachiopods, pelecypods, echinoderms, gastropods, foraminifers and red algae.

III. It consisted of brachiopods, pelecypods, echinoderms and charophyta.

Diverse fauna of this facies shows normal to near normal marine salinity. Microfacies I shows-slight variation of salinity conditions. Facies II shows normal marine salinity, whereas facies III- shows fresh water or near shore, brackish water conditions. Presence of sparite, instead of micrite due to winnowing effect, suggests high energy. Ooids are superficial to radial concentric.

5:- Ooidal grainstone. (Plate no.1b) On the basis of ooids microstructures in thin section. This facies has been sub-divided as: -

I. Oosparite with radial ooids and scarcity of fauna (Plate no.1b).

II. Oosparite with concentric ooids or ooidal grainstone.

III. Oosparite with radial concentric ooids (Plate no.2a).

IV. Oosparite with superficial ooids.

V. Oosparite with micritized ooids. (Plate no.7a).

The radial ooids with low faunal contents show quiet water lagoonal environment, ooids with concentric cortices represent high to very high-energy shoal environment. Radial concentric ooids represent deposition in moderate to high-energy shoal environments. Superficial ooids and micritized ooids show moderate energy conditions. Radial ooids are associated with low faunal content in Thai Barrier section indicating its deposition in lagoonal environment, while concentric ooids are observed in Sangar gali section with diverse faunal fragments, which show its deposition in shoal environments with agitated waters. Trough cross bedding (Plate no.8b) is observed (Fig.II. at 46 m., 96 m. 109m), which represents shallowing nature of the depositional environment.

6:- Peloidal grainstone: The presence or absence of quartz grains has been the only criterion to subdivide this facies. The bioclasts are bi and triserial foraminifers, miliolids, oysters, phylloid and dasycladacean green algae and gastropods. They show alignment at some places. Hard grounds have also been observed in the field. All these factors show restricted marine subtidal environment. The presence of quartz in some thin sections suggests near shore depositional environment. This facies was deposited in slight water movements. Such sediments gradeded into laminoid mudstone.

7: - Grainstone with aggregate grains: The grapestone of ooids and peloids are common (Plate no.2b). The observed ooids are radial concentric. This facies is deposited in very warm, shallow water with moderate circulation.

8:- Laminated to bioturbated lime mudstone with fenestral fabric: The presence of miliolids and green algae points out intertidal environment in restricted bays and lagoons.

9:- Algal stromatolitic mudstone: Laterally linked stromatolites were observed. Fine lamination has been observed in the field (Plate no.3a). This feature suggests supratidal environments. .

10:- Oncoid, oomicrite or oncoidal ooidal wackestone: This was quiet water sediment with algal balls composed of light matter (Plate no.3b), which was later on calcified.

11:- Pure Micrite or Carbonate Mudstone: Unfossiliferous micrite at places associated with quartz, shows the deposition in somewhat saline or evaporative tidal ponds of supratidal environments.

12:- Rudstone or intraclastic grainstone: This facies contained intraclasts as the main constituents. The clasts were generally of unfossiliferous micrite. The matrix is removed by winnowing. Cross bedding and orientation of pebbles have been observed in the field. The sediment is normally termed intraformational conglomerate. It is formed as a lag deposit in tidal channels.

13- Dolomicrite: It comprised of fine-grained dolomite (Plate no.4a). It resulted from the dolomitization of micrite, which provide necessary nucleation zones for the retention of original micritic fabric.

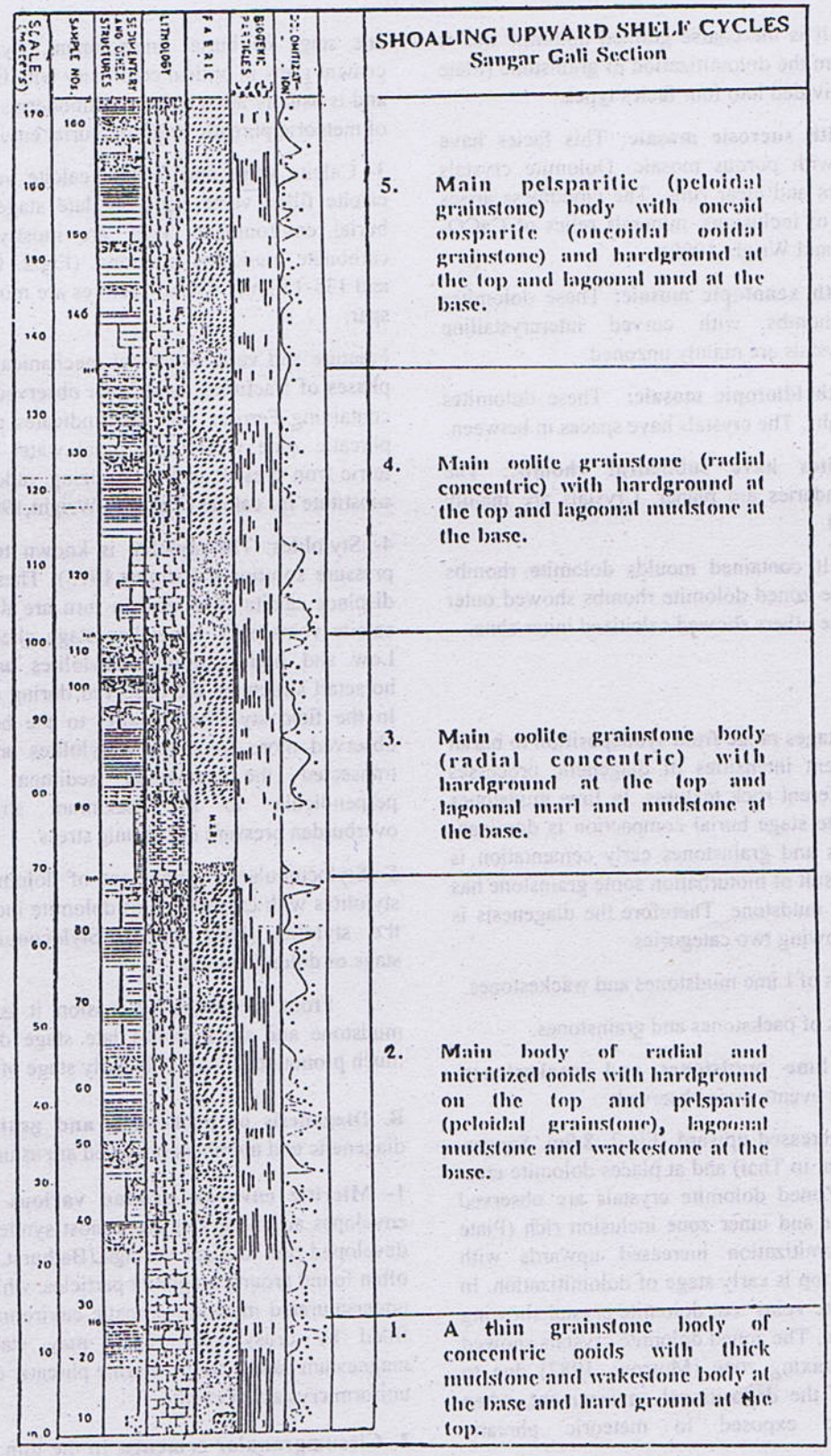

Fig. 2. Depositional and diagenetic log of the Samana Suk Formation, Sangargali Section, Abbottabad District, Pakistan.

14:- Dolosparite: It is the coarse grained dolomite this is mostly resulted from the dolomitization of grainstone (Plate no.4b). It was subdivided into four facies types.

a. Dolosparite with sucrosic mosaic: This facies have euhedral rhombs with porous mosaic. Dolomite crystals have cloudy centers and clear rims. The cloudiness arises from the presence of inclusions. minerals relics of $CaCO_3$ precursor (Tucker and Wright,1990)

b. Dolosparite with xenotopic mosaic: These dolomites have anhedral rhombs with curved intercrystalline boundaries. The crystals are mainly unzoned.

c. Dolosparite with idiotopic mosaic: These dolomites have euhedral rhombs. The crystals have spaces in between.

d. These dolomites have subhedral rhombs: The intercrytalline boundaries are planar. Crystals are mainly cloudy and unzoned.

15:- Dedolomite: It contained moulds dolomite rhombs (Plate no. 5a). Some zoned dolomite rhombs showed outer zone calcitized while others showed calcitized inner zone.

DIAGENESIS

Diagenetic stages range from syndeposition to burial compaction. Different intensities of diagenetic processes are observed in different rock textures. In lime mudstones and wackestones late stage burial compaction is dominant while in packstones and grainstones early cementation is pronounced. As a result of bioturbation some grainstone has been converted into mudstone. Therefore the diagenesis is divided into the following two categories.

A. Diagenesis of Lime mudstones and wackestones.

B. Diagenesis of packstones and grainstones.

A. Diagenesis of lime mudstones and wackestones: Following diagenetic events were observed:

1- Dolomitization increased upward (Fig.2. 8.9m. Sangargali & Fig. 3, 14.15m. in Thai) and at places dolomite crust is also observed. Zoned dolomite crystals are observed with outer zone clear and inner zone inclusion rich (Plate no.2a & 5a). Dolomitization increased upwards with dolomite crust at the top is early stage of dolomitization. In some cases, the calcite veins cut dolomite crystal showing its relatively older age. The zoned dolomite crystals showed their origin in the mixing zone (Morrow, 1982) due to shallowing nature of the depositional environment, when the sediment were exposed to meteoric phreatic environments.

2- Syntaxial overgrowth and spar cement. Syntaxial overgrowth and spar cement with uniform crystals indicated late stage of burial environment. Syntaxial overgrowth cement grew in optical continuity with the faunal fragments and is usually abundant on echinoderms. It is interpreted as of meteoric phreatic origin in burial environment.

3- Calcite veins and ferroan calcite veins. Fractures and calcite filled veins represent late stage diagenesis in the burial environment. They are mostly observed in the carbonate mudstone horizons. (Fig.2. 0-21m., 100-113m. and 135-138m.) . These fractures are mostly filled by zoned spar,

Fracture and veins represent mechanical compaction. Two phases of fracturing have been observed. The spar cement containing Ferrous iron also indicates precipitation in the phreatic zone where interstitial water has low EH. The ferric iron present in the oxidizing vadose water does not substitute for calcite (Tuker & Wright,1990).

4- Stylolites: The stylolite is known to be the result of pressure solution (Bathurst,1975). These at places cut or displace calcite veins and in turn are displaced or cut by calcite veins and show late stage chemical compaction. Low and high amplitude stylolites and stylolites with horsetail structures are observed during thin section study. In the field stylolites parallel to the bedding planes are observed more frequently. Stylolites and solution seams transected the cemented sediment and developed perpendicular to the maximum stress axis, either overburden pressure or tectonic stress.

5- Stylocumulates: Alignment of dolomite crystals along stylolites with crystal size of dolomite increasing in or near the stylolite. (Plate no. 5b). Stylocumulates showed late stage of dolomitization.

From the above discussion it is obvious that in mudstone and wackestones late stage diagenesis is very much pronounced with little early stage of diagenesis.

B. Diagenesis of packstones and grainstones: Various diagenetic end members observed are as under:

1- Micritic envelops around various grains: Micritic envelopes around grains are almost syndepositional. These developed due to algal borings (Bathurst, 1975). They are often found around aragonite particles, which leached in the undersaturated meteoric phreatic environment and later on filled by drusy spar. They may stabilize into low magnesium calcite in the marine phreatic environment with uniform crystals of calcite.

2- Circumgranular cements: In the thin section the most commonly observed circumgranular cements are:- **a:** Acicular or fibrous cement. **b:** Bladed or equant cement growing at right angles to the grain boundary (Plate no.6b).

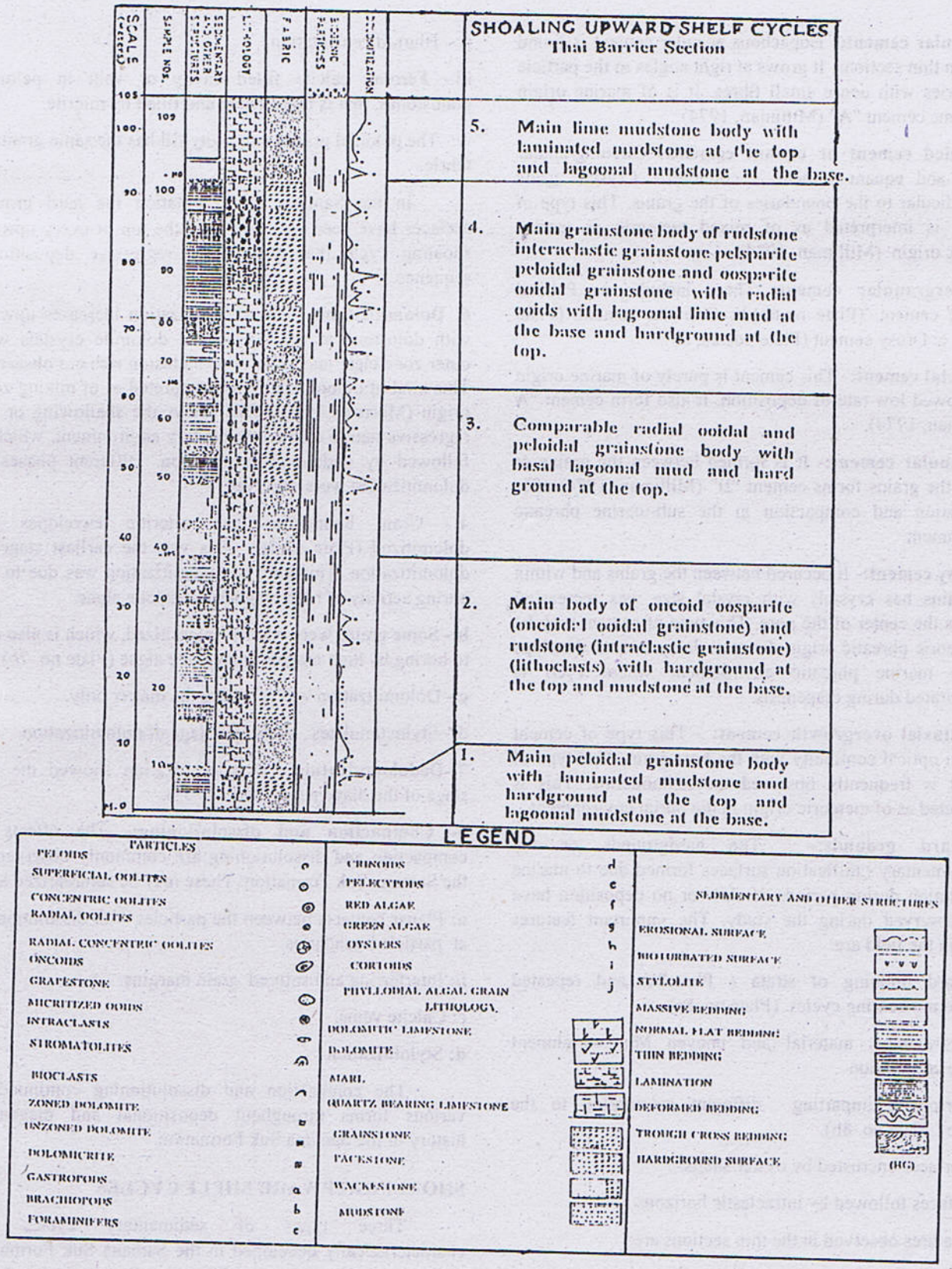

Fig. 3. Depositional and diagenetic log of the Samana Suk Formation, Thai Barrier Section, Abbottabad District, Pakistan,

a. Acicular cement:- Isopachous acicular cement is found rarely in thin sections. It grows at right angles to the particle boundaries with dense small fibres. It is of marine origin and forms cement "A" (Milliman, 1974).

b. Bladed cement or equant cement:- Circumgranular bladed and equant cement is common. Crystals grow perpendicular to the boundaries of the grains. This type of cement is interpreted as of mixed meteoric or marine phreatic origin (Milliman, 1974)

3- Intergranular cement: These include: **a:** Pelletal micritic cement. (Plate no.6b).**b:** Granular cement. (Plate no.1b). **c**: Drusy cement (Plate nos.2a, 6a).

a. Pelletal cement:- This cement is purely of marine origin and showed low rate of deposition. It also form cement "A (Milliman, 1974).

b. Granular cement:- It is formed between the grains or within the grains forms cement "B" (Milliman, 1974) after lithification and compaction in the sub-marine phreatic environment.

c. Drusy cement:- It occured between the grains and within the grains has crystals with crystal size was increasing towards the center of the pore. This type of cement may be of meteoric phreatic origin. Ferroan drusy cement develops in the marine phreatic environment where F_2O_2 is incorporated during diagenesis.

4- Syntaxial overgrowth cement: - This type of cement grew in optical continuity with the host grain. This type of cement is frequently observed on echinoderms. This is interpreted as of meteoric origin in the burial environment.

5- Hard grounds:- The hardgrounds or the synsedimentary lithification surfaces formed due to marine cementation during periods of slow or no deposition have been observed during the study. The important features found in the field are:

I-Upward thinning of strata (Plate.8a) and repeated hardground bearing cycles. (Plate no. 8a).

ii: -Ferruginous material and uneven Mn. enrichment surface colouration

iii:-Burrowing imparting different colouration to the surface (Plate no. 8b).

iv:- Surfaces encrusted by oyster shells.

v:-Surfaces followed by intraclastic horizons

The features observed in the thin sections are:

i:- Conversion of bioclastic ooidal grainstone into bioclastic ooidal lime mudstone.

ii:- Blurred cementation.

iii:- Ferroan calcite filled cavity or vein in peloidal grainstones, that is bioturbated and filled by micrite.

iv:- The peloidal grains and cavity fill has the same granular fabric.

In the Samana Suk Formation the hard ground surfaces have been observed over the top of every upward shoaling cycle that indicated a regressive depositional sequence.

6: Dolomitizition: - The dolomitization increases upward with dolostone at the top. Zoned dolomite crystals with outer zone clear and inner zone inclusion rich are observed. This kind of dolomitization is interpreted as of mixing zone origin (Morrow. 1982). This shows the shallowing or the regressive nature of the sedimentary environment, which is followed by undolomitized horizon. Different phases of dolomitization were observed: -

a:- Grain boundaries and micritic envelopes are dolomitized (Plate no.7a). This was the earliest stage of dolomitization. This kind of dolomitization was due to the boring activity of high magnesium calcite algae.

b:- Some grains were wholly dolomitized, which is also due to boring by high magnesium calcite algae (Plate no. 7b).

c:- Dolomitization was affecting the matrix only.

d:- Stylocumulates , show late stage of dolomitization.

7:-Dedolomitization:- Dedolomitization showed the last stage of the diagenesis (Plate no. 5a).

8- Compaction and dissolutioning:- The effects of compaction and dissolutioning are commonly observed in the Samana Suk Formation. These may be summarized as:-

a: Planar contacts between the particles with dissolutioning at particle boundaries.

b: Interferring and sutured grain margins.

c: Calcite veins.

d: Stylolitization .

The compaction and dissolutioning continued in various forms throughout depositional and diagenetic history of the Samana Suk Formation.

SHOALING UPWARD SHELF CYCLES

Three types of sedimentary cycles are characteristically developed in the Samana Suk Formation during periods of pure carbonate sedimentation in shelf (Wilson, 1975).

Plate -1

a:-

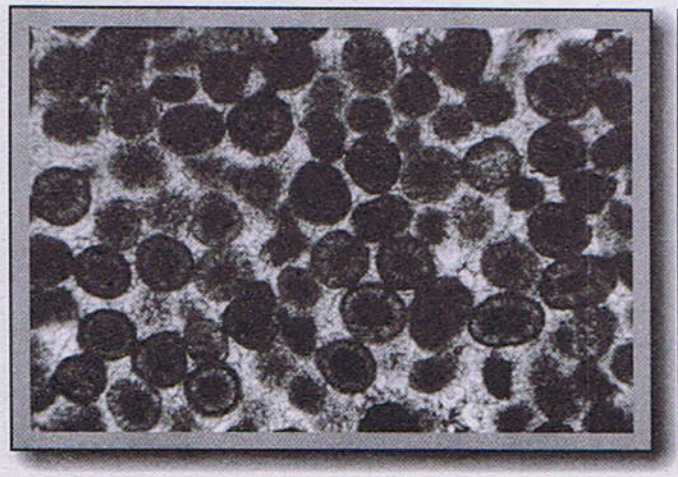

b:-

a:-Bioclasts are gastropod, bivalves, echinoid spines mudstone with diverse and well-preserved fauna. Some fossils are bimineralic, the aragonitic portion is replaced by spar. Sanger gali Section. (4x10, ppl.)

b:- Ooidal grainstone with radial ooids that possess micritic nuclei. Intergranular cement is spar. Sangar-gali Section (4x10,ppl.)

Plate -2

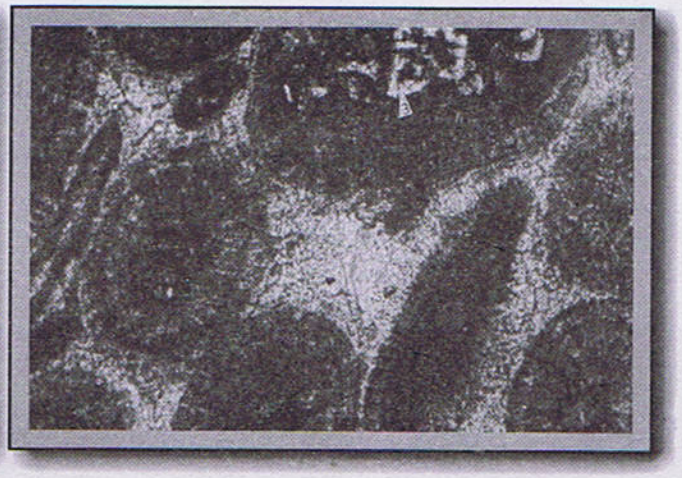

a:-

b:-

a:- Ooidal grainstone with radial concentric ooids. Two types of cements drusy (1) and circumgranular columnar (2) are prominent. Nuclei of some ooids are dolomitized with inclusion rich inner zone. Sangar gali Section (10x10, ppl.)

b:- Grainstone with aggregate grains in drusy cement. Sangar gali Section (4x10, ppl.)

Plate -3

a:-

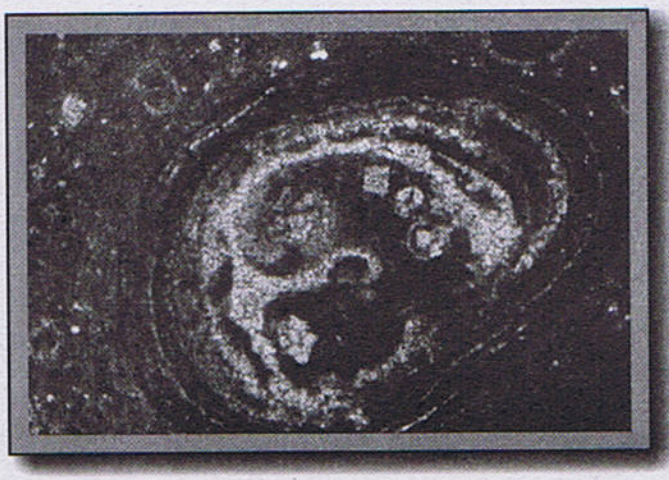

b:-

Plate -4

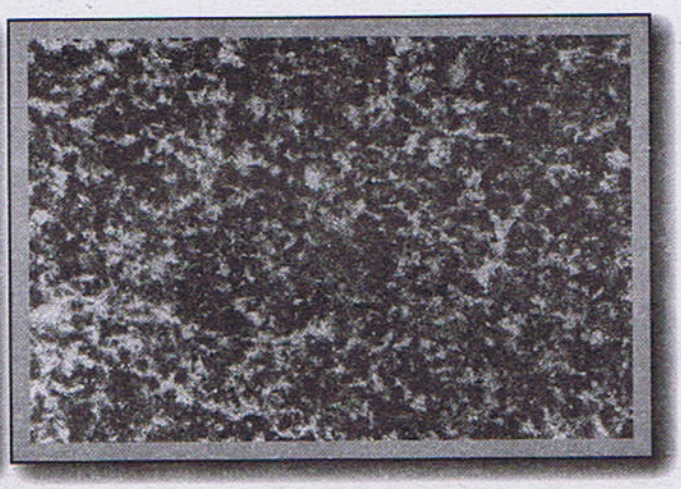

a:-

b:-

a:- Algal stromatolitic mudstone. The facies suggests supratidal environments, the algal stromatolite (1) and algal ball (2) are clearly visible in recrystallized spar cement. Thai barrier Section (4x10, ppl.).

b:- Oncoid bearing ooidal wackestone. Sangar gali (4x10, ppl).

a: Dolomicrite. Fine grained dolomite with cloudy anhedral dolomite rhombs. Thai barrier Section (10x10, ppl.).

b:- Dolosparite, with hypidiotopic mosaic. Dolomite rhombs are subhedral with mostly planar intercrystalline boundaries. Sangar gali section (20x10, ppl.)

Plate -5

a:-

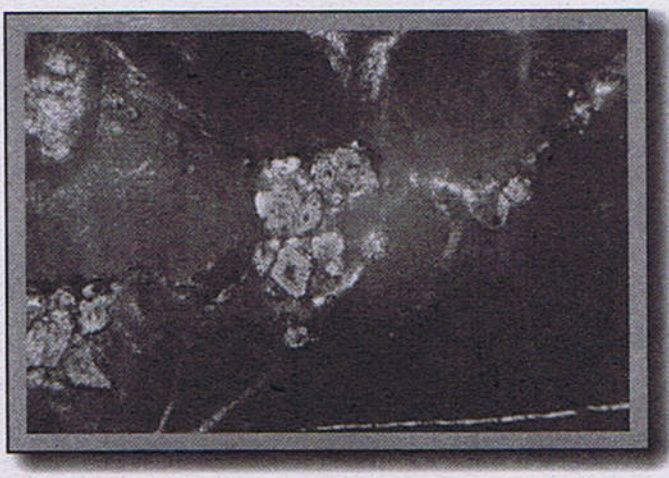

b:-

Plate -6

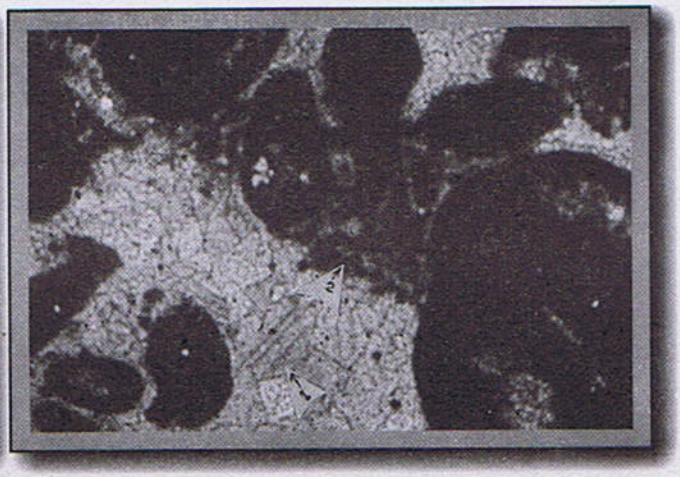

a:-

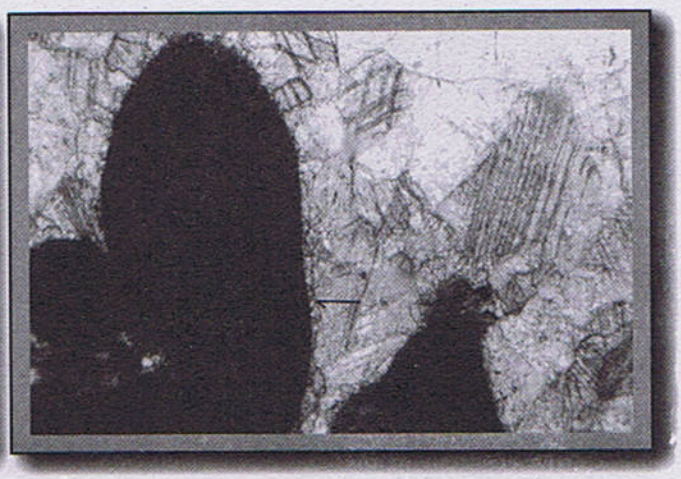

b:-

a:- Zoned dolomite crystal. Dedolomitization has produced porosity. Sangargali Section (10 x 10 ppl).

b:- Stylocumulate with dolomite rhombs aligned along low amplitude stylolites dolomite rhombs are zoned. Thai Barrier Section (10 x 10 ppl).

a:- Grainstone with drusy cement (1) and pelettal cement (2). Thai Barrier Section (4 x 10 ppl).

b:- Circumgranular equant cement (arrowed), overlain by spar of radiaxial crystal mosaic. Grains are intraclasts, Samana Suk Formation, Thai barrier Section (20x10 ppl.)

Plate -7

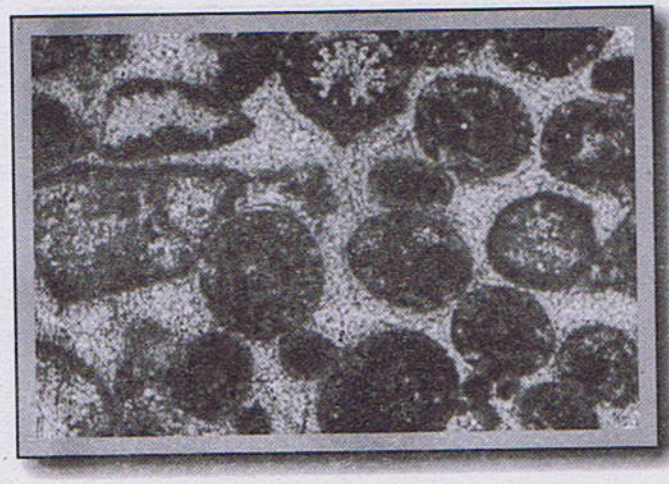

a:-

b:-

Plate -8

a:-

b :

a:- Dolomitization of peripheries of ooids. Micritized ooids are also present. Sangar gali Section (4x10, ppl.)

b:- Grain selective dolomitization. Ooids are completely dolomitized. Dolomite crystals are clear and unzoned. Sangar gali Section (10x10, ppl.).

a:- Photograph shows thinning upward (from left to right) cycles. One cycle has thick lime mudstone beds at the base and thin grainstone beds at top. Wavy bedding is also visible.

b:- Trough cross bedding in the Samans Suk Formation. Thai barrier Section.

They are as under:-

i:- Ooidal grainstone cycles:- These contain a major grainstone body commonly oolitic. generally a hardground surface occured at the top and normal marine marl or wackestone at the base and represents tropical and arid climate with moderate circulation on wide shallow shelf around basin.

ii:- Lime mudstone cycles:- They generally contained laminated tidal flat mudstone with sabkha evaporites at the top and lagoonal mudstone and marl at the base. This represented evaporitic arid climate or tropical climate with very poor marine circulation on wide shallow shelf around basins and also showed terminal filling of shallow basins.

iii:- Platform interior cycles:- It contains coarse limesand. gravel, lumps and oncoids with calcitic soil or sabkha-lagoonal to intertidal mud at the top and sand banks in wide marginal belts to bank interior mud at the base. It represents strongly seasonal evaporitic climate, intermittent good circulation and very restricted in lagoons. Considerable sea level fluctuation abrupt sub-arial exposure. These shoaling upward cycles are strong indicators of regression.

Upward shoaling cycles in Sangar gali section:-

Following shoaling upward cycles have been observed:

i:- A thin grainstone body of concentric ooids with thick mudstone and wackestone body at the base and hard ground at the top (Fig. II:- 0-13m.).

ii:-Main body of radial and micritized ooids with hardground at the top and pelsparite (Peloidal grainstone). lagoonal mudstone and wackestone at the base (Fig.II:- 13-68m.).

iii:-Main oolite grainstone body (radial concentric) with hardground at the top and lagoonal marl and mudstone at the base (Fig:-II:- 68-100m.).

iv:-.Main oolite grainstone (radial concentric) with hardground at the top and lagoonal mudstone at the base. (Fig:-II:- 100-135m.)

v:- Main pelsparite (peloidal grainstone) body with oncoid oosparite (oncoidal ooidal grainstone) and hardground at the top and lagoonal mud at the base (Fig:-II: 135-172m.).

These cycles are grainstone shoaling upward cycles showing wide shallow shelf environment with moderate circulation .

Upward shoaling cycles in Thai Barrier section:-

Following shoaling upward cycles have been observed in this section:

i:- Main peloidal grainstone body with laminated mudstone and hardground at the top and lagoonal mudstone at the base. (Fig:-III:- 0.7m).

ii:-Main body of oncoidal ooidal grainstone and rudstone (Lithoclasts) with hardground at the top and mudstone at the base (Fig:-III:- 7-38m.).

iii:-Comparable radial ooidal and peloidal grainstone body with basal lagoonal mud and hard ground at the top.(Fig:-III:-38-62m.)

iv:- Main grainstone body of rudstone intraclastic grainstone pelsparite peloidal grainstone and oosparite ooidal grainstone (radial ooids) with lagoonal lime mud at the base and hardground at the top. (Fig.:- III:-68-93m.).

v:- Main lime mudstone body with laminated mudstone at the top and lagoonal mudstone at the base (Fig:-III:- 93-105m

On the basis of shoaling upward cycles study it is concluded that Samana Suk Formation exposed at Sangar Gali section has been deposited in middle shelf with moderate open circulation of sea water. The Samana Suk Formation exposed at Thai Barrier section has been deposited in comparatively shallow shelf with restricted circulation of sea water.

CONCLUSIONS

The deposition of the Samana Suk Formation took place in open marine condition, with clear cut shoaling upward shelf cycles terminated by ooidal grainstone with hard grounds at the top. The thickness of the formation at Sangar gali is more than at the Thai barrier section. The sediments of the Samana Suk Formation show different signatures of diagenesis among which boiturbation, cementation, compaction and dolomitization are more significant. Bioturbation is restricted to grainstones forming the top of the cycles.

Cementation is the result of different diagenetic environments including marine phreatic environments near the surface and burial environments. Dolomitization is fabric selective, effecting matrix and particles at different horizons. Compaction includes both physical and chemical compaction. The chemical compaction is particularly important in the development dolomite crystals as stylocumulate.

ACKNOWLEDGEMENT

R.A.Shiekh acknowledges the receipt of research grant from University of the Punjab under Project entitled " Sedimentology of the Samana Suk Formation and Chiltan Limestone from Hazara, Kala Chitta and Ziarat Nala (Quetta) sections.

REFRENCES

Bathurst, R.G.C. (1975) carbonate sediments and their diagenesis: Development in sedimentology. 12. Elsevier, New York, pp.658.

Flugel, E. (1972) Microfacies analysis of carbonate rocks. Springer-Verlag pp. 633.

Masood, H.(1989) Samana Suk Formation, Depositional and Diagenetic history. *Kashmir Jour. Geol.*. **6&7.** pp157-161.

Milliam, J.D. (1974) Marine Carbonates. Springer-Verlag, Berlin.

Morrow, D.W. (1982) Diagenesis 2. Dolomite – Part 2. Dolomitization models and ancient dolostones. Geosci . Canda, 9, pp.95-107.

Qureshi, M.A., Baig, M.S. and Munir, M. H. (1997), Reconnaissance microfacies analysis of the upper Jurassic Samana Suk Formation, Northern Hazara, Pakistan. *Geol. Bull. Punjab Univ.* **31&32** pp. 145-152.

Tuker, M.E.,Wright, V.P (1990) Carbonate Sedimentology. Blackwell London. PP.482.

Wilson, J.L. (1975) Carbonate facies in geologic History. Springer-Verlag. New York,.

Geol. Bull. Punjab Univ. 36, 2001

SODIUM PYROXENE IN THE KOGA FELDSPATHOIDAL SYENITES, BUNER SWAT, NW PAKISTAN

BY

IFTIKHAR H. BALOCH
Institute.of Geology, University of the Punjab, Quaid-e-Azam Campus, Lahore, 54590, Pakistan

ABDUL MATEEN
Pakistan Institute of Engineering and Applied Sciences, P.O. Nilore, Islamabad, Pakistan

AND

M. NAWAZ CHAUDHRY
Institute of Geology, University of the Punjab, Quaid-e-Azam Campus, Lahore, 54590, Pakistan

Abstract:- *The Koga feldspathoidal complex predominantly comprises of foyaites, foyaitic feldspathoidal suites, garnet bearing feldspathoidal syenites and pulaskitic feldspathoidal syenites. Clinopyroxenes in these rocks suites from various intrusions and dykes have been analyzed by electron microprobe. Sodic pyroxenes are unusual and fall within the narrow field of aegirine- jadeite. Aegirine compositions range from* Ae_{75} Jd_{25} *to* Ae_{80} Jd_{20} *and hedenburgite component is absent. The chemistry of aegirine in the feldspathoidal rock suites has been interpreted and their evolutionary trend is discussed. The proxene fractionation trend established in the Koga feldspathoidal suites appears to be unique.*

INTRODUCTION

Pyroxenes are among the most important mineral phases considered for the determination of crystallization sequence and petrogenetic interpretation of syenites and nepheline syenites occurring in the alkaline igneous complexes. The sodium pyroxenes of aegirine-jadeite series exihibit extensive solid solution with the Ca-Mg-Fe pyroxenes (Morimoto et al. 1988), particularly with diopside - hedenbergite and augite. They may lead to yield Na-Ca pyroxenes of aegirine-augite series.

Pyroxene compositions fall into distinctive groups in the alkaline intrusive complexes. With the increasing Na and Fe^{3+} contents in the crystallizing alkaline magmas, the pyroxenes become enriched in acmitic component following the general trend originating from sodic - salite through aegirine - augite to aegirine (Stephenson 1972, Mitchell and Platt 1978, 1982 Platt and Woolley 1986, Woolley and Platt 1986, 1988).

Quard pyroxenes belonging to the diopside - hedenbergite series (Morimoto et al. 1988) have been reported in many alkaline complexes. Extreme enrichment of hedenbergite is observed in the Ilimaussaq intrusive (Larsen 1976), Coldwell complex (Mitchell and Platt 1978) and Dismal nepheline syenites, Antarctica (Worley et al. 1995).

Aluminous alkali pyroxenes are reported in the nepheline syenites from Malawi (Woolley et al. 1996, Eby et al. 1998), comprising of aluminian aegirine - augite, aluminian aegirine and omphacite. These are interpreted to be of igneous origin that have been metamorphosed. Similarly aluminous pyroxenes have been recorded from metamorphosed nepheline syenites from many localities (Iwasaki 1960, Curtis and Gittins 1979). Detailed mineral chemistry of aegirine has been investigated from Mont Saint-Hilaire, Quebec (Piilonen et al. 1998).

In this paper sodium pyroxene of aegirine - jadeite series occurring in the Koga feldspathoidal syenites are reported from the Koga alkaline igneous complex, NW, Pakistan. The sodium pyroxenes of the Koga syenites are different from those occurring in majority of the alkaline complexes of the world.

GEOLOGICAL SETTING

The Koga feldspathoidal syenite-carbonatite complex is the most interesting for mineralogical study from the alkaline igneous province of NW Pakistan. The Koga complex occurs in the middle of Ambela granitic complex. The feldspathoidal syenites are well exposed near

Koga village (34.23 N, 72.28 E) in the Chamla valley of Buner district, NWFP, Pakistan.

The Koga alkaline complex exhibits wide spectrum of feldspathoidal synites, essentially (pyroxene nepheline syenite suites), foyaites, sodalite-cancrinite rich foyaitic pegmatites, garnet-bearing feldspathoidal syenites, pulaskites and nordmarkites. The geology and petrology of the Koga alkaline igneous complex was described elsewhere (Siddiqui et al. 1968, Chaudhry et al. 1981, Baloch 1994, Baloch et al. 1994).

The feldsphathoidal syenite intrusions are surrounded on the northwest, west and south west, by Babaji syenites (SiO_2 - saturated and oversaturated association). The southeastern outcrop has discordant contact with metamorphosed Chingalai Granodiorite Gneiss. Small carbonatite bodies occur west of Narangi Kandao and Shapala. Well developed fenite zones are formed around carbonatite intrusions.

The feldspathoidal syenite is generally medium to coarse grained. Dykes, sills and small irregular intrusions of later generation are fine to coarse grained even pegmatitic, very often show flow foliation roughly in N-S direction. Ijolite and mafic dykes (dolerites and microgabbos), cutting nepheline syenites, occur at places particularly in Sura, Agarai, Lulu Razzar and Kharkai.

The feldspathoidal syenites contain numerous pegmatite and aplite veins of variable composition and texture. The pegmatites are both zoned and unzoned. They are either intrusions or replacement bodies (Chaudhry et al. 1981).

PETROGRAPHY

The rocks of the Koga feldspathoidal syenites are predominantly composed of nepheline (5-35wt%), mirocline (20-70wt%) , albite (trace to a few percent), cancrinite and sodalite (up to 12-15wt%). Aegirine (2-3wt%) biotite (1-4wt%) , magnetite (up to 3wt%) and sphene and garnet (up to 1 and 4 wt% respectively). Apatite and zircon are accessory minerals.

The mafic minerals occur as aggregates and clots as well as subhedral to anhedral grains. Pyroxene and biotite are generally fresh and primary crystalline phases coexisting in most of the rocks. Pyroxenes are more abundant and minor phase, fine to medium grained and of yellow green in colour. The amphiboles are absent or rare. Garnet when present is invariably associated with pyroxenes.

MINERALOGY OF SODIUM PYROXENES

Representative samples of feldspathoidal syenites were prepared for electron-probe microanalysis (EPMA). Pyroxenes were analysed on a Jeol. superprobe JXA 8600 available at the Department of Geology, University of Leicester, U.K. The equipment was fitted with an on-line computer for ZAF correction and was calibrated against appropriate natural and synthetic standards. Quantitative results were obtained on the wavelength dispersive system using the operating conditions of 15 kV acceleration voltage and 0.03 microampere current.

Representative compositions of pyroxenes are given in Table 1, calculated on the basis of 6 oxygens and 4 cations. Pyroxene compositions fall in aegirine-jadeite domain belonging to the sodium pyroxene series (Morimoto et al. 1988). The composition varies form Ae_{75} Jd_{25} to Ae_{80} Jd_{20}. The aegirines are relatively unzoned and show variation in its Na_2O contents from 12.54 to 14.14wt% Al_2O_3=3.9 to 5.41 wt%, CaO= 0.35 to 3.05 wt% and MgO=0.00 to 0.92 wt% in the samples studied.

The Q [wollastonite (Wo), enstatite(En), ferrosilite (Fo)] contents are from Q_0 to Q_{42}. The compositional variations illustrated in (Fig. 1), show that there are not more than 10 points in the field of aegirine - augite.

The sodium pyroxenes from the Koga feldspathoidal syenites are plotted on Ae+Jd - Di - Hd (Fig. 2) instead of the usual plot of Ac-Di-Hd. These analyses mostly plot on the Ae-Jd - Di line, and a very few on the hedenbergite join. The data indicates that the compositional range mostly remains in the aegirine field. Overall compositional variations show that the Koga nepheline syenites follow typical peralkaline trend (Fig. 3).

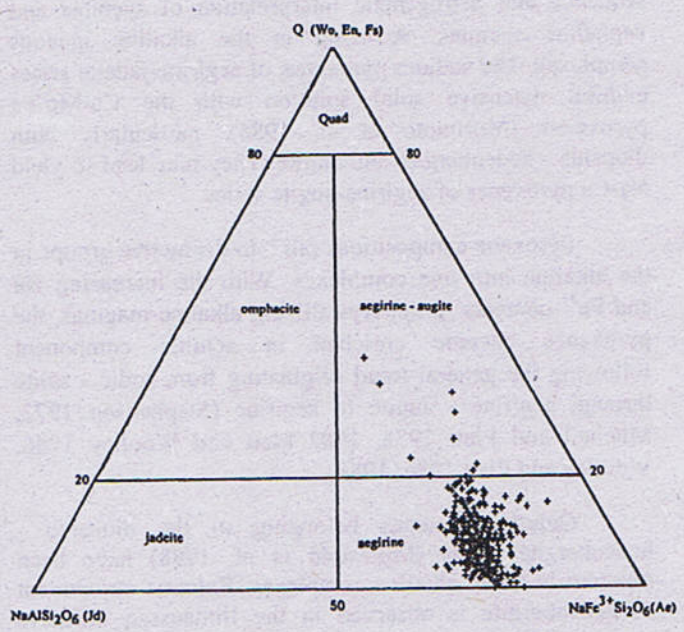

Fig. 1 Ca-Mg-Fe and Na pyroxenes with accepted names. Quard represents the Ca-Mg-Fe pyroxenes areas.

Table 1

Microprobe analyses of aegirine from the Koga Complex

Sample No.	K-3		K-4		K-5		K-6		K-8		MK-2		MK-5	
	mean	sd	mean	sd	mean	sd	mean	sd	mean	sd	mean	sd	mean	sd
SiO_2	53.48	0.55	53.78	0.23	53.23	0.85	53.47	0.80	53.53	0.31	53.20	0.66	53.84	0.43
Al_2O_3	3.90	1.30	4.69	0.58	4.84	0.78	5.13	0.71	5.46	0.75	4.88	0.66	5.40	0.47
FeO	25.16	1.32	23.71	0.85	23.84	0.72	24.48	1.05	22.61	1.03	22.54	0.69	23.26	0.62
MnO	0.20	0.08	0.22	0.11	0.18	0.07	0.22	0.19	0.29	0.25	0.11	0.08	0.00	
MgO	0.52	0.26	0.73	0.42	0.43	0.16	0.13	0.11	0.59	0.25	0.00		0.12	0.07
CaO	1.44	0.57	2.15	0.85	1.56	0.36	0.55	0.18	2.08	0.81	0.35	0.33	0.52	0.12
Na_2O	13.63	0.41	13.03	0.35	13.37	0.41	13.99	0.44	12.86	0.34	13.94	0.42	14.14	0.16
Total No.	32		8		10		29		28		7		23	
No. of cations on the basis of 6 oxygens and total of 4 cations														
Si	1.980		1.992		1.985		1.977		1.997		2.019		1.996	
Al	0.170		0.205		0.212		0.223		0.240		0.218		0.236	
Fe^2	0.000		0.009		0.000		0.003		0.017		0.018		0.000	
Fe^3	0.779		0.725		0.743		0.754		0.689		0.698		0.721	
Mn	0.006		0.007		0.006		0.007		0.009		0.004		0.000	
Mg	0.029		0.040		0.024		0.007		0.033		0.002		0.007	
Ca	0.057		0.085		0.063		0.022		0.083		0.014		0.020	
Na	0.978		0.936		0.966		1.003		0.930		1.025		1.016	

Sample No.	MK-6		MK-10		MK-21		SB-1		SB-5		SB-14		S-3	
	mean	sd	mean	sd	mean	sd	mean	sd	mean	sd	mean	sd	mean	sd
SiO_2	53.16	0.41	53.05	0.35	53.09	0.79	53.44	0.44	53.64	0.33	54.05	0.72	52.68	0.47
Al_2O_3	5.41	0.85	4.93	0.60	4.88	0.87	4.07	0.42	4.25	0.39	4.75	1.59	5.32	0.61
FeO	22.38	1.03	23.09	0.74	22.01	0.87	23.83	0.63	24.06	0.66	22.98	4.83	20.38	0.57
MnO	0.19	0.07	0.27	0.09	0.42	0.12	0.35	0.08	0.30	0.06	0.73	0.24	0.37	0.08
MgO	0.32	0.18	0.51	0.29	0.93	0.24	0.72	0.41	0.40	0.12	0.32	0.10	0.89	0.20
CaO	1.38	0.39	2.11	0.68	2.77	0.72	2.54	0.48	1.79	0.42	1.37	0.58	3.05	0.44
Na_2O	13.53	0.28	13.10	0.52	12.73	0.45	12.99	0.59	13.48	0.29	13.68	0.43	12.54	0.31
Total No.	34		19		34		7		4		36		19	
No. of cations on the basis of 6 oxygens and total of 4 cations														
Si	1.994		1.986		1.991		1.988		1.989		1.999		2.003	
Al	0.239		0.217		0.220		0.178		0.186		0.206		0.238	
Fe^2	0.001		0.002		0.000		0.010		0.000		0.008		0.000	
Fe^3	0.701		0.721		0.689		0.731		0.746		0.703		0.648	
Mn	0.006		0.008		0.013		0.011		0.009		0.023		0.012	
Mg	0.018		0.029		0.051		0.040		0.022		0.018		0.050	
Ca	0.055		0.085		0.107		0.101		0.071		0.055		0.124	
Na	0.984		0.951		0.928		0.937		0.969		0.981		0.924	

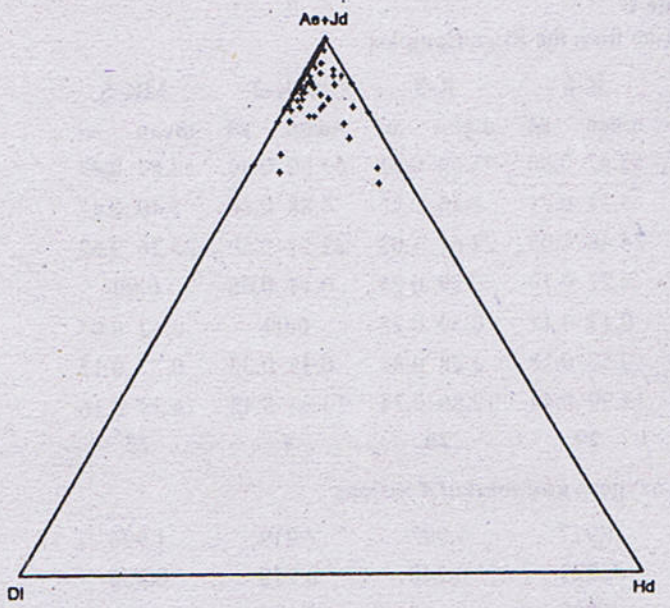

Fig. 2 Pyroxenes from the Koga feldspathoidal complex plotted on $Ae^{+}Jd$-Di-Ac system.

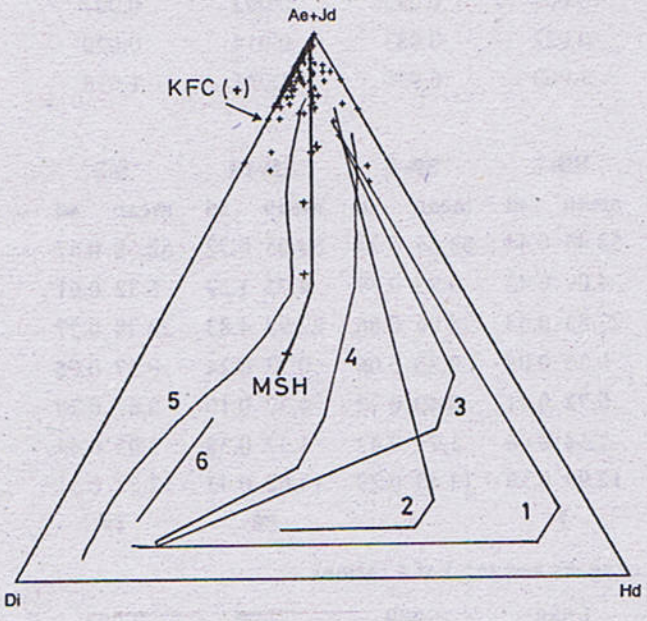

Fig.3 Pyroxene crystallization trends at the Koga feldspathoidal complex (KFC & $^{+}$ sign) compared to that obtained in similar alkaline intrusions. Mont Saint-Hilaire, (MSH) Quebec, Canada (Piilonen & Lalonde 1998), 1. Illimaussaq, Greenland (Larsen 1976), 2. Morutu, Japan (Yagi 1966), 3. South Qoroq, Greenland (Stephenson 1972), 4. Auvergne, France (Varet 1969), 5. Little Murum ultrapotassic complex, Russia (Mitchel & Vladykin 1996), 6. Fen alkaline complex, Norway (Mitchel 1980).

Fig. 4 Clots and aggregates of pyroxenes.

DISCUSSION

Pyroxene compositions in the Koga feldspathoidal suites are distinctly Al-rich sodic pyroxenes and exhibit a limited range of chemical compositions (Fig. 1). The general character of pyroxenes is the increase in Fe and Na contents leading to more acmitic compositions. The excess of Na over Fe^{3+} which forms with $NaAlSi_2O_6$ component due to replacement of Fe^{+3} - Al. The sodic pyroxene series exhibit a unique feature in the igneous environment of the Koga Complex. Such alkali-rich pyroxenes recently reported from the alkaline intrusive complexes of the North Nyasa alkaline province, Malawi (Woolley et al. 1996).

According to the classification scheme of pyroxenes (Morimoto et al. 1988), the aegirine is defined to have more than 80% of Ac end-member (Acmite: $NaFe^{3+}Si_2O_6$). Acmite (aegirine) is related to diopside due to the exchange of Na Fe^{3+}□ CaMg and to jadeite by Fe^{3+} □ Al.

The acmite component in pyroxene is common in high-pressure environment as well as in alkaline intrusives. Similarly, sodic pyroxene is related to calcic pyroxene by either the jadeite ($NaAl^{IV}Ca_{-1}Mg_{-1}$) or plagioclase ($NaSiCa_{-1}Al^{IV}$) substitution. In the Koga feldspathoidal complex, the aegirine is unusual having the composition which varies $Ae_{75}Jd_{25}$ to $Ae_{80}Jd_{20}$. The Hd component is practically absent unlike in most peralkaline igneous intrusions.

Figure 3 shows the pyroxene crystallization trends in the Koga feldspathoidal complex and the sodic peralkaline intrusive complexes such as South Qoroq, Greenland (Stephenson, 1972), Ilimaussaq, Greenland (Larsen, 1976), North Nyasa alkaline province, Malawi (Woolley et al. 1996, Eby et al. 1998) and in the Mont Saint-Hilaire Complex, Quebec (Piilonen et. al. 1998). The salic fractionation trends extend from diopsidic component (Di) towards hedenbergite (Hd) prior to the crystallization of aegirine. In the Koga Complex, extensive oxidation of iron

may have occurred within the highly evolved sodic undersaturated magma. As a result the crystallization of Fe2+ - bearing clinopyroxenes (Hd) was inhibited. The Koga feldspathoidal suites are essentially pyroxene bearing nepheline syenites and the aegirine is the only dominant mafic phase, which crystallized under low degree of competition. Thus, the pyroxene fractionation trend established in the Koga feldspathoidal suite appears to be unique.

It is generally believed that the factors, which control the evolutionary trends of pyroxenes, are oxygen fugacity and the peralkalinity of magmatic melt (Nash and Wilkinson, 1970, Larsen, 1976, Stephenson and Upton 1982, Woolley and Platt, 1986). High oxygen fugacity combined with peralkalinity must have favoured the crystallization of aegirnie within the narrow range of composition.

Jadeite pyroxenes are generally considered indicative of high pressures. Nevertheless, this may not be necessarily the case. The aluminous pyroxenes in the Red Wine rocks were formed under amphibolite-facies conditions; Curtis and Gittins (1979) suggested that the presence of jadeite and omphacitic pyroxenes in nepheline-bearing rocks do not indicate the high pressures normally attributed to silica-saturated or oversaturated rocks that contain these minerals. Although experimental work indicates that formation of pure jadeite probably does require a minimum pressure of about 7 kbar, replacement of Al by Fe3+ will probably lead to the generation of pyroxenes at much lower pressures (Deer et al. 1978). The preservation of early igneous pyroxenes of the Koga feldspathoidal syenite, dykes and intrusions suggest that the metamorphism was neither of high-pressure nor reached particularly elevated temperatures. The pressure calculated for the formation of nepheline in the complex is >1 and <5 Kbar (Baloch, 1994). The presence of pyroxenes as aggregates and clots (Fig. 4) is indicative of low pressure. Moreover, there is replacement of Al by Fe3+ and rocks do not have pure jadeite as is obvious in Fig. 1.

REFERENCES

Baloch, I. H., 1994. The Koga feldspathoidal syenite complex, Northwestern Pakistan: Mineralogy and industrial applications. Unpublished PhD thesis, Univ. of Leicester.

Baloch, I. H., Dunham. A. C. and Ghazanfar, M., 1994. Geology of the Koga feldspathoidal syenite complex of northwestern, Pakistan. *Pak. Jour. Geol.* **2(2), 3(1),** 1-8

Chaudhry, M. N., Ashraf, M. and Hussain, S. S., 1981. Petrology of Koga nepheline syenite and pegmatites of Swat District. *Geol. Bull. Punj. Univ.* **16**, 83 - 97.

Curtis, L. W. and Gittins, J., 1979. Aluminous and titaniferous clinopyroxenes from regionally metamorphosed agpaitic rocks in central Labrador. *Jour. Petrol.* **20**, 165-186.

Deer, W. A., Howie, R. A. and Zussman, J., 1978. Rock Forming Minerals. 2A. Single chain silicates. Longman, London, UK.

Eby, G. N., Woolley, A. R., Din, V. and Platt, G. R., 1998. Geochemistry and petrogenesis of nepheline syenites: Kasungu-Chipala, Ilomba, and Ulindi Nepheline Syenite Intrusions, North Nyasa Alkaline Province, Malawi. *Jour. Petrol.* **39**, (8), 1405-1424.

Iwasaki, M., 1960. Clinopyroxenes intermediate between jadeite and aegirine from Suberi-dani, Tokusima Prefacture. *Jour. Geol. Soc. Japan.* **66**, 334-340.

Larsen, L. M., 1976. Clinopyroxenes and coexisting mafic minerals from the alkaline Ilimaussaq intrusion, South Greenland. *Jour. Petrol.* **17**, 258 - 290.

Mitchell, R. H., 1980. Pyroxenes of the Fen alkaline complex, Norway. Am. Mineral. **65**, 45-54.

Mitchell, R. H. and Platt, R. G., 1978. Mafic mineralogy of ferroaugite syenite from the Coldwell complex. *Can. Jour. Petrol.* **19**, 627 - 651.

Mitchell, R. H., and Platt, R. G., 1982. Mineralogy and petrology of nepheline syenites from the Coldwell alkaline complex, Ontario, Canada. *Jour. Petrol.* **23**, 186 - 214.

Mitchell, R. H. and Vladykin, N. V., 1996. Compositional variation of pyroxene and mica from the Little Murrun ultrapotassic complex, Aldan Shield, Russia. *Mineral. Mag.* **60**, 907-925

Morimoto, N., 1988. Nomenclature of pyroxenes. *Am. Mineral.* **73**, 1123 - 1133.

Nash, W. P. and Wilkinson, J. F. G., 1970. Shonkin Sag laccolith, Montana. 1. Mafic minerals and estimates of temperature, pressure, oxygen fugacity and silica activity. *Contrib. Mineral. Petrol.* **25**, 241 - 269.

Piilonen, P. C., M. M. McDonald, A. and Lalonde, A. E., 1998. The crystal chemisrty of aegirine from Mont Saint-Hilaire, Quebec. *Can. Mineral.* **36**, 779-791.

Platt, R. G. and Woolley, A. R., 1986. The mafic mineralogy of the peralkaline syenites and granites of the Mulanje Complex, Malawi. *Min. Mag.* **50**, 85 - 99.

Siddiqui, S. F. A., Chaudhry, M. N. and Shakoor, A., 1968. Geology and petrology of the feldspathoidal syenite and associated rocks of the Koga area, Chamla valley, Swat, West Pakistan. *Geol. Bull. Punjab Univ.* 7, 1 - 30.

Stephenson, D., 1972. Alkalic clinopyroxenes from nepheline syenites of the South Qoroq Centre, South Greenland. *Lithos.* **5**, 187 - 201.

Stephenson, D. and Upton, B. G. J., 1982. Ferromagnesian silicates In a differentiated alkaline complex: Kungnat Fjeld, South Greenland. *Min. Mag.* **46**, 283 - 300.

Varet, K., 1969. Les pyroxenes des phonolites du Cantal (Auvergne, France). *Nues Jahrb. Mineral., Monatsh.*, 174-185.

Woolley, A. R. and Platt, R.G., 1986. The mineralogy of nepheline syenite complexes from the northern part of the Chilwa Province, Malawi. *Min. Mag.* **50**, 597 - 610.

Woolley, A. R. and Platt, R. G., 1988. The peralkaline nepheline syenites of the Junguni Intrusion, Chilwa Province, Malawi. *Min. Mag.* **52**, 425 - 433.

Woolley, A. R., Platt, R.G. and Eby, G. N., 1996. Relatively aluminous alkali pyroxene in nepheline syenite from Malawi: Mineralogical response to metamorphism in alkaline rocks. *Can. Min.* **34**, 423-434.

Worley, B. A., Cooper, A. F. and Hall, C. E., 1995. Petrogenesis of carbonate-bearing nepheline syenites and carbonatites from Southern Victoria Land, Antractica: origin of carbon and the effects of calcite-graphite equilibrium. *Lithos.* **35**, 183-199.

Yagi, K., 1966. The system acmite-diopside and its bearing on the stability relations on natural pyroxenes of the acmite-hedenburgite-diopside series. *Am. Mineral.* **51**, 976-1000.

Yoder, H. S. and Tilley, C. E., 1962. Origin of basalt magmas: An experimental study of natural and synthetic rock systems. *Jour. petrol.* **3**, 342.

Geol. Bull. Punjab Univ. 36, 2001

MUD TURBIDITES FROM THE MADEIRA ABYSSAL PLAIN, WEST OF GIBRALTAR, NORTH ATLANTIC.

BY

ABDUL SALAM KHAN
Department of Geology University of Balochistan, Quetta, Pakistan

GILBERT KELLING
Department of Geology, Keele University, Staff, ST5 5BG England

AND

PHIL. P.E. WEAVER
Institute of Oceanographic Sciences, Wormely, United Kingdom

Abstract: *Three cores, two (DII806) from the southern and one (D11813) from the northern area of the Madeira abyssal plain, each 15m to 18m long, were studied in detail. These cores were selected due to their thick, fine grained nature and environmental significance. The muddy sediments in these cores may be divided into hemipelagite and turbidite facies on the basis of sedimentary structures, texture and composition, Turbidites and hemipelagites regularly alternate with each other, together with a few amalgamated turbidites. The ratio of turbadite to hemipelagite in these cores ranges from 13:1 to 6:1. Hemipelagites are highly to moderately bioturbated, mottled with ring type burrows, rich in forams and nannofossils. Turbidites display a variety of primary structures that include cross lamination (T), parallel lamination (T), indistinct parallel lamination (T), homogenous mud (T6-7) and bioturbated mud (T). The internal organization of the sedimentary structures is complex showing no obvious and consistent vertical sequential arrangement, but the general upward fining from silty bases to muddy tops, the type and general sequnce of the sedimentary structures and the general restriction of bioturbation to the tops of these beds all suggest that were deposited essentially from gravity driven, initially turbulent flows that gradually waned in energy (low concentration turbidity flows). The internal variability and multiple repetition of sedimentary structures tend to favour deposition from pulsatory turbidity flows. It is believed that during earthquakes or other widespread slope failure, several slum-generated mass flows may be initiated at different points along the open margin, evolving into turbidity flows of different size and hydraulic behaviour, which ultimately may coalesce to form a large flow consisting several pulses.*

INTRODUCTION

The Madeira Abyssal Plain (MAP) lies in the North Atlantic mid-way between North-West Africa and the Mid-Atlantic Ridge and occupies the central and deepest part of the Canary Basin. It is completely flat between 30° to 30'N and 23° 30' to 25° 30'W, changing in relief by less than 10 metres. The Mid-Atlantic Ridge in this area is characterized by numerous abyssal hills elongated in a NE-SW direction and the western boundary of the abyssal plain trends NNE-SSW along the base of the ridge flank.

METHODS OF STUDY

Three mud dominated piston cores from the Madeira Basin were selected for detailed study (Fig.1). Composition texture and structures were carefully noted on the split cores. Detailed compositional and textural studies were carried out using smear slides. Sedimentary logs were made. These cores were cut into 20cm long and 0.6cm to 1cm thick slices with minimum distortion following the method of Chmelik (1967) for X-radiography to look sedimentary structures which are rarely observable to the naked eyes. The core slices were X-rayed in a Hewlett packard faxitron 43805 N using Kodak AX X-ray film at a tube voltage of 40-50KV and exposure times of 3-5 minutes depending on the thickness of the slice.

DESCRIPTION OF THE CORES

There cores (D11800, D11806, D11813), each from 15 to 18m long, were studied in detail. Cores D11800 and

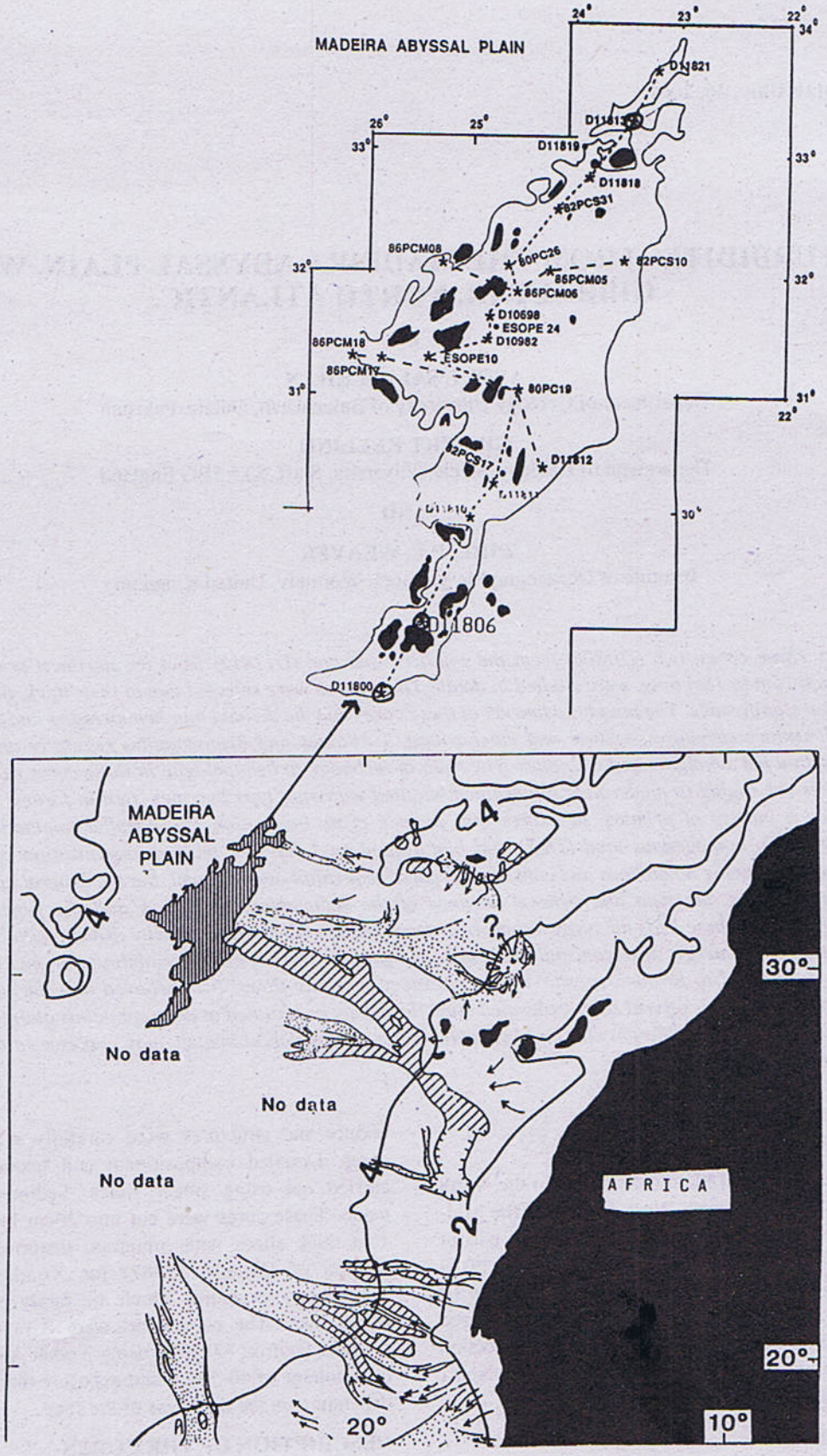

Fig. 1 Map showing location of the Medeira Abyssal Plain (vertical strip) and positions of the cores. Core D11800, D11806 and D11813 have been sescribed in the text. 2 and 4 are Bathymatric Contour in kilometer.

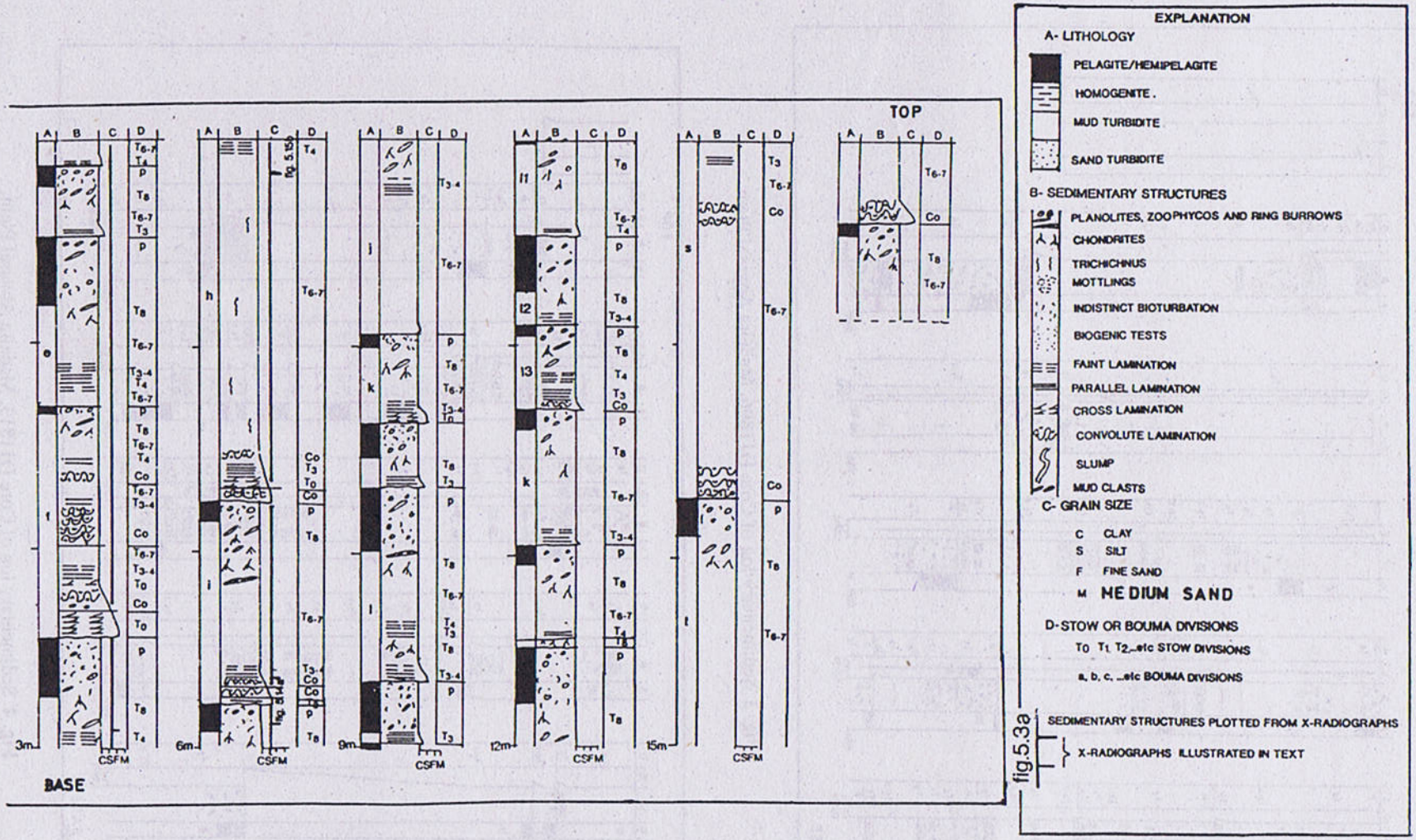

Fig. 2 Sedimentary log of Core D11800, Madeira Abyssal Plain.

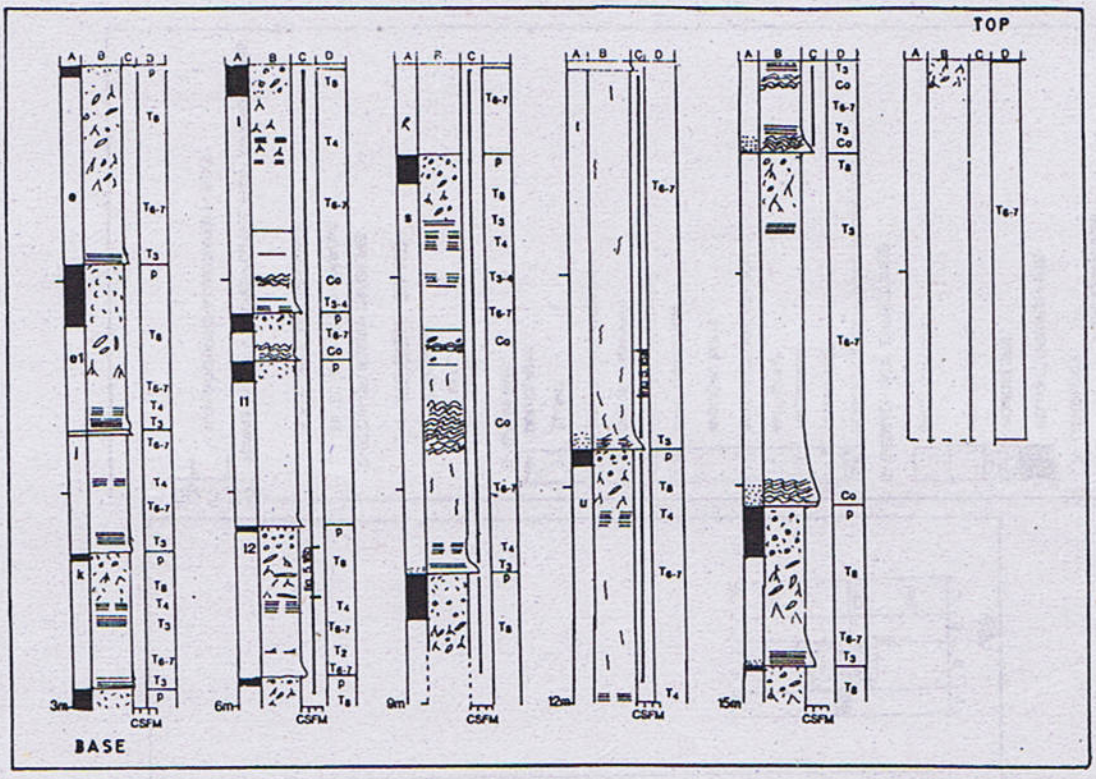

Fig. 3 Sedimentary log of Core D11806, Madeira Abyssal Plain.

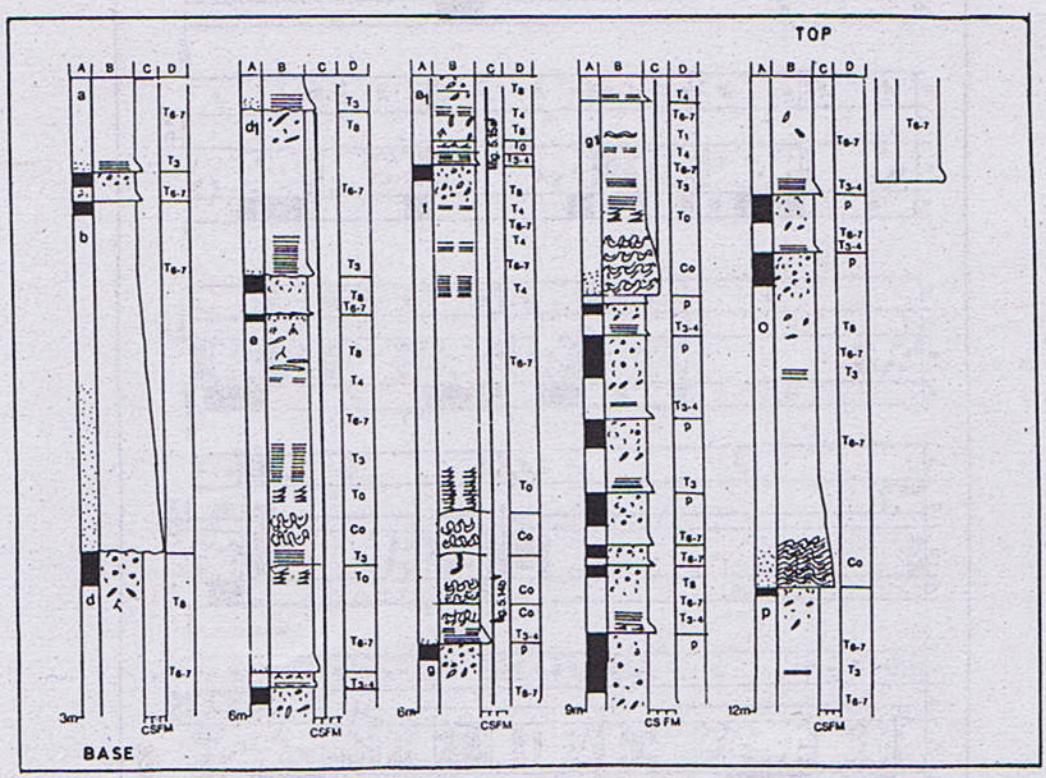

Fig. 4 Sedimentary log of Core D11813, Madeira Abyssal Plain.

D11806 are from the southern part of the Madeira Abyssal Plain, while core D11813 is located in the northern area (Fig.1). These cores were selected due to their thick, fine grained and environmental significance in the Abyssal Plain. The muddy sediments in these cores can be divided into turbidite and (hemi) pelagite units on the basis of sedimentary structures, texture and composition. Turbidites and hemipelagites regularly alternate with each other (Figs 2, 3 and 4), together with a few amalgamated turbidites. The ratio of turbidite to hemipelagite in these cores ranges from 13:1 to 6:1 Hemipelagite Facies.

Hemipelagic units can be distinguished from the intervening turbidites on the basis of texture, composition, sedimentary structures and colour (Rupke and Stanley, 1974). These hemipelagites consist of foraminiferal and nannofossil oozes, red clays and yellowish marls; and are poorly sorted silty clays. They are totally devoid of sedimentary structures. Their colour varies from pale brown (10YR5/4), dark brown, pale greyish blue to bluish white. Beds thicknesses vary from 2cm to 30cm and they constitute about 10% of the aggregate thickness of the cores examined. They are highly to moderately bioturbated, mottled with ring type burrows predominant at the base. The upper part of hemipelagic units is typically rich in forams and nannofossils, with indistinct bioturbation. The lower contact with the underlying turbidite is usually gradational while the contact with overlying turbidtes is sharp.

Turbidite Facies

Turbidites Facies comprise clay-grade muds and silts with silty sand at the base of a few beds. Their colour range from dark olive grey (5Y6/2) to light olive grey (5Y6/2) with a sharp colour change to pale green, greyish yellow and green (5GY7/2) in the upper part of the bed. This colour change is probably due to oxidation of the sediment (Weaver et al., 1986). In smear slides, no marked mineralogical differences were recognised between the lower, dark olive grey unti and the upper pale green unti in the same turbidite bed. However the lower unit contains 1-5% organic carbon and the upper pale green unit contains less than 0.5% organic carbon (Weaver et al., 1986). Some of the turbidite units are white in colour and are composed of calcareous silt and silty clay. These are very difficult to slice.

The bed thickness of these turbidites ranges from 4cm to 205cm, with beds 50cm to 100cm more common. Turbidite constitutes about 90% of the total sediment in these cores. All bads have sharp bases with slight erosion. Some of the beds show a few centimetres of silty sand at the base, followed by apparently homogeneous mud. Most of the beds are bioturbated in the upper (3 to 35cm), with a gradual upward in intensity.

Sedimentary Structures in the Turbidite Facies

It is difficult to identify sedimentary structures visually on the split cores. However, on the thin-slice x-radiographs, these turbidites display a variety of primary structures. Due to soft-sediment deformation, the laminated parts of most of these turbidites are badly distorted and show no clear original depositional features. Nevertheless, the sedimentary structures can be divided into 6 intervals:

Interval 1 (TO) : This structural interval is characterized by cross lamination (Fig. 5a) and usually occurs at the base of the bed or individual sedimentation unit within a compound bed. It is generally associated with slight internal erosion and ranges in thickness from a few mm upto 15cm and constitutes about 3% of the aggregate turbidites thickness (based on the x-radiograph data). It may occur more than once in an apparently single turbidite bed. This interval is equivalent to the TO interval of the mud turbidite model, but is usually thicker than TO in the standard mud turbidite model (Stow and Shanmugam, 1980).

Interval 2 (contorted lamination): Interval 2 is characterized by syndepositional deformed laminae. In some cases, distortions have been caused by escaping waters (Fig. 5b). it consists of a variety of contorted laminae, silt pseudonodules, variously folded laminae, loadcasts and mudclasts. Interval 2 varies in thickness from 5cm to 42 cm and constitutes about 13.5% of the total turbidite beds. Due to the highly deformed nature of this interval, it is not usually possible to identify precisely the original nature of the lamination. This interval may be correlated with the TO to T5 intervals of the mud turbidite model (Stow and Shanmugan, 1980). Where it occurs in the lower part of turbidite beds, this interval is silt-rich while in the upper part of the beds, it is mud-rich, with indistinct deformed laminae.

Interval-3 (T3) : This structural interval is characterized by parallel silt laminae (Fig. 6a). Interval 3 comprises a set of fine and regular laminae of variable thickness ranging from 0.5cm to 7cm. It constitutes about 3.9% of the aggregate thickness of turbidite examined. The thickness of the individual laminae rarely exceeds 1mm. This interval is usually structurally and texturally graded, showing a gradual upward decrease in thickness and resolution of the laminae. This interval is equivalent to the T3 interval of the mud turbidite model (Stow and Shanmugan, 1980).

Interval-4 (T4) : Interval 4 is characterized by indistinct and/or discontinuous parallel lamination (Fig. 6b). It is very laminated, and individual laminae are usually thinner than the laminae in interval 3. The thickness of this interval ranges from 0.5cm to 16cm and constitutes about 5.4% of the aggregate turbidites. Like interval 3, it is graded upwards into homogeneous mud. This interval corresponds

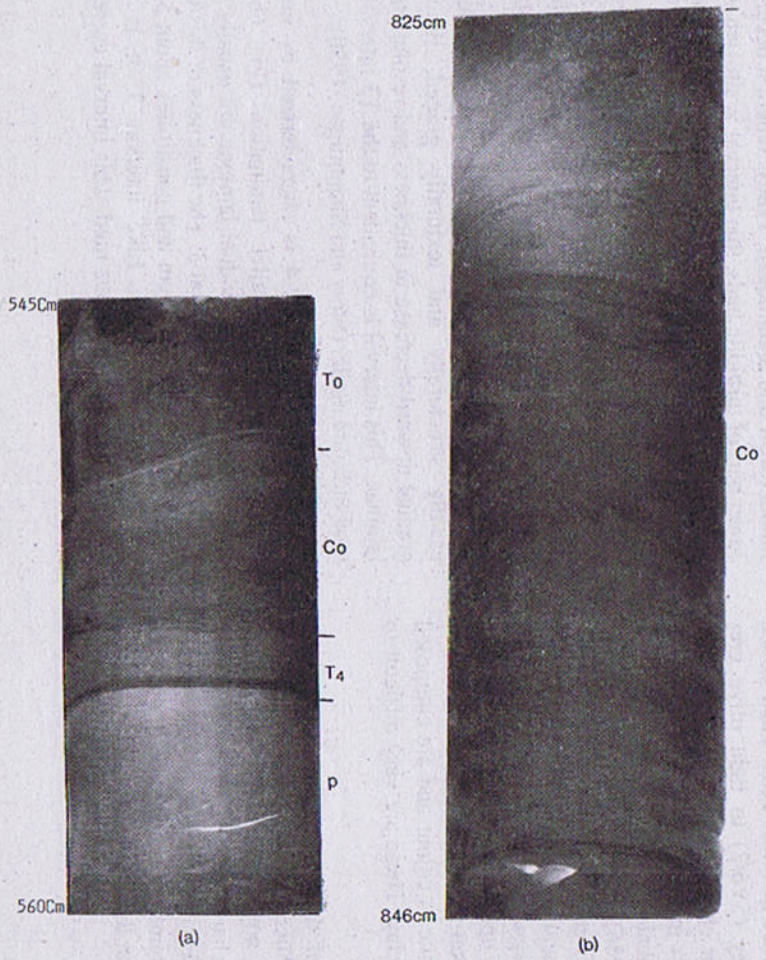

Fig. 5 (a) X-radiograph of Core D11800 (545-560cm) showing T_o Interval (erosive base and internal cross lamination).(b) X-radiograph of Core D11813 (825-846cm) showing contorted lamination. Note water escape features (E).

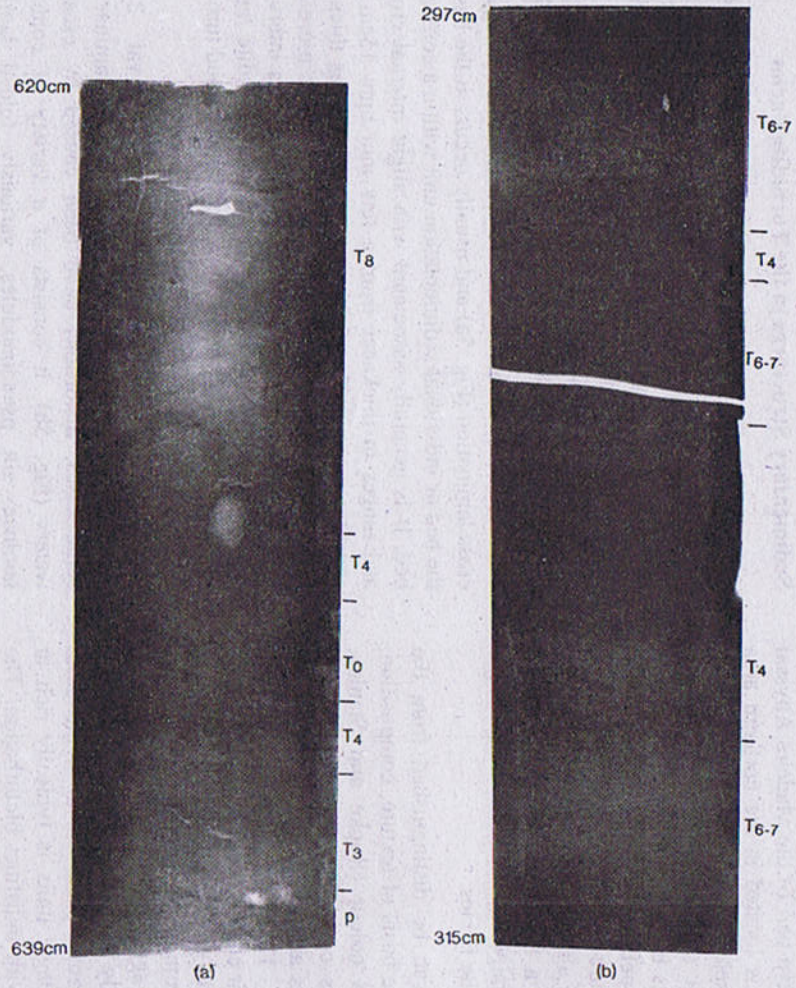

Fig. 6 (a) X-radiograph of Core D11813 (620-639cm) showing parallel lamination (T_3) at the base. (b) X-radiograph of Core D11800 (297-314cm) showing faint lamination (T_4). Note alternations of (T4) and uniform mud (T_{6-7}).

to T4 of the standard mud turbidite model (Stow and Shanmugan, 1980).

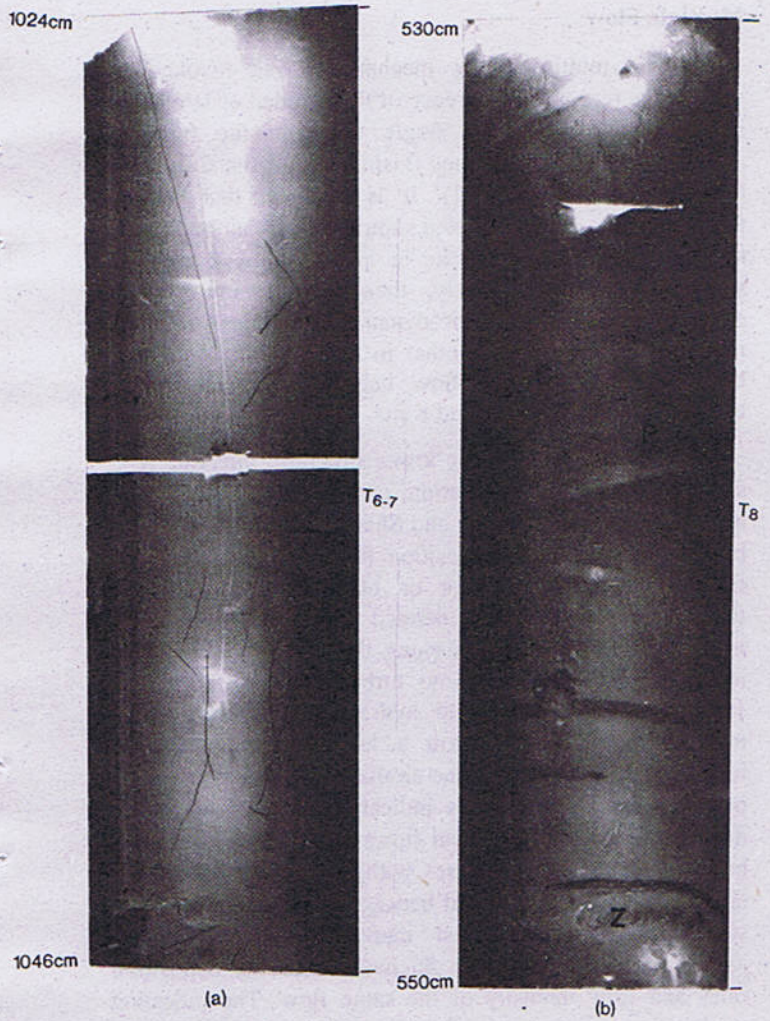

Fig. 7 (a) X-radiograph of Core D11806 (1024-1046cm) showing uniform mud (T_{6-7}).(b) X-radiograph of Core D11806 (532-553cm) showing bioturbated mud (T_8).Note Zoophycos (Z), Planolite (P)? and Chondrite burrows (C).

Interval-5 (T6-7): Interval 5 is represented by homogeneous mud (Fig. 7a). It may occasionally contain fine mud laminae, very tiny silty patches and single silt laminae with irregular vertical spacing. The thickness of this interval is very variable, ranging from less than 4cm up to 170cm and in aggregate, it constitutes the dominant interval of the turbidite beds examined (about 62%). It contains very thin (less than 0.5mm), thread-like pyritized Trichichnus burrows, sporadically distributed and vertical to subvertical to the bedding. This interval is comparable with T6-7 intervals of the mud turbidite model (Stow and Shanmugan, 1980). Precise division of this interval into T6 and T7 intervals is difficult in these turbidites bacause the tiny silty patches and wispy laminae are irregularly distributed within this interval.

Interval-6 (T8): Interval 6 is characterized by conspicuous bioturbation and burrows (Fig. 7b). It occurs in yellow-green, terrigenous mud at the top of turbidite beds. Its thickness is variable, ranging from 3cm to 35cm and constitutes about 12% of the total turbidite beds. At least three types of burrows (trace fossils) may be recognised in this interval. These are Planolites, Chondrites and Zoophycos. Planolites usually are more abundant in the upper part of the interval while Zoophycos is more common in the lower part of the interval. Planolites burrows are subhorizontal or gently inclined to the bedding and are elliptical to subcircular in cross-section, with smooth walls. Chondrites traces are represented by a network of branched (dendritic) burrows, spreading down and out from a central shaft. Zoophycos are horizontal to subhorizontal burrows with back-filled sediment forming concentric (meniscoid) arcs. In most of the turbidite beds, these trace fossils occur together as an assemblage. However, in a few turbidite beds the absence of Planolites and the overlying hemipelagic sediments indicate erosion by the overlying turbidite.

DISCUSSION

Sequences of Sedimentary Structures

The internal organization of the sedimentary structures observed in these turbidites is complex. There is no obvious and consistent vertical sequential arrangement of the sedimentary structures. Many of the turbidite beds show repetition of the same structural interval, sometimes up to four times. This repetition is irregular, and any interval can be repeated with any other interval. However, two types of repetition are more common: (i) repetition between Interval 2 (contorted laminae) and Interval 5 (homogeneous mud, T6-7), and (ii) repetition between Interval 5 and Interval 4 (T4). The first type of repetition is more common in the lower part of the beds whereas the second type is more common in the upper half of the turbidites. Amalgamated intervals may also occur.

Due to this interval variability and the multiple repetition of the sedimentary structures, it is difficult to establish a single representative model for these turbidites. However, a general tripartite vertical sequence may be established;

(a) The lower part of most of the turbidite beds tends to comprise Intervals 1,2 and 3 which may occur in any sequential order.

(b) The, middle part is characterized by multiple occurrences of Intervals 5 and 4.

(c) The top of these beds is typically represented by Interval 6 (bioturbated mud, T8).

Depositional Processes

The internal organization of the sedimentary structures observed in these thick turbidite beds is complex, but the general upward fining from silty bases to muddy topes, the type and general sequence of the sedimentary structures and the general restriction of bioturbation to the tops of these beds all suggest that they were deposited essentially from gravity driven, initially turbulent flows that gradually waned in energy (low concentration turbidity flows).

The most widely adopted mud turbidite model (Stow and Shanmugan, 1980) consists of a series of structures (TO-T8) which reflect gradual deposition from large dilute mud-rich turbidity flows that lose competency with time. However instabilities in the flow behaviour may cause departure from the ideal sequence of the mud turbidite (Stow and Piper, 1984). As mentioned above, mud turbidites from the Madeira Abyssal Plain display complex sequences of sedimentary structures, suggesting very complex hydraulic behaviour of the depositing flows. Two mechanisms are commonly considered to contribute to the complexity and repetition of the sedimentary structures in a single bed. These are reflected or reversed flows, and multiple flows.

Reflected and Reversed Flow

Recently Porebski et al. (1991), discussing the origin of Quaternary mud turbidites from the South Shetland Trench Basin, interpreted the complex nature of sedimentary structural sequences and their multiple occurrences in single turbidite bed as the result of reversal flows. According to this concept, as an elongate turbidity current reaches an adverse slope, part of it is reversed back and then propagate backwards in the opposite direction to the primary flow. Thus a series of series of pulsatory reverse flows are formed, that transport sediment from opposite directions.

The above described mechanism cannot be entirely ruled out for the Madeira units but the following points do not support the operation of this mechanism was during the deposition of these turbidites:

i. There is no clear evidence of reversed paleocurrent flow in the Madeira Abyssal Plain turbidites. Some cross laminated intervals (TO) in these turbidites appear to dip in different directions in different beds. However, this does not necessarily indicates opposite flows because the cross laminated beds could be constructed from curved ripple-forms, successive oblique sections of which may than display apparently opposite foreset dips.

ii. Solitary-type reverse waves are usually low energy flows. They are unlikely to have produced the internal erosive surfaces within the TO interval seen in the Madeira Abyssal Plain turbidites (up to 2cm of erosive relief).

Multiple Flow

The multiple flow mechanism was invoked to explain the repeated occurrence of the "graded or laminated beds" deposited from a single event in the turbidite recovered from the Guyamas Basin, Gulf of the California (Einsele and Kelts, 1982). It is believed that several turbidity flows can be initiated simultaneously along a basin margin during an earthquake or associated with massive slope failure. Subsequently, these flows may ecquire different densities and hydrodynamic properties, and thus may interfere with one another in the deeper parts of the basin. The most dense flow behave as an underflow turbidity current (Einsele and Kelts, 1982).

The repetition of the lower structural intervals (e.g. scoured bases, cross lamination, parallel lamination) of the mud turbidite model (Stow and Shanmugan, 1980) in these beds, tends to favour deposition from pulsatory turbidity flows. During earthquakes or other widespread slope failures, several slump-generated mass flows may be initiated at different points along the open margin. These mass flows may evolve into turbidity flows (Hampton, 1972), varying in size and hydraulic behaviour, which ultimately coalesce to form a large volume flow but involving several pulses. The similarity in the composition of these repeated intervals indicates that they were not deposited from nearly coeval flows from different sources but probably represent pulses within one large flow. The erosive junctions within and between some of the repeated structural intervals suggest marked variations in the hydraulic of the pulses or fluctuations in the deposition rates and flow intensity of the same flow. The pulsating mode of transport responsible for these sediments is also evident from truncated burrows within the repeated intervals, which implies that sufficent time existed for benthic organisms to excavate (escape) burrows before the next pulse arrived. The highly deformed nature of some laminated intervals and the presence of loadcasts also are consistent with very rapid deposition.

The middle part of the majority of these beds comprises a homogeneous mud (Interval 5, T6-7) which alternates irregularly with indistinctly laminated sediments (Interval 4, T4). These homogeneous mud intervals are interpreted as the deposits of dilute residual flows with relatively rapid fallout. This rapid deposition is evident from the absence of bioturbation and the presence of diffuse silty patches, suggesting insufficient time for silt to be segregated. The indistinctly laminated intervals probably have been deposited by sorting processes within the flows, similar to those described by Stow and Bowen (1980), rather than by contour currents. Contour currents are

generally associated with marginal slopes (McCave, 1984) and are unlikely to occur in the central parts of an abyssal plain.

The uppermost bioturbated mud (Interval 6, T8) of the turbidite beds is interpreted to have been deposited from the tail of the turbidity flow, and is associated with very slow fallout rates.

Some turbidite beds (e.g. turbidite t of D11806, Fig. 5.12) comprise a thick (up to 170cm) homogeneous mud with a few centimetres of silty sand at the base, displaying cross lamination. This basal silty sand layer suggests that deposition took place under bottom traction conditions from a waning flow (Stow and Shanmugam, 1980) while the overlying thick homogeneous mud appears to have been deposited from a dense non-turbulent flow that prevented individual particle settling (McCave and Jones, 1988). Probably, in this case, the depositing flow initially lost energy rapidly, allowing silts/fine sands to be segregated at the base, followed by sudden suppression of the turbulence and relative increase in flow density. Under these hydrodynamics, conditions, free settling of the coarser particles is prevented by interparticle forces. It is equally possible that this thick homogeneous mud was created by the ponding of flows against the base of the opposite slope of the Madeira basin.

CONCLUSIONS

On the basis of distinctive sedimentary structures and general characters, two main lithofacies have been recognized which include mud turbidites and hemipelagites. Mud turbidites are very thick and show surprisingly irregular organization of sedimentary structures, suggesting deposition from unstable, possible interfering turbidity flows. The hemipelagites consist of foraminiferal and nonnofossil oozes and are poorly sorted, moderately to highly bioturbated, mottled with ring type burrows.

ACKNOWLEDGEMENTS

This paper is based on part of the research work carried out by first author for his ph.D thesis under the supervision of Professor Gilbert Kelling at the University of Keele, England. ASK is grateful to the Ministry of Science and Technology, Government of Pakistan for awarding scholarship.

REFERENCES

Chmelik, F.B., 1967. Electro-osmostic core cutting. *Marine Geol.* **5,** 321-325.

Einsele, G. and Kelts, K., 1982. Pliocene and quaternary mud turbidites in the Gulf of California: sedimentology, mass physical properties and significance. In Initial Reports of the Deep Sea Drilling Project, :(Curray, J.R., Moore, D.G. et al. Eds.), US. Government Printing Agency, Washington, **64,** 511-528.

Hampton, M.A., 1972. The role of subaqueous debris flow in generating turbidity currents. *Jour. Sed. Pet.* **42,** 775-793.

Mccave, I.N., 1984. Erosion, transport and deposition of fine-grained marine sediments. In: Fine-Grained Sediments: Deep-Water Processes and Facies Stow, D.A.V. and Piper, D.J.W. Eds. *Geol. Soc. London, Spec. Publ.* **15,** 35-70.

Mccave, I.N. and Jones, K.P.N., 1988. Deposition of ungraded muds from high-density non-turbulent turbidity currents. *Nature,* **333,** 250-252.

Porebski, S.J., Meischner, D. and Corlich, K., 1991. Quaternary mud turebidites from south Shetland Trench (West Antartica): recognition and implications for turbidite facies modelling. *Sedimentology,* **38,** 691-715.

Stow, D.A.V. and Bowen, A.J., 1980. Physical model for the transport and sorting of fine-grained sediments by turbidity currents. *Sedimentology,* **27,** 31-46.

Stow, D.A.V. and Piper, D.J.W. 1984., Deep-water fine-grained sediments: facies models. In: Fine-Grained Sediments: Deep-Water Processes and Facies., Stow, D.A.V. and Piper, D.J.W. Eds. *Geol. Soc. Publ.* **15,** 611-646.

Stow, D.A.V. and Shanmugam, G., 1980. Sequences of structures in fine grained turbidites: comparison of recent deep sea and ancient flysch sediments. *Sediment. Geol.,* **25,** 23-42.

Weaver, P.P.E., Searle, R.C. and Kuijpers, A., 1986. Turbidite deposition and origin of the Medeira Abyssal Plain. In: North Atlantic Palaeoceanography, Summerhayes, C.P. and Shackleton, N.J. Eds. *Geol. Soc. London, Spec. Publ.* **21,** 131-143.

Geol. Bull. Punjab Univ. 36, 2001

THE FEASIBILITY OF THE RESISTIVITY METHODS AND HYDROCHEMISTRY FOR DETECTING THE SALINE INTRUSIONS IN THE SEDIMENTS OF MORFA BYCHAN AREA, NORTH WALES, U.K.

BY

SAEED AHMED SOOMRO AND LAL BAKHSH BOZDAR
Department of Geology, University of Sindh, Jamshoro.

Abstract:- *To detect the extent of saline intrusions in the sediments of Morfa Bychan area, a small coastal town situated between Criccieth and Porthmadog, North Wales, U.K., combined resistivity, electromagnetic soundings and chemical methods were used.*

A total of thirty one vertical electric soundings (VES) were made at selected sites using Simple Wenner & Offset Wenner arrays and twenty three electromagnetic (EM) soundings were also measured at selected Centres of the sites where previously VES were made in the study area. Several of these soundings were measured adjacent to borehole sites to aid in correlating the geophysical interpretations to chemically detected water quality data. By correlating the interpreted surface geophysical data to water quality data from the boreholes, depth to a bulk resistivity ranging from 8 ohm-m to 35 ohm-m (or chlorides concentration from 250ppm to 500ppm/ a mixing water or transition zone) and depth to a bulk resistivity of 7 ohm-m or less (or 500ppm chloride concentration or more/a saline water zone) could be mapped in an unconfined aquifer.

The permeability values of the sediments by field and laboratory tests gave additional supporting data.

The study revealed that combined electrical and chemical observations provide a dependable means for the detection and mapping of saline intrusions and that the aquifer in the area has been intruded and the extent of saline intrusions is a function of permeability, volume of fresh water, sand dunes and bed rock available to prevent inland movement.

INTRODUCTION

The application of vertical electric soundings and electromagnetic soundings to detect saline-fresh water interface is based on the fact that materials saturated with saline water represent much better "conductors" than similar materials filled with fresh water. However, the accuracy of the electrical methods depend on the geological subsurface conditions, as the presence of other good conducting sediments, such as intercalated clay layers, can affect the correct interpretations of electrical data. Nevertheless, this disadvantage can often be overcome by increasing the number of the electrical soundings and constructing vertical sections of the area. From the manner in which the resistivity values vary over large areas, it is then possible to determine whether clay layers are present or not.

The goal of this study pertaining to the Morfa Bychan area, U.K. (Fig.1), was to relate vertical electric and electromagnetic soundings to existing boreholes or to boreholes drilled for this purpose. The chloride concentrations of the water samples collected from the boreholes, were determined and simultaneously correlated with the formation resistivities & laboratory measurements of some sediment parameters from the site were also made to examine the effect of permeability on saline intrusions (Soomro, 1993).

Use direct current resistivity methods is not new to water resources investigations. Swartz (1937) used this technique for locating fresh water lenses in salt water bodies on the Hawaiian islands. Since then, much resistivity work on the detection of fresh salt water interface has continuously been done in other parts of the world (Zohdy et al., 1974; and Gorhan, 1976).

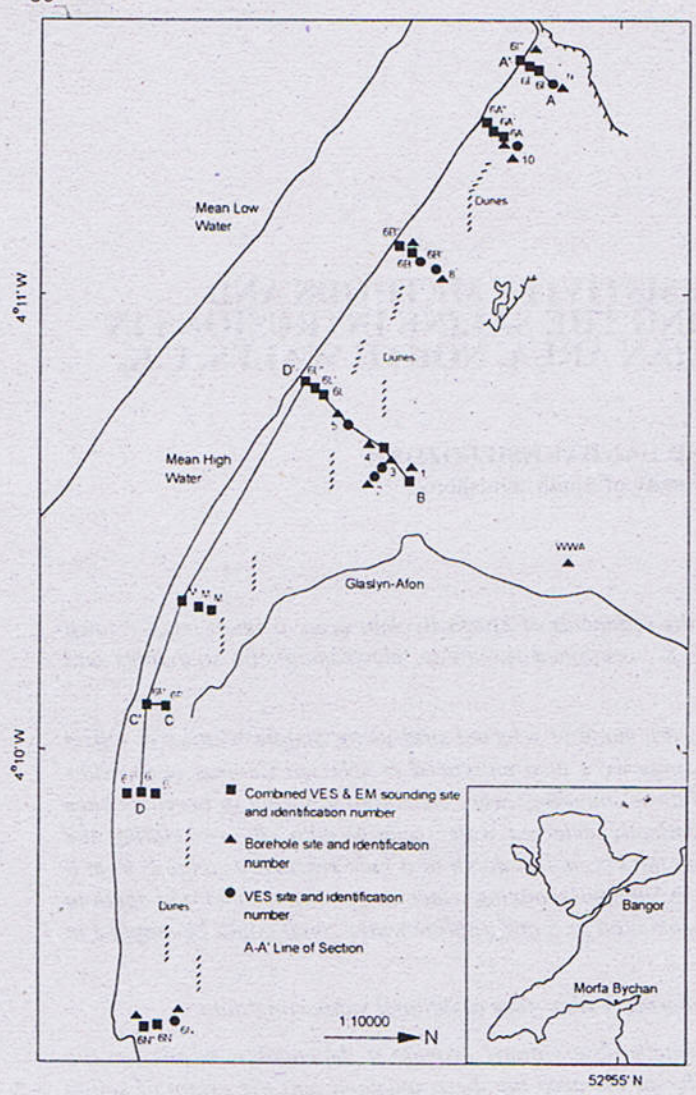

Fig.1 Map showing location of the study area, Morfa Bychan.

METHODS AND THE INSTRUMENTATION

Resistivity Methods

In the present study the techniques have been limited to one of the most commonly used Wenner electrode array, although the Wenner at some sites has made use of the Offset system (Barker, 1981).

The Offset Wenner system which has several advantages over both the Schlumberger and conventional Wenner system developed at the University of Birmingham, was also used. By this system. It is possible to overcome the lateral resistivity variations, which are not detectable by other method. It is also less time consuming. ABEM's battery operated resistivity meter, the Terrameter SAS 300.was used in measurements of all the vertical electric soundings (VES) taken under different arrays.

The electromagnetic survey was carried out with the Max-Min 1-8 (commonly known as Apex Max-Min) portable instrument. It permits the choice of eight octavely spaced operating frequencies i.e. 110, 220, 440, 880, 1760, 3520, 7040 and 14080HZ. To arrive at the much needed parameters, the most commonly used transmitter powered operating mode, MAX 1 (also known as the horizontal loop mode) is used; it is an effective mode in obtaining the resistivity and thickness of the subsurface layers.

Interpretations

Instead of the auxiliary point method (Ebert, 1943; Orellana and Mooney, 1966) for the approximate interpretation of resistivity soundings through curve matching, interpretation of VES soundings is done by computer software using Bossix and EM soundings by EMIXMM programmes both produced by the Interpex Ltd.

Conductivity of Groundwater

As conductivity is preferred rather its reciprocal resistivity, because the former increases with salt content, the conductivity of groundwater samples is determined for all the water samples obtained from most of the VES sites. The conductivity of each groundwater sample so obtained is used to calculate total dissolved solids (TDS).

The conductivity of groundwater, samples is determined by a conductivity meter called Aqua Lytic, which automatically gives water conductivity in ms/cm at a reference temperature of 25°C.

Chemical Methods to Determine Chloride Ions in Groundwater

Chloride in groundwater sample is most conveniently determined using atomic absorption spectroscopy (AAS). The first step is to quantitatively precipitate silver chloride by the addition of a known amount of sliver nitrate. The amount of chloride in the original sample is then known by the determination of excess sliver in the solution, when the preciptated silver chloride has been removed (Recichel, 1969: and Truscott, 1970).

AQUIFER RESISTIVITY ITS CORRELATION TO CHLORIDE CONCENTRATIONS

The type of dissolved solids cannot be resolved through the measurement of fluid conductivity. To derive more quantitative information about concentration of dissolved solids, an attempt has been made to correlate formation resistivities measured through direct resistivity methods to chloride concentrations.

First, water samples from 12 boreholes were collected and chemically analysed for chloride anions. The electrical conductivity for all the samples were determined and it ranged from 240 to about 100000 µs/cm at 25°C. Table 1 enlists all the details of the data obtained from the boreholes and with analysis carried thereon. The relation between chloride concentration and water conductivity on samples from boreholes was investigated. The data obtained from the site is summarized in Fig. 2. Each dot represents one sample. The correlation coefficient is equal to 0.999.

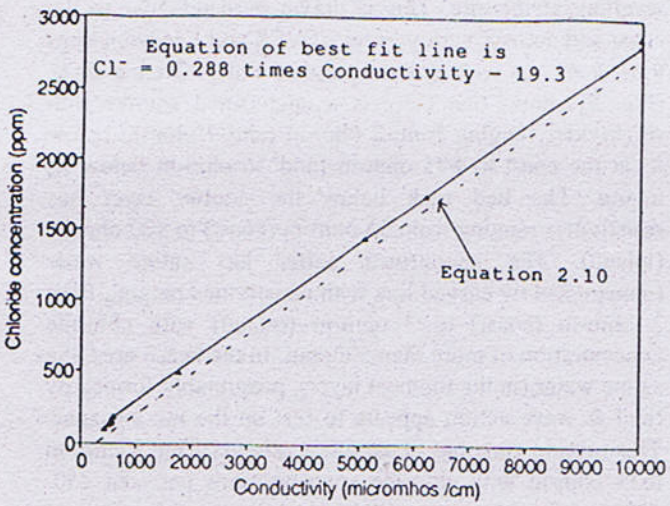

Fig.2 Relation measured between chloride concentration and fluid conductivity on water samples from Morfa Bychan area.

On the basis of Fig. 2, 500ppm chloride concentration corresponds to a fluid conductivity of about 1900 µs/cm or a fluid resistivity of about 5 ohm-m and 250ppm chloride concentration corresponds to a fluid conductivity of about 950 µs/cm or a fluid resistivity of about 10 ohm-m. This is not far away from the information summarized by Kwader (1986), who has put 500ppm chloride concentration corresponding to a fluid resistivity value of 6 ohm-m and 250ppm chloride concentration to a fluid resistivity value of 9 ohm-m. Here specially 500ppm chloride concentration has been selected because boreholes/wells that reach chloride concentration of 500ppm are considered to be significantly intruded with seawater (Goswami, 1968: and Mills et al., 1988), and is taken as a basis for the fresh-salt water interface. In the present study on the other side 250ppm chloride concentration, which also correspond to a measured bulk resistivity value of 35 ohm-m (Table 1), is selected as the basis of mixing zone (transition zone).This value is in more agreement to Mills and Ryder (1977); and Stewart et al., (1982) who have put thelower limit of the mixing zone between 200-250ppm chloride concentration than Goswami (1969) who puts the lower limit at 300ppm chloride concentration.

Table 1

Chemical Analysis of Groundwater for chloride Ions

B.H. No.	EC µs/cm at 25c	Estimated Fluid Resistivity (ohm-m)	Measured Aquifer Resistivity (ohm-m)	TDS (ppm)	Chlorides (ppm)
VS 1	421	24	95	270	103
VS 2	502	20	85	322	129
VS 3	530	19	87	340	136
VS 4	518	19	86	332	129
VS 5	600	17	55	484	180
VS 9	582	18	76	360	146
VS 6A"	3200	03.2	06	2048	880
VS 6A"	5480	02	04	3507	1402
VS 6B"	4922	02.1	04	3150	1450
VS 6B"	6600	01.5	03	4224	1820
VS 6I"	9980	01	02	6387	2870
VS 6J"	1800	06	12	1152	488

To correlelate formation resistivities to chloride concentrations, the results of the interpretation of VES measurements are compared with the chloride concentration data of groundwater samples obtained from certain depths in the boreholes.and by carefullty selecting resistivity sounding results of good quality and representative of the regional hydrologic regime, some six data points were selected for the study area. These data points are shown in Fig. 3. This figure is used for converting the aquifer resistivity into the chloride concentration of the groundwater at the location of measurement. On the basis of this figure, an aquifer resistivity of about 7 ohm-m is expected to correspond to a chloride concentration of 500ppm. This value is nearly in agreement with the work of Mills et al., (1988) and Hoekstra et al., (1990) who have shown it to correspond to a bulk resistivity of 8 ohm-m.

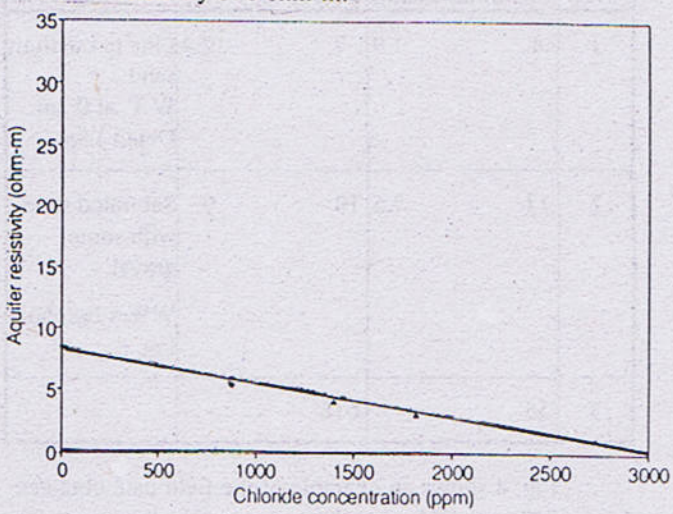

Fig.3 Relation between chloride concentration and aquifer resistivity in selected borewells

DATA ACQUISITION AND REDUCTION

In the present study, the site of investigation, Morfa Bychan area is a small coastal town lying about 2.5 miles to the west of porthmadog and on the northern extremity of Cardigan Bay, North Wales, U.K. (Fig. 1). This work was carried out in the year 1991-92 at this site. The area is bounded to the east and south by coastal sand dunes and to the north and west by low lying relatively marshy ground drained by open ditches. A small river Afon Glaslyn flows through the area. The site consists of granular material mostly sand, miner gravel, boulder clay with intrusive igneous rocks at the base. As at Morfa Bychan there is a single unconfined aquifer in the area which is in direct contact with the sea all along the coast.

Average rainfall per year in year 1991 and 1992 was 925mm. Using Cooper et al., (1964) equation, an approximate rate of flow of the fresh water to the coast is estimated to be $5m^3$/Day/m.

Thirty one VES soundings were made at selected sites (Fig. 1) with the ABEM's Terrameter resistivity meter. Simple Wenner and Offset Wenner arrays were used up to the maximum electrode spacings ranging from 80m to 150m for the Simple Wenner array and 64m to 128m for the Offset wenner array. Twenty three electromagnetic soundings were also made at the selected centres of the sites where previously VES soundings were made, using Max-Min 1-8 portable equipment. The interpreted results are given in Table 2.

Table 2
Vertical Electric & EM Soundings 61" interpreted data with geological log, Morfa Bychan area.

Layer No.	VES Sounding R(ohm-m)	Th.(m)	EM Sounding R(ohm-m)	Th(m)	Geological Drill Log
1	4	1.9	7	2.4	Fine to medium sand. W.T. at 0.3m. Depth).5m.
2	12	7.5	10	9	Saturated sand with some gravel. WWA borehole log.
3	55	-	618	-	-

Fig. 4 shows an example of the field data obtained from VES and EM soundings at site 61` together with mathematically fitted curves via the software models alongside their equivalence. The shape of the curves indicate that the current has passed through geoelectric layers. The model of VES sounding (4a) has good agreement with the model of EM sounding (4b). Table 2 shows the comparision of the geological drill log in the hand augered hole at site 61` and the Welsh Water Authority (WWA) drilled log in the area (Fig. 1) with the interpreted results of the VES & EM soundings carried out at the same site.

A geoelectric section Figure 5 A-A` has been drawn after taking into account the ground surface levelling at the site. This is drawn perpendicular to the coast and acrosss various sites of VES and EM soundings 9,61 & 61" as well as hand augered holes. Section A-A` (Fig. 5) shows that there is a unconfined aquifer with resistivities ranging from 2 ohm-m (and 7 ohm-m below it) at the coast to 895 ohm-m (and 76 ohm-m below it) inland. The bed rock below the aquifer layer has resistivities ranging from 55 ohm-m (coast) to 400 ohm-m (inland). The unconfined aqifer has saline water (demarcated by curved line with resistivities ranging from 2 ohm-m (coast) to 7 ohm-m (inland) with chloride concentration of more than 500ppm. In the beach area, the saline water (in the topmost layer), presumably formed by tidal & wave action appears to rest on the mixing zone. This mixing zone has resistivities ranging from 8 ohm-m to35 ohm-m with chloride concentrations between 250-500ppm,. Another curved line drawn in the figure, shows that the mixing zone separated from fresh water. The saline water zone & mixing zone abruptly end at the seaward foot of the sand dunes, which suggests that the large amount of fresh water regularly received by the aquifer from rainwater prevents the saline water from penetrating further inland. It is evident from the figure that the fresh water gradient is towards the sea.

Two more geoelectric sections B-D` & C-C` (Fig. 1) are also drawn perpendicular to the coast, wheras the fourth & the last section D-D` (Fig. 1) is drawn parallel to the coast.

The last stage of the detection of the saline-fresh water interface is the construction of the saline-fresh water interface contour maps in order to detect the extent to which saline water has intruded inland. All the geoelectric sections previously discussed have been used in the construction of these maps of the study area. The maps (Figs. 6 and 7) show the extent of contamination and saline zones.

Permeability of the Sediments: Guelph permeameter tests in the field and grain size & constant head permeameter tests in the laboratory were used to calculate the permeability of the sediments. Table 3 Permeability values measured or estimated by different methods have been summarized.

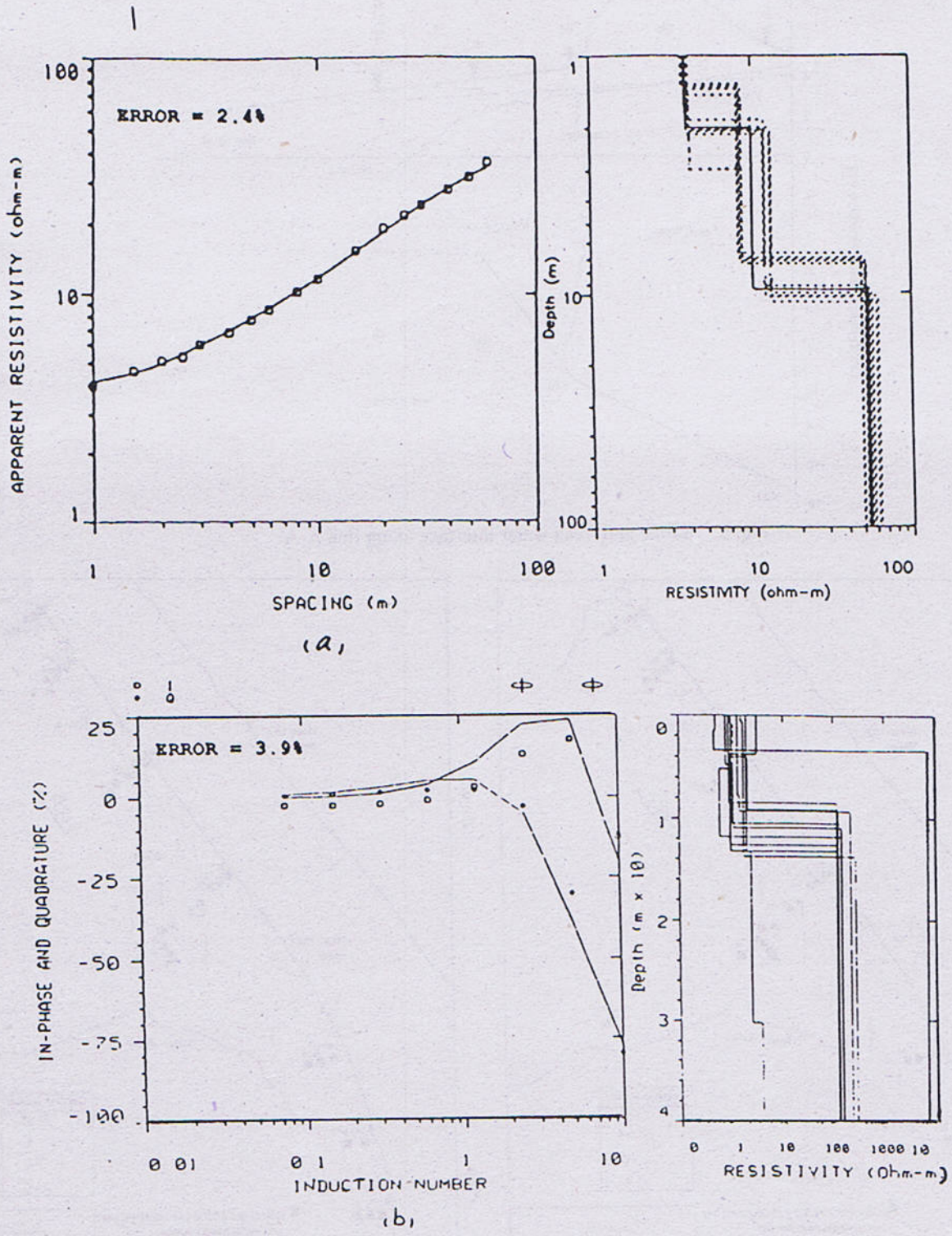

Fig.4. Vertical electric sounding curve (a) and electromagnetic sounding curve (b) at site (6I') based on field data points, alongside their equivalence curves.

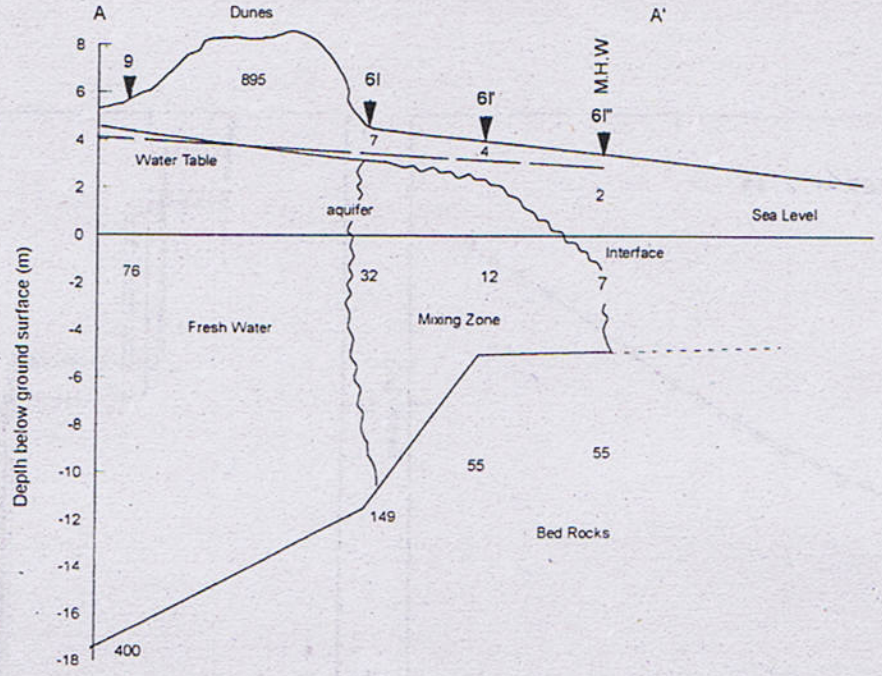

Fig. 5. Saline and fresh water interface along line A-A'.

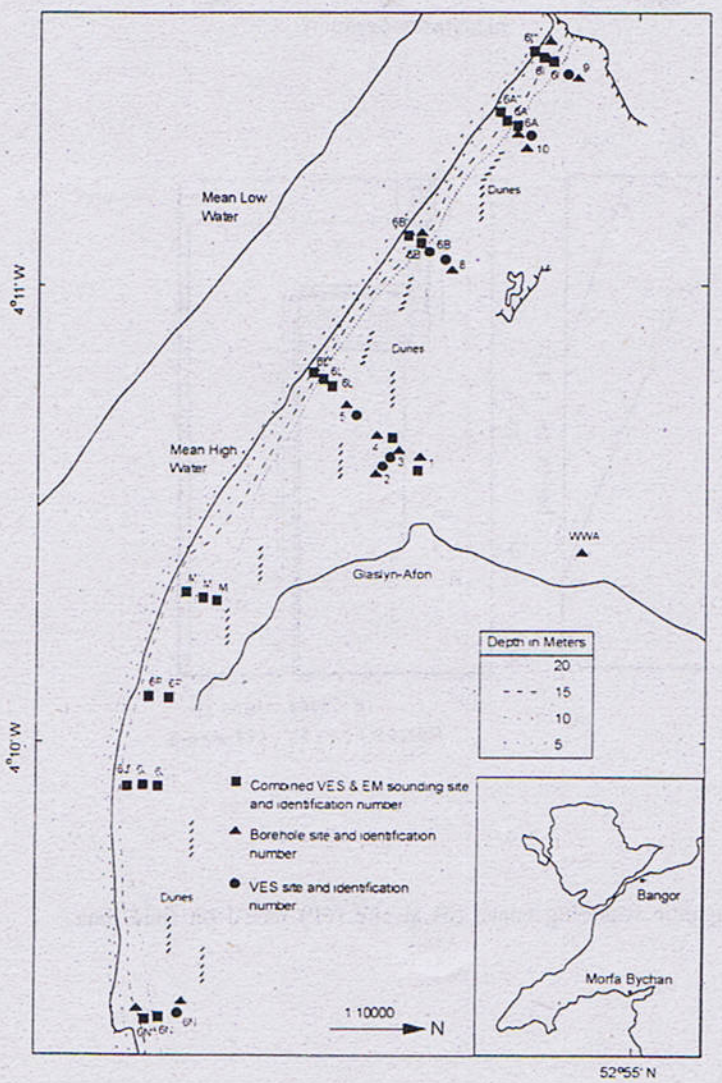

Fig. 6. Depth to the bulk resistivity of les than 35 ohm-meters (or more than 250ppm chloride concentration), Morfa Bychan.

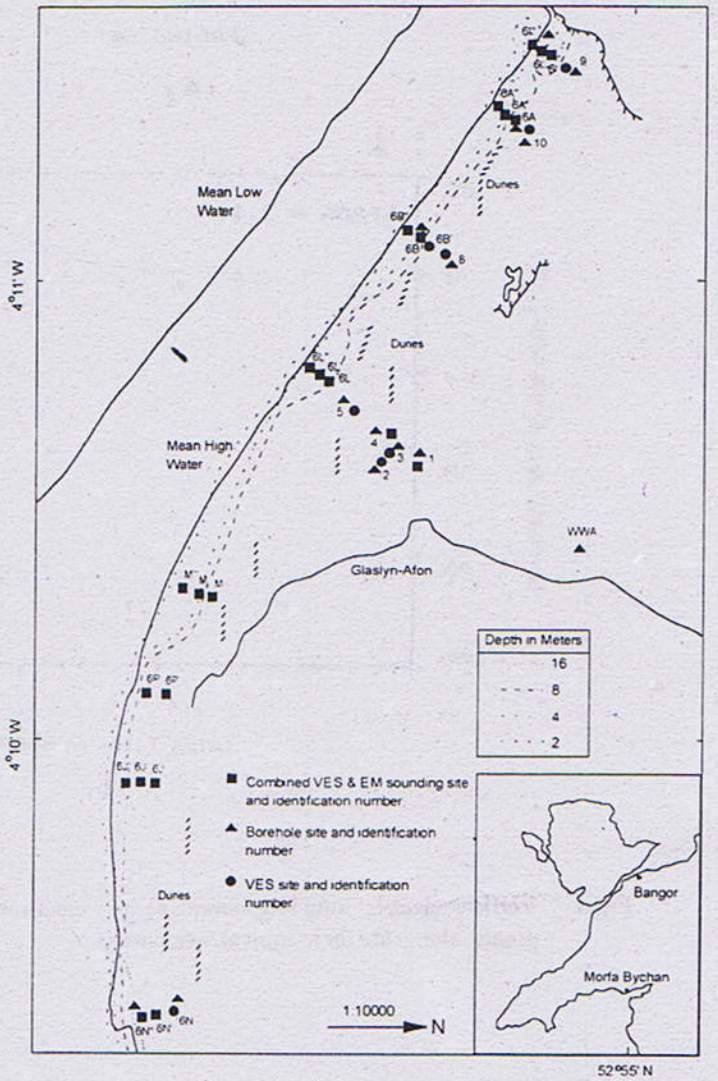

Fig.7 Depth to a bulk resistivity of less than 7 ohm-meters (or more than 500ppm chloride concentration) Morfa Bychan.

Table 3.
Shows a list of the permeability values measured or calculated by different methods.

Methods	Permeability (m/sec) Min.	max.
1. By Guelph permeameter (field test)	7.5×10^{-3}	1.0×10^{-3}
2. Constant head permeameter (laboratory test)	1.0×10^{-4}	3.2×10^{-4}
3. Grain size (Hazen's formula)	1.1×10^{-4}	3.6×10^{-4}
4. Grain size (Kozeny-Carman)	1.2×10^{-4}	2.9×10^{-4}
5. By using electrical formation factor.	2.4×10^{-4}	

DISCUSSION

It is observed that the continuous supply of fresh water in Afon (river) Glaslyn from upstream restricts the saline intrusions to a greater depth as well to the narrowest strip as compared to the coastal area surrounding the Afon Glaslyn. Sand dunes in the area also prevent the inland advance of the saline intrusions as the heavy rainfall is quickly infiltrated towards the sea, which helps in maintaining the fresh water gradient towards the sea, as D' Andrimont (1905) and Hubbert (1940) have shown.

The permeability values are more of moderate magnitude and thus this is another important reason in minimizing the rate of landward advance of intruding saline water, as Howard (1987) has shown.

It is also observed that the Afon Glaslyn's present course still lies along its old route and there has been no deviation with the passage of time.

CONCLUSIONS

Electrical resistivity depth probing (VES), electromagnetic soundings (EM) and chemical tests on groundwater samples obtained from boreholes indicate the existance of a saline-fresh water interface and zone of mixing in the study area.

The extent of saline intrusions is a function of permeability and the volume of fresh water (either from rainfall or river flow or both) available to prevent inland movement; it is also a function of the availability of any surface feature like sand dunes or any sub-surface natural barrier such as bed rock.

Geophysical observations provide dependable means for the detection & mapping of saline intrusions.

A bulk resistivity of 7 ohm-m or less & chlorides of 500ppm or more defined saline groundwater and the zone of mixing water (transition zone) was defined by resistivities ranging from 8 ohm-m to 35 ohm-m with chlorides from 250ppm to 500ppm.

ACKNOWLEDGEMENTS

Special thanks are due to Professor Denzil Taylor Smith, Head of School of Ocean Sciences, University of Wales, Bangor, U.K, for his valuable supervision, guidance and permission to carry research work in the Laboratories of the School of Ocean Sciences, University of Wales, Bangor. U.K.

REFERENCES

Barker, R.D., 1981. The offset system of electrical resistivity sounding and its use with a multicore cable. *Geophy Prospect,* **29,** 128-143.

Cooper, H.H.Jr., Kohout, F.A., Henry, H.R. and Glover, R.E., 1964. Seawater in coastal aquifers. *U.S. Geol. Surv. Water Supply Paper,* **1613-C,** C12-C32.

D. Andrimont, R., 1905. Note preliminaire sur une nouvelle methode pour etudier experimentalement l'allure des neppes aquifers dans les terrains permeables en petit. *Soc. Geol. Belg. Au., Liege,* **32,** 115-120.

Ebert, A., 1943. Grundlagen zur Auswertung geoeleektrischer Tiefenmessungen en. Beitr. *Angew. Geophys.* **10,** 1-17.

Gorhan, H.L., 1976. The determination of the saline-fresh water interface by resistivity soundings. *Bull. Assn. England Geol.,* **13,** 163-175.

Geoswami A. B., 1968. A study of salt water encroachment in the coastal aquifer at Digha, Midnapore district, West Bengal, India. *Bull. Inter. Assoc. Scio. Hydrol.,* **13(3),** 77-87.

Hoekstra, P. and Blohm, M.W., 1990. Case Histories of time domain electromagnetic soundings in environmental geophysics. *Geotech. Environ. Geophys.*, **11,** 1-15.

Howard, K.W.F., 1987. Beneficial aspects of seawater intrusion. *Ground Water,* **25(4),** 398-406.

Hubbert, M.K., 1940. The theory of groundwater motion. *Jour. Geol.,* **48,** 785-944.

Kwader, T., 1986. The use of geophysical logs for determining formation water quality. *Ground Water,* **24,** 11-15.

Mills, L.R. and Ryder, P.D., 1977. Salt water intrusion in the Floridan aquifer, coastal Citrus and Hermando Counties, Florida, 1975. *US geol. Surv. Water Resour. Invest.,* 77-100.

Mills, T., Hoekstra, P., Blohm, M.W. and Evans, L., 1988. Time domain electromagnetic soundings for mapping seawater intrusion in Monterey county, CA. *Ground Water,* **26,** 771-782.

Orellana, E. and Mooney, H.M., 1966. Master tables and curves for vertical electric soundings over layer structures. *Interciencia, Madrid,* **34.**

Reichel, W., 1969. *Analyt. Chem., Acs. L.,* **41(13),** 1886-1969.

Soomro, S. A., 1993. Detection of Saline Intrusions in Coastal and Estuarine Sediments. Unpubl. Ph.D thesis. University of north Wales, Bangor, U.K.

Stewart, M., Lizanec, T. and Layton, M. 1982. Application of DC resistivity surveys to regional hydrgeologic investigations, collier county, Florida. South Florida Press, West Palm Beach.

Swartz, J.H., 1937. Resistivity studies of some salt water boundries in the Hawaiian Islands. *Trans Amer. Geophys Union., Truscott, E.D., 1970.* Ibid., **42(13),** 16557.

Zohdy, A.A.R., Eaton, G.P. and Maybey, D.R., 1974. Application of surface geophysics to groundwater investigations. *US. Geol. Surv.,* **116.**

Geol. Bull. Punjab Univ. 36, 2001.

CONODONTS FAUNA FROM COL DES TRIBES, MONTAGNE NOIRE, FRANCE

BY

FAZLI RABBI KHAN
National Centre of Excellence in Geology, University of Peshawar.

AND

SARFRAZ AHMED
Institute of Geology, University of the Punjab, Lahore-54590, Pakistan.

Abstract:- *The Study of Conodonts in a 37 meters thick stratigraphic section of the Griote Formation at Col des Tribes (Mont Peyroux), was carried out. As a result of the analysis, 23 species of the genera Ancyrodella, Ancyrognathus, Icriodus, Palmatolepis and Polygnathus were discovered which indicate the zones of Rhenana, Traingularis, Crepida, Rhomboidea and Marginifera.*

INTRODUCTION

The Col de Tribe, (Mont Peyroux) MONTAGNE NOIRE is located at Lambert, X=660.50, Y=132.75,topographic sheet of 1:50,000, the Saint Chining, fig. 1and fig1a. The purpose of the present study is to document conodont fauna, interpret age and depositional environments of the rocks.

The zonal conception resembles that of the Late Devonian standard conodont zonation of Sandberg & Ziegler (1973), to a very high degree but these but two of the main zones ie Rhenana and Triangularis are marked by the appearance of morphotypes

Lys & SERR (1957a.d) were the first to discover conodonts from a red calcareous zone of Col de Tribe at Coumiac and Saint-Nazaire of Ladarez. Further discoveries were made from Pie de Bissous, Cabrieres (ZIEGLER1959), Escondologue (REMACK-PETITOT, 1960) and Caunes Minervois and dans (FEIST& SCHONLAUB. 1973, 1974). They were followed by FEIST & KLAPPER (1985), FETST & SCHONLAUB & BULTYNCK, 1985, KLAPPER, G. (1989), FEIST, 1990. Recently, Schuike (1999) has described an area adjacent to the type sections of Tourrier, Cabrieres. He worked out just the Triangularis and Cripida zones of the La Serre trench and Causses et Veyran sections. It is to be noticed that the species Crepida was discovered for the first time by the author in 1993.See thesis plate 3 fig.6.

LITHOLOGIC SETUP

TheFrasnian and lower Famennien sediments of Serre Formation were deposited in often badly ventilated second order basins formerly laterally adjacent to the carbonate ramp of the Mont Peyroux nappe. The beds are overturned and represent well-oxygenated Carbonates.

The lower member of Serre Formation consists of well-bedded grey limestones, dark grey shales, platy marls, nodular limestone and some black laminated limestone beds. Hematitic fossils may occur in shale and marl horizons and sometimes can be found together with lower Famennian fossils of identical preservation due to hillwash and downhill transport. At the top of the Serre Formation there are typically light to medium grey limestone beds that can contain rich benthic assemblages. Subsequently, there is a return to hypoxic sedimentation simultaneously with the Upper Kellwasser Event. However, organic-rich shales and dark limestone extend up to a level high in the lower Nehdenian which corresponds to the onset of the Famennian regression in many different sedimentary provinces around the world. The overlying Griotte Formation includes either light gray microspantes or more

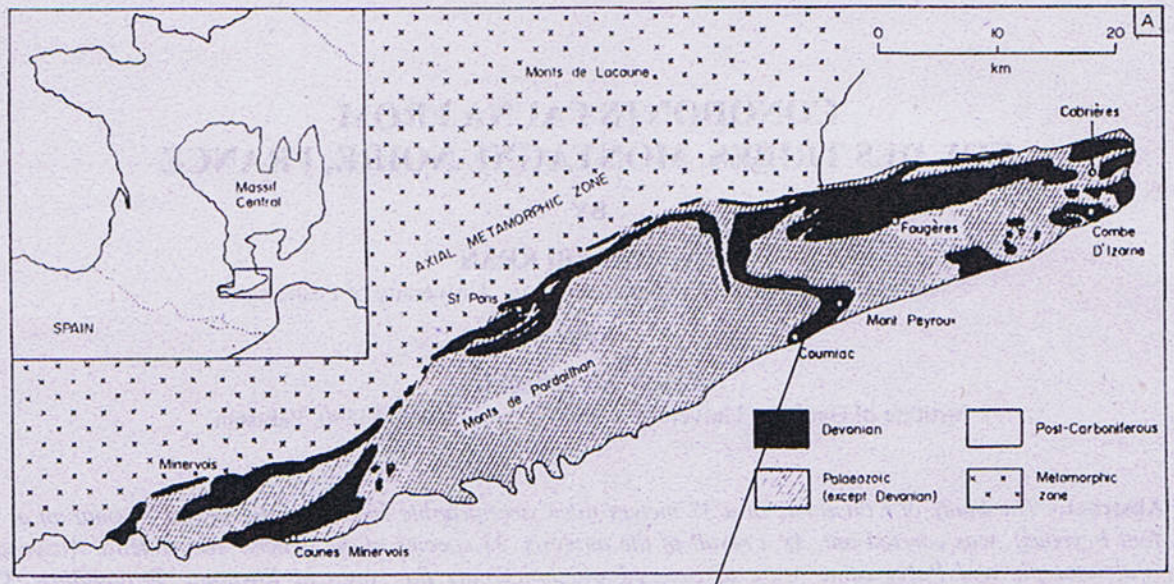

Fig.1. Geographic and geologic map of the study area

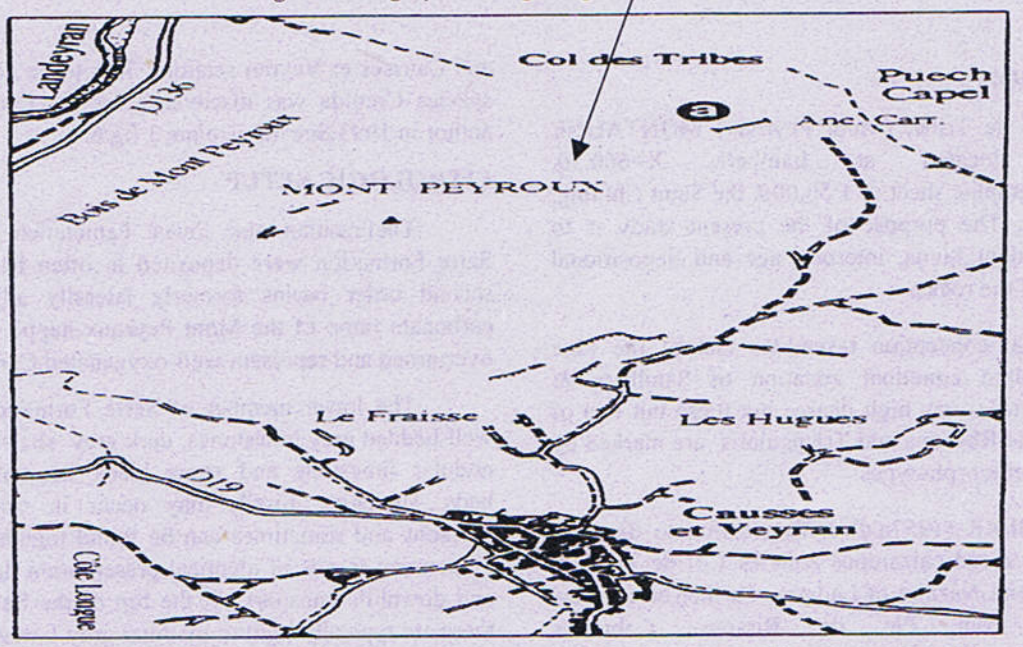

Fig.1a. Road map of the section of Col De Tribe

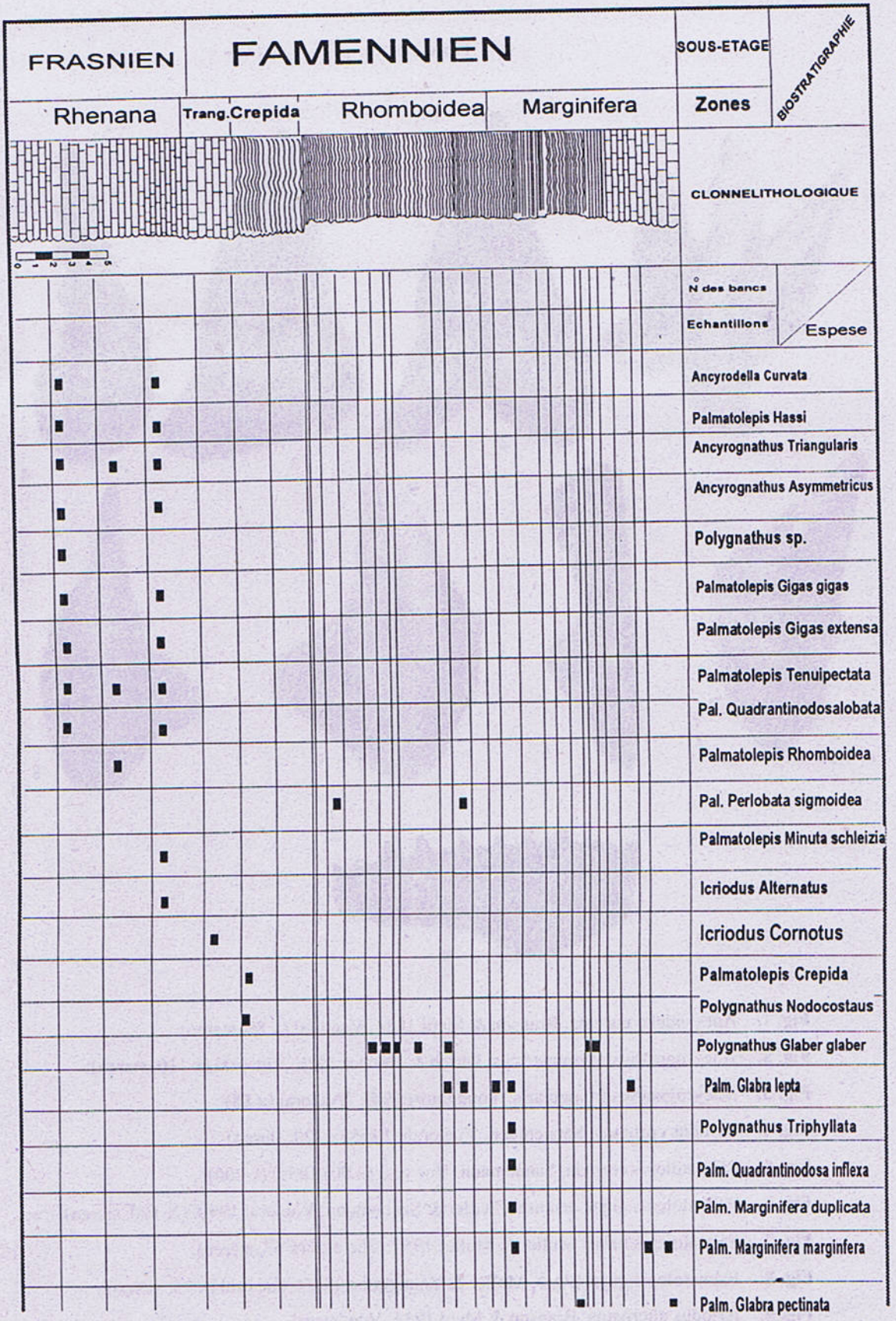

Fig. 2 Conodont species of the section at Col Des Tribes France.

Plate 1

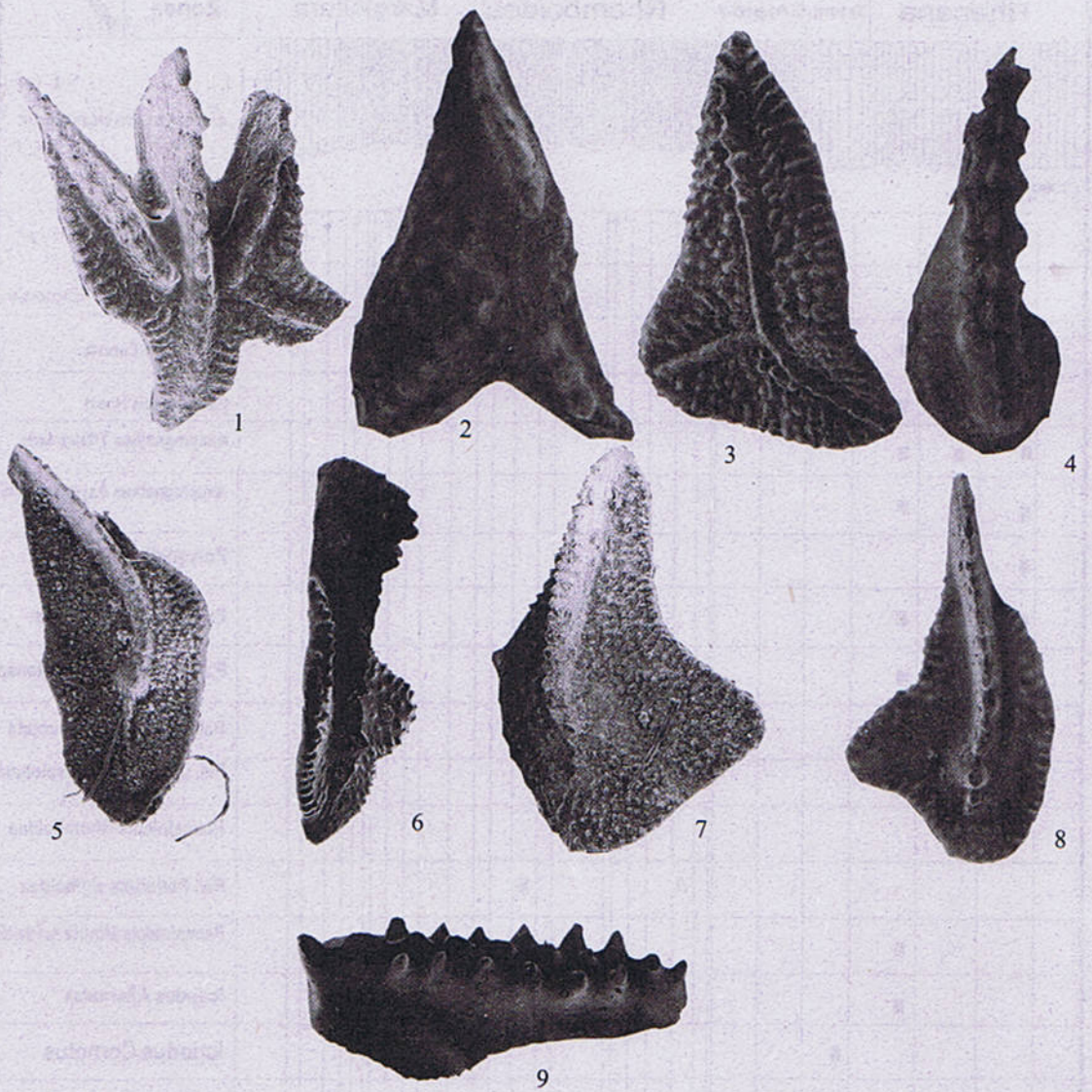

Fig. 1. Ancyrodella curvata, Branson & Mehl.1934. Vue oral (x 80, stereo).

Fig. 2. Ancyrognathus asymmetricus, Ulrich & Bassler.1926. Vue oral (x 110, stereo).

Fig. 3. Ancyrognathus triangularis, Youngquist.1945. Vue oral (x 88).

Fig. 4. Icriodus cornutus, Sannemann. Vue orale.1955 (x 120, stereo).

Fig. 5. Palmatolepis crepida, Sannemann. Vue oral (x 90).1955. (x 200).

Fig. 6. Palmatolepis gigas extensa, Ziegler & Sannemann. Vue oral.1990. (X 100, stereo).

Fig. 7. Palmatolepis hassi, Muller & Muller.1957. Vue oral (x 63, stereo).

Fig. 8. Palmatolepis gigas gigas, Muller & Youngquist.1945. Vue oral (x 75, stereo).

Fig. 9. Icriodus alternatus, Branson & Mehl.1934. Vue lateral.

Plate 2

Fig. 1. Polygnathus Triphylatus, Ziegler. 1960 Vue oral (x 84)

Fig. 2. Palmatolepis glabra pectinata, Ziegler.1962 Vue oral (x 70, stereo).

Fig. 3. Palmatolepis minuta schleizia, Helms.1963. Vue oral (x 70).

Fig. 4. Palmatolepis perlobata sigmoidea, Ziegler.1962. Vue oral (x 75).

Fig. 5. Palmatolepis quadrantinodosa inflexa, Muller.1956b. Vue oral (x 225, stereo).

Fig. 6. Palmatolepis marginifera duplicata, Sandberg & Ziegler.???? Vue oral (x 70, stereo).

Fig. 7. Palmatolepis marginifera marginifera, Helms.1959. Vue oral (x 125, stereo).

Fig. 8. Palmatolepis quadrantinodosalobata, Sannemann.1955. Vue oral (x 100, stereo).

Plate 3

Fig. 1. Palmatolepis rhomboidea, Sannemann.1955a. Vue oral (x 175).

Fig. 2. Palmatolepis stopelli, Sandberg & Ziegler.1973. Vue oral (x 120, stereo).

Fig. 3. Palmatolepis tenuipectata. Sannemann .1955. Vue oral (x 81, stereo).

Fig. 4. Polygnathus glaber glaber, Ulrich & Bassler.1926. Vue oral (x 95, stereo).

Fig. 5. Polygnathus sp.Anderson.1966. Vue oral (x 95).

Fig. 6. Polygnathus nodocostatus, Branson & Mehl.1934. Vue aboral (x 80)

Griotte type limestone, which is the locality chosen for this study.

THE STRATIGRAPHIC SECTION AT COL DES TRIBES

This section is of a total thickness of 37 meters and is located at 37 meters North East of the Mount Peyroux. Which has been divided into three different lithological units from bottom towards top. Discovery of the fauna is accordingly mensioned at fig.2.

1. Lower Unit: It is 12.4 meters of yellowish, micritic calcarious stuff. Sometime shining. It has bioclasts, Gonietites and Ostrocodes, bioterbated. The Conodonts fauna discovered in this unit is *Ancyrodella curvata, Ancyrodella afi. curvata, Palmatolepis hassi, Palmatolepis rotunda, Polygnathus sp. 1, 2, 3, Ancyrognathus triangularis, Lonchodina sp., Polygnatellus sp, Ancyrognathus, asymmetricus, Paimatolepis tenmpunctata, Hindeodella sp, Palmatolepis gigas extensa n. sp., Palmatolepis gigas gigas, Palmatolepis quadrantinodosalobata, Palmatolepis minuia minuta, Palmatolepis perlobata helmsi.*

2. Middle Unit: It is 19.9 meters of nodular Limestone of reddish color with intense bioturbation . The crakes are filled with ferogenous material. It contains a visible fauna of Crinoids, Goniatites. The Conodont fauna received are *Palmatolepis crepida, Palmatolepis rhomboidea / tenuipunctata, Palmatolepis perlobata, Bispathodus sp.,Palmatolepis minuta schleizia, Polygnathus nodocostatus, Polygnathus glaber glaber, Icriodus alternatus, Icriodus cornutus, Palmatolepis glabra lepta, Polygnathus sp., Palmatolepis perlobata sigmoidea ,Polygnathus triphyllatus, Palmatolepis schindewotfi, Palmatolepis glabra pectinata, Palmatolepis quaarantinodosa,inflexa,Palmatolepis - Quadrantinodosa marginifera, Palmatolepis perlobata schindewolfi, Palmatolepis gracilis gracilis, Palmatolepis glabra acuta, Palmatolepis tenuipunctata.* It gives us Faminian age 20 meters from Crepida, Rhomboidea and half of the lower Marginifera zone.

3 Upper Unit: It is 5 meters thick grey Limestone of secondary dolomitic nature. It contains the conodonts fauna *Ancyrognathus sinelaminus, Palmatolepis quadrantinodosalobata, Icriodus cornutus, Polygnathus sp. cf. brevilaminus, Polygnathus sp., Ligonodina sp. (element M "Synprioniodiforme"),Ligonodina panderi (element Sc "Hindeodelliforme"), Palmatolepis glabra prima, Nothognathella brevidonta, Potygnathus nodocostatus, Alternognathus regularis.* It is of Faminian age (Zone marginifera and lower Velifer). See fig 2 for the lithological description, faunal distribution and zonal establishment. The fauna discussed is documented in plates 1, 2 and 3 of this paper.

CONCLUSION

From the above study we can conclude three main things.

1. Paleoenvironment. 2. Paleoecology. 3. Age of the strata.

The strata can be assigned the age of Frasnien and Famennien on the basis of presence of fauna that are Ancyrodella, crepida, rhomboidea, margmifera and valifer. Each of these index fossils represents separate zones, and accordingly five zones are marked that are also reported from all over the world with slight modifications. These are Rhenana, Triangularis, Crepida, Rhomboidea and marginifera. On the bases of the presence of these fossils and conodont faunal composition, a Carbonate ramp environment is suggested for these strata.

REFERENCES

Anderson, W. I., 1966, Upper Devonian conodonts of Iowa. *Journal of Paleont.,* **40,** n°2, p. 414, pi. 51, fig. 2-4.

Branson, E. & Mehl M. G., 1934a,. Conodonts from the Grassy Creek Shale of, Missouri. Univer. *Missouri Studies,* **8,** n°3 p .173-259 9pl fig.

Feist R, & Schonlaub H.P., 1973,. Le passage siluro-devonien de la Montagne Noire orientate. C. R. Acad. Paris, t. 276, p. 1267-1270.

Feist R, & Schonlaub H.P.,1974, Zur Silur/Devon-Grenze in der Ostlichen Montagne Noire Siid-Frankreichs. N. Jb. *Geol. Palaont. Mh.,* H.4, p. 200- 219, 6 figs., 2 tabl., 2 pis.

Feist, R. & Klapper G,. 1985, Stratigraphy and conodonts in pelagic sequences a cross the Middle-Upper Devonian boundary (Montagne Noire, France). Paleontographica, Stuttagart, n° 188, p. 1-18, 9 text-figs.

Feist, R. Schonlaub H.P. & Bultynck P.,1985, Facies et biostradgraphie (conodontes) du passage Devonien inferieur-moyen de la Montagne Noire. Hercynica, **1.** n°2. p. 81-87, 4 figs., 2 tabl... 3 pis.

Feist, R., 1990, The Frasnian-Famennian boundary and adjacent strata of the eastern Montagne Noire. Guide book of the field meeting, Montagne Noire, p. 1-69, 36

Helmms, J.,1959,Conodonten aus dem Saalfelder Oberdevon (Thuringen). Geologie,vol. 8, p. 634-677, 3figs.6pls,

HELMS, J.M.,1963, ZurPhylogenese und TaxinomievonPalmatolepis (Conodontica Oberdevon). Geologic. V01. 12, p. 449-485, 3 text-figs. 4pls.

Khan, F.R.,1993, Les Conodonts\es des Calcaires Griottes du Devonien superieur de la Montagne Noire (Inventaire, Biostratigraphie et Paleonvironments). THESE presentee devant I' Universite Claude Bernard-Lyon I pour I'obtention du Diplome de Doctorat.

Muller, K. J., 1956, Taxonomy, nomenclature, orientation and stratigraphic evaluation of conodonts. J. Paleont. Tulsa, vol.30, n° 6, p.1324-1340. pi, h,t. 145.

Muller, K. J. & Muller E. M.,1957, Early upper Devonian (independence) conodonts from Iowa, Parti. Journ. Paleont., vol.31, p.1069-1108, 8 pis.

Sannemann, D.,1955a, Beitrage zur Untergliederimg des Oberdevons nach Conodonten. Neues JB. Geol, u Pahontol. Abh., 100,p.324-331, 1 pl.text-fig..ltabl

Sannemann, D.,1955b,Oberdevonische Conodonten (toJ-)Senckenbergiana 1 Lethaea, n°36, p. 123-156, 6pls., 3 text-figs.

Schulke, I., 1999, Early Famennian Conodont biostratigraphy of the stratotype area (Montagne Noire, Southern France). Bulletino della societa paleontologica Italiana, 37(2-3), 1998. ISSN 0375-7633, 375-391, 2pls Modena, Novembere 1999. Sud- rankneichs.N.jb Geol. Palaont. Mn, h.4, p. 200-219.

Ulrich, E. 0. & Bassler R.S.,1926, A classification of the toothlike fossils Conodonts, with the description of American Devonian and Mississipian species. U. S Na. Museum, Proc; vol.68. n"2613, p 1-63, 1 Ipl,, 5 fig.

Youngquist, W., 1945, Upper Devonian conodonts from the Independance Shale (?) of Iowa jour. *Paleont,*, **19,** p.355-367. 3pls.

Ziegler, W., 1962b, Taxionomie und Phylogenie Oberdevonishe Conodonten und ther stratigraphische Bedeutung. Hessisches Landesamt Bodenforschung Abhandlungen.

Ziegler, W., 1960, Conodenten aus dem Rheinischen Unterdevon (Gedinnium) des Remscheider Sattels (Rheinisches Schiefergebirge). Palaont. Zeitschr. Bd. 34, p. 169-201, 3 pis., 2 figs.

Ziegler, W., ed., 1973, Catalogue of conodonts. E. *Schweizerbart 'sche Verlagsbuchhandlung,* **1,** 504 p., 23 figs., 27 pis.. Stuttgart.

Geol. Bull. Punjab Univ. 36, 2001.

SOME MONOSACCATE POLLEN FROM THE TOBRA FORMATION OF THE NILAWAHAN GORGE, CENTRAL SALT RANGE, PAKISTAN

BY

QAISER MAHMOOD KHAN
Botany Department, Govt. College of Science, Allama Iqbal Town, Lahore, Pakistan.

SARFRAZ AHMED, KAMRAN MIRZA
Institute of Geology, University of the Punjab, Lahore-54590, Pakistan.

AND

FAZLI RABBI KHAN
National Centre of Excellence in Geology, University of Peshawar, Pakistan

Abstract:- *A preliminary palynological study of the Tobra Formation, Nilawahan Gorge, Central Salt Range has yielded a relatively rich and well preserved palynoflora dominated by miospores and pollen grains. The palynoflora is dominated by gymnosperm pollen grains of both monosaccate and bisaccate origin. These are Aratrisporites fischeri, Cannanoropollis niazuddinii, Densipollenites indicus, Nuskoisporites cf. N. dulhuntyi, Plicatipollenites indicus, Plicatipollenites trigonales. All of these are monosaccate pollen which are described here systematically.*

INTRODUCTION

Permian sedimentary rocks have been described palynologically from different parts of the Salt Range (see location map). Only a few sequences have been analysed and this undoudtedly reflects the more limited studies of the Permian rocks. No one has published on the Tobra Formation from the Nilawahan Gorge. This work is the first of its origin in which an attempt has been made to describe some pollen from that area. All of these six pollen grains are of monosaccate type and an early Permian age is given to this stratigraphic rock unit. It is of interest to note that monosaccate pollen in the Tobra Formation are dominated in quantity than the bisaccate pollen; the former ones 47% while the latter ones 37%. Trilete spores are recorded upto 13% while Cyadopites are only 3%. The palynoflora indicates glacial condition of deposition.

The rock samples were prepared by means of standard palynological techniques using hydrofluoric acid to remove the mineral matter, followed by oxidation of the organic residue with conc. nitric acid at various stages of oxidation were applied with maximum time of approximately 24 hours for the best result. No alkalis were used. Strew mounts were made using "cellosize" dispersalagent and Canada Balsam as mounting medium.

SYSTEMATIC PALYNOLOGY

ANTETURMA:	POLLENITES POTONIE 1931.
TURMA:	SACCITES ERDTMAN, 1947.
SUBTURMA:	MONOSACCITES CHITALEY EMEND POTONIE AND KREMP, 1954.
INFRATURMA:	ALETISAACITI LESCHIK, 1955.
GENUS:	DENSIPOLLENITES BHARADWAJ, 1962.
TYPE SPECIES:	DENSIPOLLENITES INDICUS BHARADWAJ, 1962.
	Densipollenites indicus Bharadwaj, 1962.
	Plate 1, fig. 1.
Material:	71 specimens.

Dimension

Total breadth:	85(105) 130 µm
Total height:	73(87) 110 µm
Corpus diameter:	40(51) 60 µm
Maximum breadth of saccus:	16-20 µm

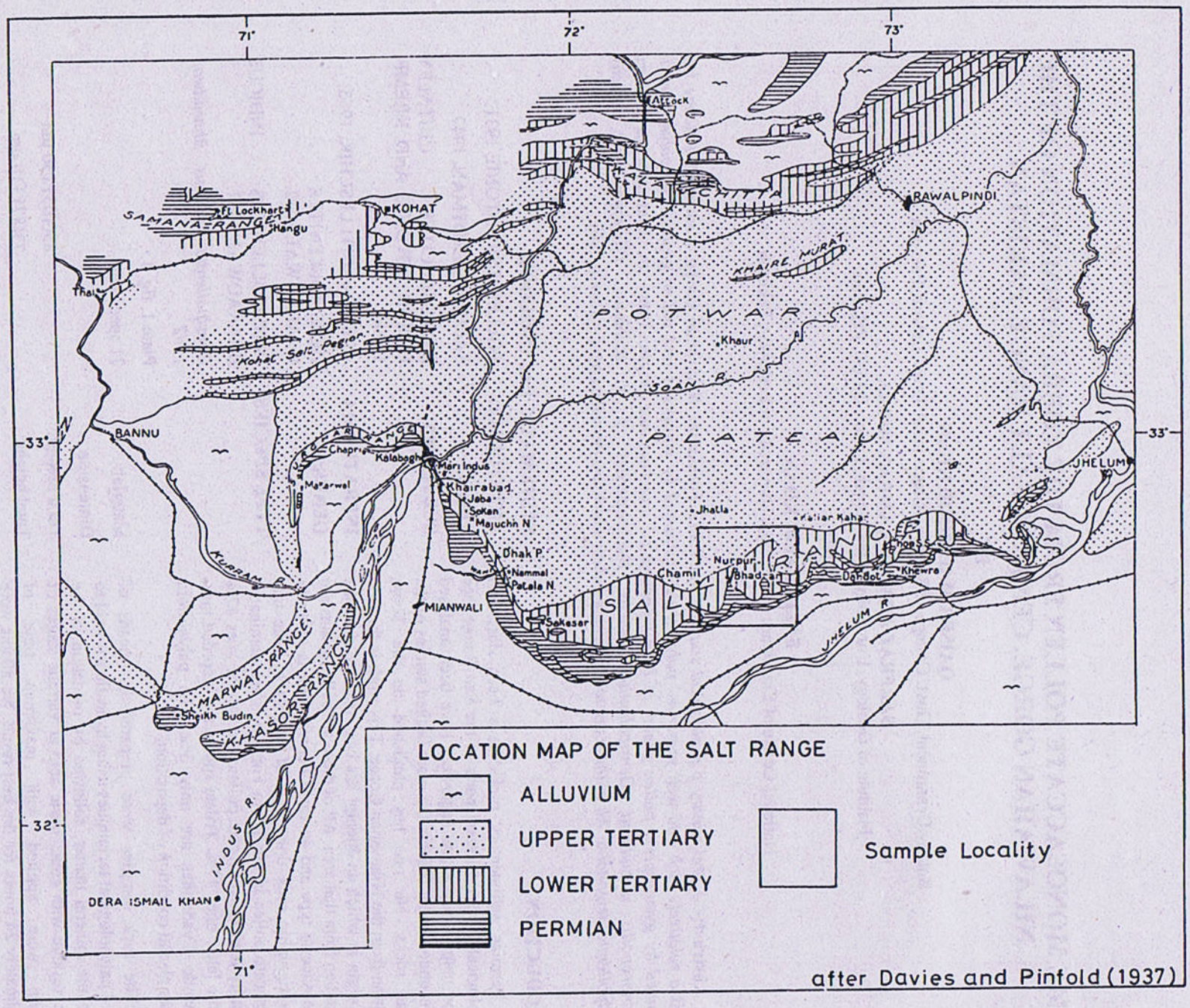

Fig. 1 Location Map of the Salt Range.

Description

Pollen grain, monosaccate, radial symmetrical, anisopolar trilete marking absent, alete. Corpus circular to subcircular, with sharply defined demarcating boundry. Corpus centrally placed. Exine of corpus dark brown, punctate, equatorial thickened, forming bended collar at equatorial line, compression folds absent. Exoexine of saccus intra-reticulate, partly detached from endoexine (corpus) on proximal and partly on distal pole, brochi 3-6 µm in diameter, muri ± 3 µm thick, some of the sculpturing element of margin of saccus undulating to ragged, limbus present.

Remarks and Comparison

Densipollenites indicus Bharadwaj (in Balme 1970, p.354, pl.7, fig.8) is the nearest in its gross morphology and size range. Balme (1970) recorded his specimen from Chidru Formation (Upper Permian). The present writers recorded this specimen for the first time from the Dandot Formation of Lower Permain age from Nilawahan Gorge.

AGE: Lower Permain.

SLIDE NO: 1018/4-3, 1018/4-10, 1018/4-11, 1018/6-2-17, 1018/6-2-19, 943/3-15.

FILM NO: 84/150693313, 1/120790/5.

INTRATURMA: TRILETISACCITI LESCHIK, 1955.

GENUS: CANNANOROPOLLIS POTONIE AND SAH, 1960.

Type Sp.: *Cannanoropollis niazuddinii masood, 1983.*

Plate 1, Fig.2.

Material: 10 specimens.

Dimension

Total breadth: 85(97) 122 µm

Total height: 73(84) 109 µm

Corpus diameter: 47(52) 56 µm

Breadth of saccus: 15-25 µm

Description

Pollen grain, monosaccate, radiosymmetrical, contour circular to subcircular, trilete marking distinct, open, arms straight 1/2 to 1/3 of the spore radius. Central body clearly defined a darker region around the "Y" marking, zone of corpus marked by diffused to distinct limbus exine of central body infraforveolate, saccus equatorial attached, saccus exoexine ragged with infrareticulate veination.

Remarks and Comparison

Cannanoropollisf niazuddinii Masood, 1983, pl.49, fig.1, recorded from Dandot Formation Central Salt Range giving an average size of 24 x 112 µm seems to be somewhat similar, but slightly differentiated due to its oval outline, whereas the diagnosis given for the genus by Potonie and Sah (1960, p.127, pl.1.2, fig.16), suggests that the grains are "equator circular, subcircular to very round triangular, saccus small more or less equal width, with an irregular and slightly notched to sinuate border", giving a size range 95 µm to 133 µm. It is noted that Masood (1983) described it his species as radiosymmetrical but provided the average size of 112 x 124 µm showing a somewhat spheriodal outline. Thus the present sporomorph is closely related with Cannanoropollis niazuddinii Masood (1983, pl.49, fig.1).

AGE: Early Permian.

SLIDE NO: 943/3-18.

FILM NO: 67/120790/5.

INFRACTURMA: TRILETISACCITI LESCHIK, 1955

GENUS; NUSKOISPORITES POTONIE AND KLAUS, 1954.

Type of Sp. *Nuskoisporites (cf.) N. dulhuntyi Potonie & Klaus, 1954.*

Plate 1, Fig.3.

Material: 9 specimens.

Dimension

Total breadth: 82(93) 97 µm

Total height: 82(93) 97 µm

Corpus diameter: 58 µm

Maximum breadth of saccus: 26 µm

Description

Pollen grain, monosaccate, spherical, corpus spherical, trilete; Trilete closed to open, half the length of central body radius, lips raised suture straight, proximal exine punctate, limbus well marked, saccus attachment proximal, saccus uniformily wide 26 µm, undulating, exine of saccus intrafoveolate, foveolae radially arranged.

Remarks and Comparison

Guskoisporites c/i Guskoisporites bulhuntd., Potonie and Klaus (1954, Tschudy and Kosanke, 1955, pl. 2, fig. 44), has somewhat nearest comparison.

AGE: Upper Permian

SLIDE NO: 943/3-28

FILM NO: 39/140790/5

INFRATURMA: APERITACORPITI LELE, 1964.

GENUS: PLIACTIPOLLENITES LELE, 1964.

Type species: Plicatipollenites indicus Lele, 1964, p.152-154, pl.1, figs.6-10

Plicatipollenites indicus Lele, 1964

Plate 1, Fig.4; Text Fig.1

Material: 74 specimens

Dimensions

Total breadth:	102(105) 112 µm
Corpus:	53(57.5) 59 µm
Maximum breadth of saccus:	21(24) 28 µm

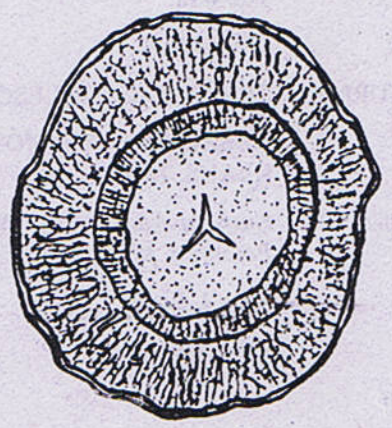

Text Fig. 1. *Plicatipollenites indicus* Reconstruction in proximal view X 475.

Description

Pollen grain, monosaccate, light brown, radiosymmetrical, contour spherical to slightly oval. Central body transluscent with discernible Y-marking area not exceeding to µm. Central body bounded by well marked limbus, with dark and light radially arranged bands. Saccus attachment proximally inclined, variable in width from 13-25 µm, 1.0 µm thick, muri very fine.

Remarks and Comparison

The present specimen has very close similarity with Plicatipollenites indicus described by Balme (1970, p.357, pl.7, fig.9). Surprisingly, Balme (1970) did not mention about the arms of "Y" radii.

The present specimens were found frequently in Tobra Formation, Nilawahan Gorge, Central Salt Range, Pakistan.

AGE: Early Permian.

HORIZON: Tobra Formation, Nilawahan Gorge.

SLIDE NO: 943/3-14, 943/3-26 1014/10,10147 1014-17, 1014-42,1014-47, 101054, 1014-A, 4 8/120790/4, 15/290790/11

Type Species

Plicatipollenites trigonalis Lele, 1964.

Plate 1, Fig.5; Text Fig.2.

Holotype: *Plicatipollenites trigonalis* Lele, 1964.

Material: 24 specimens

Dimensions

Total breadth:	109(114) 122 µm
Total length:	100(104) 109 µm
Corpus breadth:	65(70) 79 µm
Corpus height:	55(65) 75 µm
Maximum breadth of saccus:	17(20) 25 µm

Text Fig. 2. *Plicatipollenites trigonalis* Reconstruction in proximal view X 480.

Description

Pollen grain, monosaccate, radiosymmetrical or bilateral symmetrical, subcircular to broadly convex triangular, margins ragged or undulating. Amb of Corpus subcircular to triangular, contact area distinct, "Y" marking clearly defined, laesurae open straight ± 13 µm long, extending upto 1/3rd of radius, compression folds present. Saccus not uniform 17 µm to 25 µm in width, slightly narrower in the inter-radial region in triangular form, saccus exine microreticulate with smooth undulating ragged margin.

Plate-1

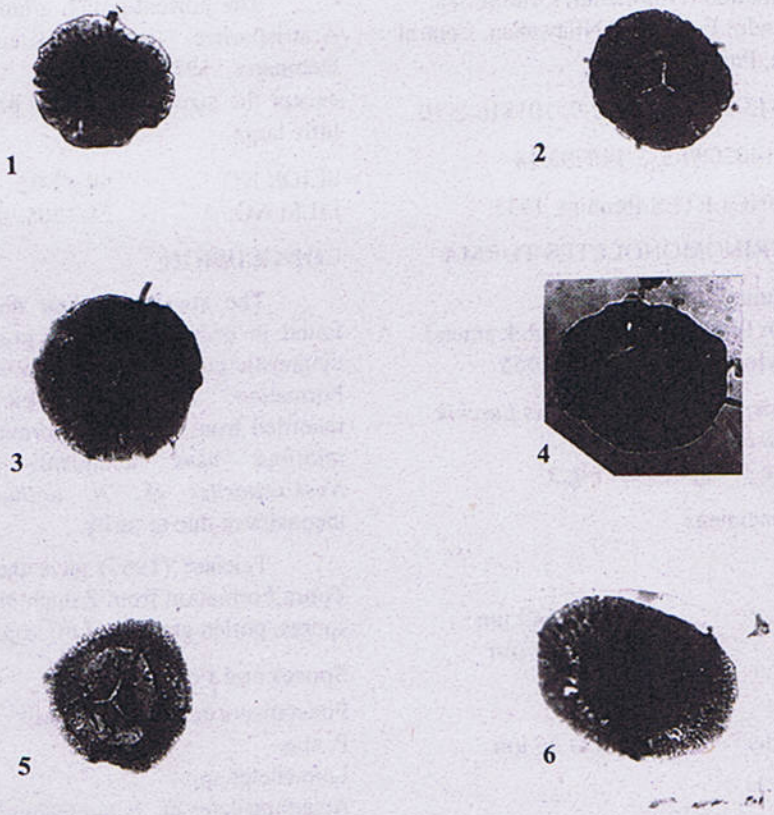

Explanation of Plate

Fig. 1. *Densipollenites indicus* Bharadway, 1962 x 450.

Fig. 2. *Cannanoropollis niazuddinii* Masooq, 1983 x 450.

Fig. 3. *Nuskoisporites* (cf) *N. dulhuntyi* potonie & Klaus, 1954 x 375.

Fig. 4. *Plicatipollenites indicus* Lele, 1964, x350.

Fig. 5.*Plicatipollenites trigonalis* Lele, 1964, x 300.

Fig. 6. *Aratrisporites fischeri* (Klaus) Balme, 1970, x 350.

Remarks and Comparison

Plicatipollenites trigonalis Lele, 1964, p.2, figs.13-14 from Lower Permian of Talchir stage, India, seems to be similar with the present palynorph, although the exact size range of the palynomorph is not exactly known, but the figured specimen shows a maximum size ± 109 µm.

AGE: Early to Late Early Permain

HORIZON Tobra Formation (Nilawahan) Central Salt Range, Dandot Formation Nilawahan, Central Salt Range, Pakistan.

SLIDE NO: 94313-26, 101816-2-9, 101816-2-10

FILM NO: 30/1407090/5, 3/140793/14

TURMA: MONOLETES Ibrahim, 1933

SUPRASUBTURMA:PERINOMONOLETES TURMA

TURMA: Erdtman, 1947

GENUS: ARATRISPORITES Leschik emend. Playford and Dettmann, 1965

Type species: *Artrisporites parvispinosus Leschik*
Aratrisporites fischeri
Plate 1, Fig.6; Text Fig.3

Material: 8 specimens

Dimensions

Total breadth:	134(141) 149 µm
Total height:	97(103) 109 µm
Corpus breadth:	73 µm
Corpus height:	59 µm
Maximum breadth of saccus:	20 µm to 36 µm

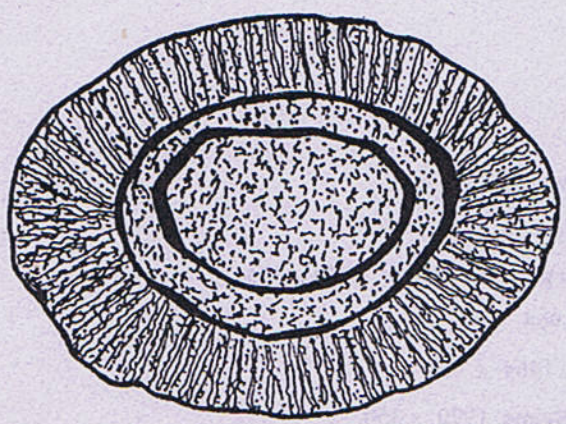

Text Fig. 3. *Aratrisporites fisheri* Reconstruction in proximal view X 500.

Description

Pollen grain, monosaccate, dark brown amb oval, central body dark brown, trilete marking discernible, laesurae indistinct. Saccus attachment proximally inclined, saccus variable in thickness, 25 µm to 36 µm wide, saccus exine intrareticulate, muri radially oriented.

Remarks and Comparison

The present pollen grain has close resemblance with Aratrisporites fischeri (Klaus). 1960 Playford and Dettmann, 1965 in Balme, 1970, p.351, pl.7, figs.5-7, except the size range of the present pollen grain which is little large.

SLIDE NO: 943/3-25
FILM NO: 28/120590/5

CONCLUSION

The species studied during this investigation are found in excellent state of presentation and they are age diagnostic confirming the Lower Permian age of the Tobra Formation. This palynological assemblage is newly recorded from the Tobra Formation of this area. All of the mioflora have abundantly been recorded except *Nuskoisporites* cf., *N. dulhunting*. It is sporadic or inconsistent due to rarity.

Teichert (1967) gave the lithological details of the Tobra Formation from Zaluch Nala and listed the following spores, pollen grains and micropalankton:

Spores and Pollen Grains

Punctatisporites cf. P. gretensis
P. spp.
Leiotriletes spp.
Acanthotriletes cf. A. tereteangulatus
Apiculatisporis sp.
Protohaploxypinus sp.
Striatopodocarpites sp.
Potonieisporites sp.
Kraeuselisporites
Cf. Nuskoisporites sp.

Microplankton

Leiosphaeridia spp.
? Cymatiosphaera sp.

These are observed from unit 2 of C Member and established the Permian age of the Tobra Formation on the basis of age diagnostic palynomorphs.

However, these typical genera have not been recorded during the present investigations. It is proposed that a detailed study should be carried out for a comprehensive record of palynological assemblage from this area.

REFERENCES

Balme, B.E., 1970. Palynology of Permian and Triassic strata in the Salt Range and Surghar Range, West Pakistan. In: Stratigraphic Boundry Problems. Permian and Traissic of West Pakistan. (Ed. Kummel, B. and Teichert C.). *Kansas Univ. Spec. Publ.*, **4,** 305-453.

Bharadwaj, D.C., 1962. The miospore genera of coals of Ranigunj stage (Upper Permian), India. *Palaeobotanist*, **9,** 8-106.

Erdtman, G., 1947. Suggestion for the clarification of fossils and Recent pollen grains and spores. Svensk *Botanisti Tidskult*, **41(1),** 104-114.

Hart, G.F., 1965. The Systematics and distribution of Permian Miospore. Witwaterssand Univ. John Johansberg, 1-253.

Ibrahim, A.C., 1933. Sporenformen des "Agirhorizontes des Ruhrreviers. Q.es.*Techn. Hochschule, Berlini*, 1-46.

Klaus, W., 1958. Some Lower Mesophytic Microspores of Europe with remarks on their relation to the Gondwona Microflora. *Jour. Pal. Soc. India, Lucknow, Birbal Sahnii Mem.* **2,** 151-155.

Lele, K.M., 1964. Studies in Talchir Flora of India 2. Resolution of the spore genus Nuskoisporites Potonie in Potonie and Klaus. *Palaeobotanist*, **12,** 147-168.

Leschik, 1956. Spore aus dem saitzon des Zechsteine Von Meuhof (beifulda): *Palaeontographica*, 100, 122-142.

Masood, K.R., 1983. Studies on the Gondwana Flora of the Salt Range Pakistan. Ph.D. thesis (Punjab University, Lahore, Pakistan).

Potonie, R. and Kremp, G., 1954. Die Gattangen der Polaozoischen sporae dispensae und ihre stratigraphic, *Geol. Jahrb.* **69,** 11-94.

Potonie, R. and Klaus, W., 1954. Einige Sporen Gattungen des Alpinen Salzge irges. *Geol. Jahrb.*, **68,** 517-544.

Potonie, R. and Sah, S.C.D., 1960. Sporae dispersae of the lignites from Cannanore Beach on the Malabar. *Coast of India.*

Srivastava, S.C., 1970. Mioloral investigation in some coals of Talchir Colfield (Orissa) India.

Teichert, C. 1967. Nature of Permian glacial record, Salt Range and Khisor Range, West Pakistan. N.Jb.Geol.Palaont.Abh, 129, 2, 167-184, Stuttgart.

Geol. Bull. Punjab Univ. 36, 2001.

GEOTECHNICAL EVALUATION OF A WEIR SITE ON KURRAM RIVER, MIANWALI

BY

SAEED FAROOQ AND N.TAMEEM

Institute of Geology, University of the Punjab, Lahore-54590, Pakistan.

Abstract:- *Exploring of sub surface soil and rock condition has long been an item of interest for those involved in evaluation of soil and rock as a foundation material. Horizontal and vertical variations of soil and rocks have introduced a large scatter of engineering characteristics of these materials. The need of detailed investigations prior to any engineering activity has increased with increasing scientific knowledge. The purpose of this paper is to present the variation of various engineering characteristics and parameters of an area near Isakhel in Mianwali District on Kurram River.*

INTRODUCTION

The study includes sub-surface exploration in order to depict the engineering behavior of the subsoil under structural stresses.

A number of test pits were excavated to determine the engineering behavior of soils at shallow depths. Two boreholes to a depth of 55 ft each were also drilled to establish soil profile of the area. Necessary field testing in boreholes and test pits were conducted simultaneously during exploratory works.

Disturbed and undisturbed soil samples were tested in the Laboratory for classification and determination of strength parameters. The foundation evaluations have also been presented in this paper.

FIELD STUDIES

Field studies include

i. Drilling of two boreholes by auger/ light percussion method upto 55 ft. depth.

ii. Excavation of eight test pits at appropriate locations upto maximum depth of 10 ft.

iii. Preparation of field logs on the basis of visual classification.

iv. Carrying out standard penetration tests in each hole at 5 ft depth interval.

v. Collection of disturbed and undisturbed soil samples from boreholes and test pits.

vi. Execution of field density tests.

Drilling of Boreholes

The boreholes marked on Fig.1 were drilled down to 55 ft depth by auger and light percussion method from natural surface level (NSL). Steel casing was used to control the caving-in of the holes.

Excavation of Test Pits

Eight test pits were excavated down to 10 ft depth from NSL. In addition, auger holes were drilled at the bottom of pits down to 15ft depth at three locations in order to supplement the test pits data. Standard Penetration Tests were conducted in the auger holes and subsequently the small disturbed samples were taken.

Field Logs

The logs of boreholes and test pits were prepared carefully and necessary description of lithology was noted during drilling and excavation of test pits, (Fig.1). Data of field tests and other information like groundwater levels and sample locations were also recorded on the logs. Visual soil classification noted on the logs were corrected after completing the laboratory tests on soil samples.

Standard Penetration Tests

Standard Penetration Tests are imperative to depict the in-situ conditions of soil and infer many other prameters like density friction etc. (Chellis,1962), (Teng,1977) , (Bowles,1988)

The Standard Penetration Tests were conducted generally at every five feet depth interval in the

boreholes. The tests were performed in accordance with ASTM D—1586. (Table-1 & Table-2)

Field Density Tests

Field density tests were executed to determine in place compactness of shallow soil. Sand replacement method was used for the tests in which in-situ soil is replaced by uniform sand of known density with a series of weight measurements. The density of soil was calculated at site. Soil moisture contents were determined in the laboratary on samples collected in small tins from each test location to determine dry density of in place soil. The results have been presented in the summary of test results. (Table-3)

Field density is an important parameter which reflects the general engineering behavior of sub soil (Tomlinson, 1986)

Sampling

Disturbed and undisturbed sampling is an important aspect of geotechnical studies as laboratory studies cannot be accomplished without good quality samples (Lee et.al, 1983). A number of disturbed samples were collected during field work from SPT split spoon sampler. Undisturbed samples were obtained through thin walled Shelby tubes. These were carefully waxed and preserved for various laboratory tests. Bulk samples from test pits were collected to perform laboratory compacion tests.

LABORATORY TESTING

Physical characteristics were measured through precise laboratory testing on selected soil samples (Tomlinson, 1986). Engineering behavior of the subsoil was determined by the laboratory test data for evaluating the geotechnical parameters of subsoil material. Laboratory tests performed on soil samples collected from the field are discussed;

Grain Size Analysis

Sieve and hydrometer analysis (where ever applicable) on a number of soil samples were carried out conforming to ASTM designation D 421 and 422. The results were plotted as particle size distribution curves and a test summary was also prepared which is annexed as Table 4.

Atterberg's Limits

Atterberg's limits were required for the classification and for predicting engineering properties of cohesive soils in addition to grain size. It also gives fair idea about compressibility and swell characteristics etc. (Tomlinson, 1986). These tests were conducted on two samples in accordance with ASTM designation D 431—84. The results are presented in Table-4

Natural Moisture Content

Moisture is considered to be the most deterioratic factor for strength characteristics of sub soil. (Tomlinson, 1986).

A number of tests were performed on soils samples of the study area to determine the moisture content. These tests were executed conforming to ASTM designation D 221-80. The results are given in Table-4 showing variation from 15.69% to 20.26%.

Specific Gravity

Specific gravity tests were performed on soil samples obtained from various horizons in accordance with ASTM, D 854-83. The results of these tests presented in Table-4 exhibit variation from 2.64 to 2.69.

Unconfined Compression

Cohesive soil found in borehole AH-2 and collected through thin walled Shelby tube samplers were tested to determine the unconfined compressive strength, q_u. Two tests were conducted and results are presented in Table-4.

Direct Shear Tests

These tests were carried out on remoulded sandy samples compacted to the field density. To determine the cohesion 'c' and angle of internal friction 'ϕ', only peak values were plotted. These tests concluded the angle of internal friction 'ϕ' of sandy soils between 30° and 33° with negligible cohesion, 'c'.

Results of these tests have been presented in Table-4

Bulk Density

In addition to field density determination by sand replacement in the field, bulk densities of the undisturbed samples were also determined and results are given in Table-4.

Chemical Analysis

Chemical tests were performed including determination of sulphate and chloride contents. The test results are also presented in Table-4.

DATA INTERPRETATIONS

Correction of Standard Penetration Tests

Standard penetration test data gathered during field exploration was corrected by the equations suggested by Bazara (1967)

$$N' = \frac{4N}{1+2P_o} \quad \text{for } P_o < 1.5 \text{ KSF}$$

Table-1
SPT data of boreholes at wier site

BH	Depth	Field	GWL	γ_b	Po	Soil Below GWL,	γ_s, soil below GWL,	Po total		4 x N	3.25+0.5Po	N'
No.	ft	N	Ft.	pcf	psf	ft	pcf	psf	KSF			
AH-1	5	3	4	115	460	1.0	55	515	0.515	12	3.51	3
	10	10	4	115	460	6.0	55	790	0.790	40	3.65	10
	15	9	4	115	460	11.0	55	1065	1.065	36	3.78	9
	20	13	4	115	460	16.0	55	1340	1.340	52	3.92	13
	25	16	4	115	460	21.0	55	1615	1.615	64	4.06	16
	30	19	4	115	460	26.0	55	1890	1.890	76	4.20	19
	35	22	4	115	460	31.0	55	2165	2.165	88	4.33	20
	40	27	4	115	460	36.0	55	2440	2.440	108	4.47	24
	45	26	4	115	460	41.0	55	2715	2.715	104	4.61	23
	50	29	4	115	460	46.0	55	2990	2.990	116	4.75	24
AH-2	5	5	4	115	460	1.0	55	515	0.515	20	3.51	6
	10	9	4	115	460	6.0	55	790	0.790	36	3.65	12
	15	8	4	115	460	11.0	55	1065	1.065	32	3.78	8
	20	5	4	115	460	16.0	55	1340	1.340	20	3.92	5
	25	18	4	115	460	21.0	55	1615	1.615	72	4.06	18
	30	20	4	115	460	26.0	55	1890	1.890	80	4.20	19
	35	24	4	115	460	31.0	55	2165	2.165	96	4.33	22
	40	21	4	115	460	36.0	55	2440	2.440	84	4.47	19
	45	27	4	115	460	41.0	55	2715	2.715	108	4.61	23
	50	29	4	115	460	46.0	55	2990	2.990	116	4.75	24
	55	27	4	115	460	51.0	55	3265	3.265	108	4.88	22

Table-2
SPT data of augar holes along canal alignment

TP No.	Depth ft	Field N	GWL ft.	γ_b pcf	Po psf	Po total psf	Po total KSF	4 x N	1+2po	N'
TP-2	5	6	-	110	110	1100	1.100	24	3.20	6
	10	8	-	110	110	1650	1.650	32	4.30	8
	15	11	-	110	110	1650	1.650	44	4.30	11
TP-3	5	6	-	110	110	550	0.550	24	2.10	6
	10	21	-	110	110	1100	1.100	84	3.20	26.3
	15	14	-	110	110	1650	1.650	56	4.30	14
TP-4	5	10		110	110	550	0.550	40	2.10	10
	10	9		110	110	1100	1.100	36	3.20	9
	15	12		110	110	1650	1.650	48	4.30	12
TP-5	5	5		110	110	550	0.550	20	2.10	5
	10	8		110	110	1100	1.100	32	3.20	8
	15	11		110	110	1650	1.650	44	4.30	11
TP-6	5	5		110	110	550	0.550	20	2.10	5
	10	9		110	110	1100	1.100	36	3.20	9
	15	13		110	110	1650	1.650	52	4.30	13
TP-7	5	9		110	110	550	0.550	36	2.10	9
	10	10		110	110	1100	1.100	40	3.20	10
	15	13		110	110	1650	1.650	52	4.30	13
TP-8	5	5		110	110	550	0.550	20	2.10	5
	10	6		110	110	1100	1.100	24	3.20	6
	15	7		110	110	1650	1.650	28	4.30	7
TP-9	5	6								6
	10	7								7
	15	10	8.5	110	935	6.5	50	325	1260	10

Table-3
Field density test data

TP No.	Depth m.	Field Density gm/cc	NMC %	Dry Density gm/cc
2	2	1.67	3.66	1.61
3	2	1.62	1.71	1.59
4	2	1.6	3.44	1.55
5	2	1.36	1.01	1.35
6	2	1.56	2.8	1.52
7	2	1.62	4.88	1.55
8	2	1.53	7.36	1.43
9	2	1.49	3.7	1.44

Table-4
Summary of laboratory test data

BH	Depth	NMC	Grain Size Analyses			Sp.	Direct Shear		Atterberg's Limits			Bulk Density		qu	Chemical Analyses	
No.	ft.	%	Sand %	Silt %	Clay %	Gr.	'c' psi	ϕ	LL %	PL %	PI %	pcf	N.M.C.	T/sq.ft.	Sulphate %	Chloride %
AH-1	5	20.26	96	4	-											
	10	18.49	97	3	-	2.64									0.014	0.002
	15	19.17	95	5	-											
	25	18.85	97	3	-											
	30		98	2	-	2.67	0	33								
	35		98	2	-											
	40		96	4	-											
	45		96	4	-											
AH-2	5	18.99	86	14	-	2.66	0.5	30								
	10		96	4	-											
	15.3	18.46	29	64	7										0.012	0.001
UDS	17				-				Non Plastic			117.8	19.17	0.83		
UDS	22		6	70	24				26	19	7	119.2	18.85	0.89		
	30	15.69	95	5	-	2.69										
	35		98	2	-											
	40		96	4	-											
	50		95	5	-											

Table-5
Single Pile Load Carrying Capacities

Depth Pile,m.	γ_b Pcf	γ_s pcf	GWL ft.	p1 tsf	p2 tsf	Pile Dia ft.	20xDia ft.	Area sq.ft	Length ft	Circum area/ft	Nq	Khc	'N'	ϕ	3/4 ϕ δ	Tan δ	Qult (Tons)	Qall (Tons)
15	110	60	8.5	0.42	1.53	1.83	36.7	2.64	49	5.76	10	0.7	9	29.5	22.13	0.407	130.7	43.6
18	110	60	8.5	0.42	1.80	1.83	36.7	2.64	59	5.76	10	0.7		29.5	22.13	0.407	182.9	61.0
20	112	65	8.5	0.43	2.12	1.83	36.7	2.64	66	5.76	10	0.7	9	29.5	22.13	0.407	232.8	77.6
22	110	65	8.5	0.42	2.30	1.83	36.7	2.64	72	5.76	12	0.7		30.5	22.88	0.422	296.9	99.0
24	112	65	8.5	0.43	2.50	1.83	36.7	2.64	79	5.76	14	0.7	17	30.5	22.88	0.422	363.1	121.0
26	112	65	8.5	0.43	2.70	1.83	36.7	2.64	85	5.76	14	0.7		30.5	22.88	0.422	420.2	140.1
28	112	65	8.5	0.43	2.89	1.83	36.7	2.64	92	5.76	14	0.5		30.5	22.88	0.422	374.5	124.8
30	112	65	8.5	0.43	3.08	1.83	36.7	2.64	98	5.76	17	0.5	19	32.5	24.38	0.453	470.8	156.9

Notes:

Qult Ultimate Load Carrying Capacity of Single Pile
Qall Allowable Load Carrying Capacity of Single Pile, with FOS=3
γ_s Submerged density, assumed.
γ_b Bulk density of soil above GWL, assumed.
p1 Eff. O.B. pressure above GWL
p2 Eff. O.B. pressure at pile tip
δ Friction angle between pile and soil
Khc Ratio of H to V Eff. Stress.

Table-6
Allowable bearing capacities of structures along canal alignment

TP No.	γ_b pcf	γ_b ton/ft^2	Po Psf	po ton/ft^2	Depth ft.	ϕ	0.67 tanϕ	$\tan^{-1}\phi$	ϕ^*	Nq	Width ft.	Nγ	Qult Ton/ft^2	Qall ton/ft^2
TP-2	104.2	0.047	1042	0.47	10	29	0.371	0.356	20.4	6.4	8	5.39	2.94	0.98
TP-3	101.1	0.046	1011	0.46	10	31	0.403	0.383	22	7.82	10	7.13	3.73	1.24
TP-4	100	0.045	1000	0.45	10	30	0.387	0.369	21	7.07	12	6.20	3.37	1.12
TP-5	84.9	0.039	849	0.39	10	29	0.371	0.356	20	6.40	10	5.39	2.40	0.80
TP-6	97.4	0.044	974	0.44	10	29	0.371	0.356	20	6.40	10	5.39	2.81	0.94
TP-7	101.1	0.046	1011	0.46	10	30	0.387	0.369	21	7.07	10	6.20	3.31	1.10
TP-8	95.5	0.043	955	0.43	10	29	0.371	0.356	20	12.7	10	5.39	5.47	1.82
TP-9	93	0.042	930	0.42	10	29	0.371	0.356	20	12.0	10	5.39	5.03	1.68

Table-7
Allowable bearing capacities of wier foundations

BH. No.& Ele. in m.	γ_s pcf	γ_s ton/ft^2	p_o psf	p_o ton/ft^2	D (ft.)	'N' value	ϕ	ϕ^*	Nq	Width ft.	Nγ	Qult ton/ft^2	Qall ton/ft^2
AH-1													
710	60	0.027	1560	0.71	26	17	31.5	21.1	7.07	30	6.2	5.73	1.91
710	60	0.027	1560	0.71	26	17	31.5	21.1	7.07	50	6.2	6.69	2.23
718	65	0.029	1170	0.53	18	15	31	20.8	7.07	30	6.2	4.39	1.46
718	65	0.029	1170	0.53	18	15	31	20.8	7.07	50	6.2	5.16	1.72
AH-2													
710	60	0.027	840	0.38	14	8	29.5	19.8	6.4	30	5.39	2.73	0.91
710	60	0.027	840	0.38	14	8	29.5	19.8	6.4	50	5.39	3.18	1.06
718	65	0.029	390	0.18	6	6	28.5	19.1	5.8	30	5.39	1.19	0.40
718	65	0.029	390	0.18	6	6	28.5	19.1	5.8	50	5.39	1.41	0.47

$N' = \frac{4N}{3.25+0.5 P_o}$ = for $P_o > 1.5$ KSF

where

N = Measured N - value in field.

N' = Corrected N - value.

P_o = Effective Overburden pressure, in KSF

The corrected N-values are presented in Table -1 and Table-2.

Field and laboboratory test data was used to evaluate the geo-engineering character of sub soil at this location. In view of engineering behavior of sub soil, various options of foundations were analyzed and presented in the following paras.

Correction of Shear Strength Parameters

$H = H_o + D$

$Q_{ult} = P_T N_q A_T + \Sigma (K_{HC})(P_o)(TAN\ \delta)(S)$

$H = H_o$ (NAVFAC DM 1983)

Where Q_{ult} = Ultimate pile load capacity in compression, T/sf.

P_T = Effective vertical stress at pile tip

H_o = Depth of water table,8.5 ft.

D = Depth of pile below water table.

N_q = Bearing capacity factor, depending on 'ϕ' (=10).

A_T = Area of Pile tip,sq.ft.

K_{HC} = Ratio of horizontal to vertical effective stress on side of pile in compression, (0.7)

P_o = Eff. vertical stress over length of embedment, D

δ = Friction Angle between pile and soil (3/4 ϕ).

S = Surface area of pile per unit length.

Pile capacity calculations have been presented in Table-5. A factor of safety of 3 has been applied.

Individual and strip footings

The ultimate bearing capacity non cohesive soils have been determined using following equation. (Tomlinson, 1986)

$q_{ult\ (net)} = P_o (N_q - 1) + 0.5\ \gamma\ B\ N\gamma$ (for strip foundations)

$q_{ult\ (net)} = P_o (N_q - 1) + 0.4\ \gamma\ B\ N\gamma$ (for square or circular foundations)

These equations are based on assumption that D<=B since ground water level was at 8.5 ft, submerged density of 60 pcf have been taken to compute P_o. The results are presented in Table-6 & Table-7.

Almost all the bearing capacity equations are based on general shear failure assumption. This failure is really sudden and catastrophic. In loose and relatively compressible soils punching or local shear failure may occur. To approximate the local or punching shear failure. The bearing capacity factors have been calculated with reduced strength characteristics c* and ϕ defined as

$c^* = 0.67c$

$\phi = \tan^{-1}(0.67 \tan)$ (NAVFAC DM 1983)

FOUNDATION DESIGN CONSIDERATIONS

Pile foundation

Load carrying capacity of pile was determined using following expression

CONCLUSIONS

Following conclusions can be drawn in the light of field and Laboratories studies.

The sub soil in the area of study predominantly is fine sand with some silt and light grey to grey in color. Concretions and gravels are also found at places and soil is generally loose to medium dense and dense. A 5 ft thick layer of clayey silt encounters at

about 19 ft depth (left bank of the Kurram River) while thin clay layers were also found at different horizons.

Groundwater table was shallow and encounters at about 4 ft depth from Natural Surface Level (NSL).

The partical size distribution curves indicate the range of grain size ,

D 10 range between 0.01 mm to 0.1 mm

D 30 range between 0.002 mm to 0.15 mm

D 60 range between 0.045 mm to 0.18 mm.

Natural moisture content above water table varies from 1.01% to 7.36% while bulk densities range from 1.36 g/cc to 1.67 g/cc and dry densities are in the range of 1.35 g/cc to 1.61 g/cc (Table-3).

The geo-engineering character of the sub soil suggests that lighter structures could be supported by strip or individual footings while heavy structures should be constructed on pile foundations.

Allowable bearing capacities for shallow foundations at about 10 ft depth came out to 0.94 to1.82 tons/sq ft which vary from place to place. (Table-6)

The single allowable pile capacity came out to 43.6 to 156.9 tons with depth from 49 ft to 98 ft and diameter of 20 inches (Table-5)

REFERENCES

Bazara , A.R. (1967), "Use of The Standard Penetration Tests For Estimating Settlement of Shallow Foundations On Sand", Ph.D. thesis, University of Illinois, Urbana, 379 pp.

Bowles Joseph E. (1988) "Foundation Analyses and Design", Mc Graw Hill International Editions 219 – 222 pp

Chellis R.D. (1962) "Foundation Engineering", Mc graw Hill Book Co. New York, 643 pp.

Lee I.K. (1983) "Geotechnical Engineering", Pitman Publishing Inc, Massachusetts, 58 pp.

NAVFAC Design Manual 7.2 (1983) " Foundations and Earth Structures", USA Department of Navy, Naval Facilities Engineering Command, 130 – 193 pp.

Teng W.C.(1977) "Foundation Design", Prentice Hall of India, New Delhi, 117 – 120 pp.

Tomlinson M.J. (1986) "Foundation Design and Construction", English Language book Society / Longman, 20 – 122 pp.

Geol. Bull. Punjab Univ. 36, 2001.

ENVIRONMENTAL CONCERNS OF DERA GHAZI KHAN AREA PUNJAB, PAKISTAN

BY

SAJID RASHID, SARFRAZ AHMAD
Institute of Geology, University of the Punjab, Lahore - 54590, Pakistan.

SHEIKH MOHAMMAD IQBAL
111-Tariq Block Garden, Lahore, Pakistan

AND

FAZLI RABBI KHAN
National Centre of Excellence in Geology, University of Peshawar, Pakistan

Abstract:- *Environmental geological study of the Dera Ghazi Khan area has been carried out through five maps of environments to maintain natural environments. The maps inform about geology, natural resources, land use planning, water resources and its management and geological hazards about development of the area. These information are helpful to the financial advisors, urban planners and government advisors for fast development of the area without loss of life and property.*

INTRODUCTION

The Metropolitan area of Dera Ghazi Khan Quadrangel lies between longitudes 70° 30' and 70° 45' and latitudes 30° 00' and 30° 15' N in the Dera Ghazi Khan district, Punjab. Dera Ghazi Khan city is a planned city and is located at foothills of the Sulaiman Range and the Lower Indus Plain. It is well connected to all parts of the country by G.T. Road, Railway track and by air. It is also approachable through network of metalled and fair weathered jeepable roads as shown in fig. 1.

The altitude generally increases north westwards with local relief about 300m with minimum and maximum heights of 450m from average mean sea level respectively.

Drainage of the area is controlled by Indus Rier while Chabbri Wah, Johlu nala, Rod Koli and Phullar nala are the main streams. These streams form a dendritic drainage pattern in the area.

The city of Dera Ghazi Khan and the adjoining urban centers have been expanding continuously and also encroaching the older flood plains. The major part of the Dera Ghazi Khan city is developed on the alluvial plain and at places, the soil has swelling characteristic. There has been a growing national awareness by using the geological, land-use planning, hydrological information and the geological satellite imaginary to design the urban area. Its importance increases when the human activity changed the setting of natural resources of the urban area. Thus environmental geology is very important to planners, architects, engineers, government officials and officials of financial agencies who make land-use decisions for safety and property of the urban community.

Iqbal et al (1990) conducted environmental geology studies of Dera Ghazi Khan Quadrngle. Sheikh Iqbal et al (1993) carried out environmental geological studies of Shahdan Lund area district D.G. Khan and its special areas. Sheikh Iqbal et al (1995) described the geology and health hazards of the Dera Ghazi Khan city.

To keep the normal conditions and setting of environments, it needs extensive and thoughtful planning for future development of natural and water resources for urban area. Environmental cancers depend upon the process of urban development, availability of groundwater and construction material and proper disposal of liquid and solid waste material.

ENVIRONMENTAL CONCERNS

The Metropolitan area of Dera Ghazi Khan Quadrangle has urban concentration in the southern part. The rest of the area is rural area where gravel and sand are

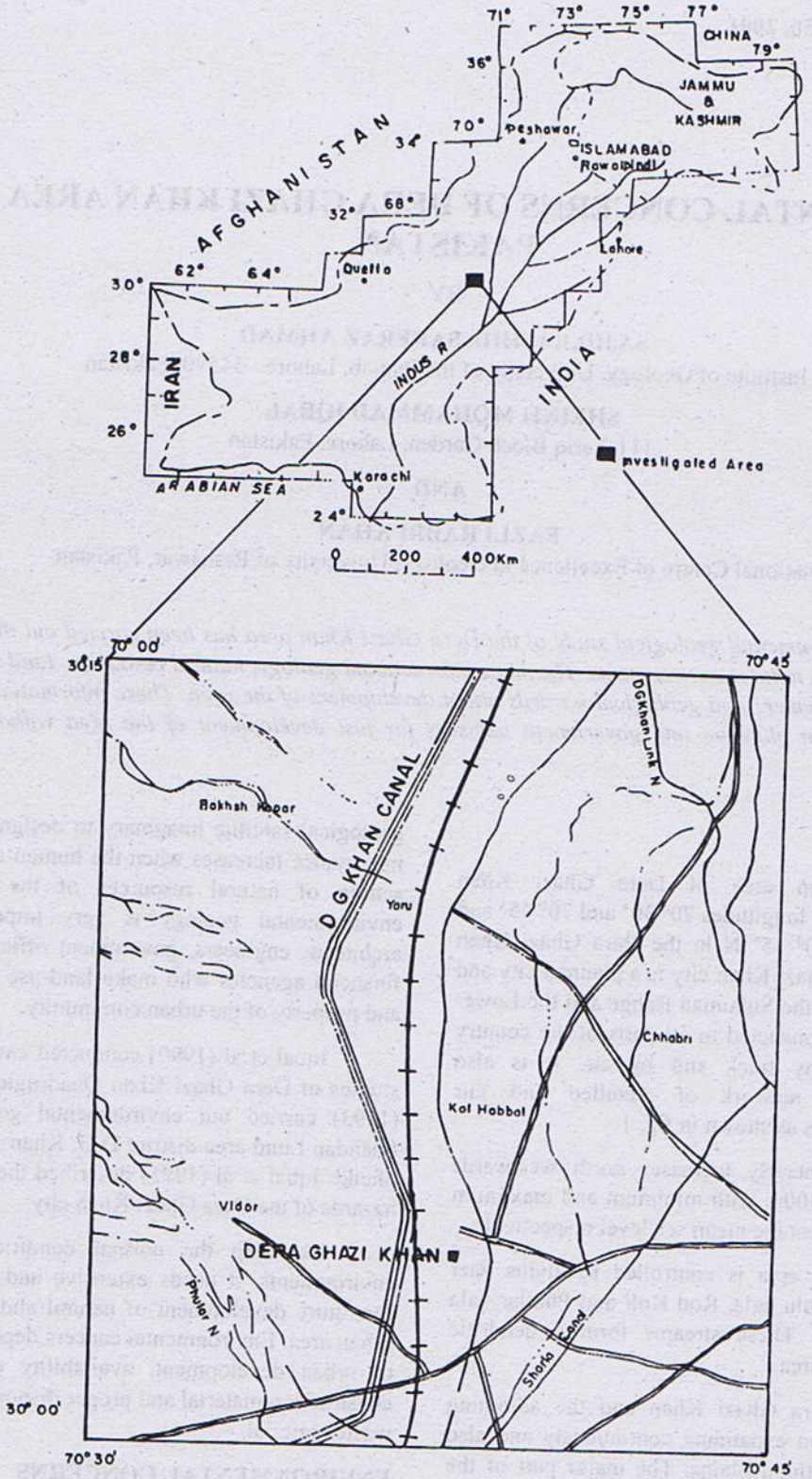

Fig.1. Location Map

abundant. The urban development in alluvial plain unit is maximum. This unit comprises clay, loamy clay and sand. The gravel, sand and clay are specially important for urban development because of reasonable construction material reserves is available in the area. Gravel is primary source for groundwater aquifer. Clay of alluvial plains is mined as a raw material for brick kilns.

Following are the parameters for environmental concern study of Dera Ghazi Khan Metropolitan Area.

- Water Resources
- Construction Material Resources
- Geology/Geomorphology and Landuse Planning
- Engineering Geology
- Geological Constraints
- Pollution

This paper provides data and guideline to concerned agencies for solving environmental issues of the environmental aspects including degradation of environments and mitigation's hazards in the Dera Ghazi Khan city to maintain the natural environment. This data of the following target maps has been achieved here by contributing:

- Location Map
- Geological Map
- Water Recourses Map
- Construction Material Resources Map
- Landuse Planning Map

GEOLOGY/GEOMORPHOLOGY AND LANDUSE PLANNINGS

General Geology:

Dera Ghazi Khan Quadrangle is underlain by Pliocene to Pleistocene sedimentary rocks and Quaternary deposits of Holocene age. The geological map of Dera Ghazi Khan area is shown in fig. 2. (For detail see Geological Bulletin No. 29, pp. 35-41 1994, Institute of Geology, Punjab University, Lahore).

Generalized stratigraphic sequence exposed in the area is given in Table No. 1 from top to bottom.

Table No. 1:

Tope	Rock units	Age
	Stream channels deposits	H
	Sand	O
	Younger Floodplain Deposits	L
	Alluvial Flood Plain Deposits	O
	Alluvial Fan Deposits	C
	Terrace Gravel Deposits	E
		N
		E
	----------Unconformity----------	
Bottom	**Chaudhwan**	**Pliocene**
	Base not Exposed	Sheikh et al. (1995)

Structurally area is simple with moderate dips and recent faulting is marked in the nala cuttings.

Geomorphology:

D.G. Khan Metropolitan Area consists of combination of plains and hilly terrain's. Major part of the area is occupied by plain of lower Indus where as northern part is hilly terrain which includes the low hill of chaudhwan formation of Pliocene age. (Iqbal et al. 1997)

WATER RESOURCES

Indus River, D.G. Khan Canal, Shora Canal are surface water resources of D.G. Khan area. The water is scare and brackish in the northwestern part whereas northeastern and southeastern parts have reasonable groundwater resources. But water is heavy and saline due to

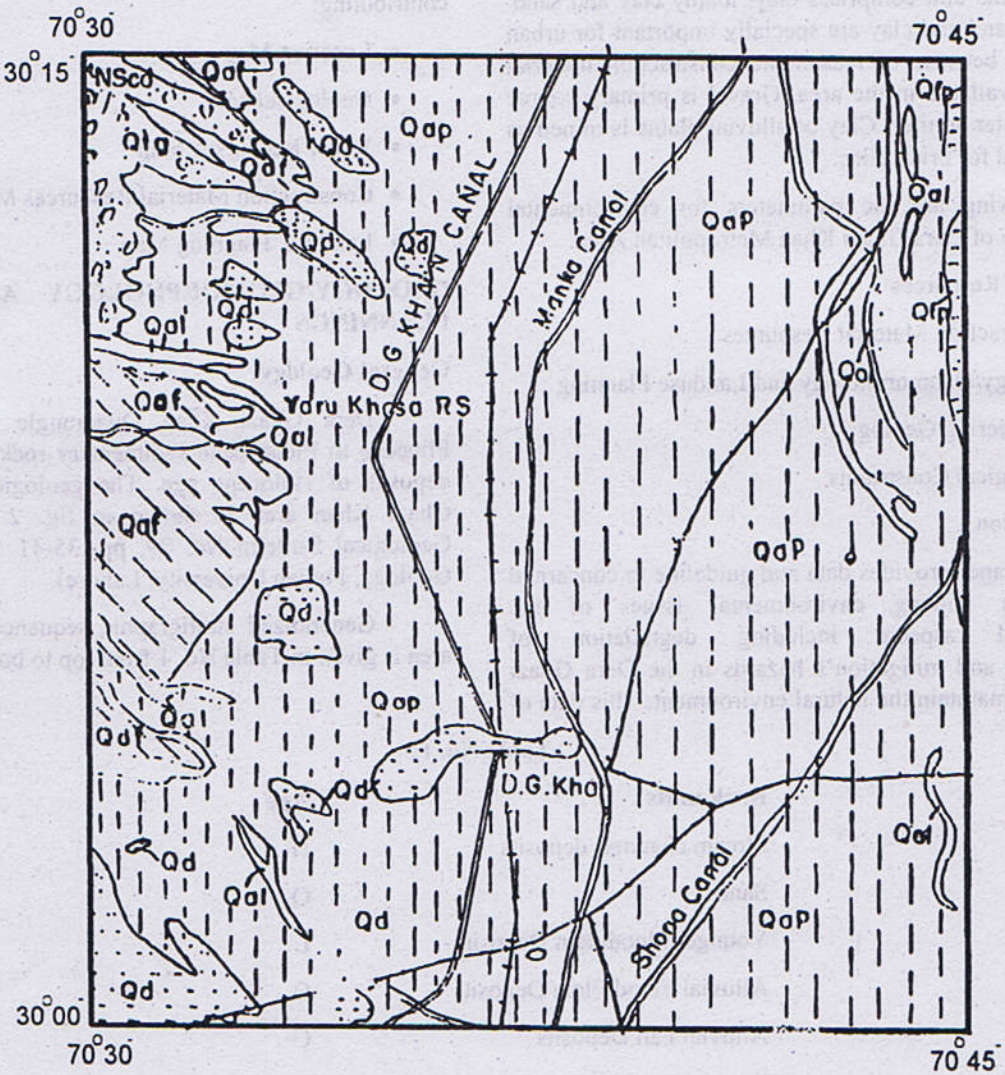

Fig.2. Geological map of D. G. Khan, Pakistan.

evaporite deposits present in the Sulaiman Range. Sweet water is only present in the older flood plain deposits of Indus River and along D.G. Khan Canal, Manka Canal and Shora Canal where tubewells and hand pumps are supplying water to the whole city and surrounding areas as shown in fig. 3. In groundwater assessment studies for D.G. Khan city area, that is not only the quantity of water but also the quality of water, which plays a major role. The water quality of groundwater in the area is generally good along Indus River and D.G. Khan Canal, Manka Canal and Shora Canal but gradually starts deteriorating towards west and southwestern end.

Records from Meteorological department for Dera Ghazi Khan city indicate that there is little increase of temperature. This rise of temperature is effects in the environment of surrounding area and agricultural production and also reduces of work capability of the people. It brings early ripe of crops and vegetation and reduces production of cotton and vegetables in the area. During the field survey, chemical quality of 37 water samples from tubewells, hand pumps, canals and drains were collected and checked from chemical lab Lahore.

Field data have been used to determine the change of groundwater quality in arial extent. The TDS values of different tubewells and hand pumps are given in the table 2. But in western portion, the water deteriorates very fastly where its TDS values ranges from 2000-3500 ppm. This sort of water is not useable for domestic purposes. To construct artificial ponds from canal water, which may be cleaned, filtered and used for domestic uses.

Indus River and D.G. Khan Canal are main sources of recharge to aquifer under D.G. Khan city. Rate of recharging is in accordance with water level heads in the river, therefore, data on discharge and recharge of Indus and Irrigation canals are very important to study the interaction between canal and river.

The details of the tubewells and hand pumps is under:

Tubewells	65
Rural Tubewells	30
Hand Pumps	More than hundred

During field surveys 43 samples of water were conducted for its ppm value regarding to World Health Organization on the basis of Total Solid Dissolved of the project area can be divided into three main zones.

I	Excellent water	0-500 ppm
II	Fresh water	500-1500 ppm
III	Saline water	1500-3000 ppm

CONSTRUCTION MATERIAL RESOURCES

The most important mineral resources of Dera Ghazi Khan Quadrangle are construction material resources including gravel for concrete, sand for mortar and clay for bricks, tiles and pottery. These stuffs are quite abundant is quantity and are being used in construction as shown in fig. 4.

Aggregate:

The gravel to be used as crushed stone and aggregate for construction of multi story buildings and road buildings. There are 15 gravel crushers in operation along Sakhi Sarwar and D.G. Khan – Taunsa Road. Most aggregate resources are obtained by digging alluvial gravel, terrace gravel and stream channel deposits. Sand is obtained from pits of sand. Bricks clay is dug from clay pits scattered in the northern parts of D.G. Khan are where loamy clay is sufficient and good in quantity as shown in fig. 4. There are 10 gravel crushers in operation in the area.

Sand:

Sand is being mined from Vidor, Sakhi Sarwar Road and Kucha Wandani localities by locals and government agencies. The leases are controlled by DMD. Sand is medium to coarse grained and is excellent in quality.

Clay:

Alluvial clay is dominantly used for brick industry. The clay comprises silty clay which is calcareous and plastic. It is used for tiles and pottery in the area. Bricks kilns are widely developed in the area. All production is maintained by manually and no mechanical system is used. There are almost 27 brick kilns present in the area.

LANDUSE PLANNING:

Land is finite resource and its utility must be maintained by its suitability and capabilities. It depends upon geological and biological setting and morphology of the area. (Eleven land-use units have been established for future planning and fast development as show in fig. 5).

Cultivated land (C):

The alluvial plains are usually cultivated land and comprises loamy clay and clay having fine texture with minor sand and stones. This unit covers almost 67% of the area and is irrigated through Dera Ghazi Khan Canal and its branches. This land is easily converted to urban use. Primary crops are wheat, cotton, sugar cane, rice and seasonal vegetables.

Barren Land (B):

The barren land is composed of alluvial plain, which is mainly covered with sand dune. This land is convertible to farmland due to availability of canal water.

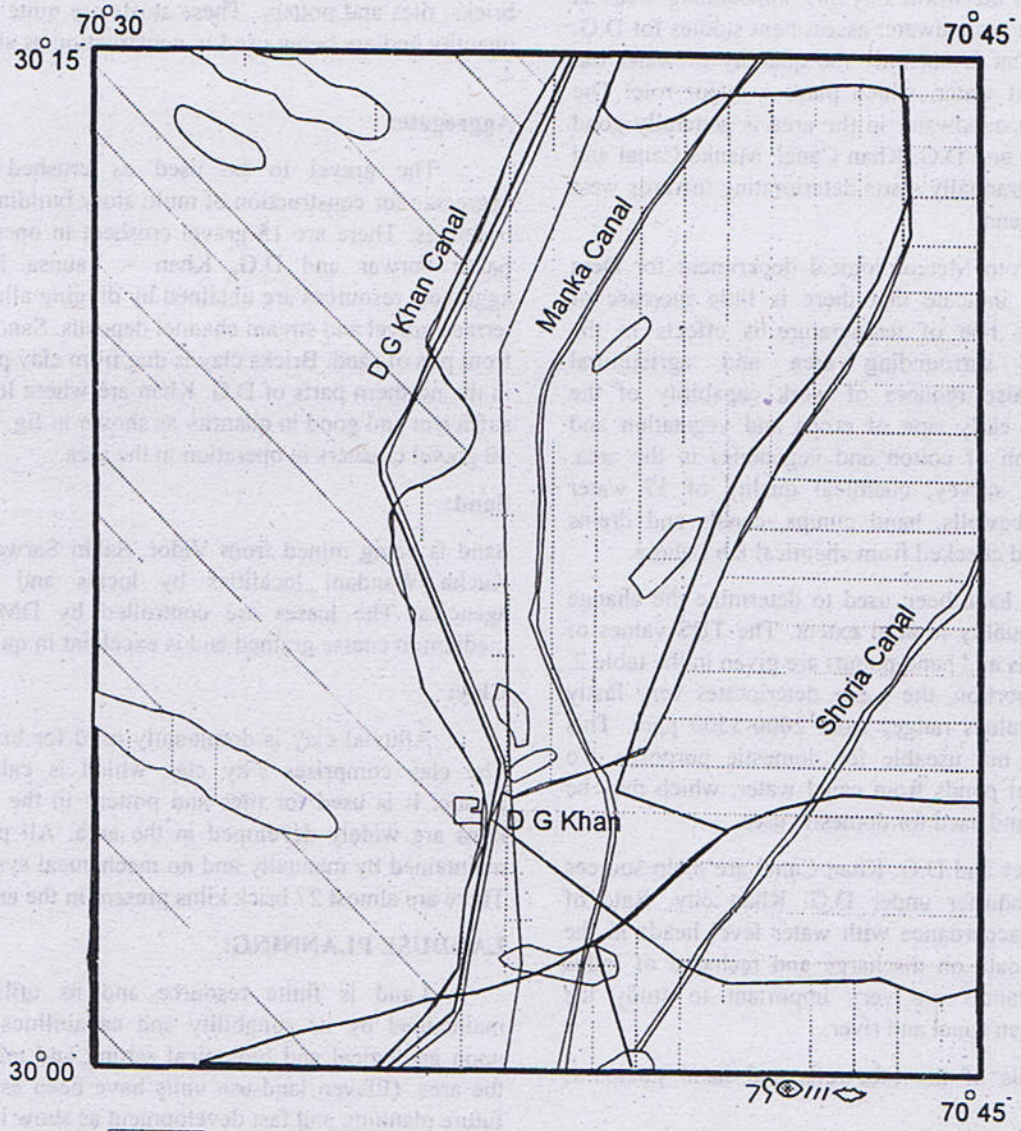

Fig. 4. Construction material resources map of D.G. Khan, Pakistan.

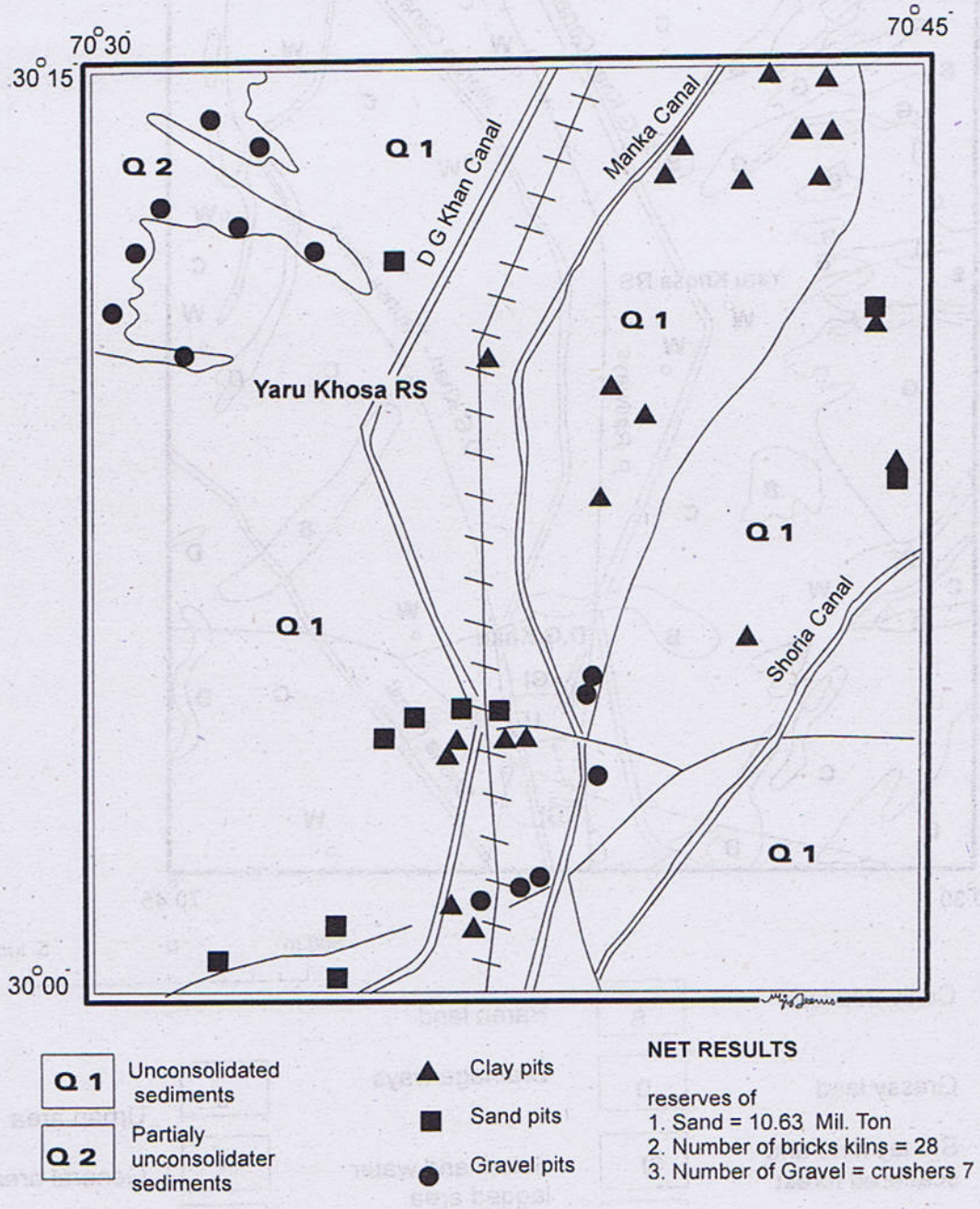

Fig. 4. Construction material resources map of D. G. Khan, Pakistan.

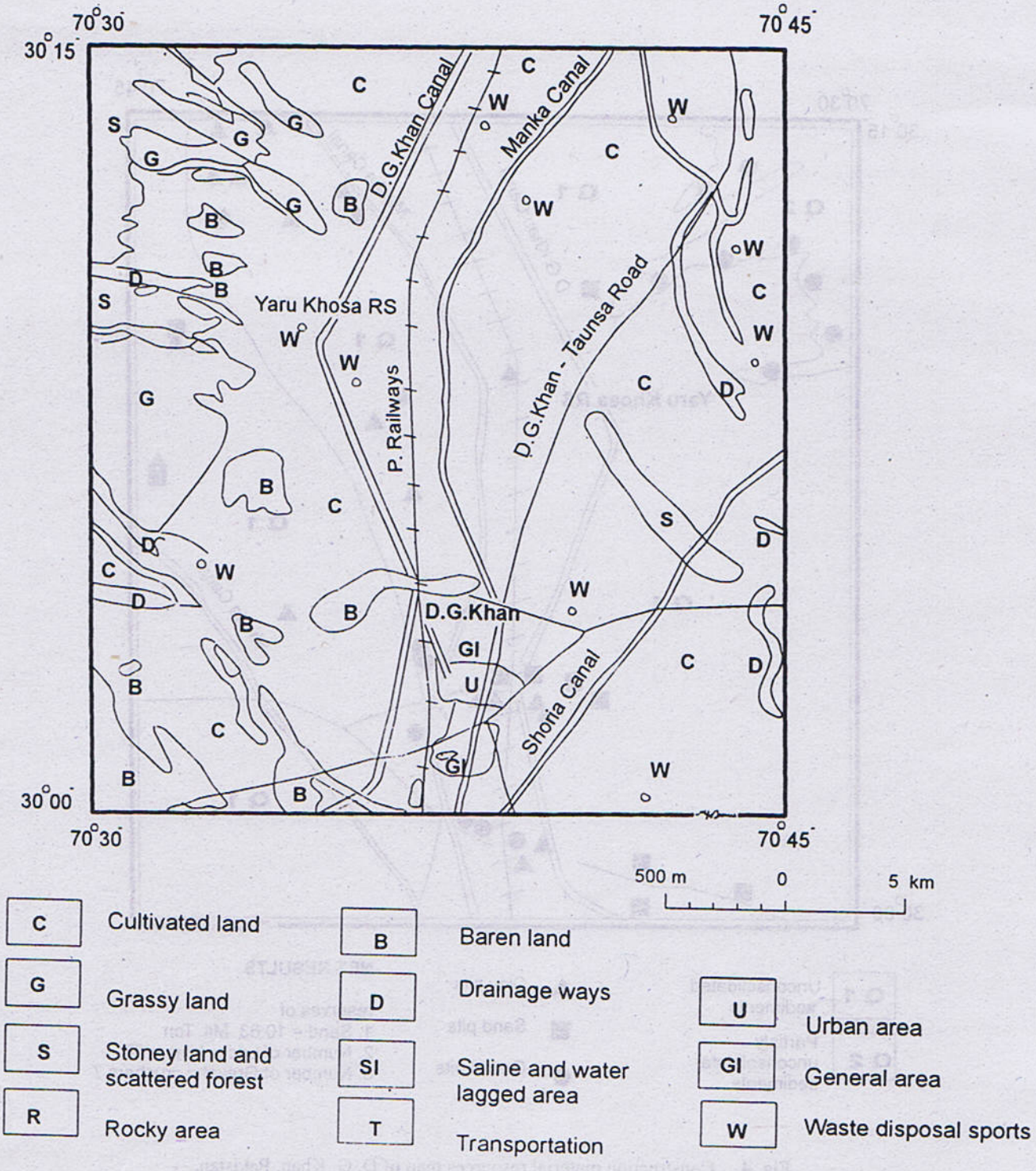

Fig. 5. Land - Use planning map of Dera Ghazi Khan, Pakistan.

Grass Land (G):

The grass land comprises chuadhwan formation and terrace gravel deposits and is covered with grass and bushes and small trees. It cannot be converted into urban use because of difficult to excavate and having no water.

Forest Land (F):

The forest land is mainly with scattered trees, bushes and grass. This unit can be used for grazing of animals and goats and recreation parks. The plantation of trees may be maintained to control the soil erosion and is good for beauty of the area.

Clay pits and Brick Kilns (CI):

This unit consists of loamy clay of alluvial plain deposits. It is more calcareous and plastic and is suitable for pottery and brick industry in the area. These pits are useable for urban use and parks and agriculture use.

Urban Area (U):

It includes the old city and new localities in its vicinity. It is thickly and more polluted with less amenities such as open sewage and no provision of dumping of solid and semi solid garbage in this parts. In this unit, shopping centers and hotels throw their waste on open ground which is becoming problem for residents due to dirty smell emitting from these dumps of garbage.

Planned Residential Area (P):

The area comprises Government residential and newly constructed colonies of Dera Ghazi Khan city. It has sewage and garbage dumping spots and parks.

Institutional Area (1)

This unit is dominantly for school, colleges, hospitals and government offices.

Transportation (T):

This unit includes all kinds of roads through which city is connected with other parts of city as well as with country.

Waste Disposal Areas (W):

These are spots where domestic and industrial waste is being dumped daily. But Municipal Corporation dumps garbage along road depression and abounded places. They are not adopting "landfill method" for dumping of garbage. Due to old method, contamination of groundwater is more susceptible.

Artificial Ponds (P):

Artificial ponds are developed by Municipal Corporation in western part of city where no good quality water is available.

Drainage Ways (D):

The drainage ways are D.G. Khan Canal with its branches and seasonal streams, which carry out extra water in rainy season and recharge the aquifer through seepage.

Saline And Waterlogged Area (S):

This area is being used for different industries such as cotton, flour mills and ice cream and ice factories and railway workshops.

ENGINEERING GEOLOGY

There are no foundation problems except some cracks have been developed in some buildings of Dera Ghazi Khan city. This is mainly caused by swell/shrinkage of soil due to presence of evaporite deposits in Sulaiman Range. For example, a new building for hospital where cracks have been developed due to presence of gypsum content in the soil material, being used in its construction. Special tests are recommended to determine the physical properties of the soil before start of construction of the any building or multistory building especially bearing capacity, moisture content, bulk density, specific gravity, swelling soil and consolidating tests.

GEOLOGIC CONSTRAINTS

Seismic Risk:

Dera Ghazi Khan city does not fall in seismically active zone of folded belt of Sulaiman Range and Lower Indus plain but it lies in the foredeep of Suleiman Range. No seismic survey has been conducted in this area recently.

Urban Flooding and Drainage

Dera Ghazi Khan is located on a part of water way of Indus River. All flood plains, however, are subject to periodic flooding. The old and new part of the city is located on flood plains. During monsoon rainy season, road, lanes and main shopping centers are remained under water for couple of days. In flood season, Sakhi Sarwar Road is blocked due to sand and debris flow.

Natural drainage with gutters, storm sewers may be constructed. Urban paving and drainage channelization accelerate and increase run off. Storm drainage network can mitigate local flooding. In rural area, flood water may hit the Kucha houses and damage them. Build small check dams, which can reduce intensity of flood damage in rural area.

POLLUTION

Pollution in the area is due to the dumps of garbage and solid waste and thick canopy of smoke, dust and other gases in the atmosphere. The air pollution effects on the temperature of the area and decreases production of agricultural land.

EFFECTS

I. Increase the temperature due to CO_2

II. Breathing problems respiratory ailments.

III Sulphur compounds from coal may cause of cancer quaintly in the atmosphere.

IV Plants are also affected due to more CO_2.

REMEDY

I. Install dust collectors at cotton mills.

II. Install smoke filters at silencers of vehicles.

III. Increase farmland and forest area.

IV. Plantation along road and industrial area.

POLLUTION OF WATER

Sources

I. Discharge of domestic and municipal sewage.

II. Discharged of industrial water.

III. Use of agricultural chemical (pesticides and Insecticide).

IV. Not dumping of garbage of landfill method.

CONCLUSIONS

All these information from environmental geological map its related maps of Dera Ghazi Khan area provide full picture of the whole area for city planners, municipal management and financial advisers for solving their problems of urban as well as rural areas with rapid growth of population with content of environmental geologists. These information will help planners and engineers and local public and leaders for better planning, money saving and better management of the urban area under develop part of this region.

ACKNOWLEDGEMENTS

Thanks are due to Director General and Deputy Director General of Geological Survey of Pakistan for technical support.

REFERENCES

Bajwa, M.S. 1986, Geology of Dalana Area, D.G. Khan District Punjab, Pakistan. Information Release No. 239.

Hemphil, W.R. & Kidwai, A.H. 1973, Stratigraphy of Bannu and Dera Ismail Khan areas, Pakistan. *U.S. Geol. Surv. Prof paper* 716-B, 36pp., Reston va.

Iqbal, M. Sheikh, M.K. Pasha & Van William, 1993, Environmental Geology of Islamabad Area. GSP Pakistan and U.S. Geological Survey, Prof. Paper No. (IR)PK-109-3A.

Iqbal, M. sheikh, Khan M.A. & Ahmed, S; 1994, Urban Geology of Dera Ghazi Khan area Southern Punjab Pakistan, *Geol. Bull, Punjab Univ.***28**. pp. 35-41.

Iqbal, M. Sheikh, Akhtar, M.K; Hasan, M. & Raza, Q; 1995, Environmental Geology and solid & Liquid waste disposal of Dera Ghazi Khan Area, Punjab, Pakistan; Vol. 12 Nepal Geological society, Special Bulletin, 1st Geological Congress, Nepal.

Iqbal, M. Sheikh and Mahmood-ul-Hasan, 1995, Geology of Shahdan Lund, D.G. Khan District, Punjab Pakistan; Information Release No. 611.

Iqbal, M. Sheikh and Mahmood-ul-Hasan, M. Kaleem Akhtar and S.Q. Raza, 1995, Environmental Geology of Shahdan and D.G. Khan District, Punjab Pakistan.

Iqbal, M. Sheikh, Khan M.A & Ahmed, S; 1997 Role of Earth Sciences in Urbanization of Dera Gahzi Khan city Punjab Pakistan, *Geol. Bull. Peshawar* **30,** pp. 119-130.

Iqbal, M.W.A; & Shah, S.M.I; 1980 A guide to the Stratigraphy of Pakistan *Geol. Surv. Pak. Recs;* **53**.

Kazmi, A.H; & Rana, R.A; 1982, Tectonic Map of Pakistan. Scale 1:2,000,000. Geol. Surv. Pak map series; Quetta.

Geol. Bull. Punjab Univ. 36, 2001.

STAFF LIST OF THE INSTITUTE OF GEOLOGY, UNIVERSITY OF THE PUNJAB ON 31ST DECEMBER, 2001

1. Teaching Staff

Name and Qualifications	Field of Specialization
Professors	
Dr. Shafeeq Ahmad (Director) M.Sc. (Pb)., Ph.D. (Pb)	Geochemistry, Environmental Geology, Ore-microscopy
Dr. Zulfiqar Ahmad M.Sc. (Pb), Ph.D. (U.K) (on Ex-Pakistan leave)	Mineralogy, Economic Geology
Dr. Munir Ghazanfar M.Sc. (Pb)., M.Sc. (Sheffield) Ph.D. (Pb)	Geomorphology, Tectonics
Associate Professors	
Mr. Umar Farooq M.Sc. (Pb), M.Sc., D.I.C. (London)	Exploration Geophysics
Dr. Sarfraz Ahmad M.Sc. (Pb), Ph.D. (London)	Stratigraphy, Palynology, Palaeontalogy
Mr. Zahid Karim Khan M.Sc. (Pb)	Engineering. Geology, Geohydrology, Aggregate Materials
Assistant Professors	
Dr. Iftikhar Hussain Baloch M.Sc. (Pb), M.Sc. (Hull), Ph.D. (Leicester)	Industrial Mineralogy
Dr. Akhtar Ali Saleemi M.Sc. (Pb), M.Sc. (Leicester), Ph.D. (Leicester)	Industrial Mineralogy, Economic Geology
Dr. Nazir Ahmad M.Sc. (Pb), Ph.D. (Leicester)	Structural & Petroleum Geology, Sedimentology
Mr. Syed Alim Ahmad M.Sc. (Pb)	Mineralogy, / Petrology

Dr. Muhammad Hafeez M.Sc. (Pb), Ph.D. (U.K.) (On study leave)	Geohydrology
Dr. Muhammad Saeed Farooq M.Sc. (Pb), Ph.D. (Pb)	Engineering Geology, Geohydrology
Dr. Riaz Ahmad Sheikh M.Sc. (Pb), D.I.C., Ph.D. (London)	Petroleum and Structural Geology, Sedimentology
Mr. Muhammad Ashraf Siddiqui M.Sc. (Pb), PGD (Leicester)	Industrial Mineralogy
Dr. Shahid Jameel Sameeni M.Sc. (Pb), Ph.D. (Pb)	Paleontology / Stratigraphy
Mr. Sajid Rashid M.Sc. (Pb)	Engineering Geology, Geohydrology
Mr. Syed Mahmood Ali Shah M.Sc. (Pb), M.Sc. (SA)	Mineralogy/Petrology

Lecturers

Mr. Abdus Sattar M.Sc. (Pb)	Geochemistry, Mineralogy
Mr. Abdur Rauf Nizami M.Sc. (Pb)	Sedimentology, Petroleum Geology, Remote Sensing
Mr. Kamran Mirza M.Sc. (Pb)	Micropaleontology/Stratigraphy
Mr. Naveed Ahsan M.Sc. (Pb)	Petroleum & Structural Geology, Tectonics, Sedimentology
Miss Farzana Aslam M.Sc. (QAU), M.Phil (QAU)	Physics
Mr. Shahid Ghazi M.Sc. (Pb)	Petroleum Geology, Stratigraphy & Sedimentology
Mr. Tariq Javed Bhatti M.Sc. (Pb), M.Sc. (Norway)	Engineering Geology, Hydropower Development

2. Technical and Service Staff

Mr. Masood Ahmad Khan Lodhi	Administrative Officer
Mr. Muhammad Suleman	Assistant (Accounts)
Ch. Muhammad Siddique	Assistant
Mr. Nadeem Younas	Senior Stenographer
Vacant	Stenographer

Mr. Muhammad Asghar	Senior Clerk
Mr. Muhammad Arif	Senior Clerk
Mr. Muhammad Farrukh Javed	Junior Clerk
Mr. Ali Akbar Sandhu	Junior Clerk
Malik Muhammad Nazir	Library Attendant
Vacant	Maintenance Engineer
Mr. Masud Minhas	Geological Illustrator
Mr. Zafarullah Butt	Senior Technician
Mr. Muhammad Yaseen	Store Supervisor
Mr. Liaqat Ali S/o Ilam Din	Junior Technician
Vacant	Junior Technician
Mr. Muhammad Younas	Museum Assistant
Mr. Riaz Qadeer	Lab. Assistant
Mr. Muhammad Ilyas	Lab. Assistant
Mr. Liaqat Ali S/o Barkat Ali	Lab. Attendant
Mr. Samiullah Khan	Lab. Attendant
Mr. Haq Nawaz	Lab. Attendant
Mr. Nazir Ahmad	Lab. Attendant
Mr. Ghulam Mustafa	Lab. Attendant
Mr. Muhammad Yaqoob	Lab. Attendant
Mr. Muhammad Rafi	Lab. Attendant
Drivers	2
Service Staff	3